UNIVERSITY *of*
TASMANIA
AUSTRALIA

Polymer-Inorganic Hybrid Nanoparticles via Polymerization-Induced Self-Assembly

by

Guo Hui Teo

BE (Hons.)

A thesis submitted in fulfilment of the requirements for the degree of Doctor of Philosophy at

The University of Tasmania in September 2018

Abstract

Silica nanoparticles are commonly integrated within polymeric matrices to form composite materials, due to their non-toxic nature, chemical resistance and physical properties. Polymer-silica colloidal nanocomposites are the most studied class of hybrid nanoparticles and their applications can be tailored based on synthetic approaches. The aims of this work were to prepare polymer-silica colloidal nanocomposites via a combination of reversible deactivation radical polymerization, self-assembly and sol-gel chemistry. This approach enabled the preparation of hybrid nanoparticles with controllable shape and size. The influences of compositional design (e.g. block copolymer architecture), solvent and initiating systems were also studied.

Firstly, polymer nanoparticles were prepared by Polymerization-Induced Self-Assembly (PISA) in ethanol where the solvophilic block was an alkoxysilane-functional methacrylate. Spherical nanoparticles and polymeric vesicles were successfully prepared. A solid silica shell was successfully grown from the particle surface via subsequent hydrolysis and condensation of tetraethyl orthosilicate. Secondly, block copolymer self-assembly was studied where the alkoxysilane functionality was present in the core-forming block. This approach was not viable by aqueous PISA emulsion polymerization. A solvent-mediated self-assembly approach was thus adopted, yielding spherical nanoparticles in water, and a mixture of spheres and vesicles in *n*-hexane. Finally, the reactivity of alkoxysilane-functional methacrylates was exploited to prepare triblock copolymers as surfactants where the interfacial block could be crosslinked via hydrolysis and condensation. Triblock copolymers were either formed separately (and used to stabilize oil-in-water miniemulsions) or *in-situ* via the PISA method. The encapsulation of Nile Red in the particle core was achieved in parallel with self-assembly and the retention rate was improved through interfacial crosslinking.

Declaration by Candidate

This thesis is written based of my original research work, and contains no material that has been accepted for a degree or diploma by the University or any other institution, except by way of background information and duly acknowledged in the thesis. To the best of my knowledge and belief no material has been previously published or written by another person except where due acknowledgement is made in the text of the thesis, nor does the thesis contain any material that infringes copyright.

The publishers of the papers included within Chapters 3 and 4 hold the copyright for that content, and access to the material should be sought from the respective journals. The remaining non-published content of the thesis may be made available for loan and limited copying and communication in accordance with the Copyright Act 1968. I allow the University of Tasmania Library to keep an electronic version of my thesis based on the policies and procedures of The University of Tasmania.

The contributions by each co-author to the published works that I have incorporated in this thesis have been clearly stated. The contribution of others to this thesis such as editorial advice and sample analysis is also stated.

All materials included in this thesis have been clearly cited. The copyright of these materials resides with the copyright holders. This thesis has been submitted for plagiarism checking through Turnitin® software and the similarity report can be provided upon request.

Candidate's signature:

Guo Hui Teo

Publications and Conferences during Candidature

Peer-Reviewed Papers:

G. H. Teo, R. P. Kuchel, P. B. Zetterlund and S. C. Thickett, Polymer-Inorganic Hybrid Nanoparticles of Various Morphologies via Polymerization-Induced Self-Assembly and Sol–Gel Chemistry, *Polymer Chemistry*, **2016**, 7, 6575-6585. DOI: 10.1039/C6PY01447J

M. Rowe, G. H. Teo, J. Horne, O. Al-Khayat, C. Neto and S. C. Thickett, High Glass Transition Temperature Fluoropolymers for Hydrophobic Surface Coatings via RAFT Copolymerization, *Australian Journal of Chemistry*, **2016**, 69, 725-734. DOI: 10.1071/CH15787

G. H. Teo, R. P. Kuchel, P. B. Zetterlund and S. C. Thickett, Self-Assembly of Block Copolymers with An Alkoxysilane-Based Core-Forming Block: A Comparison of Synthetic Approaches, *Journal of Polymer Science Part A: Polymer Chemistry*, **2018**, 56, 420-429. DOI: 10.1002/pola.28911

Conference Proceedings

G. H. Teo, Y. H. Ng, N. Wood, P. B. Zetterlund and S. C. Thickett, Hollow Polymer-Graphene Oxide Microcapsules via Pickering Miniemulsion Polymerization, 35th Australasian Polymer Symposium (APS), July 2015, Gold Coast, Queensland, Australia (poster presentation).

G. H. Teo, Y. H. Ng, N. Wood, P. B. Zetterlund and S. C. Thickett, Hollow Polymer-Graphene Oxide Microcapsules via Pickering Miniemulsion Polymerization, 9th Graduate Research Conference, September 2015, Sandy Bay, Tasmania, Australia (poster presentation).

G. H. Teo, R. P. Kuchel, P. B. Zetterlund and S. C. Thickett, Polymer-Inorganic Hybrid Nanoparticles via Polymerization-Induced Self-Assembly, 10th Graduate Research Conference, September 2016, Sandy Bay, Tasmania, Australia (poster presentation).

G. H. Teo, R. P. Kuchel, P. B. Zetterlund and S. C. Thickett, Polymer-Inorganic Hybrid Nanoparticles via Polymerization-Induced Self-Assembly, 36th Australasian Polymer Symposium (APS), November 2016, Lorne, Victoria, Australia (poster presentation).

Statement of Co-Authorship

The following people and institutions contributed to the publication of work undertaken as part of this thesis:

Candidate	Guo Hui Teo, School of Natural Sciences (Chemistry), UTas
Author 1 (Primary Supervisor)	Dr. Stuart C. Thickett, School of Natural Sciences (Chemistry), UTas
Author 2	Dr. Rhiannon P. Kuchel, Mark Wainwright Analytical Centre, UNSW
Author 3	Professor Per B. Zetterlund, Centre for Advanced Macromolecular Design, UNSW

Author details and their roles:

Paper 1, *Polymer-Inorganic Hybrid Nanoparticles of Various Morphologies via Polymerization-Induced Self-Assembly and Sol–Gel Chemistry*

Located in Chapter 3.

Candidate was the primary author (50 %) and contributed to the conception and design of the research project, planning, execution, preparation of the work for the paper and data analysis.

Author 1 (30 %) contributed to the conception and design of the research project, data analysis, drafted significant parts of the paper and refinement.

Author 2 (10 %) contributed to the electron microscopy and refinement.

Author 3 (10 %) contributed to the conception and design of the research project and refinement.

Paper 2, *Self-Assembly of Block Copolymers with An Alkoxysilane-Based Core-Forming Block: A Comparison of Synthetic Approaches*

Located in Chapter 4.

Candidate was the primary author (50 %) and contributed to the conception and design of the research project, planning, execution, preparation of the work for the paper and data analysis.

Author 1 (30 %) contributed to the conception and design of the research project, data analysis, drafted significant parts of the paper and refinement.

Author 2 (10 %) contributed to the electron microscopy and refinement.

Author 3 (10 %) contributed to the conception and design of the research project and refinement.

We the undersigned agree with the above stated "proportion of work undertaken" for each of the above published papers contributing to this thesis:

Signed

Candidate: ..... Author 2: .....

Author 1 : ..... Author 3: .....

Contributions by Others to This Thesis

The author (candidate) acknowledges the following individuals who have contributed and supported to this thesis:

- Dr. Stuart C. Thickett for contributing and supporting to the experimental ideas, designs, data analysis and revisions of this thesis.

- Dr. Siva Shanmugam and Mr Eh Hau Pan for running Size Exclusion Chromatography and measuring polymer molecular weights and distributions (Chapter 3 and 4).

Statement of Parts of The Thesis Submitted to Qualify for The Award of Another Degree

None.

Acknowledgements

First of all, I would like to express my sincere appreciation to my primary supervisor Dr. Stuart Thickett for his patience, encouragement, enthusiasm, brilliant ideas and continuous support to my PhD study and research work. His excellent guidance directed and helped me to work professionally and think broadly in solving obstacles.

I would like to convey my gratitude to The University of Tasmania for generous scholarship support and School of Natural Sciences (Chemistry) for providing a dedicated workplace.

I acknowledge the Central Science Laboratory for providing facilities and scientific instruments. I would also like to thank the competent people who kindly assisted me on technical and instrumental issues: Dr James Horne for silicon (^{29}Si) NMR support, Dr. Karsten Goemann and Dr. Sandrin Feig for Scanning Electron Microscopy (SEM) support, Dr Olivier Bibari for Transmission Electron Microscopy (TEM) support and Dr. Petr Smejkal for Size Exclusion Chromatography (SEC) support.

I am thankful to Mr Murray Frith for helping me in arranging chemical orders and Miss Trish McKay for smoothing the administrative work. I also want to thank A/Prof Jason Smith (Head of Discipline, Chemistry) for his continuous support during my candidature.

I would like to express my gratitude to colleagues and friends for their direct or indirect help in my research work and for their genuine friendship.

Last but not least, I am indebted and would like to thank my parents and family for their warmly supports and encouragement during my PhD study.

Keywords

RAFT polymerization, self-assembly, Polymerization-Induced Self-Assembly (PISA), hybrid nanoparticles.

Australian and New Zealand Standard Research Classifications (ANZSRC)

ANZSRC code: 030306 Synthesis of Materials, 30%

ANZSRC code: 030301 Chemical Characterisation of Materials, 25%

ANZSRC code: 091202 Composites and Hybrid Materials, 30%

ANZSRC code: 090406 Powder and Particle Technology, 15%

Fields of Research (FoR) Classification

FoR code: 0303 Macromolecular and Materials Chemistry, 55%

FoR code: 0912 Materials Engineering, 30%

FoR code: 0904 Chemical Engineering, 15%

Table of Contents

List of Figures

List of Tables

Abbreviations Used in This Thesis

ACVA	4,4′ -Azobis(4-cyanovaleric acid)
BzMA	Benzyl methacrylate
CDTSPA	4-Cyano-4-[(dodecylsulfanylthiocarbonyl)sulfanyl]pentanoic acid
CPADB	4-Cyano-4-(phenylcarbonothioylthio)pentanoic acid
DCC	N,N'-Dicyclohexylcarbodiimide
DMAP	4-Dimethylaminopyridine
DMF	Dimethylformamide
DMSO	Dimethyl sulfoxide
DP	Degree of polymerization
d_{pred}	Predicted *Z*-average diameter
DP_{th}	Theoretical degree of polymerization
d_z	*Z*-average diameter
E_a	Activation energy
H_2SO_4	Sulphuric acid
HCl	Hydrochloric acid
HD	Hexadecane
IPS	3-(Triisopropoxysilyl)propyl methacrylate
LMA	Lauryl methacrylate

M_n	Number-average molecular weight
M_p	Peak molecular weight
MPS	3-(Trimethoxysilyl)propyl methacrylate
MWCO	Molecular weight cut off
NH_4OH	Ammonium hydroxide
PBzMA	Poly(benzyl methacrylate)
PDI ($Đ$)	Dispersity
PEG	Poly(ethylene glycol) methyl ether
PEGMA	Poly(ethylene glycol) methyl ether methacrylate
PIPS	Poly(3-(triisopropoxysilyl)propyl methacrylate
PISA	Polymerization-induced self-assembly
PLMA	Poly(lauryl methacrylate)
PMPS	Poly(3-(trimethoxysilyl)propyl methacrylate
RAFT	Reversible Addition–Fragmentation chain Transfer polymerization
SiNPs	Silica nanoparticles
TBHP	tert-Butyl hydroperoxide
TEA	Triethylamine
TEOS	Tetraethyl orthosilicate
THF	Tetrahydrofuran
TMS	Tetramethylsilane

Chapter 1 : Introduction and Aims

This chapter provides a background of silica nanoparticles and hybrid materials consisting of both polymer and silica domains. In Section 1.1, silica nanoparticle synthesis and their applications will be briefly discussed. In Section 1.2, the main methods of chain growth polymerization and the approaches to integrate silica-based materials into polymers are discussed. Primary heterogeneous polymerization methods and the polymerization of silicon containing monomers through heterogeneous techniques are examined in Section 1.3. In Section 1.4, self-assembly of block copolymers (with and without a silicon containing block) via various methods are presented. The aims and objectives of this work are given in Section 1.5 and the thesis outline is described in Section 1.6.

Chapter 1

1.1 Silica Nanoparticles

Silicon dioxide (SiO_2; commonly referred to silica) nanoparticles have been applied in multidisciplinary research, spanning advanced applications in biomedical engineering through to applications in everyday life (e.g. kitchenware, sealant and casings). The rise of silica nanoparticles as an effective and multipurpose material in different areas is primarily due to its high melting point, chemically inert nature, low toxicity and easy surface functionalization.[1] A brief scheme of silica nanoparticle synthesis is shown as Figure 1-1.

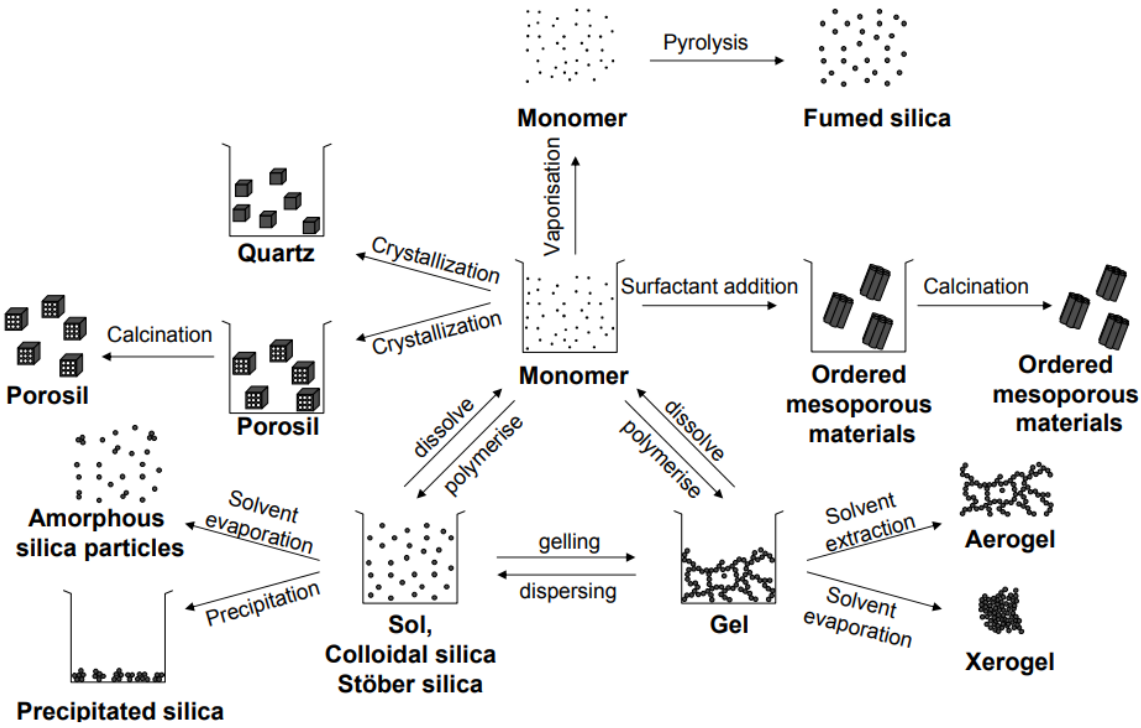

Figure 1-1: Brief scheme for silica particles synthesis via using silane-based monomers. Reprinted with permission from reference 2. Copyright 2010 BioMed Central Ltd.

1.1.1 Methods of Silica Nanoparticles Preparation

A variety of different approaches to synthesize silica nanoparticles with different sizes, morphologies and physicochemical properties have been reported. Two of the most popular methods for silica nanoparticle synthesis are the Stöber and microemulsion methods. Both methods rely on sol-gel chemistry in the presence of either an acid or base catalyst. Acid catalysis produces chain-like networks while basic conditions produces a highly condensed and branched network.[3] This is due to the different rates of hydrolysis (of the silica sol) and condensation (to form siloxane linkages) as a function of pH. At low pH the rate of hydrolysis is high and condensation is low; the reverse is true at high pH.[4] The crosslinking rate is also affected by the size of alkoxy group.[5] The sol-gel process is shown in Figure 1-2**.**

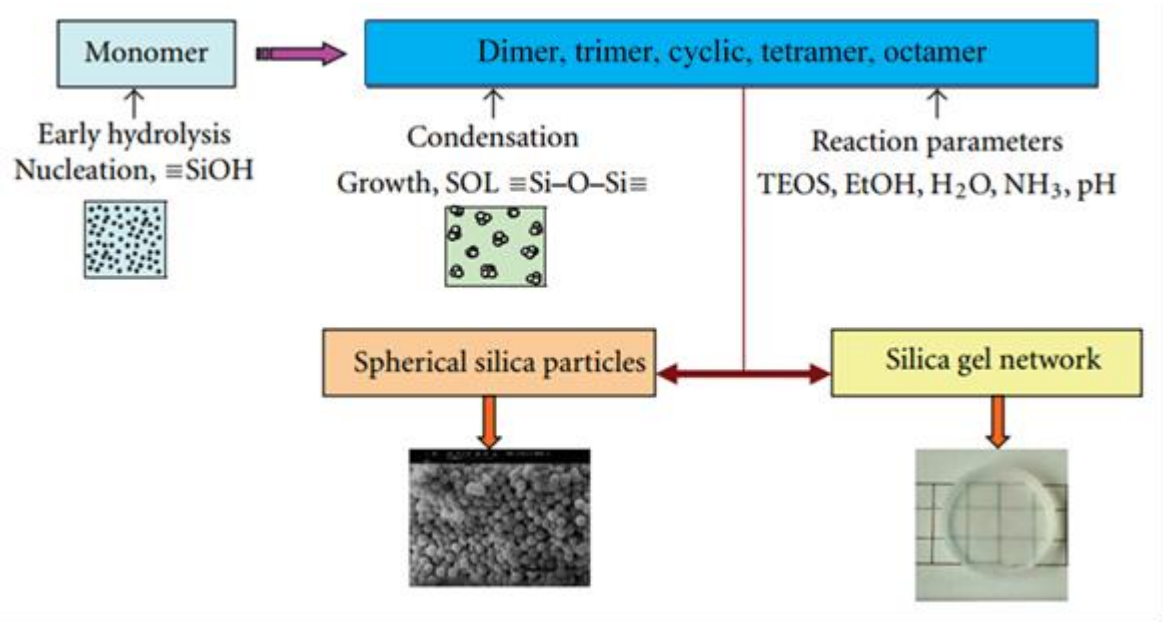

Figure 1-2: Flow chart of sol-gel process. Reprinted with permission from reference 6. Copyright 2012 Hindawi Limited.

1.1.1.1 The Stöber Method

A method of silica particle synthesis was first presented by Gerhard Kolbe in 1956.[7] He synthesized spherical silica particles by hydrolysing tetraethylorthosilicate (TEOS) in the presence of ammonia catalyst. Following this, Werner Stöber improved the synthetic process in 1968.[8] A variety of synthetic methods are available now, however the Stöber process is still the most popular technique for preparing silica nanoparticles to date, given it is the simplest and most effective way to synthesize monodisperse silica spheres. Furthermore, the conditions in the Stöber process involve readily available starting materials and non-stringent reaction conditions. In the simplest form of the Stöber process to prepare colloidal particles, the only reaction is the sequential hydrolysis and condensation of alkyl silicates under alkaline catalysis in alcoholic media. For an example, monodisperse and nonporous silica spheres with a diameter range from 20 to 100 nm were produced by using Stöber process.[9] The particle diameter was highly influenced by water concentration, TEOS concentration, temperature and ammonia concentration. Figure 1-3 shows the silica nanoparticles produced from different conditions via Stöber method. In their work, the standard conditions were set to 0.37 mol L^{-1} TEOS, 0.25 mol L^{-1} ammonia, 3.95 mol L^{-1} water and 25 ^{o}C.[9]

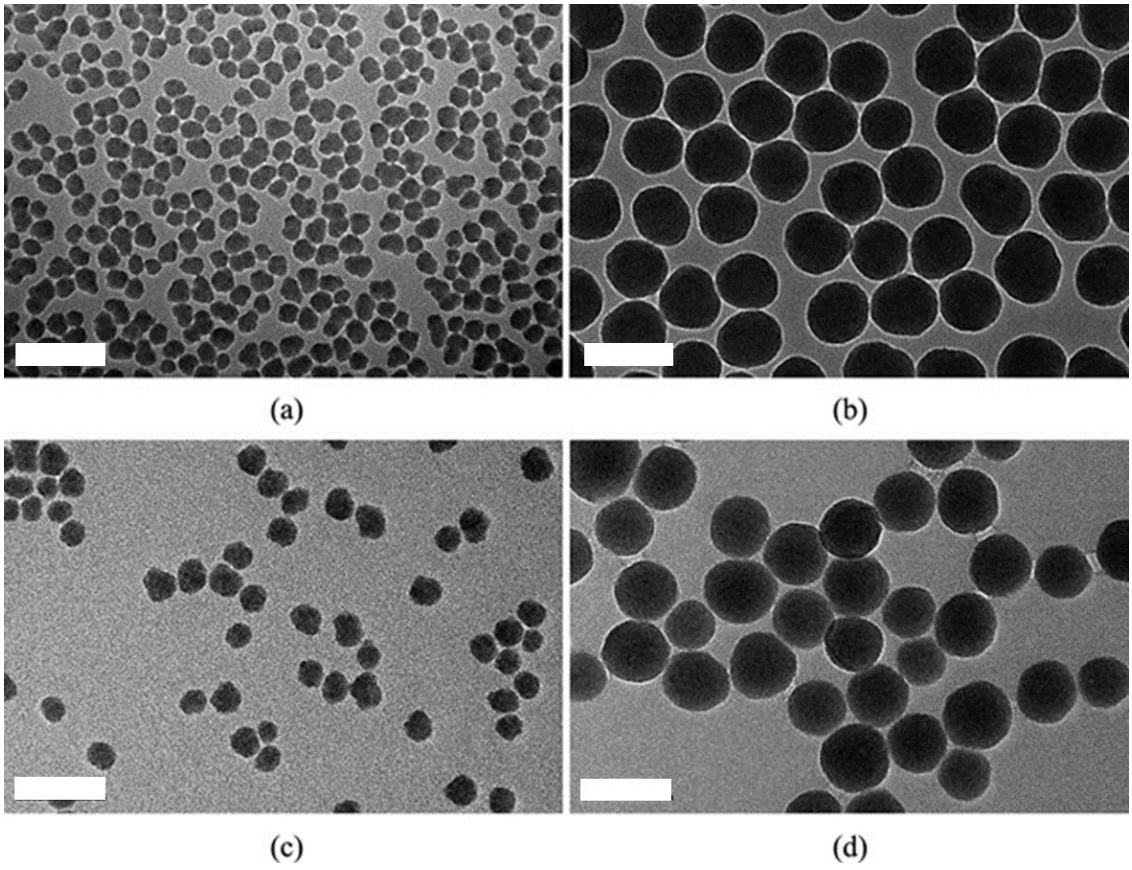

Figure 1-3: TEM images of silica nanoparticles produced from different conditions via Stöber method: (a) TEOS = 0.37 mol L^{-1}, ammonia = 0.20 mol L^{-1}, water = 3.95 mol L^{-1}; (b) TEOS = 0.37 mol L^{-1}, ammonia = 0.45 mol L^{-1}, water = 3.95 mol L^{-1}; (c) TEOS = 0.37 mol L^{-1}, ammonia = 0.25 mol L^{-1}, water = 3.95 mol L^{-1}; (d) TEOS = 0.37 mol L^{-1}, ammonia = 0.25 mol L^{-1}, water =8.34 mol L^{-1}. All scale bars are 100 nm. Reprinted with permission from reference 9. Copyright 2017 Taylor & Francis.

In addition to colloidal silica, the Stöber method can be used to prepare hybrid materials through encapsulation. Some precious metal nanoparticles can be protected by coating with a layer of silica shell in addition to functionalize the hybrid nanoparticles with specific ligands via utilizing and conjugating the interface silanol (Si-OH) groups. Gold colloids have been evenly coated with a silica shell through Stöber process.[10] The thickness of silica shell had an impact on optical properties of gold-silica hybrid nanoparticles. To extend the application, silica coated Fe_3O_4 magnetic nanoparticles (via using Stöber method) was surface

functionalized with different organosilane such as APTES (3-aminopropyltriethoxysilane) and MPTMS (3-mercaptopropyltrimethoxysilane).[11] This surface functionalization was used to immobilize the enzyme lipase. A range of products can be prepared via the Stöber process and the overview is shown in Figure 1-4.

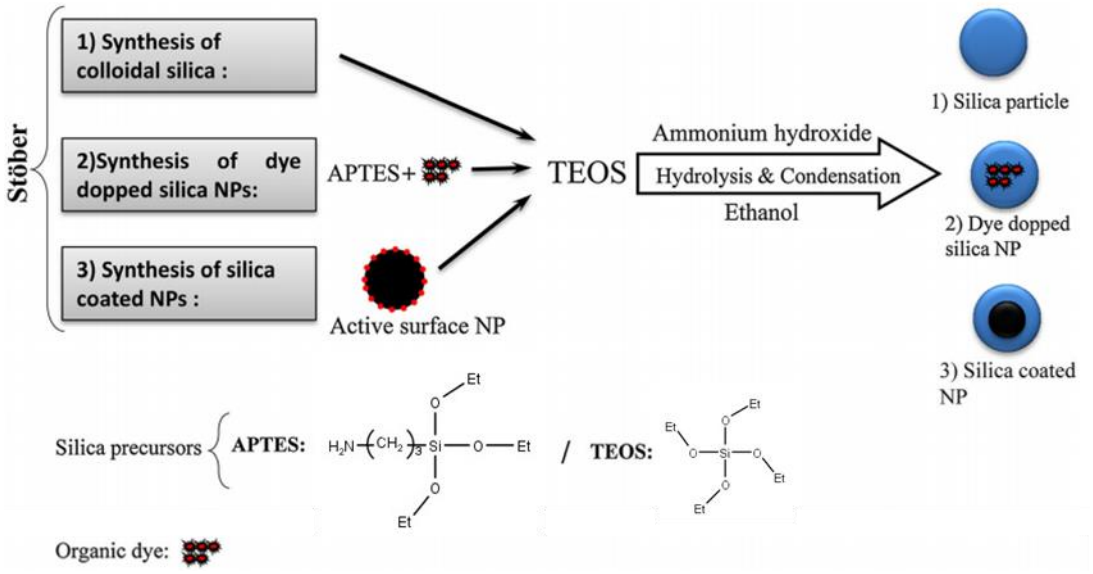

Figure 1-4: The versatility of Stöber process in producing different silica nanoparticles. Reprinted with permission from reference 12. Copyright 2014 John Wiley and Sons.

Besides solid sphere nanoparticles, mesoporous structures are also possible by the Stöber method with the assistance of magnesiothermic reduction process.[13] The resultant spherical mesoporous particles had high specific surface area and average pore size of 9.7 nm. A modified Stöber method can improve the control in producing spherical mesoporous silica nanoparticles in terms of size distribution, pore diameter and synthesis time.[14, 15]

1.1.1.2 Microemulsion Method

In addition to the Stöber process, highly monodisperse and spherical silica nanoparticles can be obtained through the microemulsion technique. In general, silica nanoparticles can be produced in either an oil-in-water (O/W)[16, 17] or water-in-oil (W/O)[18, 19] emulsion. Surfactants are used to stabilize the system and the thermodynamically stable nanodroplets will transform into "nanoreactors" where the hydrolysis and condensation of the alkoxysilyl groups takes place in the presence of catalyst. The size of resultant nanoparticles in this method is impacted by the nature of the surfactant and ratio of water to surfactant.[12] As the reaction occurs within the "nanoreactors", the volume of micelles also controls the size distribution of silica nanoparticles. The overview of microemulsion method can be seen in Figure 1-5.

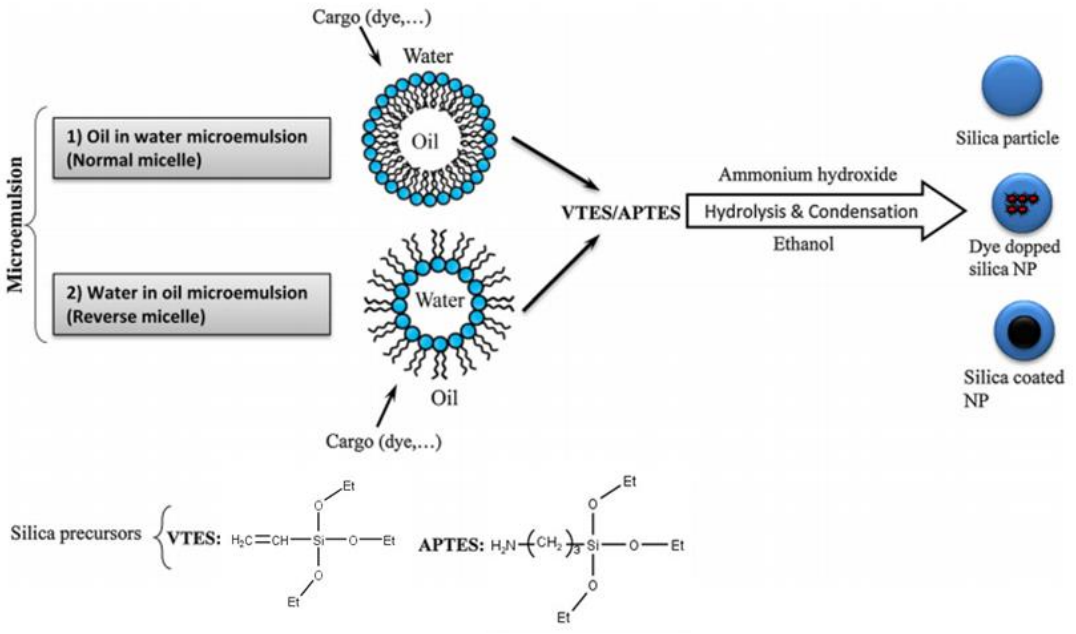

Figure 1-5: Overview of the microemulsion method. Reprinted with permission from reference 12. Copyright 2014 John Wiley and Sons.

1.1.2 Size, Shape and Surface Chemistry

1.1.2.1 Size

The size of silica nanoparticles can be varied based on the synthetic method used.[20] For example, Stöber and co-workers successfully produced spherical silica nanoparticles with controlled size up to 1.5 μm in diameter.[7, 8] Much smaller sizes could be prepared in a non-ionic reverse micellar system, where 50 to 70 nm diameter of silica nanoparticles were produced by hydrolysis of the tetraethoxysilane (TEOS).[21] In such a system, the particle size decreased when the water to surfactant molar ratio increased.

The size of silica nanoparticles is strongly affected by solvent choice and amounts of the reactants and catalysts.[22] In addition to this, the stability of generated silica nanoparticles in the dispersion medium, and the rate of hydrolysis and condensation of silica precursor molecules also play an important role in governing the final silica nanoparticle size.[23] The surface potential of silica nanoparticles and the ionic strength of the solvent strongly affect the particle formation through the aggregation of siloxane substructures. This has been reported by using tetraethoxysilane as a starting material.[23] In that work, the growth of silica spheres occurred via a limited surface condensation of hydrolysed monomers and the particle growing rate was controlled by the first-order hydrolysis of the alkoxysilyl groups. The final particle size (20 nm to 180 nm) was influenced by the ionic strength of the solvent and the concentration of ammonia and water. Highly stable and small silica particles were most successfully formed in dilute ammonia solution.[23]

1.1.2.2 Shape and Structure

The shape of silica nanoparticles is important with respect to specific applications. Due to recent synthetic advances, silica nanoparticles can be prepared with various morphologies such as cones,[24] hexagonal platelets[25] and ellipsoids.[26] From a biomedical perspective, the morphologies of silica nanoparticles are crucial to improve their pre-designed functions. For example, the shape of mesoporous silica nanoparticles (MSN) has a significant effect to pharmacokinetics. Long rod-like silica nanoparticles had a greater residence time in the gastrointestinal tract and highest bioavailability than short rod-like and spherical nanoparticles.[27] Rod shape particles also improved their oral absorption. The structures of these MSNs are shown in Figure 1-6. Intracellular reactive oxygen species (ROS) levels in cells were also affected by the particle shape.[28] Long rods were an ideal antioxidant carrier to protect cells from oxidative injury while the short rods could improve "oxidative therapy" for tumour treatment. Spherical silica particles acted as antioxidants to reduce ROS levels. Additionally, nanorods have a higher surface area to volume ratio than spheres, which can boost the efficiency in drug loading and delivery.[29]

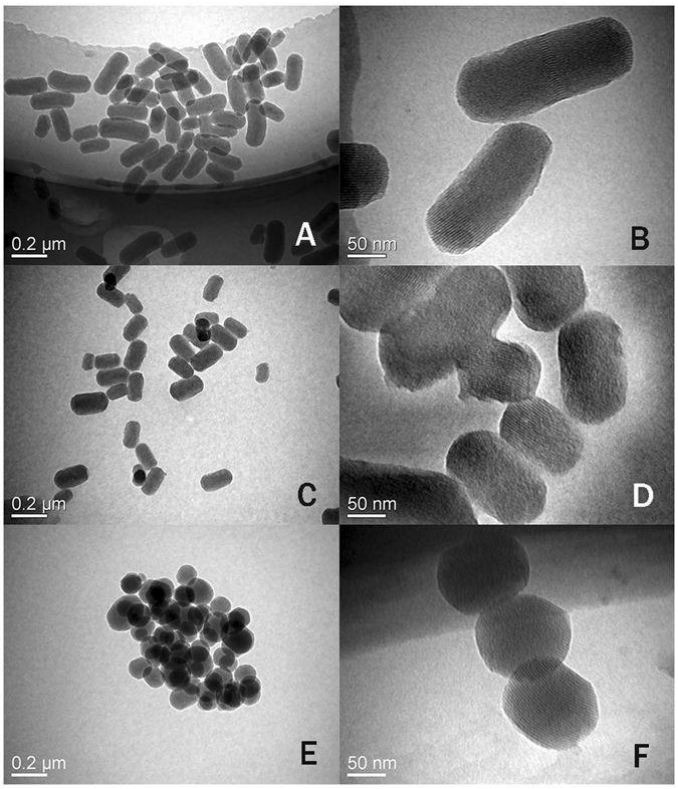

Figure 1-6: TEM images of mesoporous silica nanoparticles: (A, B) = long rods; (C, D) = short rods; (E, F) = spheres. Reprinted with permission from reference 27. Copyright 2017 Springer Nature Limited.

The preparation of silica nanoparticles with different shapes often involves the uses of templates. Two types of templating methods are used; soft templating (using micelles[30] and microemulsions/emulsions[31, 32]) and hard templating (using inorganic/metallic oxide particles[33]). The soft templating method is typically considered more attractive than hard templating, as it offers greater flexibility in tailoring the particle morphology and the template is easily removed. Hollow silica colloids with different conformations (pseudocubes, ellipsoids, capsules and peanuts) have been successfully revealed recently by applying hard template-based methods.[34] Hematite colloidal particles with different shapes were coated with silica to form hybrid hematite core-silica shell microparticles, followed by shell crosslinking and core removal in hydrochloric acid to form hollow structures. These hollow particles had potential to be used in catalytic supports and gas sensing due to the presence of tiny pores on the surface

and greater permeation than solid spherical particles.[34] Figure 1-7 illustrates the synthesis of hollow silica nanoparticles using hematite. An example of using soft-template to prepare mesoporous silica nanoparticles with changeable pore structure and morphology has also been demonstrated recently.[35] In that work, cetyltrimethylammoniumbromide (CTAB) was used as structure directing agent, ethyl acetate as co-template, with ethanol and water as co-solvents. When the initial volume of ethanol under basic condition was altered, the morphology and pore structure of the resulting particles were changed accordingly.

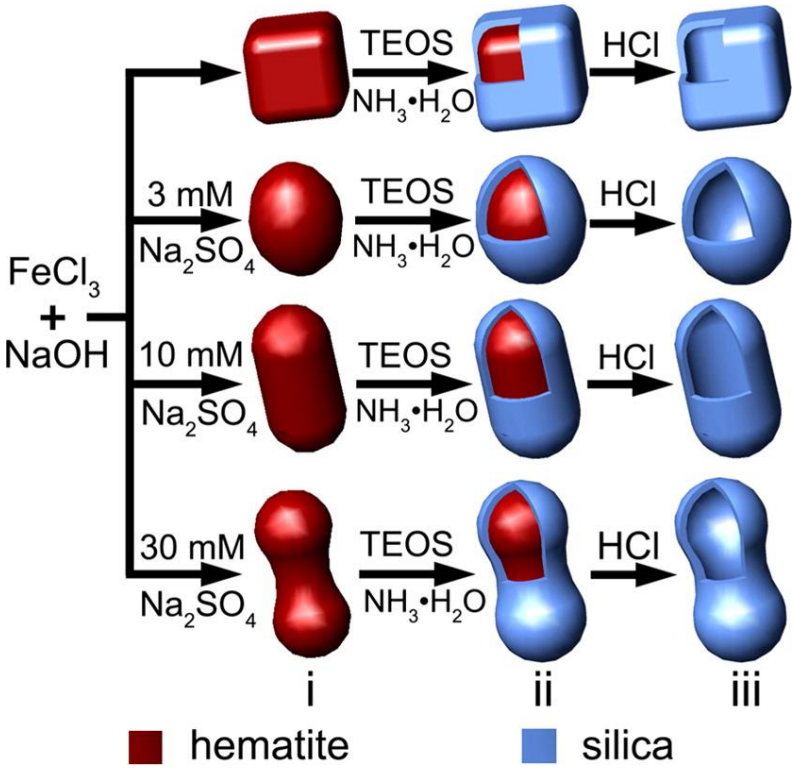

Figure 1-7: Different shapes of hollow silica nanoparticles by using hard-template method. Reprinted with permission from reference 34. Copyright 2013 American Chemical Society.

1.1.2.3 Surface Chemistry

The surface characteristics of silica nanoparticles determine the interaction patterns between particles and the surrounding environment. Silica nanoparticles have a modifiable surface chemistry where various organic functional groups or biomolecules can be attached. The negative charge of deprotonated silanol groups on the particle surface causes particle repulsion and contributes to colloidal stability.[36] However this can be a problem when dispersing silica nanoparticles into high ionic strength solvent, as particles will aggregate and phase separate from the dispersion medium. In order to maintain effective dispersion and colloidal stability, the surface of silica particles can be modified with different types of organosilanes.[37] As a large number of different organosilanes are commercially available, different functional groups are readily grafted from the surface of silica nanoparticles.

The surface of silica nanoparticles also can be modified with polymers, mainly through covalent attachment. Particularly important examples involve poly(ethylene glycol) PEG based polymers; for example the preparation of high density PEG coated silica nanoparticles has been reported.[36] This example demonstrated the functionalization of silica nanoparticles with PEG in a one pot reaction. PEG is a well-known polymer to prevent or minimize biomolecule adsorption. Because of its hydrophilic nature and outstanding biocompatibility, poly(ethylene glycol) methyl ether methacrylate (PEGMA) has been applied to decorate the surface of silica core forming nanoparticles. Silica nanoparticles were coated with PEGMA brushes via surface initiated living radical polymerization.[38]

Target ligands can also be used to modify the surface of silica nanoparticles. The tetradentate tris(2-aminoethyl)amine ligand has been used to prepare functionalized silica nanoparticles.[39] These nanoparticles were used as absorbents for eliminating copper and lead ions in paper mill wastewater.

The surface chemistry of silica nanoparticles also sees these materials readily used as a Pickering-type emulsifier. A Pickering emulsion is an emulsion stabilized by solid particles adsorbed at the oil-water interface.[40-45] Pickering emulsions are more resistant to coalescence compared to the use of traditional surfactants, increasing the variety of potential applications. Examples of Pickering stabilizers include carbon nanotubes,[46, 47] clay,[48, 49] and magnetic (Fe_3O_4) nanoparticles,[50, 51] however silica stabilizers are the most common as they are easily obtained and modified.[52, 53] Unmodified silica particles typically stabilize oil-in-water (O/W) Pickering emulsions due to the hydrophilic character resulting from Si-OH groups on the particle surface, while hydrophobic silica (via surface modification) can stabilize W/O Pickering emulsions.[54] In the last few decades, a range of solid stabilizer morphologies were explored in addition to traditional spherical shapes. Silica nanowires were used as a stabilizer in Pickering emulsion,[55] and it was shown that stability of the emulsion was highly dependent on the length of nanowires. The hydrophilicity and length of silica nanowires could determine whether W/O or O/W Pickering emulsion. Mesoporous modified silica nanoparticles are versatile and they are used as stabilizers in Pickering emulsion as well as catalytic sites.[56] Porous silica has much higher catalytic efficiency than non-porous at a comparable size, due to abundant pores for reactions to take place without sacrificing the emulsion stability.

1.1.3 Polymer-Silica Hybrid Materials

The preparation of organic-inorganic hybrids is a heavily researched topic in polymer science, and these materials are normally made by incorporating silica into a polymer matrix via various chemical interactions. As some polymers have undesirable chemical and physical properties (e.g. low melting point and/or glass transition temperature.), mixing silica into polymers can improve mechanical properties (e.g. flexural characteristic and tensile strength) of the hybrid material.[57] An example of bulk silica incorporation into a polymeric material was shown via the copolymerization of vinyl acetate (VAc) with commercially available silane coupling agents (vinyltrimethoxysilane (VTS) and 3-(trimethoxysilyl) propyl methacrylate (MPS)), followed by a sol-gel process with TEOS to create silica domains, with a view to enhancing thermal and optical characteristics.[58] The thermal decomposition temperatures of PVAc-PVTS-TEOS and PVAc-PMPS-TEOS hybrids were much higher than PVAc-TEOS. This was explained by the presence of strong covalent bonding interactions between the copolymer and silica domains that could resist thermal decomposition and increase the hardness (or mechanical characteristic) of the material. Inorganic materials play an important role in composite network formation, as they are robust fillers that provide interfacial sites for the various organic components, typically resulting in significant increases in the elastic moduli and stiffness of hybrid materials. Furthermore, both hybrid materials were transparent under visible light and no macrophase separation was observed.[58]

Besides improving material properties, silica also can be used as a template for producing polymer particles with different shapes. The synthesis process involves either grafting from silica template or directly polymerize at the surface of silica template. A range of polymer

shapes have been demonstrated such as nanospheres,[59-61] ordered mesoporous polymers,[62] nanocapsules (buckled spheres),[63] nanowires,[64] and rods.[65] For potential application, the silica template can be removed with hydrofluoric acid (HF) that will form nanoparticles with a hollow structure to potentially load cargo molecules.

The directed self-assembly of silica nanoparticles also can be achieved via the use of block copolymers as directing agents. The self-assembly of block copolymers can be tuned based on temperature and pH, which can influence the resultant morphology. For example, poly(ethylene oxide) (PEO) and poly(propylene oxide) (PPO) are thermoresponsive and become hydrophobic when the temperature is above 80 and 20 ºC respectively.[66] This method can provide control in the morphology of silica nanoparticles. A series of Pluronic® polymers ((PEO-PPO-PEO) copolymers) were used as mediators to assemble solid spherical silica nanoparticles (~ 15 nm to 30 nm in diameter) into vesicular,[67] ring,[68] and rod-like[69, 70] architectures. The surface morphology of silica nanoparticles was influenced by the molecular weight of the Pluronic® polymers which is shown in Figure 1-8. Yao *et al.* showed a method to prepare multi-lamellar silica vesicles via self-assembly.[71] Amphiphilic comb-like polymers with a siloxane backbone and Pluronic P123 were used as flexible co-templates to accommodate vesicle aggregation and fusion. The hardness of the vesicles could be enhanced via the hydrolysis and condensation of tetraethoxysilane (TEOS). Figure 1-9 shows the structure of multi-lamellar silica vesicles produced at different temperatures.

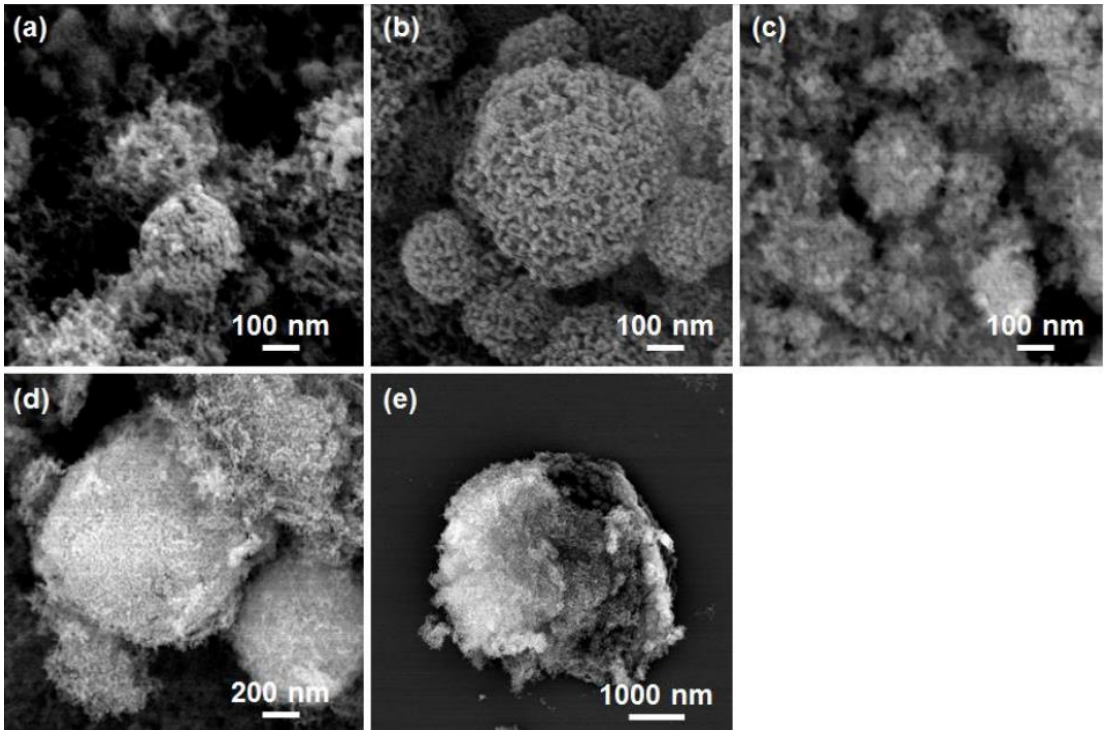

Figure 1-8: SEM images of silica nanoparticles vesicles prepared with different molecular weight of Pluronic® polymers after hydrothermal treatment: (a) 4400 g mol^{-1}, (b) 5750 g mol^{-1}, (c) 2900 g mol^{-1}, (d) 3400 g mol^{-1}, and (e) 12600 g mol^{-1}. Reprinted with permission from reference 67. Copyright 2015 American Chemical Society.

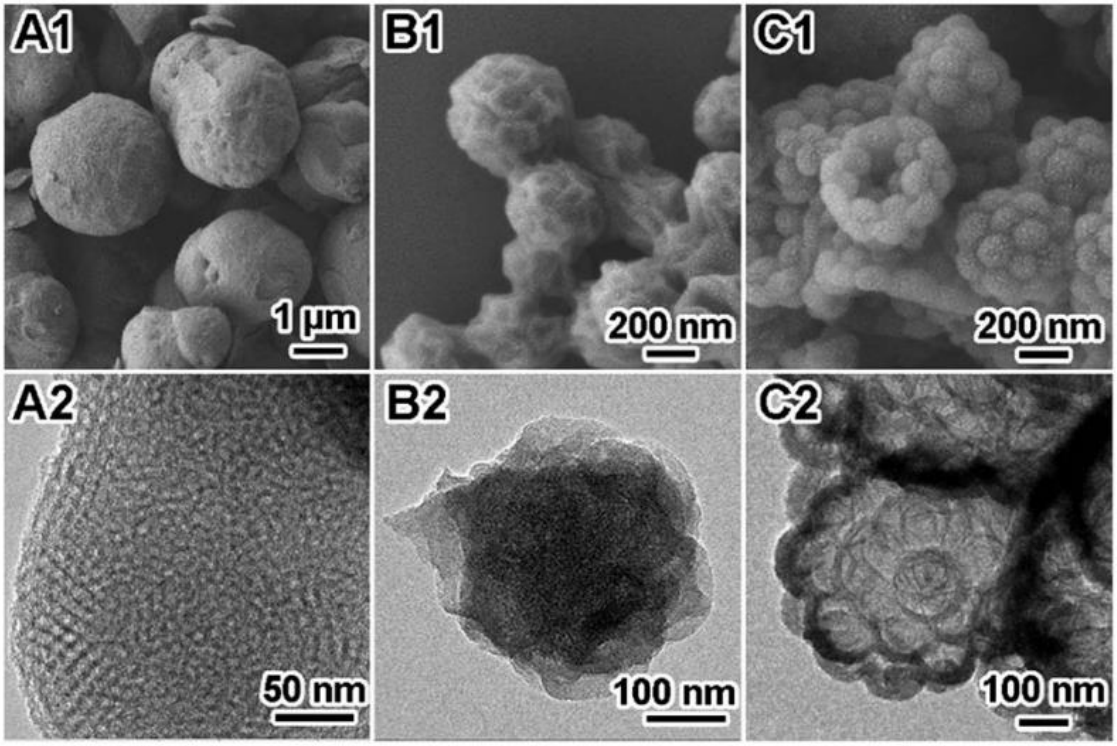

Figure 1-9: SEM and TEM images of multi-lamellar silica vesicles produced under different temperatures: (A) 40 °C, (B) 55 °C, and (C) 80 °C. Other conditions were maintained at standard. Reprinted with permission from reference 71. Copyright 2015 Royal Society of Chemistry.

1.2 Chain Growth Polymerization Methods

Pure silica nanomaterials may have some drawbacks that limit or restrict use in particular applications. In order to fully utilise silica nanomaterials, the preparation of polymer-silica hybrid materials is popular and has been heavily investigated for several decades. The incorporation of silica nanomaterials into a polymer matrix during polymerization is relatively easy, and in addition the polymers can give different properties to the resulting material (e.g., degradable, biocompatible, thermoresponsive, etc.). With recent developments in polymer chemistry, silicon-containing monomers have been commercialised, that enables silicon incorporation directly into a polymer network. This has also enabled the preparation of composite nanoparticles consisting of a polymer phase and a silica phase, through common techniques such as emulsion or miniemulsion polymerization. In order to chain individual unit together, polymerization is the process that uses to connect smaller molecules (repeating units known as monomers) together to form three-dimensional networks or long polymer chains. Numerous polymerization mechanisms exist, such as step growth, chain growth, ring opening and metathesis, with arguably the largest sub-class being free-radical polymerization (FRP). In its simplest form, FRP is conducted with a vinyl compound (monomer) and an initiator – a small molecule capable of forming free radicals via decomposition. In this thesis, a sub-class of FRP known as Reversible Deactivation Radical Polymerization (RDRP) is utilized, as RDRP methods provide both molecular weight control and the ability to form block copolymers. Features of FRP and RDRP are discussed below.

1.2.1 Free Radical Polymerization (FRP)

Free radical polymerization (FRP) is arguably the main chain growth polymerization method. The mechanism of FRP consists of multiple competing steps: initiation, propagation, termination, in addition to chain transfer (intra- and inter-molecular). Initiation of polymerization can take place by one of multiple methods, such as thermal decomposition of a small molecule,[72] redox initiation[73] or radiation (including UV,[74] laser and visible light[75, 76]). Chain growth occurs via propagation, resulting in sequential addition of monomer units to an active chain. Chain termination occurs either via combination or disproportionation, resulting in "dead" chains that are unable to facilitate further chain growth. FRP is considered uncontrolled, in that the resultant polymer has a wide distribution of different chain lengths in addition to a variety of chain topologies (linear and branched).

1.2.2 Reversible Deactivation Radical Polymerization (RDRP) Techniques

Polymer chains produced by FRP are "dead" (they are unable to be re-initiated) and typically possess a broad chain length distribution (characterized by the dispersity *Đ*, the ratio of the weight-average and number-average molecular weight of the distribution). To create a polymer with low dispersity, every chain must be initiated and propagate at a comparable rate to grow polymer chain length in the absence of termination or other side reactions.[77] This concept, in addition to re-initiation of polymer chains to consume more monomer, is known as "living polymerization." Michael Szwarc was the first person to lay the groundwork on living polymerization in 1956.[78] He observed the formation of "living" polystyrene with two living ends and the radical flux was not exhausted. He suggested this may be due to the polymers not

undergoing termination, allowing propagation until all monomers in the system were consumed, i.e. a "living" polymer. This exploration was the first step towards managing polymer architectures such as narrow molecular weight distribution and composition (e.g. block or triblock copolymers). The suppression of termination and unwanted chain transfer reactions establish a linear relationship between molecular weight and conversion of monomer to polymer. The initial work was performed using anionic polymerization, which has restrictions in terms of monomer selection and strict reaction conditions (e.g anhydrous solvents), as well as sensitivity to various functionalities and impurities.[79,80]

Since the initial work in living ionic polymerization, Reversible Deactivation Radical Polymerization (RDRP) has become the dominant method in preparing polymers with controllable molecular weight and architecture. RDRP is a chain growth polymerization where minimal termination occurs, as long as monomer is still available in the system for propagation. RDRP solves many of the challenges in living anionic/cationic polymerizations. RDRP has much higher tolerance in reaction conditions and the process is relatively versatile; if performed well, the growing chains should increase in molecular weight and decrease in dispersity with increasing conversion.[79] An ideal RDRP should have less than 10 % dead polymers (i.e. chains that have undergone irreversible termination), comparing to over 99 % of dead polymers in a conventional free radical polymerization.[81] The arrival of RDRP has greatly aided the design of polymeric materials and their potential applications (e.g. surfactants, biomedical applications, membranes etc.).[79] A comparison between free radical and Reversible Deactivation Radical Polymerization is showed in Figure 1-10.

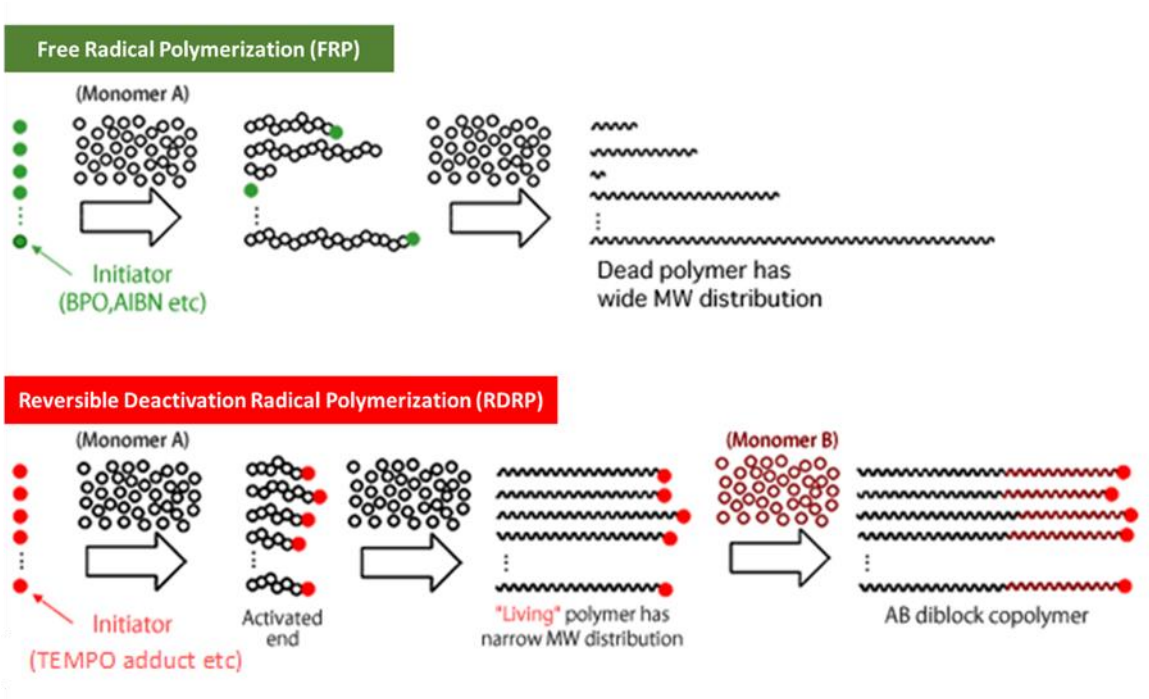

Figure 1-10: Comparison between FRP and RDRP. (Top): FRP produces polymers with random chain length and the produced polymers are dead. (Bottom): RDRP produces almost even chain length polymers and the resultant polymers are "living" and suitable for subsequent chain extension with another type of monomer. Reproduced from reference 82. Copyright 2018 Otsuka Chemical Co., Ltd.

There are three major RDRP methods that differ on the basis of the control agent used and the mechanism of control (i.e. reversible termination, or degenerative chain transfer). These methods are known as nitroxide mediated polymerization (NMP), atom transfer radical polymerization (ATRP), and reversible addition-fragmentation chain transfer (RAFT). RAFT polymerization is the RDRP method used exclusively in this thesis and as a result is described in detail below. NMP and ATRP have been reviewed extensively previously in the literature.[83-90]

1.2.2.1 Reversible Addition-Fragmentation Chain Transfer polymerization (RAFT)

Reversible Addition-Fragmentation Chain Transfer polymerization (RAFT) is one of the major RDRP techniques. RAFT can form polymer with low dispersity and be applied in different reaction environments (bulk, solution, emulsion etc.) to a greater extent than NMP and ATRP.[91] RAFT also has the widest potential to polymerize a broad variety of monomers with different functional groups.

The mechanism of RAFT polymerization is shown in Figure 1-11. It involves reversible chain transfer via a series of addition-fragmentation processes. The initiation is identical to conventional FRP where the initiator generates active radicals to initiate monomers. After initiation, propagating radical ($P_n^{\bullet}$) adds to a compound containing a thiocarbonylthio group (Species 1 in Figure 1-11). The intermediate radical (Species 2) forms upon addition and can fragment to generate a polymer capped with a thiocarbonylthio group (Species 3) and a new radical derived from the leaving group (R•). This radical (R•) can continue to initiate monomers and form a new propagating radical ($P_m^{\bullet}$). A rapid chain equilibration between active propagating radicals ($P_n^{\bullet}$ and $P_m^{\bullet}$) and dormant polymeric thiocarbonylthio-capped chains offers an increased probability for all polymeric chains to grow simultaneously with low dispersity. Active polymeric chains may terminate with each other to form dead polymer via radical combination or disproportionation. When all radicals are exhausted, the majority of polymeric chains contain the thiocarbonylthio endgroup and can be isolated and purified as stable polymeric materials.

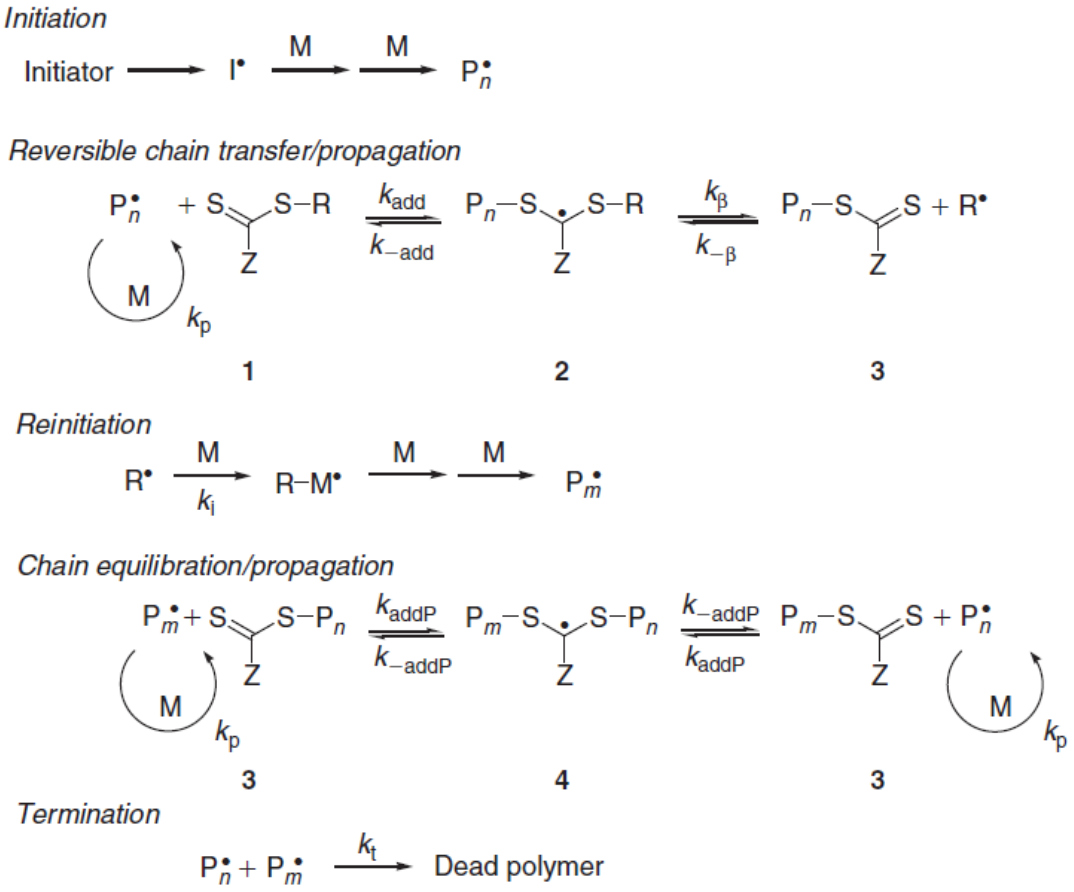

Figure 1-11: Mechanism of RAFT polymerization. Reproduced from reference 92. Copyright 2006 CSIRO Publishing.

1.2.2.1.1 Initiators, RAFT Agents, and Monomer Selections

Initiation in RAFT polymerization can be successfully achieved by numerous methods; using conventional thermal initiators such as azo and peroxy compounds, as well as various radiation sources (e.g. gamma,[93, 94] UV and visible light[95-98]). The radicals (I•) from thermal decomposition of initiators can potentially add to monomers before adding to the chain transfer agent. For an ideal RAFT polymerization, chains should be initiated by the RAFT agent leaving group (R•) to control the molecular weight of polymers produced.[80] RAFT polymerization can minimize the number of dead chains to below 5% of the total chain population through the use of a high ratio of CTA to initiator.[99]

RAFT agents can be categorised into several classes such as dithioesters, xanthates, dithiocarbamates and trithiocarbonates. The chemical structures of these RAFT agents are shown in Figure 1-12. Inappropriate RAFT agent choice may lead to retardation, long induction period and loss of control over the polymerization for a specific monomer. The relevance of RAFT agent for a given monomer is determined by substituents of R and Z groups; each group will have a different effect towards controlling the polymerization.

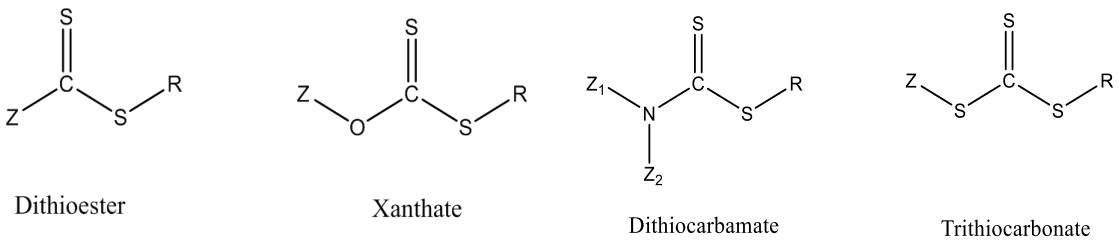

Figure 1-12: Basic structures of different RAFT agents

The Z group of the CTA (the "stabilizing group") is used to amend the rate of addition of propagating radicals (Pn•) to the RAFT agent and the rate of fragmentation of the intermediate radical (Species 2 in Figure 1-11).[77] The reactivity of the RAFT agent is highly influenced by the chemical groups surrounding the thiocarbonylthio group.[77] In addition, the Z group also stabilizes the intermediate radical; if too stable, the fragmentation rate will be reduced and thus increasing the likelihood of termination.[100, 101] The presence of electron withdrawing groups in the Z group will enhance the transfer constant to the RAFT agent, regardless of the class of RAFT agent.[102] The R group of the RAFT agent (the "leaving group") is important in determining the reactivity of the RAFT agent towards polymerization. R must typically be a good homolytic leaving group with respect to propagating radicals (Pn•) and should also be able to reinitiate polymerization to avoid retardation.[77, 103]

In addition to the R and Z groups of the RAFT agent, the choice of RAFT agents is also dependent on the monomer type, which are typically classified as more-activated monomers (MAMs) and less activated monomers (LAMs). The monomer classification is determined by the position of double bond in monomer. The double bond of MAMs is conjugated to an aromatic ring (styrene), a carbonyl group (methyl methacrylate), or a nitrile (acrylonitrile) while the double bond of LAMs is adjacent to saturated carbon (diallyldimethylammonium chloride), an oxygen or nitrogen lone pair (vinyl acetate, N-vinylpyrrolidone), or heteroatom of a heteroaromatic ring (N-vinylcarbazole).[104] Dithioesters and trithiocarbonates are well suited for polymerizing MAMs whereas the low transfer constant xanthates and dithiocarbamates are compatible with LAMs. In order to well control the polymerization of methacrylates or methacrylamides, the R group should form a secondary or tertiary radical.[105,106] For polymerizing monomers with a high propagation rate coefficient (e.g. acrylates, acrylamides, vinyl esters), a primary or secondary R group is strongly preferred.[77]

At the conclusion of the reaction, the terminal groups of resultant polymers typically consist of the R (e.g. hydroxyl, carboxylic acid, succinimidyl ester, etc.) and Z (e.g. dithiobenzoates, trithiocarbonates, dithiocarbamates, and xanthates) groups of the RAFT agent. The chemistry of these terminal groups is dictated by RAFT agent selection.

1.2.2.1.2 RAFT Polymerization with Silicon Containing Monomers in Homogeneous Systems

RAFT polymerization is suitable for silyl-containing monomers and many examples have been reported. 3-[Tris(trimethylsilyloxy)silyl]propyl methacrylate (TRIS) (Figure 1-13) is an important building block for making contact lenses due to high content of Si-O group, which can improve oxygen penetration in the material. TRIS monomer has been polymerized with both cumyl dithiobenzoate (CDB) and 2-cyanoprop-2-yl dithiobenzoate (CPDB) in RAFT bulk polymerization.[107] It was found that inhibition and retardation were significant for CDB compared to CPDB. The retardation in CDB-mediated polymerization was due to high stability of intermediate macroRAFT radicals. Both resultant polymers had low dispersity (<1.1) at high conversion (> 90%).

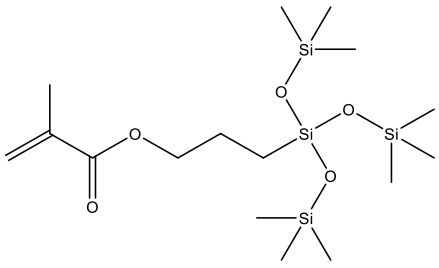

Figure 1-13: Chemical structure of 3-[tris (trimethylsilyloxy) silyl] propyl methacrylate (TRIS).

RAFT is considered as the best candidate in producing controllable silyl-based polymers due to its wide tolerance of different functional groups and monomer species. A further example is the polymerization of bis(trimethylsiloxy)methylsilyl methacrylate (MATM 2) with S-(2-cyanoprop-2-yl)-S-dodecyltrithiocarbonate (CTA-0610) and 2-Cyanoprop-2-yl dithiobenzoate (CPDB) RAFT agents in xylene.[108] The chemical structures of MATM 2, CTA-0610, and CPDB are shown as Figure 1-14. The polymer of MATM 2 is used to create a self-polishing and antifouling surface due to its similarity to other alkylsilyl methacrylates monomers that have been tested as an effective antifouling coating.[109, 110] The homopolymerization of MATM 2 with CPDB and CTA-0610 followed first order kinetics and their resultant polymers were well controlled in terms of low dispersity and high molecular weight at high conversion. Chain extension with methyl methacrylate (MMA) to form a diblock copolymer was performed to create a material with lower surface energy and less susceptibility to hydrolysis.[108]

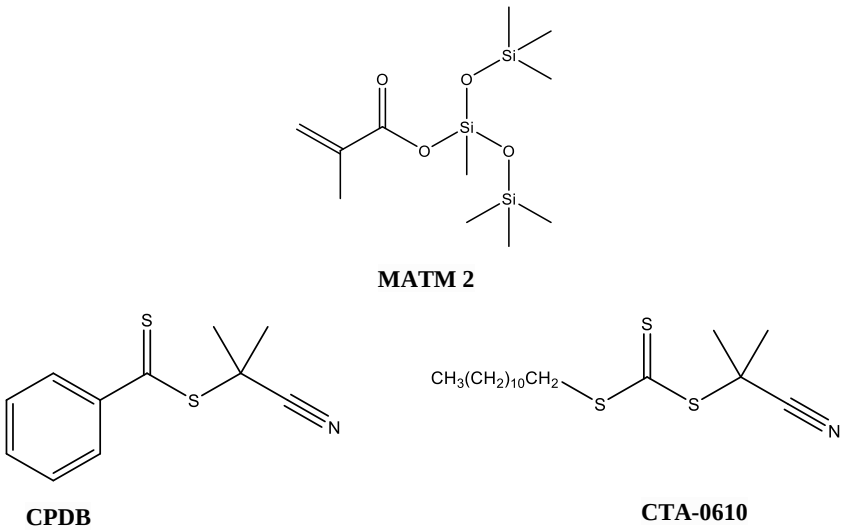

Figure 1-14: Chemical structures of MATM 2, CTA-0610, and CPDB

Furthermore, 2-phenyl-2-propyl benzodithioate (CDB) and CPDB RAFT agents have shown good control over the polymerization of tert-butyldimethylsilyl methacrylate (TBDMSMA, Figure 1-15) in toluene.[111] Both RAFT agents were successful to produce low dispersity polymers (< 1.3) at high conversion. Polymers of TBDMSMA are similar to MATM 2 as it is often applied in anti-erosion and fouling resistance paint.

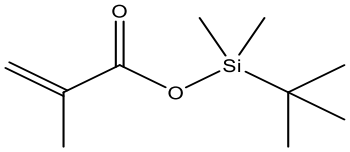

Figure 1-15: Chemical structure of tert-butyldimethylsilyl methacrylate (TBDMSMA)

1.3 Heterogeneous Methods of Polymerization

Polymerization methods can be divided into two main groups: homogeneous and heterogeneous. Homogeneous polymerization involves the polymerization of monomer(s) either in bulk (no solvent) or dissolved in a compatible solvent. Bulk polymerization is the simplest given that the only components are monomer(s) and initiator, however in bulk the system becomes extremely viscous even at moderate conversion. This makes the system very difficult to control heat transfer and dissipation can be problematic. This can be partially overcome by working in solution, however solvent selection is key as chain transfer to solvent may occur and the molecular weight distribution of the polymer will be affected.

In contrast, heterogeneous polymerization relates systems where the polymer formed exists in a discrete dispersed phase, typically as particles, dispersed in a continuous phase (the solvent). Most heterogeneous polymerization systems require surfactants or stabilizers to avoid coagulation of the polymeric dispersed phase. Heterogeneous polymerization is applied extensively in industry due to it being an efficient method to reduce heat transfer and viscosity problems of bulk and solution systems. Heterogeneous polymerization systems are often classified by various parameters, such as monomer solubility in the continuous phase, stabilizer loading, dispersed phase stability, droplet size and polymerization mechanism. Three of the major heterogeneous polymerization techniques are known as dispersion, emulsion, and miniemulsion polymerization. These are discussed briefly below.

1.3.1 Dispersion Polymerization

In a typical dispersion polymerization, the monomer is soluble in the continuous phase but its corresponding polymer is insoluble. A dispersion polymerization begins as a homogeneous solution (a mixture of monomer, initiator, stabilizer, and solvent). Upon the start of polymerization, polymer chains become longer and ultimately become insoluble in the continuous phase. In the presence of stabilizers (typically polymeric stabilizers), the insoluble polymer remains dispersed in the continuous phase without precipitation, forming a polymer particle phase. The remaining monomer in the dispersed phase will diffuse into the core of swollen polymeric particles for continuous polymerization and subsequent increase in particle size. At the end of the process, the dispersion polymerization is a heterogeneous turbid dispersion consisting of nanoparticles with an insoluble polymer core and a shell of polymeric stabilizer. The process of dispersion polymerization with polymeric stabilizer is illustrated in Figure 1-16.

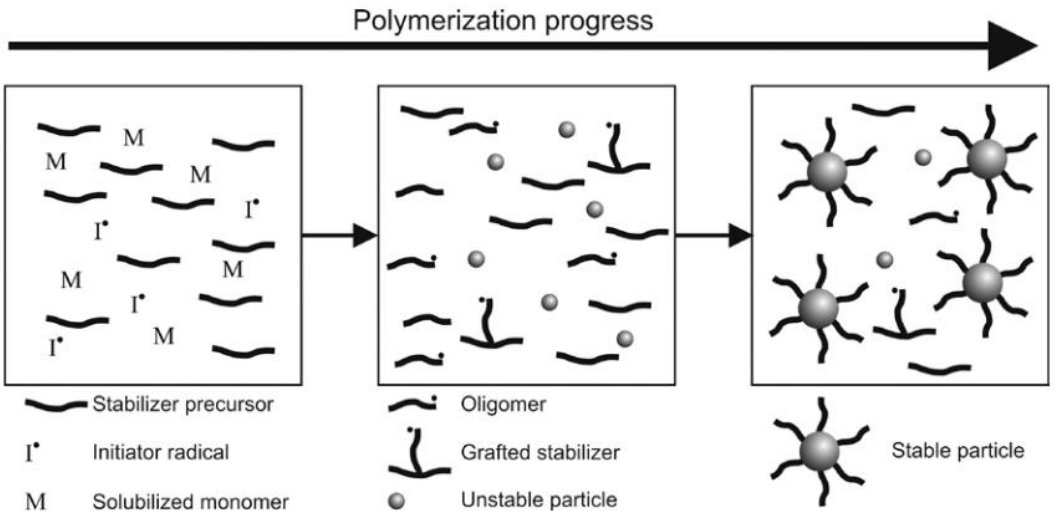

Figure 1-16: Dispersion polymerization with polymeric stabilizer. Reprinted with permission from reference 112. Copyright 2014 John Wiley and Sons

1.3.2 Emulsion Polymerization

An emulsion polymerization differs from a dispersion polymerization in that both the monomer and polymer are insoluble in the continuous phase, which is most typically water. Emulsion polymerization is typically performed using a monomer, solvent, initiator (that is soluble in the solvent) and surfactant. A sufficient shearing force (e.g. mechanical agitation such as overhead stirring) is required to emulsify the monomer into small droplets, and potentially form monomer-swollen micelles if surfactant is present above the critical micelle concentration (CMC). Nucleation in emulsion polymerization occurs either via micellar or homogeneous nucleation which depends on the surfactant level present.[112-115] Following particle nucleation, particle growth occurs due to consumption of monomer, however, the concentration of monomer in the polymer particles is maintained via monomer diffusion from monomer droplets through the aqueous phase. Therefore, the polymerization rate is relatively constant and no new polymer particles form. After the depletion of monomer droplets, the monomer concentration in polymer particles decreases over time until all monomer is consumed.

1.3.3 Miniemulsion Polymerization

Miniemulsion polymerization involves the formation of nano-sized monomer droplets (typically 50 – 500 nm) in a continuous phase that can be converted to polymer particles via polymerization. Miniemulsion polymerization uses high amounts of surfactant that are adsorbed on the monomer droplet surface and therefore no micelles form. Miniemulsion polymerization differs from dispersion and emulsion polymerization as nucleation mainly occurs in monomer droplets and does not require mass transfer through the aqueous phase.

Because of this, every monomer droplet can act as an independent nanoreactor and the nucleation can be shielded from external disturbance. A typical miniemulsion system requires a small amount of an ultrahydrophobe (typically a long chain alkane) that is dissolved in the dispersed phase to retard Ostwald ripening of monomer droplets.[116] A miniemulsion is usually produced via high energy mixing (e.g. ultrasonication) to disperse the monomer phase into a narrow distribution of monomer droplets. Miniemulsion process is briefly illustrated in Figure 1-17.

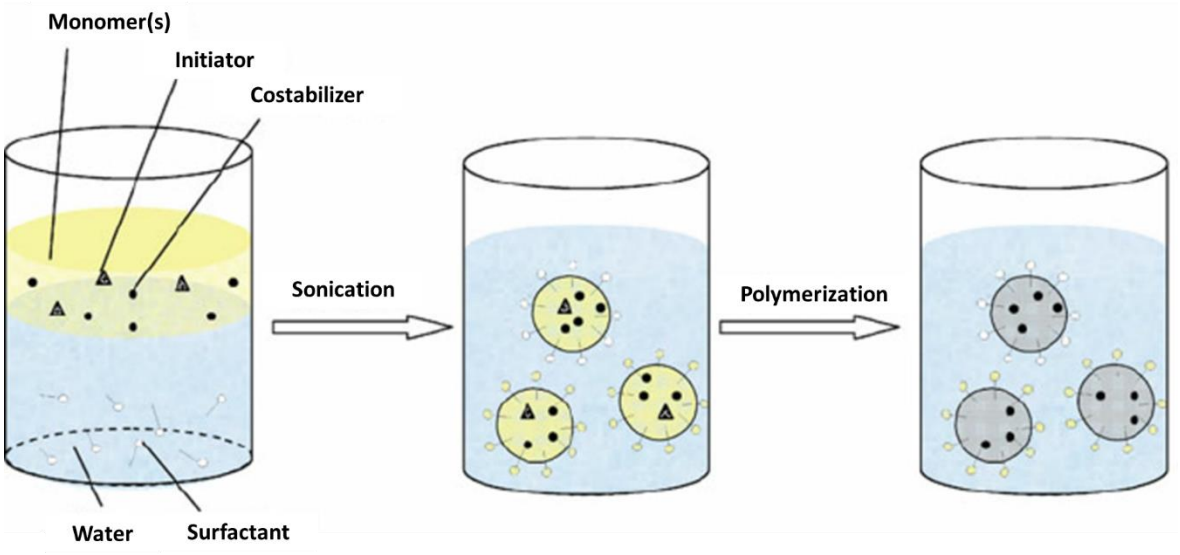

Figure 1-17: Oil-in-water miniemulsion process. (Left): A system containing oil phase (monomer, initiator and costabilizer/ultrahydrophobe) and water phase (water and surfactant). (Middle): Strong sonication is used to disperse oil phase into small droplets. (Right): Stable polymer particles are produced after polymerization. Reprinted with permission from reference 117. Copyright 2010 Springer Nature.

1.3.4 Heterogeneous Polymerization involving Silicon-Containing Monomers

In addition to homogeneous methods, heterogeneous polymerization techniques such as emulsion polymerization have been used to create hollow silica nanoparticles. Silica core or silica shell nanoparticles can be created based on the experimental setup. Tissot and coworkers reported the preparation of latex particles in water (by *ab initio* emulsion polymerization) and the resultant particles were coated with a shell of silica.[118, 119] The silica coated particles were synthesized via a two-step process: 3-(trimethoxysilyl)propyl methacrylate (MPS) was incorporated into polystyrene latex particles followed by a sol-gel reaction with tetraethoxysilane in water to form a silica shell on the surface. Dodecyldimethylpropylammonium sulfonate and potassium persulfate (KPS) were used as surfactant and initiator respectively. Because of the high melting point of the silica shell, hollow particles were produced via thermal degradation of the polystyrene core under calcination. The dimensions of particles could be easily adjusted by changing the amount of surfactant or monomer. Various reaction conditions of the emulsion copolymerization of styrene and MPS latex were also studied.[120] The size of hybrid nanoparticles was affected by the pH of the aqueous phase (Figure 1-18).

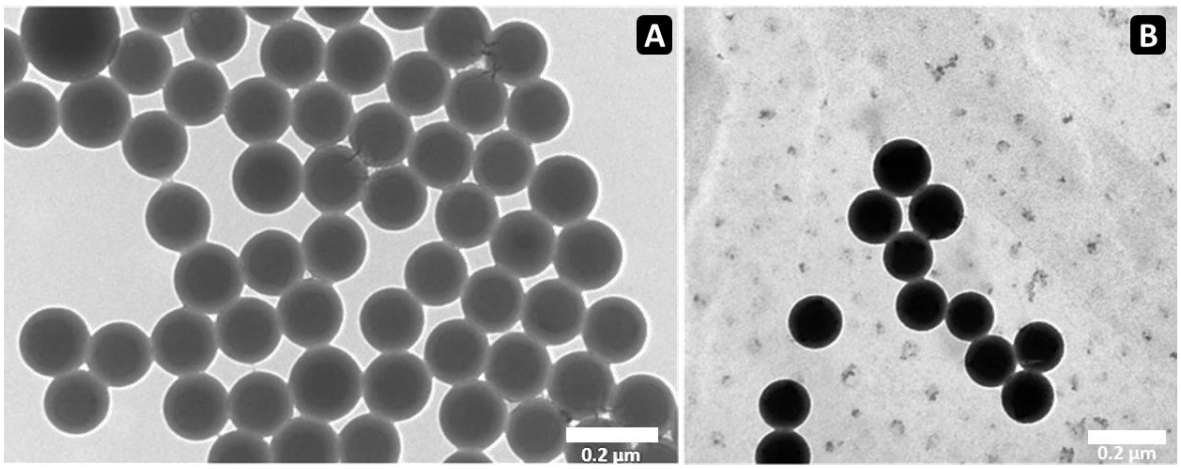

Figure 1-18: Different sizes of polystyrene core- silica shell nanoparticles were produced at various pH: (A) pH 7, and (B) pH 8.5. All scale bars are 200 nm. Reprinted with permission from reference 120. Copyright 2005 American Chemical Society.

Polyacrylate latex particles incorporating both fluorine and silicon in the shell have been synthesized by a seeded emulsion polymerization approach.[121] The core consisted of methyl methacrylate (MMA), butyl acrylate (BA) and methacrylic acid (MAA). Dodecafluoroheptyl methacrylate (DFMA) and γ-(methacryloxy) propyltrimethoxy silane (KH-570) were used as functional monomers to form the shell. Three types of surfactants were used in this emulsion polymerization: a sulphonated anionic fluorosurfactant (S-100), anionic ammonium allyloxtmethylate nonylphenol ethoxylates sulfate (DNS-86), and non-ionic octylphenol polyoxyethylene ether (OP-10). The hydrophobicity and thermal stability of the particles were improved due to the enrichment of silicon and fluorine at the interface. The surface energy also decreased with the increasing amount of DFMA and MPS.

Besides producing particles with a silica shell, emulsion polymerization also can prepare nanocomposites consisting of a silica core and polymeric shell. Formation of silica core/polymer shell particles were made by using a dispersed silica sol and a monomer mixture

(MMA, BA, and MAA).[122] Poly(ethylene oxide)-type reactive non-ionic surfactants (ADECA REASOAP NE-10 and NE-30) were used. The emulsion was initiated either by ammonium peroxydisulfate (APS) or a redox system. Spherical hybrid nanoparticles were observed under TEM, and the resultant emulsion used to prepare nanocomposite films. The transparent film had a high resistance against organic solvents due to the strong interaction between the silica and polymeric phases.

Miniemulsion polymerization is a versatile method to prepare silicon-containing particles as the nucleation occurs within monomer droplets, which can suppress the premature hydrolysis and condensation of alkoxysilyl groups. Silanol-functionalized polystyrene latex nanoparticles have been successfully prepared in miniemulsion using MPS as the functional monomer.[123, 124] The final particle size was not affected by MPS concentration but was influenced by surfactant concentration. As the latex interface was enriched with alkoxysilyl groups, the surface of polystyrene latex could be functionalized or coated with a silica shell. The kinetics of the miniemulsion copolymerization of styrene and MPS were studied and a series of variables (MPS/St weight ratio, nature and amount of initiator, pH, and surfactant concentration) were also investigated.[125] Besides styrene (St) monomer, MPS also has been copolymerized with other acrylates (butyl acrylate, BA) and methacrylates (methyl methacrylate, MMA) via miniemulsion to form random copolymers.[126] Figure 1-19 shows the nanoparticles produced by the copolymerization of MPS with other monomers. Figure 1-19(a)-1 shows particles are 'linked' due to hydrolysis and condensation of MPS. The linked coagulum produces coarse and irregular dark region as seen in Figure 1-19(a)-1. A typical nanoparticle structure of poly(MMA-co-MPS) is showed in Figure 1-19(a)-2 and this image is looked similar to other systems.

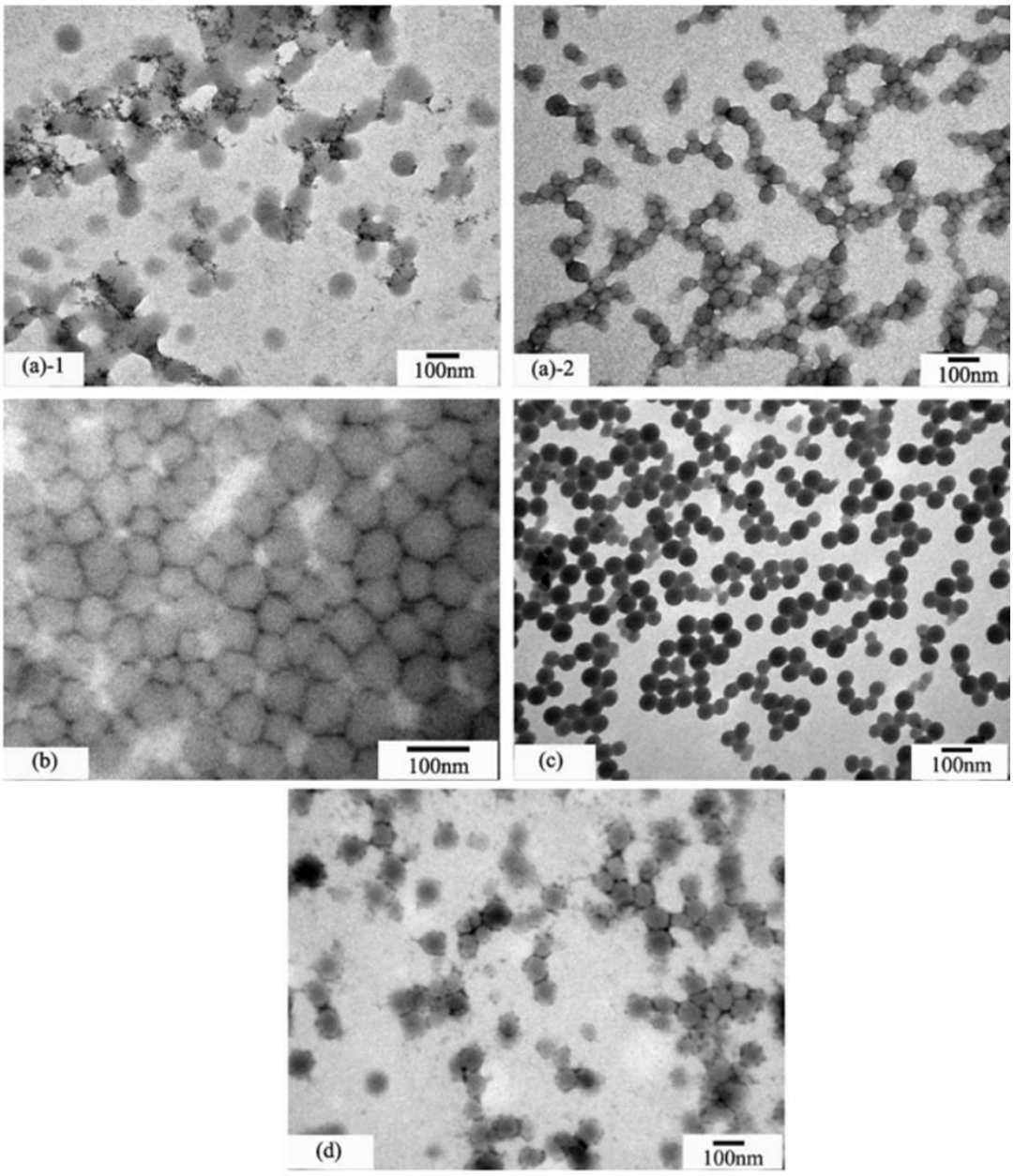

Figure 1-19: TEM images for nanoparticles produced by MPS copolymerization with different types of monomers in miniemulsion: (a) poly(MMA-co-MPS), (b) poly(MMA-co-BA-co-MPS), (c) poly(St-co-MPS), and (d) poly(St-co-BA-co-MPS). Reprinted with permission from reference 126. Copyright 2006 Elsevier.

In addition to emulsion and miniemulsion polymerizations, monodisperse crosslinked hybrid polymer particles also can be synthesized in conventional dispersion polymerization.[127] Styrene and MPS were copolymerized together in a methanol/water mixture, and the resultant micron-size particles were then crosslinked to form high density siloxane network.

1.4 Self-Assembly of Block Copolymers

Block copolymers can be prepared through a diverse range of synthesis techniques such as anionic and cationic polymerizations, and more recently Reversible-Deactivation Radical Polymerization (RDRP).[128] Block copolymers consist of two chemically distinct domains that can self-assemble into a variety of different nanostructures (e.g. spheres, cylinders and vesicles) when dispersed into a solvent that is selective for one block. For example in aqueous solution, a block copolymer with hydrophilic (poly(acrylic acid)) and hydrophobic (polystyrene) domains will aggregate to form micellar structures with a hydrophilic polymer shell and hydrophobic core.[129] Self-assembly of block copolymers is also observed in bulk resulting in microphase separation as a function of copolymer composition and the Flory-Huggins parameter, again into a variety of different shapes.[130]

Block copolymer self-assembly has attracted greater attention than small molecule (amphiphile) self-assembly due to the stability of block copolymer aggregates in solution, in addition to their potential applications in fields such as biomedical engineering.[131] Block copolymer self-assembly in solution has been intensively studied over the last few decades and numerous different morphologies have been produced.[130] For block copolymer self-assembly in solution, the block copolymer is initially designed and synthesized in a good solvent that solvates both blocks, followed by introducing an external stimulant (e.g. feeding a non-solvent,[132-134] changing temperature[135] or pH[136]) into the homogeneous solution. As a result, the block copolymers aggregate and form micelles that predominantly depend on the composition and concentration of the polymer, however kinetically trapped structures can be observed. Dialysis may be required in some cases to remove the remaining good solvent. This traditional self-

assembly technique is usually time-consuming due to the series of steps involved and can only be performed in dilute solution (typically < 1 wt%).[137] The self-assembly process of block copolymer in solution is essentially controlled by three main factors: the degree of stretching of the core-forming block, interfacial tension between the micelle core and the solvent outside the core and the repulsive interactions among corona chains.[130, 138, 139]

The geometry of self-assembled block copolymer objects can be predicted by using the packing parameter (*p*). The equation is defined as follows:

$$p = \frac{v}{a_o l_c}$$

where 'v' and 'l_c' are the volume and length of the hydrophobic polymer segment while 'a_o' is the surface area of the block junction/ head group. The morphology of self-assembled objects will change with respect to the packing parameter, such as spheres ($p \leq 1/3$), cylinders/rods ($1/3 < p \leq 1/2$) and vesicles ($1/2 < p \leq 1$). Figure 1-20 shows the relationship between packing parameter and shape. Spherical micelles are predicted when the hydrophilic block mass fraction (*f*) is greater than 45%.[140] Cylindrical particles can be obtained at f < 50%,[141] while polymersomes/vesicles and inverted micelles will form when $f \approx 35 \pm 10\%$ and f < 25% respectively.[140]

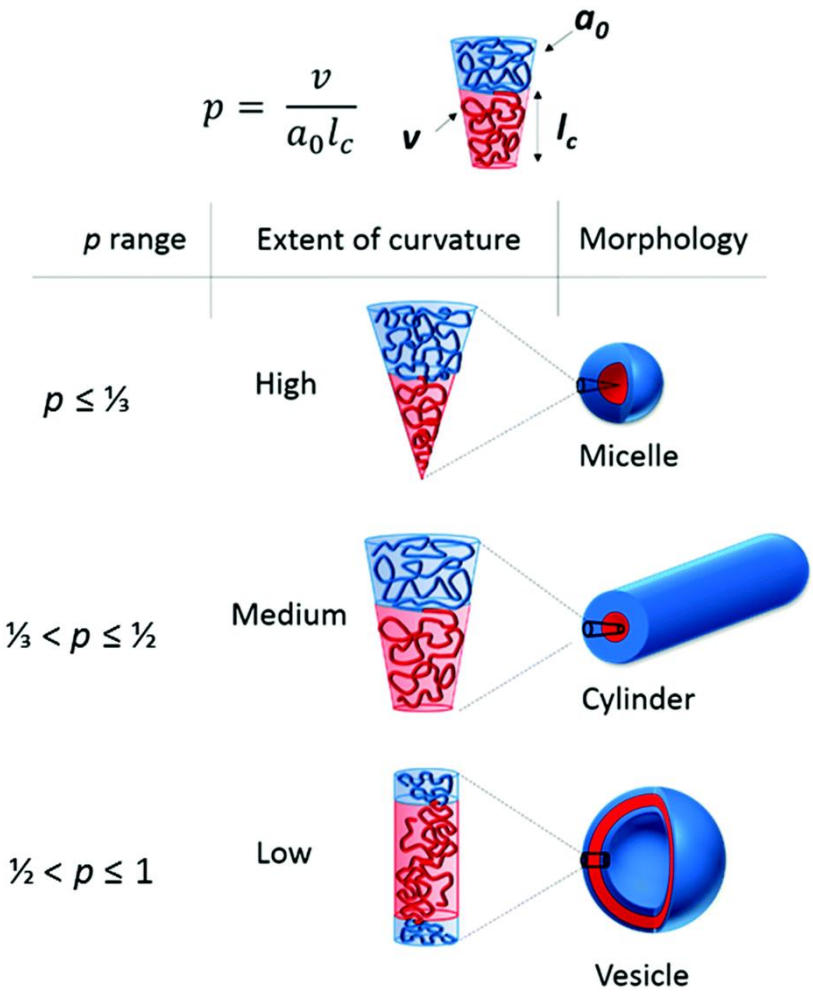

Figure 1-20: Packing parameter (p) is determined by the block copolymer aggregation. The corresponding morphology is controlled by the p value. Reprinted with permission from reference 142. Copyright 2017 Royal Society of Chemistry.

1.4.1 Solvent-Driven Self-Assembly of Silicon-Containing Block Copolymers

Block copolymers consisting of a silicon-containing block have been extensively explored due to many favourable features such as beneficial physical and chemical properties,[143] ready post-assembly modification[144] and applications in lithography.[145] Some examples of polymer-silicon hybrid nanocomposites prepared by living polymerization and their subsequent self-assembly induced by external solvent are reported below.

Various compositions of poly(acryloxypropyltriethoxysilane)-b-poly(styrene) (PAPTES-b-PS) diblock copolymers were prepared by nitroxide-mediated polymerization (NMP).[146] The self-assembly of block copolymer started when methanol was added slowly to a solution of the block copolymer in dioxane until the solvent composition was dioxane:methanol = 40/60 w/w. Methanol is a poor solvent for the PS block but a good solvent for the PAPTES block. After the formation of spherical block copolymer nanoparticles, hydrochloric acid was added to crosslink the PAPTES shell and maintain the shape for subsequent analysis. Figure 1-21 shows the self-assembly of PAPTES-b-PS block copolymer induced by methanol.

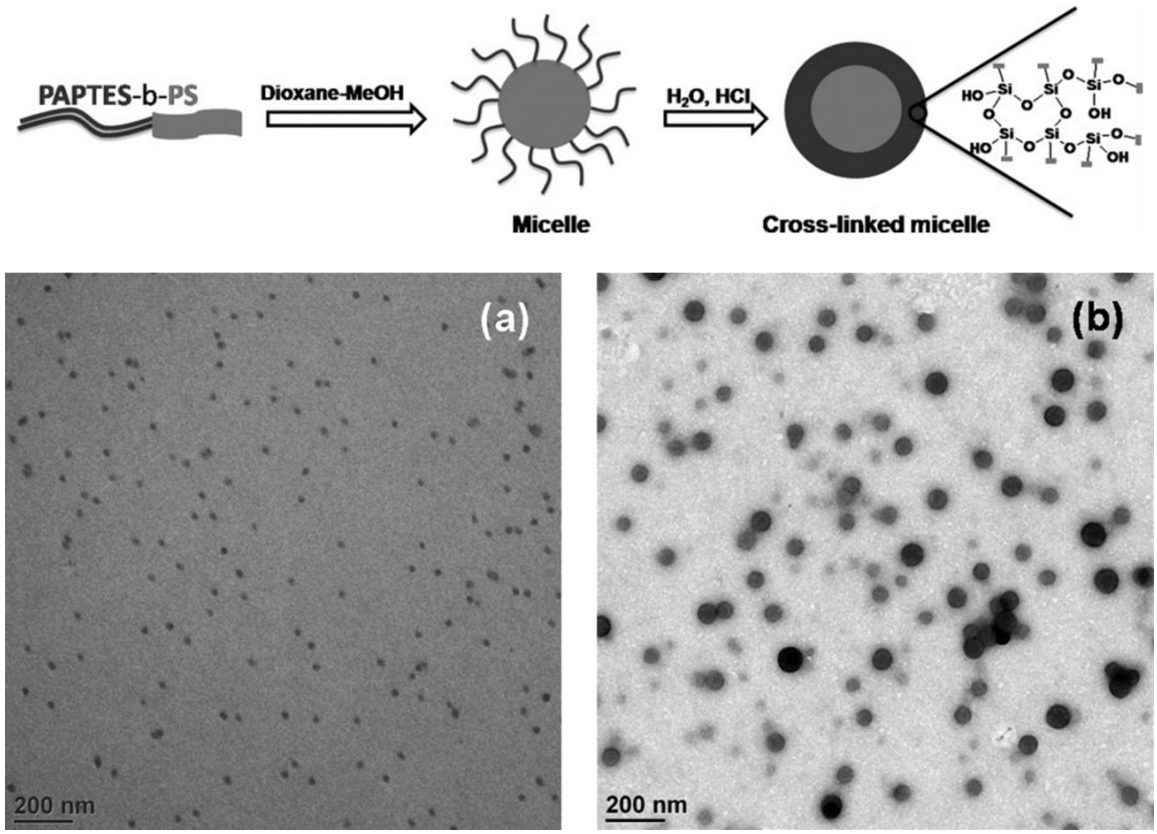

Figure 1-21: Self-assembly of block copolymer (PAPTES-b-PS) induced by methanol. (Top): schematic diagram of self-assembly and crosslinking of PAPTES-b-PS, (Bottom): TEM images of self-assembled particles made up of different chain lengths of PS in 40/60 (w/w) dioxane/methanol solutions- (a) $PAPTES_{91}$-b-PS_{34}, and (b) $PAPTES_{91}$-b-PS_{175}. Reprinted with permission from reference 146. Copyright 2010 Elsevier.

A series of silicon containing triblock copolymers (poly(ethylene oxide)-b-poly(3-(trimethoxysilyl) propyl methacrylate)-b-poly(methyl methacrylate) (PEO-b-PMPS-PMMA)) were synthesized via ATRP.[147] The triblock copolymers were initially dissolved in a good solvent (dimethylformamide, DMF) and then self-assembly was induced by adding water into DMF (until the water content reached 51.4 wt%) to form nanospheres with PEO corona. As each individual sphere consisted reactive trimethoxysilyl groups, triethylamine was then used to catalyse the hydrolysis and condensation process of alkoxysilane groups to form solid hybrid nanospheres.

In addition to NMP and ATRP methods, silica core-polymer shell nanoparticles also can be prepared via RAFT polymerization. A dithiobenzoate RAFT agent (S-benzyl dithiobenzoate) was used to control the polymerization of N-isopropylacrylamide (NIPAM) and the resultant homopolymer was isolated.[148] This macroRAFT agent was then chain extended with silicon containing monomers (3-(trimethoxysilyl) propyl methacrylate (MPS)) to form a block copolymer (PNIPAM-b-PMPS) that could undergo self-assembly. The block copolymer was dissolved in a good solvent (DMF) and self-assembly was induced by adding water. Nanospheres were produced with a PMPS hydrophobic core and PNIPAM shell. The PMPS core was also crosslinked with triethylamine (TEA). By changing the degree of polymerization of PNIPAM, the nanospheres could be varied in size. When the temperature was above 32 ^{o}C, the particle size decreased due to the thermoresponsive nature of PNIPAM.

1.4.2 Polymerization-Induced Self-Assembly

With continuous developments in controlled/living radical polymerization (especially RAFT), a relatively new self-assembly technique has emerged, known as polymerization-induced self-assembly (PISA).[149-151] The PISA process involves *in-situ* self-assembly during the chain growth of solvophobic block, representing a different approach to traditional self-assembly. PISA can also be performed in a one-pot approach, comparing to the two separate steps needed in conventional self-assembly. The PISA technique has increased the flexibility in designing nanoparticles with unique morphologies (such as spheres, rods or "worms", and vesicles), at high solids content (up to 50 % w/w polymer). Many variables can be tuned to produce desirable nanocomposite structures such as solvent choice, temperature and monomer selection.

In a typical PISA approach, a solvophilic block is firstly prepared by RAFT polymerization, and second block monomer (solvophobic block) is subsequently introduced and chain extension is allowed to take place. When the chain length of solvophobic block increases, the diblock copolymer self-assembles into micelles and the morphology evolves from spheres to worms or vesicles, based on the packing parameter of the block copolymer as a function of composition. As a result, solvophobic block forms the core of the self-assembled structure and stabilized by the solvophilic block on the surface. PISA works well with organic and inorganic polymers and can be applied in various media. Over the last decade, PISA mediated by RAFT polymerization has been demonstrated in emulsion and dispersion polymerizations;[152,153-159] each system is able to produce pure spheres, worms or vesicles at high solid content.

1.4.2.1 PISA via RAFT Dispersion Polymerization

RAFT dispersion polymerization is slightly different to traditional dispersion polymerization in that a RAFT agent is added. The key to PISA via RAFT dispersion polymerization is determined by the selection of the monomer for the second block. The second block monomer should be soluble in the continuous phase and initially form a homogeneous solution. When the second block reaches a certain degree of polymerization, the block becomes insoluble in the reaction medium. This also changes the polymerization system from homogeneous to heterogeneous. With stabilization from the solvophilic block/macroRAFT agent, the block copolymer begins to aggregate into nanoparticles, ultimately forming stable particles that can evolve in morphology from sphere to vesicles along with the increasing chain length of the hydrophobic block.

One of the most common classes of solvents for RAFT dispersion polymerizations are low molecular weight alcohols such as methanol and ethanol. Semsarilar and colleagues used benzyl methacrylate (BzMA) as a core forming block instead of styrene.[160] This is primarily due to styrene is a less reactive monomer with low conversion after several days polymerization whereas benzyl methacrylate propagates at a much greater rate and high conversion can be achieved.[161, 162] For the chain extension of BzMA, poly(methacrylic acid) (PMAA) was used as a stabilizer block and 4-cyano-4-(2-phenylethanesulfanylthiocarbonyl) sulfanylpentanoic acid (PETTC) was utilised as RAFT agent. Diverse morphologies and hydrodynamic diameters were tuneable by the chain length of core forming block and solid concentration. When the chain length of BzMA increased, spherical nanoparticles grew into worms and vesicles. After high conversion of the second monomer and narrow polymer molecular weight distributions

of the PMAA-b-PBzMA were obtained, a further chain extension to form a triblock copolymer was carried out. PMAA-PBzMA was used as the macroCTA for chain extension with 2,2,2-trifluoroethyl methacrylate (TFEMA). Once the TFEMA monomer was added to the system, the initially turbid solution became clear due to the effect of co-solvent to the PBzMA block. As the DP of the TFEMA block became larger, the solution became milky again and the morphology evolved from spheres to vesicles. The schematic diagram for this experiment is shown as Figure 1-22.

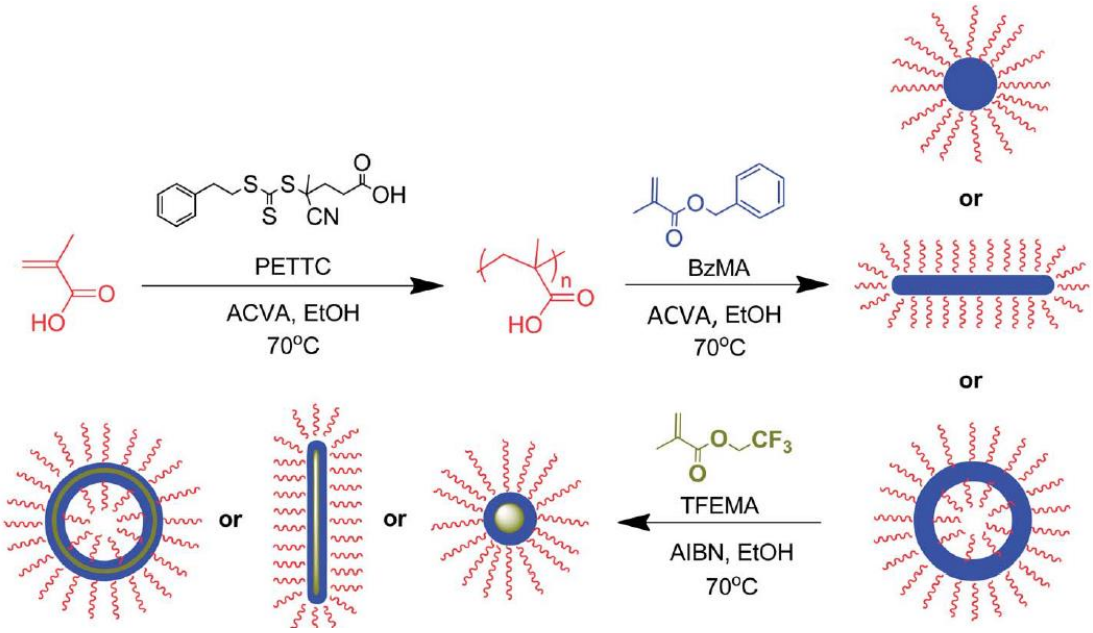

Figure 1-22: Synthesis of diblock (PMAA-PBzMA) and triblock copolymer (PMAA-PBzMA-PTFEMA) in ethanol. Reprinted with permission from reference 160. Copyright 2014 Royal Society of Chemistry.

In addition to polar solvents, non-polar hydrocarbons also can be used as solvents in PISA via RAFT dispersion polymerization. A diblock copolymer of poly(lauryl acrylate)−poly(benzyl acrylate) (PLA−PBzA) was prepared in three different *n*-alkane solvents (*n*-heptane, *n*-dodecane, and isohexadecane) via RAFT polymerization.[163] Under this one-pot approach, high conversions were achieved in all reactions and various morphologies (sphere, worms, and vesicles) were observed. When the solvent hydrophobicity increased, the block copolymers in isohexadecane formed a gel at much lower target PBzA DP than in dodecane and heptane. The gel phase was interpreted as the presence of worms.

The PISA process also enables encapsulation of guest molecules within nanoparticle structures. Karagoz *et al.* reported high efficiency loading of hydrophobic guest molecules into nanoparticles during the one-pot PISA process.[164] An asymmetric poly(poly(ethylene glycol) methyl ether methacrylate)-block-poly(styrene) (PEGMA-b-PSt) copolymer was prepared via RAFT polymerization in methanol. When the chain length of polystyrene increased, the PISA process began and nanoparticles self-assembled into various morphologies. Figure 1-23 shows the particle size increased over polymerization time and a range of morphologies were obtained. Because of the hydrophobic polystyrene core, the hydrophobic dye Nile Red was successfully loaded into the nanoparticle core during the self-assembly process without affecting the morphology or polymerization kinetics. The Nile Red loading increased with the size of hydrophobic core.

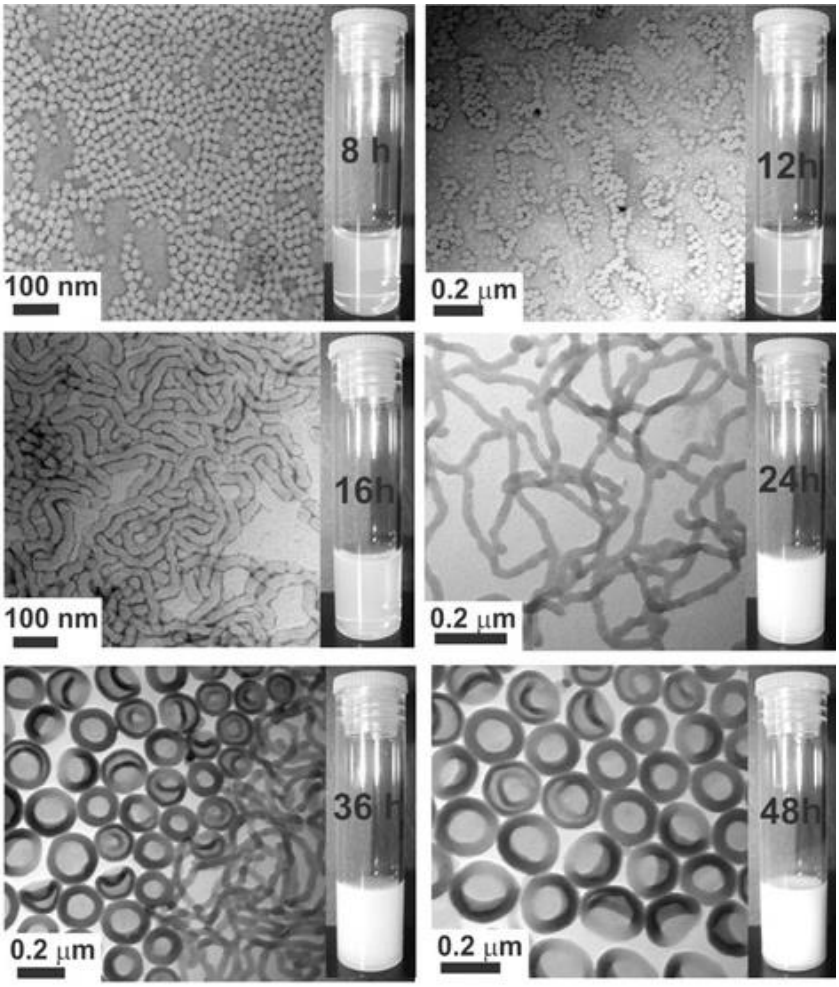

Figure 1-23: TEM images of block copolymer (PEGMA-b-PSt) morphology changing with the conversion over 48 hours. Reprinted with permission from reference 164. Copyright 2013 John Wiley and Sons.

Self-assembly of silicon containing block copolymers via a one-pot approach is rare, typically due to the need for stringent reaction conditions and the instability of the monomer. A relatively stable silicon containing monomer (based on polyhedral oligomeric silsesquioxane (POSS)) has been used to prepare hybrid nanoparticles via RAFT and PISA processes using a one-pot method.[165] Different morphologies were produced via controlling the compositions of block copolymers. In the experiment, cumyl dithiobenzoate (CDB) was used as a RAFT agent and polymerized with 3-(3,5,7,9,11,13,15-heptaisobutyl-pentacyclo [9.5.1.13,9.15,15.17,13]-octasiloxane-1-yl) propyl methacrylate (MAiBuPOSS). The resultant macroRAFT agent was

then chain extended with styrene at 120 ^{o}C in octane (a poor solvent for the PSt block) to produce diblock copolymers (PMAiBuPOSS-b-PSt). Although the conversion was low (< 50%), the molecular weight (17000-74000 g mol^{-1}) and dispersity ($Đ$ = 1.15-1.9) were considered as satisfactory. Different morphologies were observed (sphere, rod, vesicles and large porous particles) by electron microscopy and these morphologies were influenced by the degree of polymerization of the PS core block and the chain length of PMAiBuPOSS macroCTA. The obtained morphologies were also found to be sensitive to the cooling rate from the polymerization temperature; the block copolymer was completely soluble at high temperature and only self-assembled at room temperature.

1.4.2.2 PISA via RAFT Emulsion Polymerization

Water-soluble and surface-active chain transfer agents have been utilised in RAFT aqueous emulsion polymerization to improve colloidal stability, in addition to offering an alternative strategy to replace traditional surfactants. Surface-active chain transfer agents in RAFT emulsion polymerization also provide better control over the molecular weight distribution by localizing the polymerization growth and avoiding transportation of the RAFT agent in aqueous medium.[166] The polymerization typically consists of two steps: firstly to prepare a hydrophilic macroRAFT/stabilizer block and secondly to perform chain extension with water-immiscible monomers to grow micelles under RAFT control. When the chain length of hydrophobic block increases, the micelles become bigger and eventually aggregate into stable particles via the PISA process. PISA via RAFT emulsion polymerization has attracted much interest due to many benefits such as self-assembly at high solids content, high conversion, and the use of environmental friendly solvents such as water. This approach also can produce

alternative morphology such as nanofibers and vesicles,[167-171] which were never seen previously in conventional emulsion polymerization (which is limited to spherical structures only[172-177]). The pathway of PISA via RAFT emulsion polymerization is shown in Figure 1-24.

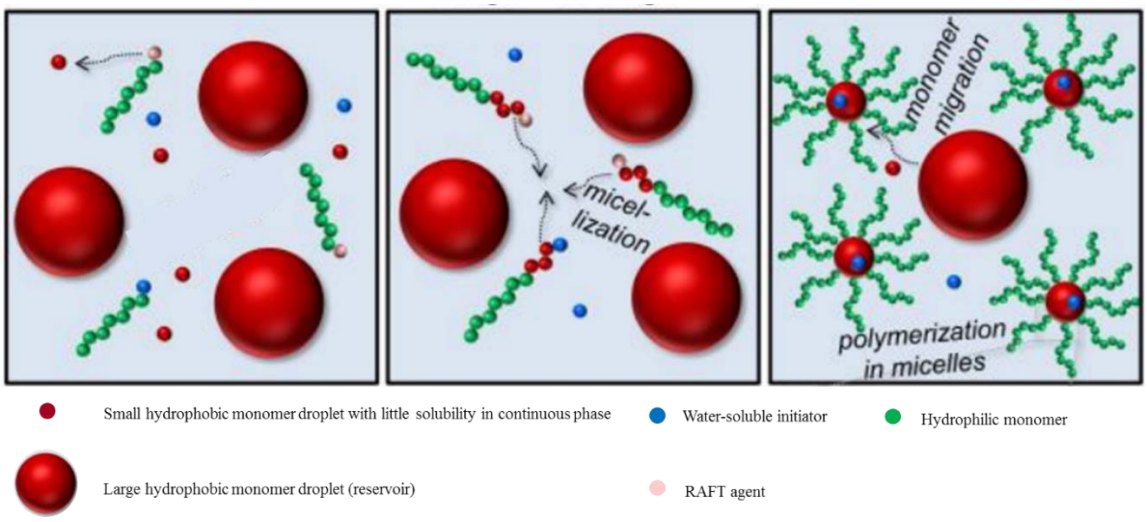

Figure 1-24: A brief mechanism of PISA via RAFT emulsion polymerization. (Left): hydrophilic macroRAFT agent is dissolved in continuous phase and prepared for chain extension with hydrophobic monomers. (Middle): macroRAFT agent chains start to aggregate and form micelles after chain extension with a few hydrophobic monomer units. (Right): large monomer droplets breakdown slowly as monomer diffuses into micelles stabilized by macroRAFT agent and continue polymerization and chain extension. Reprinted with permission from reference 178. Copyright 2017 MDPI Publisher.

Some examples of PISA via RAFT emulsion polymerization are described below. Phenyl acrylate (PhA) has been recently applied in three different PISA formulations: RAFT aqueous emulsion polymerization, RAFT dispersion polymerization in ethanol, and RAFT dispersion polymerization in *n*-heptane.[179] For the PISA via RAFT emulsion polymerization, poly(dimethyl acrylamide) (PDMAC) was selected as a macroRAFT agent and chain extended with PhA in water. High conversion was achieved and the molecular weight increased with

target degree of polymerization of PhA (between 50 and 500 units). Only spherical structures were observed in RAFT aqueous emulsion polymerization due to kinetic trapping of this morphology. This is in contrast to PISA via RAFT dispersion polymerizations in ethanol and heptane, which generated diverse morphologies such as spheres, worms, and vesicles.

An intermediate water solubility monomer (2-hydroxybutyl methacrylate, HBMA; ~20 g dm^{-3} at 70 ^{o}C) was used as a core block in RAFT aqueous emulsion polymerization and PISA approach.[180] In the experiment, poly((methacrylic acid), PMAA) macroRAFT agent was chain extended with HBMA in pH 5 buffer. When the chain length of HBMA increased, the morphology changed from spheres to "monkey nuts." A further increase of the HBMA block (DP 300, 1000 and 1500) resulted large spheres only. Figure 1-25 shows the synthesis of PMAA-b-PHBMA in buffer and nanoparticles obtained at different chain length of PHBMA. "Monkey nut" structures (Figure 1-25(c)) were caused by the 1D fusion of spheres, due to the intermediate aqueous solubility HBMA monomers that can plasticise the core block effectively.

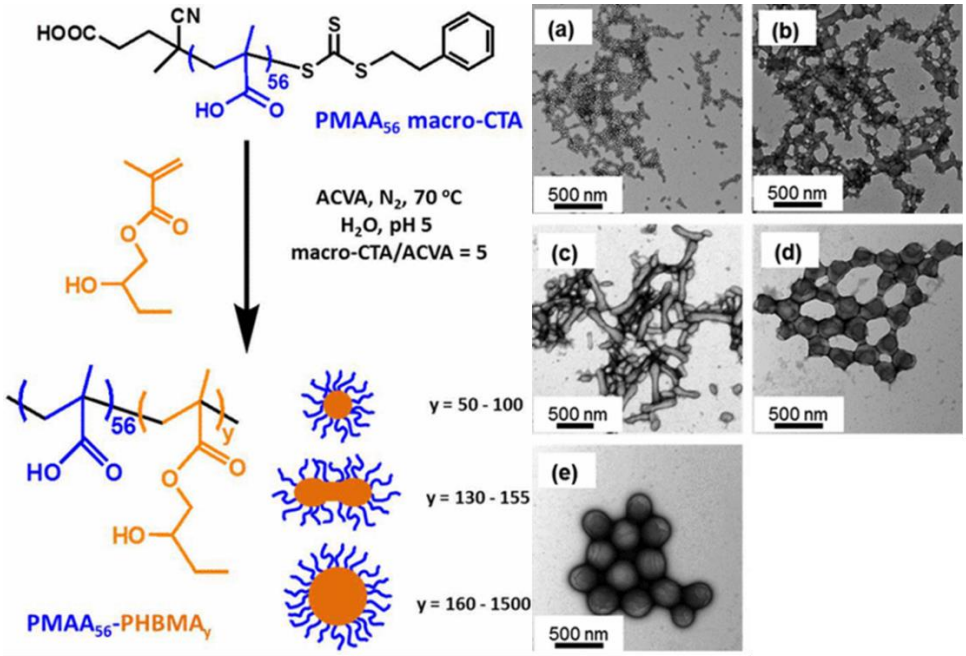

Figure 1-25: Self-assembly of PMAA-b-PHBMA. (Left) Preparation of PMAA-b-PHBMA via RAFT aqueous emulsion polymerization, (Right) TEM images of nanoparticles with different chain lengths PHBMA – (a) $PMAA_{56}$-b-$PHBMA_{50}$, (b) $PMAA_{56}$-b-$PHBMA_{130}$, (c) $PMAA_{56}$-b-$PHBMA_{150}$ (monkey nut), (d) $PMAA_{56}$-b-$PHBMA_{300}$, and (e) $PMAA_{56}$-b-$PHBMA_{1000}$. Reprinted with permission from reference 180. Copyright 2017 American Chemical Society.

Polymeric nanofibers were obtained via RAFT emulsion polymerization of styrene through the PISA process.[181] A hydrophilic trithiocarbonate based macroRAFT agent (poly(acrylic acid)-gradient-poly(ethylene glycol) methyl ether acrylate (PEGA), PAA-*grad*-PEGA) was used to chain extend styrene in aqueous media with different pH and salt concentrations. As the styrene block grew, the continuous phase became turbid. However, residual macroRAFT agent was detected at pH > 6 due to reported effect of pH[182] and less efficient chain extension in emulsion polymerization (due to multiphasic nature of emulsion polymerization). Non-spherical structures (such as vesicles or fibres) were observed at acidic pH or high salt concentration.

As emphasised above, under the PISA approach, access to higher order morphologies (worm and vesicles) is much more challenging in RAFT aqueous emulsion than RAFT dispersion polymerization. RAFT aqueous emulsion polymerization often produces spherical morphologies even at highly asymmetric diblock compositions[183-187] and this limitation is still not well understood. Khor and co-workers found the macroRAFT agent end group hydrophobicity and radical initiator concentration were the critical keys to access higher order morphology via PISA in RAFT aqueous emulsion polymerization.[188] N-hydroxyethyl acrylamide (HEAA) and poly(ethylene glycol) methyl ether acrylate (PEGA) were used to prepare two macoRAFT agents with different end groups: 4-cyano-4-(ethylthiocarbonothioylthio)pentanoic acid (ECT) or methylated-ECT (ECT-Me). Both macroRAFT agents were then chain extended with styrene in water to form nanoparticles (PHEAA-b-PEGA-b-PSt). When the macroRAFT agent with ECT-Me was used, vesicles structure was obtained. At a similar chain length of styrene block, only spherical structures were obtained with ECT endgroup macroRAFT agent. This might due to the ECT-Me endgroup increasing the packing parameter and chain aggregation number. For the methyl-terminated macroRAFT agent, reducing the radical concentration by half changed the morphology from vesicles to spheres. This decreased the number of growing polymer chains. Conversely, doubling or tripling the radical concentration could produce vesicles from spheres in the RAFT emulsion polymerization of styrene with the macroRAFT agent with ECT endgroup.

1.5 Aims and Objectives of the Work

Based on a review of the literature across the topics of polymer-silica hybrid materials, reversible deactivation radical polymerization and self-assembly, there is a clear knowledge gap with respect to the preparation of colloidal nanocomposites (consisting of polymer and silica domains) via various self-assembly methods. The overall aim of this work is therefore a fundamental investigation of the use of silicon-containing monomers for the rational preparation of hybrid nanocomposites of controllable size and shape.

This overall aim can be broken down as a series of sub-aims, described as follows:

a) To investigate the synthesis and preparation of hybrid polymer-silica nanoparticles through a combination of reversible deactivation radical polymerization, self-assembly and orthogonal sol-gel chemistry;
b) To specifically prepare polymer/silica nanoparticles with controllable size and shape, including anisotropic particles such as rods, ‘worms’ and vesicles;
c) To develop a greater understanding of the experimental conditions used in both homogeneous and heterogeneous polymerizations of silicon-containing monomers for the controlled synthesis of copolymers and resulting nanoparticles;
d) To investigate the compositional design of such polymer nanoparticles, including the use of silicon-containing monomers in the i) stabilizer block; ii) core-forming block and iii) interfacial block, and to study potential applications such as encapsulation of various payloads.

1.6 Thesis Outline

This thesis is written based on the guidelines and rules of the University of Tasmania, Australia. This thesis consists of six chapters, including this Introduction. The contents of the following chapters are briefly summarized below:

Chapter 2: Experimental Methods and Characterisations

This chapter reports all the chemical reagents and preparation methods used in this thesis. The conditions used in each characterisation technique are also shown.

Chapter 3: Polymer-Inorganic Hybrid Nanoparticles of Various Morphologies via Polymerization-Induced Self-Assembly and Sol–Gel Chemistry

This chapter reports synthesis of polymer-silica hybrid nanoparticles of various morphologies via polymerization-induced self-assembly (PISA) using an alkoxysilane-based methacrylate as the solvophilic block. A range of variables were studied such as choice of alkoxysilane monomers, types of RAFT agent, and the length of both solvophilic and solvophobic blocks (benzyl methacrylate). The presence of reactive alkoxysilane groups at the particle surface enabled a silica shell to be grown from the surface via condensation of tetraethylorthosilicate (TEOS) in a controlled approach.

Chapter 1

Some of the content of this chapter was published as an article entitled "Polymer-Inorganic Hybrid Nanoparticles of Various Morphologies via Polymerization-Induced Self-Assembly and Sol–Gel Chemistry", *Polymer Chemistry*, 2016, 7, 6575-6585. (DOI: 10.1039/C6PY01447J)

Chapter 4: Self-Assembly of Block Copolymers with an Alkoxysilane-Based Core-Forming Block: A Comparison of Synthetic Approaches

This chapter reports the comparison of two methods (PISA and traditional solution-based self-assembly) to prepare polymer nanoparticles bearing an alkoxysilane based core-forming block. The limitations and benefits of each method are discussed. Using the solution self-assembly method, stable nanoparticles of differing shapes and sizes were formed in both water and hexane, based on the nature of the macroRAFT agents used. The steric bulk of the alkoxysilane block was also studied with respect to change in resultant particle morphology.

Sections of this chapter were published with the title of "Self-Assembly of Block Copolymers with An Alkoxysilane-Based Core-Forming Block: A Comparison of Synthetic Approaches", *Journal of Polymer Science Part A: Polymer Chemistry*, 2017, 56, 420-429. (DOI: 10.1002/pola.28911)

Chapter 5: Preparation of Aqueous Capsules with a Crosslinked Interface via Using Silicon Containing Triblock Copolymers

This chapter reports the preparation of ABC-type triblock copolymers by two different methods, where the central B block contained a reactive alkoxysilane functionality. These triblock copolymers were examined for their use as stabilizers in oil-in-water miniemulsions (or prepared *in-situ* via the PISA methodology), followed by base-catalysed crosslinking of the interfacial block. The success of interfacial crosslinking, colloidal stability and particle morphology by both methods was studied. Encapsulation efficiency was also investigated.

Chapter 6: Conclusions and Future Work

This chapter reports conclusions of this thesis and proposals for future work.

1.7 References

1. A. Aras, A. R. Khokhar, M. Z. Qureshi, M. F. Silva, A. S. Kupiec, E. A. G. Pineda, A. A. W. Hechenleitner and A. A. Farooqi, *Asian Pacific Journal of Cancer Prevention*, 2014, **15**, 3865-3871.
2. D. Napierska, L. Thomassen, D. Lison, J. Martens and P. Hoet, *Particle and Fibre Toxicology*, 2010, **7**, 39.
3. U. Schubert, in *In The Sol‐Gel Handbook (eds D. Levy and M. Zayat)*, John Wiley & Sons, 2015, DOI: 10.1002/9783527670819.ch01, pp. 1-28.
4. P. Innocenzi, in *The Sol to Gel Transition*, Springer International Publishing, 2016, DOI: 10.1007/978-3-319-39718-4_2, pp. 7-25.
5. R. J. Hook, *Journal of Non-Crystalline Solids*, 1996, **195**, 1-15.
6. I. A. Rahman and V. Padavettan, *Journal of Nanomaterials*, 2012, **2012**, 15.
7. H. Giesche, *Journal of the European Ceramic Society*, 1994, **14**, 189-204.
8. W. Stöber, A. Fink and E. Bohn, *Journal of Colloid and Interface Science*, 1968, **26**, 62-69.
9. D. Qi, C. Lin, H. Zhao, H. Liu and T. Lü, *Journal of Dispersion Science and Technology*, 2017, **38**, 70-74.
10. L. M. Liz-Marzán, M. Giersig and P. Mulvaney, *Langmuir*, 1996, **12**, 4329-4335.
11. B. Thangaraj, Z. Jia, L. Dai, D. Liu and W. Du, *Arabian Journal of Chemistry*, 2016, DOI: 10.1016/j.arabjc.2016.09.004, 1-13.
12. V. Shirshahi and M. Soltani, *Contrast Media & Molecular Imaging*, 2015, **10**, 1-17.
13. Y. K. Park, S. Lee, S. Yoon and J. W. Lee, *Journal of Nanoscience and Nanotechnology*, 2017, **17**, 8468-8474.
14. T. W. Kim, P. W. Chung and V. S. Y. Lin, *Chemistry of Materials*, 2010, **22**, 5093-5104.
15. K. Schumacher, M. Grün and K. K. Unger, *Microporous and Mesoporous Materials*, 1999, **27**, 201-206.
16. R. Kumar, I. Roy, T. Y. Ohulchanskyy, L. N. Goswami, A. C. Bonoiu, E. J. Bergey, K. M. Tramposch, A. Maitra and P. N. Prasad, *ACS Nano*, 2008, **2**, 449-456.
17. V. Shirshahi, F. Shamsipour, A. H. Zarnani, J. Verdi and R. Saber, *Cancer Nanotechnology*, 2013, **4**, 27-37.
18. F. J. Arriagada and K. Osseo-Asare, *Journal of Colloid and Interface Science*, 1999, **211**, 210-220.
19. K. S. Finnie, J. R. Bartlett, C. J. A. Barbé and L. Kong, *Langmuir*, 2007, **23**, 3017-3024.
20. L. Tang and J. Cheng, *Nano today*, 2013, **8**, 290-312.
21. K. Osseo-Asare and F. J. Arriagada, *Colloids and Surfaces*, 1990, **50**, 321-339.
22. J. W. Kim, L. U. Kim and C. K. Kim, *Biomacromolecules*, 2007, **8**, 215-222.
23. A. Van Blaaderen, J. Van Geest and A. Vrij, *Journal of Colloid and Interface Science*, 1992, **154**, 481-501.
24. F. Hagemans, E. B. van der Wee, A. van Blaaderen and A. Imhof, *Langmuir*, 2016, **32**, 3970-3976.
25. Sujandi, S. E. Park, D. S. Han, S. C. Han, M. J. Jin and T. Ohsuna, *Chemical Communications*, 2006, **0**, 4131-4133.
26. N. Hao, L. Li and F. Tang, *Journal of Materials Chemistry A*, 2014, **2**, 11565-11568.
27. Y. Zhao, Y. Wang, F. Ran, Y. Cui, C. Liu, Q. Zhao, Y. Gao, D. Wang and S. Wang, *Scientific Reports*, 2017, **7**, 4131.

28. N. Hao, H. Yang, L. Li, L. Li and F. Tang, *New Journal of Chemistry*, 2014, **38**, 4258-4266.
29. Y. You, L. He, B. Ma and T. Chen, *Advanced Functional Materials*, 2017, **27**, 1703313.
30. A. Khanal, Y. Inoue, M. Yada and K. Nakashima, *Journal of the American Chemical Society*, 2007, **129**, 1534-1535.
31. M. Zhao, L. Zheng, X. Bai, N. Li and L. Yu, *Colloids and Surfaces A: Physicochemical and Engineering Aspects*, 2009, **346**, 229-236.
32. Z. C. I. and I. A., *Advanced Materials*, 2005, **17**, 924-928.
33. K. Han, Z. Zhao, Z. Xiang, C. Wang, J. Zhang and B. Yang, *Materials Letters*, 2007, **61**, 363-368.
34. Y. Wang, X. Su, P. Ding, S. Lu and H. Yu, *Langmuir*, 2013, **29**, 11575-11581.
35. L. Wu, Z. Jiao, M. Wu, T. Song and H. Zhang, *RSC Advances*, 2016, **6**, 13303-13311.
36. I. M. Rio-Echevarria, F. Selvestrel, D. Segat, G. Guarino, R. Tavano, V. Causin, E. Reddi, E. Papini and F. Mancin, *Journal of Materials Chemistry*, 2010, **20**, 2780-2787.
37. R. P. Bagwe, L. R. Hilliard and W. Tan, *Langmuir*, 2006, **22**, 4357-4362.
38. K. Ohno, T. Akashi, Y. Tsujii, M. Yamamoto and Y. Tabata, *Biomacromolecules*, 2012, **13**, 927-936.
39. A. Shahbazi, H. Younesi and A. Badiei, *Korean Journal of Chemical Engineering*, 2014, **31**, 1598-1607.
40. S. U. Pickering, *Journal of the Chemical Society, Transactions*, 1907, **91**, 2001-2021.
41. Q. Monégier du Sorbier, A. Aimable and C. Pagnoux, *Journal of Colloid and Interface Science*, 2015, **448**, 306-314.
42. V. B. Menon and D. T. Wasan, *Colloids and Surfaces*, 1988, **29**, 7-27.
43. R. Aveyard, B. P. Binks and J. H. Clint, *Advances in Colloid and Interface Science*, 2003, **100-102**, 503-546.
44. Y. Chevalier and M. A. Bolzinger, *Colloids and Surfaces A: Physicochemical and Engineering Aspects*, 2013, **439**, 23-34.
45. W. Ramsden, *Proc. Royal Soc. London*, 1903, **72**, 156-164.
46. N. Briggs, A. K. Y. Raman, L. Barrett, C. Brown, B. Li, D. Leavitt, C. P. Aichele and S. Crossley, *Colloids and Surfaces A: Physicochemical and Engineering Aspects*, 2018, **537**, 227-235.
47. N. M. Briggs, J. S. Weston, B. Li, D. Venkataramani, C. P. Aichele, J. H. Harwell and S. P. Crossley, *Langmuir*, 2015, **31**, 13077-13084.
48. B. Brunier, N. Sheibat-Othman, M. Chniguir, Y. Chevalier and E. Bourgeat-Lami, *Langmuir*, 2016, **32**, 6046-6057.
49. N. P. Ashby and B. P. Binks, *Physical Chemistry Chemical Physics*, 2000, **2**, 5640-5646.
50. J. Zhou, X. Qiao, B. P. Binks, K. Sun, M. Bai, Y. Li and Y. Liu, *Langmuir*, 2011, **27**, 3308-3316.
51. Q. Lan, C. Liu, F. Yang, S. Liu, J. Xu and D. Sun, *Journal of Colloid and Interface Science*, 2007, **310**, 260-269.
52. J. Frelichowska, M. A. Bolzinger and Y. Chevalier, *Colloids and Surfaces A: Physicochemical and Engineering Aspects*, 2009, **343**, 70-74.
53. X. Zhao, G. Yu, J. Li, Y. Feng, L. Zhang, Y. Peng, Y. Tang and L. Wang, *ACS Sustainable Chemistry & Engineering*, 2018, **6**, 4105-4114.
54. Y. Yang, Z. Fang, X. Chen, W. Zhang, Y. Xie, Y. Chen, Z. Liu and W. Yuan, *Frontiers in Pharmacology*, 2017, **8**.
55. H. Yan, B. Zhao, Y. Long, L. Zheng, C. H. Tung and K. Song, *Colloids and Surfaces A: Physicochemical and Engineering Aspects*, 2015, **482**, 639-646.
56. Y. Zhao, X. Zhang, J. Sanjeevi and Q. Yang, *Journal of Catalysis*, 2016, **334**, 52-59.

57. S. K. Singh, A. Kumar and A. Jain, *Materials Today: Proceedings*, 2018, **5**, 6339-6344.
58. J. Jang, J. Bae and D. Kang, *Journal of Applied Polymer Science*, 2001, **82**, 2310-2318.
59. L. Guangyu, L. Longyu, Y. Xinlin and D. Zhao, *Polymers for Advanced Technologies*, 2008, **19**, 1922-1930.
60. G. D. Fu, Z. Shang, L. Hong, E. T. Kang and K. G. Neoh, *Macromolecules*, 2005, **38**, 7867-7871.
61. K. Zhang, L. Zheng, X. Zhang, X. Chen and B. Yang, *Colloids and Surfaces A: Physicochemical and Engineering Aspects*, 2006, **277**, 145-150.
62. S. A. Johnson, P. J. Ollivier and T. E. Mallouk, *Science*, 1999, **283**, 963-965.
63. X. Huang, D. Appelhans, P. Formanek, F. Simon and B. Voit, *ACS Nano*, 2012, **6**, 9718-9726.
64. M. J. Mulvihill, B. L. Rupert, R. He, A. Hochbaum, J. Arnold and P. Yang, *Journal of the American Chemical Society*, 2005, **127**, 16040-16041.
65. O. Shimoni, Y. Yan, Y. Wang and F. Caruso, *ACS Nano*, 2013, **7**, 522-530.
66. F. Stephan and P. Thomas, *Angewandte Chemie International Edition*, 2002, **41**, 688-714.
67. S. Zhou, A. S. Narutaki, S. Tsuboike, J. Wang, A. Shimojima and T. Okubo, *Langmuir*, 2015, **31**, 13214-13220.
68. S. Zhou, Y. Oda, A. Shimojima, T. Okubo, S. Aoshima and A. S. Narutaki, *Polymer Journal*, 2014, **47**, 128-135.
69. M. Fukao, A. Sugawara, A. Shimojima, W. Fan, M. A. Arunagirinathan, M. Tsapatsis and T. Okubo, *Journal of the American Chemical Society*, 2009, **131**, 16344-16345.
70. S. Zhou, T. Sakamoto, J. Wang, A. S. Narutaki, A. Shimojima and T. Okubo, *Langmuir*, 2012, **28**, 13181-13188.
71. Y. Yao, J. Feng, L. Han and S. Che, *RSC Advances*, 2015, **5**, 102256-102260.
72. N. Charton, A. Feldermann, A. Theis, M. H. Stenzel, T. P. Davis and C. B. Kowollik, *Journal of Polymer Science Part A: Polymer Chemistry*, 2004, **42**, 5170-5179.
73. A. C. Mortamet and R. A. Pethrick, *Journal of Applied Polymer Science*, 2012, **123**, 1539-1547.
74. Q. Yu, S. Nauman, J. P. Santerre and S. Zhu, *Journal of Applied Polymer Science*, 2001, **82**, 1107-1117.
75. G. Zhang, I. Y. Song, K. H. Ahn, T. Park and W. Choi, *Macromolecules*, 2011, **44**, 7594-7599.
76. R. K. Sadhir, J. D. B. Smith and P. M. Castle, *Journal of Polymer Science: Polymer Chemistry Edition*, 1985, **23**, 411-427.
77. G. Moad, E. Rizzardo and S. H. Thang, in *Fundamentals of Controlled/Living Radical Polymerization*, The Royal Society of Chemistry, 2013, DOI: 10.1039/9781849737425-00205, pp. 205-249.
78. M. Szwarc, M. Levy and R. Milkovich, *Journal of the American Chemical Society*, 1956, **78**, 2656-2657.
79. P. B. Zetterlund, Y. Kagawa and M. Okubo, *Chemical Reviews*, 2008, **108**, 3747-3794.
80. A. E. Smith, 3416305 Ph.D., The University of Southern Mississippi, 2010.
81. K. Matyjaszewski, in *Handbook of Radical Polymerization*, John Wiley & Sons, Inc., 2003, DOI: 10.1002/0471220450.ch8, pp. 361-406.
82. Otsuka-Chemical, High Performance Polymers Using Living Radical Polymerization Technology, https://www.otsukac.co.jp/en/advanced/living/, (accessed 17 July 2018, 2018).
83. J. Nicolas, Y. Guillaneuf, C. Lefay, D. Bertin, D. Gigmes and B. Charleux, *Progress in Polymer Science*, 2013, **38**, 63-235.
84. S. Armido and S. Tobias, *The Chemical Record*, 2005, **5**, 27-35.

85. C. J. Hawker, A. W. Bosman and E. Harth, *Chemical Reviews*, 2001, **101**, 3661-3688.
86. V. Sciannamea, R. Jérôme and C. Detrembleur, *Chemical Reviews*, 2008, **108**, 1104-1126.
87. K. Matyjaszewski, *Macromolecules*, 2012, **45**, 4015-4039.
88. T. E. Patten and K. Matyjaszewski, *Advanced Materials*, 1998, **10**, 901-915.
89. K. Matyjaszewski and J. Xia, *Chemical Reviews*, 2001, **101**, 2921-2990.
90. P. Krys and K. Matyjaszewski, *European Polymer Journal*, 2017, **89**, 482-523.
91. B. Radhakrishnan, R. Ranjan and W. J. Brittain, *Soft Matter*, 2006, **2**, 386-396.
92. G. Moad, E. Rizzardo and S. H. Thang, *Australian Journal of Chemistry*, 2006, **59**, 669-692.
93. H. Yu, Q. Chen, Z. Zhang, J. Zhu, Z. Cheng, N. Zhou, W. Zhang and X. Zhu, *Reactive and Functional Polymers*, 2012, **72**, 153-159.
94. J. F.Quinn, T. P.Davis, L. Barner and C. B. Kowollik, *Polymer*, 2007, **48**, 6467-6480.
95. S. Muthukrishnan, E. H. Pan, M. H. Stenzel, C. B. Kowollik, T. P. Davis, D. Lewis and L. Barner, *Macromolecules*, 2007, **40**, 2978-2980.
96. J. F. Quinn, L. Barner, C. B. Kowollik, E. Rizzardo and T. P. Davis, *Macromolecules*, 2002, **35**, 7620-7627.
97. T. G. McKenzie, Q. Fu, E. H. H. Wong, D. E. Dunstan and G. G. Qiao, *Macromolecules*, 2015, **48**, 3864-3872.
98. Y. Huiwen, Z. Haimei, L. Lican, L. Pengsheng and C. Yuanli, *Journal of Polymer Science Part A: Polymer Chemistry*, 2007, **45**, 5091-5102.
99. A. E. Smith, X. Xu and C. L. McCormick, *Progress in Polymer Science*, 2010, **35**, 45-93.
100. Y. Kwak, A. Goto, Y. Tsujii, Y. Murata, K. Komatsu and T. Fukuda, *Macromolecules*, 2002, **35**, 3026-3029.
101. R. T. A. Mayadunne, E. Rizzardo, J. Chiefari, Y. K. Chong, G. Moad and S. H. Thang, *Macromolecules*, 1999, **32**, 6977-6980.
102. J. Chiefari, R. T. A. Mayadunne, C. L. Moad, G. Moad, E. Rizzardo, A. Postma and S. H. Thang, *Macromolecules*, 2003, **36**, 2273-2283.
103. N. V. Tsarevsky and B. S. Sumerlin, *Fundamentals of Controlled/Living Radical Polymerization*, Royal Society of Chemistry, 2012.
104. G. Moad, E. Rizzardo and S. H. Thang, *Australian Journal of Chemistry*, 2012, **65**, 985-1076.
105. E. Rizzardo, M. Chen, B. Chong, G. Moad, M. Skidmore and S. H. Thang, *Macromolecular Symposia*, 2007, **248**, 104-116.
106. C. Li and B. C. Benicewicz, *Journal of Polymer Science Part A: Polymer Chemistry*, 2005, **43**, 1535-1543.
107. S. Saricilar, R. Knott, C. B. Kowollik, T. P. Davis and J. P. A. Heuts, *Polymer*, 2003, **44**, 5169-5176.
108. M. Lejars, A. Margaillan and C. Bressy, *Polymer Chemistry*, 2014, **5**, 2109-2117.
109. M. N. Nguyen, C. Bressy and A. Margaillan, *Polymer*, 2009, **50**, 3086-3094.
110. C. Bressy, M. N. Nguyen, B. Tanguy, V. G. Ngo and A. Margaillan, *Polymer Degradation and Stability*, 2010, **95**, 1260-1268.
111. M. N. Nguyen, C. Bressy and A. Margaillan, *Journal of Polymer Science Part A: Polymer Chemistry*, 2005, **43**, 5680-5689.
112. R. Tomovska, J. C. d. l. Cal and J. M. Asua, in *Monitoring Polymerization Reactions: From Fundamentals to Applications*, eds. W. F. Reed and A. M. Alb, John Wiley & Sons, 2013, DOI: 10.1002/9781118733813.ch4, pp. 59-77.
113. W. J. Priest, *The Journal of Physical Chemistry*, 1952, **56**, 1077-1082.
114. W. D. Harkins, *Journal of the American Chemical Society*, 1947, **69**, 1428-1444.

115. S. C. Thickett and R. G. Gilbert, *Polymer*, 2007, **48**, 6965-6991.
116. K. Landfester, in *Colloid Chemistry II*, ed. M. Antonietti, Springer Berlin Heidelberg, 2003, DOI: 10.1007/3-540-36412-9_4, pp. 75-123.
117. K. Landfester and A. Musyanovych, in *Chemical Design of Responsive Microgels*, eds. A. Pich and W. Richtering, Springer Berlin Heidelberg, 2011, DOI: 10.1007/12_2010_68, pp. 39-63.
118. C. N. I. Tissot, F. Lefebvre, and E. B. Lami, *Macromolecules*, 2001, **34**, 5737-5739.
119. I. Tissot, J. P. Reymond, F. Lefebvre and E. Bourgeat-Lami, *Chemistry of Materials*, 2002, **14**, 1325-1331.
120. K. F. Ni, G. R. Shan, Z. X. Weng, N. Sheibat Othman, G. Fevotte, F. Lefebvre and E. Bourgeat-Lami, *Macromolecules*, 2005, **38**, 7321-7329.
121. X. Xinyan and X. Rui, *Journal of Applied Polymer Science*, 2011, **119**, 1576-1585.
122. M. Tsutomu, A. Koji, M. Masatoshi and K. Yoshiharu, *Journal of Applied Polymer Science*, 2006, **99**, 659-669.
123. S. W. Zhang, S. X. Zhou, Y. M. Weng and L. M. Wu, *Langmuir*, 2006, **22**, 4674-4679.
124. K. F. Ni, G. R. Shan and Z. X. Weng, *Macromolecules*, 2006, **39**, 2529-2535.
125. Z. H. Cao, G. R. Shan, G. Fevotte, N. S. Othman and E. Bourgeat-Lami, *Macromolecules*, 2008, **41**, 5166-5173.
126. Y. Luo, H. Xu and B. Zhu, *Polymer*, 2006, **47**, 4959-4966.
127. J. B. Jun, J. K. Hong, J. G. Park and K. D. Suh, *Macromolecular Chemistry and Physics*, 2003, **204**, 2281-2289.
128. P. Samaddar, A. Deep and K. H. Kim, *Chemical Engineering Journal*, 2018, **342**, 71-89.
129. L. Zhang and A. Eisenberg, *Science*, 1995, **268**, 1728-1731.
130. Y. Mai and A. Eisenberg, *Chemical Society Reviews*, 2012, **41**, 5969-5985.
131. G. Riess, *Progress in Polymer Science*, 2003, **28**, 1107-1170.
132. H. Cai, G. Jiang, Z. Shen and X. Fan, *Soft Matter*, 2013, **9**, 11398-11404.
133. L. Zhang and A. Eisenberg, *Macromolecules*, 1999, **32**, 2239-2249.
134. K. Yu, L. Zhang and A. Eisenberg, *Langmuir*, 1996, **12**, 5980-5984.
135. J. Weiss and A. Laschewsky, *Langmuir*, 2011, **27**, 4465-4473.
136. Y. Li, T. Zhao, C. Wang, Z. Lin, G. Huang, B. D. Sumer and J. Gao, *Nature Communications*, 2016, **7**, 13214.
137. L. A. Fielding, J. A. Lane, M. J. Derry, O. O. Mykhaylyk and S. P. Armes, *Journal of the American Chemical Society*, 2014, **136**, 5790-5798.
138. L. Zhang and A. Eisenberg, *Journal of the American Chemical Society*, 1996, **118**, 3168-3181.
139. L. Zhang and A. Eisenberg, *Polymers for Advanced Technologies*, 1998, **9**, 677-699.
140. D. E. Discher and A. Eisenberg, *Science*, 2002, **297**, 967-973.
141. D. E. Discher and F. Ahmed, *Annual Review of Biomedical Engineering*, 2006, **8**, 323-341.
142. K. E. B. Doncom, L. D. Blackman, D. B. Wright, M. I. Gibson and R. K. O'Reilly, *Chemical Society Reviews*, 2017, **46**, 4119-4134.
143. T. C. Ngo, R. Kalinova, D. Cossement, E. Hennebert, R. Mincheva, R. Snyders, P. Flammang, P. Dubois, R. Lazzaroni and P. Leclère, *Langmuir*, 2014, **30**, 358-368.
144. H. Kaddami, F. Surivet, J. F. Gérard, T. M. Lam and J. P. Pascault, *Journal of Inorganic and Organometallic Polymers*, 1994, **4**, 183-198.
145. Y. S. Jung and C. A. Ross, *Nano Letters*, 2007, **7**, 2046-2050.
146. C. G. Gamys, E. Beyou and E. Bourgeat-Lami, *Journal of Polymer Science Part A: Polymer Chemistry*, 2010, **48**, 784-793.
147. J. Du and Y. Chen, *Macromolecules*, 2004, **37**, 6322-6328.

148. Y. Zhang, S. Luo and S. Liu, *Macromolecules*, 2005, **38**, 9813-9820.
149. M. J. Derry, L. A. Fielding and S. P. Armes, *Progress in Polymer Science*, 2016, **52**, 1-18.
150. N. J. Warren and S. P. Armes, *Journal of the American Chemical Society*, 2014, **136**, 10174-10185.
151. A. B. Lowe, *Polymer*, 2016, **106**, 161-181.
152. W. D. He, X. L. Sun, W. M. Wan and C. Y. Pan, *Macromolecules*, 2011, **44**, 3358-3365.
153. Y. Pei, L. Thurairajah, O. R. Sugita and A. B. Lowe, *Macromolecules*, 2015, **48**, 236-244.
154. S. L. Canning, G. N. Smith and S. P. Armes, *Macromolecules*, 2016, **49**, 1985-2001.
155. B. Charleux, G. Delaittre, J. Rieger and F. D Agosto, *Macromolecules*, 2012, **45**, 6753-6765.
156. R. Jutta, *Macromolecular Rapid Communications*, 2015, **36**, 1458-1471.
157. J. T. Sun, C. Y. Hong and C. Y. Pan, *Polymer Chemistry*, 2013, **4**, 873-881.
158. W. M. Wan, C. Y. Hong and C. Y. Pan, *Chemical Communications*, 2009, **0**, 5883-5885.
159. J. L. d. l. Haye, X. W. Zhang, I. Chaduc, F. Brunel, M. Lansalot and F. D. Agosto, *Angewandte Chemie International Edition*, 2016, **55**, 3739-3743.
160. M. Semsarilar, V. Ladmiral, A. Blanazs and S. P. Armes, *Polymer Chemistry*, 2014, **5**, 3466-3475.
161. X. Zhang, J. Rieger and B. Charleux, *Polymer Chemistry*, 2012, **3**, 1502-1509.
162. M. Semsarilar, E. R. Jones, A. Blanazs and S. P. Armes, *Advanced Materials*, 2012, **24**, 3378-3382.
163. L. P. D. Ratcliffe, B. E. McKenzie, G. M. D. Le Bouëdec, C. N. Williams, S. L. Brown and S. P. Armes, *Macromolecules*, 2015, **48**, 8594-8607.
164. B. Karagoz, C. Boyer and T. P. Davis, *Macromolecular Rapid Communications*, 2014, **35**, 417-421.
165. Y. Deng, C. Yang, C. Yuan, Y. Xu, J. Bernard, L. Dai and J. F. Gérard, *Journal of Polymer Science Part A: Polymer Chemistry*, 2013, **51**, 4558-4564.
166. J. Zhou, H. Yao and J. Ma, *Polymer Chemistry*, 2018, **9**, 2532-2561.
167. X. Zhang, S. Boissé, W. Zhang, P. Beaunier, F. D Agosto, J. Rieger and B. Charleux, *Macromolecules*, 2011, **44**, 4149-4158.
168. W. Zhang, B. Charleux and P. Cassagnau, *Macromolecules*, 2012, **45**, 5273-5280.
169. B. Stéphanie, R. Jutta, P. Gaëlle, B. Patricia and C. Bernadette, *Journal of Polymer Science Part A: Polymer Chemistry*, 2011, **49**, 3346-3354.
170. W. Zhang, F. D Agosto, O. Boyron, J. Rieger and B. Charleux, *Macromolecules*, 2012, **45**, 4075-4084.
171. W. Zhang, F. D Agosto, P. Y. Dugas, J. Rieger and B. Charleux, *Polymer*, 2013, **54**, 2011-2019.
172. T. Taner, O. Oğuz and S. I. Çetin, *Journal of Applied Polymer Science*, 1996, **61**, 485-493.
173. A. R. Goodall, M. C. Wilkinson and J. Hearn, *Journal of Polymer Science: Polymer Chemistry Edition*, 1977, **15**, 2193-2218.
174. U. John, H. F. Knut and L. Svein, *Die Makromolekulare Chemie*, 1974, **175**, 507-521.
175. H. Ni, Y. Du, G. Ma, M. Nagai and S. Omi, *Macromolecules*, 2001, **34**, 6577-6585.
176. H. Kobayashi, E. Miyanaga and M. Okubo, *Langmuir*, 2007, **23**, 8703-8708.
177. A. M. Telford, B. T. T. Pham, C. Neto and B. S. Hawkett, *Journal of Polymer Science Part A: Polymer Chemistry*, 2013, **51**, 3997-4002.
178. S. Eggers and V. Abetz, *Polymers*, 2017, **9**, 668.

179. S. L. Canning, V. J. Cunningham, L. P. D. Ratcliffe and S. P. Armes, *Polymer Chemistry*, 2017, **8**, 4811-4821.
180. A. A. Cockram, T. J. Neal, M. J. Derry, O. O. Mykhaylyk, N. S. J. Williams, M. W. Murray, S. N. Emmett and S. P. Armes, *Macromolecules*, 2017, **50**, 796-802.
181. S. Boisse, J. Rieger, K. Belal, A. Di Cicco, P. Beaunier, M. H. Li and B. Charleux, *Chemical Communications*, 2010, **46**, 1950-1952.
182. X. Wang, Y. Luo, B. Li and S. Zhu, *Macromolecules*, 2009, **42**, 6414-6421.
183. V. J. Cunningham, A. M. Alswieleh, K. L. Thompson, M. Williams, G. J. Leggett, S. P. Armes and O. M. Musa, *Macromolecules*, 2014, **47**, 5613-5623.
184. J. Rieger, W. Zhang, F. Stoffelbach and B. Charleux, *Macromolecules*, 2010, **43**, 6302-6310.
185. N. P. Truong, M. V. Dussert, M. R. Whittaker, J. F. Quinn and T. P. Davis, *Polymer Chemistry*, 2015, **6**, 3865-3874.
186. W. Zhang, F. D Agosto, O. Boyron, J. Rieger and B. Charleux, *Macromolecules*, 2011, **44**, 7584-7593.
187. I. Chaduc, A. Crepet, O. Boyron, B. Charleux, F. D Agosto and M. Lansalot, *Macromolecules*, 2013, **46**, 6013-6023.
188. S. Y. Khor, N. P. Truong, J. F. Quinn, M. R. Whittaker and T. P. Davis, *ACS Macro Letters*, 2017, **6**, 1013-1019.

Chapter 2 : Experimental Methods

This chapter reports all the experimental and instrumental procedures applied in this thesis.

2.1 Materials

3-(Trimethoxysilyl) propyl methacrylate (MPS; 98%), benzyl methacrylate (BzMA; 96%), lauryl methacrylate (LMA; 96%), poly(ethylene glycol) methyl ether (PEG; average M_n = 2000), poly(ethylene glycol) methyl ether methacrylate (PEGMA; average M_n 300 and 950), 4-cyanopentanoic acid dithiobenzoate (CPADB; >97%), 4-cyano-4-[(dodecylsulfanylthiocarbonyl) sulfanyl] pentanoic acid (CDTSPA; 97%), tetraethyl orthosilicate (TEOS; 98%), 1,3,5-trioxane (>99%), N,N'-dicyclohexylcarbodiimide (DCC; 99%), 4-(dimethylamino)pyridine (DMAP; >99%), p-toluenesulfonic acid (99%), triethylamine (TEA; >99%), octylamine (99%), hexadecane (HD; 99%), tertbutylhydroperoxide (70% w/w in water), L-ascorbic acid (reagent grade), 4-tert-butylcatechol (97%), chromium(III) acetylacetonate (97%), Nile Blue A (>75%), and 1,4-dioxane (>99%) were purchased from Sigma Aldrich, Australia. 4,4-Azobis(4-cyanovaleric acid) (ACVA; 98%) was purchased from Alfa Aesar, and ammonium hydroxide (30% w/w aqueous solution) was purchased from ChemSupply. Hydrochloric acid (HCl; 37%) was purchased from Scharlau. Sulphuric acid (H_2SO_4; 98%) was purchased from Ajax Finechem. All the reagents were used as received unless otherwise stated. Benzyl methacrylate and lauryl methacrylate were deinhibited through a basic alumina column and stored in the freezer prior to use. A pH 7 buffer was prepared from potassium dihydrogen phosphate and di-sodium hydrogen phosphate (ionic strength = 0.01 M). Methanol, ethanol, isopropanol, toluene,

petroleum spirit (60–80 ºC), diethyl ether, dimethylformamide (DMF), tetrahydrofuran (THF) and *n*-hexane used were analytical reagent (AR) grade and the water used was Milli-Q standard.

2.2 Monomer Synthesis

2.2.1 Synthesis of 3-(Triisopropoxysilyl) Propyl Methacrylate (IPS)

The synthesis of 3-(triisopropoxysilyl) propyl methacrylate (IPS) was modified slightly from previous procedures.[1, 2] *p*-Toluenesulfonic acid (0.1 g) and 4-tert-butylcatechol (0.02 g) were dissolved in isopropanol (40 mL). MPS (10 g, 9.6 mL) was added to the solution that was distilled at 110 °C for 5 hours, with further addition of isopropanol (20 mL) every 30 minutes. After 5 hours the mixture was allowed to cool, then poured into a saturated aqueous sodium bicarbonate solution (100 mL), followed by extraction into hexane (3 × 50 mL). The combined hexane layers were washed with a saturated aqueous sodium chloride solution (∼100 mL) and the resultant hexane layer was dried over anhydrous magnesium sulphate overnight. Hexane was removed via rotary evaporation and the product then dried under vacuum at room temperature for 3 hours. The product was purified by passage through a basic alumina column and stored at 4 °C until needed. IPS was a clear and pale yellow liquid. The yield was around 65%. ^{1}H NMR (400 MHz, $CDCl_3$, δ(ppm)): 0.577–0.726 (dd, 2H, CH_2), 1.15–1.26 (d, J = 6.03 Hz, 18H, $(CH_3)_6$), 1.72–1.85 (m, 2H, CH_2), 1.95 (s, 3H, CH_3), 4.08–4.16 (m, 2H, CH_2), 4.17–4.28 (m, 3H, $(CH)_3$), 5.54 (s, 1H, CH_2), and 6.1 (s, 1H, CH_2). The ^{29}Si NMR spectrum of IPS consisted of a T^0 peak (−50.2 ppm) as well as a minor T^2 peak at −56.6 ppm, suggesting a small degree of condensation in the monomer (this peak corresponded to Si atoms with two Si–O–Si linkages).[3]

2.3 MacroRAFT Agent Syntheses

2.3.1 MPS-based MacroRAFT Agents

An example procedure for a target DP of 40 units using CPADB is described. MPS (2.377 mL, 10 mmol), CPADB (69.9 mg; 0.25 mmol), 1,3,5-trioxane (150 mg, 1.67 mmol) and ACVA (28 mg, 0.1 mmol; [CPADB]/[ACVA] ratio = 2.5) were dissolved in 1,4-dioxane (9 mL) in a Schlenk flask. The solution was deoxygenated via three freeze–pump–thaw cycles, filled with high purity Ar gas, and then placed in a pre-heated oil bath at 65 °C overnight with magnetic stirring. Following polymerization, the flask was allowed to cool, opened to the air and the polymer isolated by precipitation into a tenfold excess of hexane. After precipitation, the solid was transferred to a glass vial, partial air dried for 5 minutes, dissolved in ethanol at a concentration of ~100 mg mL^{-1} and stored in the freezer until needed. The hexane content in the ethanolic solution was never more than 0.4 mol % by ^{1}H NMR. Similar reaction conditions were used to synthesize PMPS-based macroRAFT agents with a differing DP or different RAFT agent (CDTSPA).

2.3.2 IPS-based MacroRAFT Agents

PIPS macroRAFT agent (CPADB and CDTSPA) with DPs of 40 and 65 were synthesized by applying an identical procedure to that described for PMPS (Section 2.3.1), except the polymer was precipitated into a methanol/water (8:2 volume ratio) mixture.[1, 4]

2.3.3 PEGMA-based MacroRAFT Agents

Three different chain lengths of PEGMA (M_n 950)-based macroRAFT agents were prepared with targeting average degrees of polymerization (DP) of 10, 20, and 40 units. A typical method for a target DP of 20 units using CDTSPA is described as follows. PEGMA (M_n 950; 2 g, 2.11 mmol), CDTSPA (0.0425 g, 0.105 mmol), ACVA (0.0118 g, 0.0421 mmol; [CDTSPA]/[ACVA] ratio = 2.5), and 1,3,5 trioxane (0.032 g, 0.351 mmol, acting as internal reference) were dissolved in 1,4-dioxane (4.726 mL) in a Schlenk flask. The solution was deoxygenated via three freeze–pump–thaw cycles, filled with high purity Argon gas, and then placed in a pre-heated oil bath at 80 ^{o}C for 24 hours with magnetic stirring. After polymerization, the flask was allowed to cool, exposed to air and the homopolymer was isolated via precipitation into a 10-fold excess of diethyl ether. The collected polymer was dried at 30 ^{o}C under vacuum overnight prior to characterization. Fractional conversion of monomer to polymer was determined by ^{1}H NMR spectroscopy and was 0.87, 0.89, and 0.89 respectively for the three macroRAFT agents. The PEGMA (M_n 950) macroRAFT agents were denoted as $PEGMA_{9}$, $PEGMA_{18}$, and $PEGMA_{36}$, the subscript reflecting the theoretical DP of the polymer.

PEGMA (M_n 300) macroRAFT agents with DP of 20, 40, and 60 were using a similar approach that described in PEGMA (M_n 950), except the temperature was 65 ^{o}C and the resultant polymer was precipitated into *n*-hexane. The PEGMA (M_n 300) macroRAFT agents were denoted as $PEGMA_{19}$, $PEGMA_{39}$, and $PEGMA_{58}$, the subscript reflecting the theoretical DP of the polymer.

2.3.4 LMA-based MacroRAFT Agents

PLMA macroRAFT agent with DP of 40 was synthesized by applying an identical procedure to that described for PEGMA (M_n 950; Section 2.3.3), except the reaction temperature was set to 65 ^{o}C and polymer was precipitated into a methanol. The theoretical DP of PLMA macroRAFT was 38 and subsequently denoted as $PLMA_{38}$.

2.4 PEG-Trithiocarbonate based RAFT Agent Synthesis

The preparation of PEG-trithiocarbonate based RAFT agent was conducted via esterification of the carboxylic acid group (from RAFT agent) with PEG bearing a hydroxyl endgruop. The process used in this work adopted the method in published papers with some modifications[5-8] and carried out as follows. PEG (2000 Da nominal mass) (0.7 g, 0.35 mmol), DMAP (0.0385 g, 0.32 mmol), and CDTSPA (0.17 g, 0.42mmol) were dissolved in 5 mL of THF. The solution was bubbled with argon at 0 ^{o}C for 10 minutes. After 10 minutes bubbling, 2.5 mL of THF containing DCC (0.13 g, 0.63 mmol) was added via syringe and needle. The whole solution was stirred for 24 hours at room temperature. The obtained solution was filtered and the filtrate was precipitated into large excess of cold hexane:diethyl ether (1:1 v/v). The collected yellow solid was dissolved in THF and precipitated into cold hexane:diethyl ether again. The recovered yellow solid was then dried at 30 ^{o}C under vacuum overnight. The yield was around 35%. A reaction scheme can be viewed in Figure 4-5.

2.5 Nile Red Synthesis

Nile Red was synthesised according to a previously published procedure.[9] Briefly, Nile Blue (0.4619 g, 0.63 mmol) was dissolved in 250 mL of 0.5% H_2SO_4 and the solution was heated under reflux condition for 2 hours. After cooling to room temperature, the product was extracted using toluene until a light pink colour appeared in the organic phase. Toluene was removed by rotary evaporation, leaving a dark purple residue (0.112 g; yield = 57%). The compound (referred to as Nile Red) was confirmed by using ^{1}H NMR (400 MHz, DMSO-d_6, δ(ppm)): 1.15-1.21 (t, 6H, $(CH_3)_2$), 3.48-3.56 (q, 4H, $(CH_2)_2$), 6.30-6.32 (s, 1H, CH), 6.67-6.71 (d, 1H, CH), 6.84-6.89 (dd, 1H, CH), 7.63-7.68 (d, 1H, CH), 7.71-7.76 (td, 1H, CH), 7.79-7.84 (td, 1H, CH), 8.12-8.16 (dd, 1H, CH), and 8.56-8.60 (dd, 1H, CH).

2.6 Polymerization-Induced Self-Assembly (PISA)

2.6.1 PISA of BzMA Using a MPS or IPS-Based MacroRAFT Agent

MPS-based macroRAFT agents were chain extended with benzyl methacrylate (BzMA) in ethanol via RAFT dispersion polymerization. An example of the synthesis of $PMPS_{40}$-b-$PBzMA_{400}$ at 20% w/w solids is given. Deinhibited BzMA (0.795 mL, 4.69 mmol), ACVA (0.7 mg, 0.0025 mmol; [macroCTA]/[ACVA] ratio = 5), and 1,3,5-trioxane (70 mg, 0.777 mmol) were dissolved in ethanol (3.666 mL, 2.892 g). Then, 1 mL of ethanol containing $PMPS_{40}$ macroRAFT agent (0.111 g, 0.0117 mmol) was added to the mixture. The reaction mixture was deoxygenated by three freeze–pump–thaw cycles and filled with Argon gas. The reaction flask was placed in preheated oil bath with stirring at 65 °C for 24 hours. The block

copolymer was isolated by precipitation into ten-fold hexane and partial air dried prior to NMR and SEC analyses. For PISA experiments with the PIPS macroRAFT agent, the resultant copolymer was precipitated into methanol/water (8:2 volume ratio) mixture. A general reaction scheme can be viewed in Figure 3-3.

2.6.2 Attempted PISA of MPS in Water Using PEGMA-based MacroRAFT Agent

Below is a typical approach at performing PISA of MPS in water using the PEGMA (M_n 950)$_{18}$ macroRAFT agent. To prepare PEGMA (M_n 950)$_{18}$-b-PMPS$_{100}$ at 10% w/w, PEGMA (M_n 950)$_{18}$ macroRAFT agent (0.1826 g, 0.0099 mmol) was added to a reaction flask along with MPS (0.235 mL, 0.99 mmol), ACVA (0.0011 g, 0.004 mmol; [macroRAFT]/[ACVA] = 2.5) and pH 7 buffer (3.843 mL). The reaction solution was purged via bubbling with Argon gas for 15 minutes in an icebath. The flask was immersed in a preheated oil bath at 65 ^{o}C and polymerization was allowed to proceed for 24 hours with magnetic stirring. The reaction was halted via exposure to air and cooling to room temperature. For PISA approach of MPS with PEG2000-CDTSPA, an approach used in PEGMA (M_n 950)$_{18}$-PMPS was applied. When redox initiation (TBHP/ascorbic acid) was used to initiate polymerization, a similar procedure to that stated above was used, however the reaction temperature was 25 ^{o}C. The [macroRAFT]: [initiator] ratio was held at 2.5. Deoxygenated solutions of TBHP and ascorbic acid were added sequentially via syringe, with 2 minutes of Argon bubbling prior to each addition. DMF was used as an internal standard in both attempted PISA experiments (at 65 ^{o}C with thermal initiation and 25 ^{o}C with redox initiation). A general reaction scheme can be viewed in Figure 4-1.

Due to difficulties with re-dissolving vacuum dried poly(MPS) in good solvents as a result of intra- and inter-molecular crosslinking in the solid state, the nanoparticle dispersion was first dialyzed against water (to remove dissolved salts) then subsequently THF prior to SEC analysis.

2.6.3 PISA of ABC-Type Triblock Copolymers with an MPS-based "B" Block and the Simultaneous Encapsulation of Nile Red

ABC-type triblock copolymers were prepared via RAFT polymerization and PISA approach via a one-pot approach. A representative synthesis of PEGMA (M_n 300)$_{19}$-b-PMPS$_{20\text{-}y}$-b-(PMPS$_y$-grad-PBzMA$_{400}$) at 10% w/w solids is given. *y* is the remaining MPS monomers after chain extension with PEGMA (M_n 300)$_{19}$ macroRAFT agent. MPS monomer (0.1 mL, 0.42 mmol), ACVA (2.4 mg, 0.0086 mmol; [macroCTA]/[ACVA] ratio = 2.5) and 1,3,5-trioxane (6.3 mg, 0.07 mmol) were dissolved in isopropanol (1.819 mL, 1.43 g). PEGMA (M_n 300)$_{19}$ macroRAFT agent (0.133 g, 0.021 mmol) was dissolved in isopropanol (1 mL, 0.786 g) under gentle heating with hot water due to the temperature-dependent solubility (UCST) of the PEGMA block in this solvent.[10] Both solutions were mixed together and deoxygenated by three freeze-pump-thaw cycles and filled with Argon gas. The reaction flask was placed in a preheated oil bath with stirring at 65 ^{o}C for 24 hours. An aliquot was taken at the end of the reaction to determine the conversion of MPS into polymer via ^{1}H NMR. No polymer purification was carried out due to difficulties in isolating the polymer while avoiding crosslinking and gelation, likely due to crosslinking of MPS units. The mass of PEGMA (M_n 300)$_{19}$-b-PMPS$_{20\text{-}y}$ macroRAFT agent was estimated by using the MPS conversion and the dry mass of PEGMA (M_n 300)$_{19}$ macroRAFT agent. Then, deinhibited BzMA (1.423 mL, 8.4 mmol), ACVA (2.4 mg, 0.0086 mmol; [macroCTA]/[ACVA] ratio = 2.5), and 1,3,5-trioxane

(0.12 g, 1.3 mmol) were dissolved in a mixture of isopropanol (17.267 mL, 13.58 g) and MilliQ water (0.837 mL, 0.837 g). This solution was transferred into the same flask and mixed with PEGMA (M_n 300)$_{19}$-b-PMPS$_{20\text{-}y}$ macroRAFT agent (0.2192 g, 0.021 mmol) solution. After mixing, the whole solution was made up to a composition of isopropanol:MilliQ 96:4% v/v to avoid precipitation of the triblock copolymer at room temperature. The solids content was still maintained at 10% w/w. The reaction flask was deoxygenated by three freeze-pump-thaw cycles and placed in an oil bath with stirring at 65 ^{o}C for 24 hours. A general reaction scheme can be viewed in Figure 5-15.

The simultaneous encapsulation of an organic dye into the particle core was achieved via using the same protocol of PEGMA (M_n 300)$_{19}$-b-PMPS$_{20\text{-}y}$-b-(PMPS$_y$-grad-PBzMA$_{400}$) synthesis in the presence of Nile Red. The process was performed via using a one-pot approach. Nile Red was dissolved in the mixture that consisted of BzMA monomer, ACVA initiator, trioxane, PEGMA-b-PMPS macroRAFT agent, and isopropanol:MilliQ water (96:4 % v/v). Then, the purple-red solution followed the same procedure described in above for deoxygenation, reaction conditions, and purification. Nile Red was added to a constant amount with respect to the dry mass of PEGMA macroRAFT agent (0.6% w/w).[11] The excess Nile Red was removed via dialysis against isopropanol:MilliQ water (96:4 % v/v) for 3 days. The isopropanol:MilliQ water (96:4 % v/v) was changed daily.

2.7 Solvent-Induced Self-Assembly of Block Copolymers

2.7.1 Self-Assembly of PEGMA (M_n 950)-b-PMPS and PEGMA (M_n 950)-b-IPS in Water

3-(Trimethoxysilyl) propyl methacrylate (MPS) was used to chain-extend PEGMA (M_n 950)-based macroRAFT agents in 1,4-dioxane via RAFT solution polymerization, for a variety of different DPs of the MPS block. An example of the synthesis of PEGMA $(M_n\ 950)_{18}$-b-$PMPS_{100}$ at 10% w/w solids content is given. PEGMA $(M_n\ 950)_{18}$ macroRAFT agent (0.1504 g, 0.00909 mmol), MPS (0.216 mL, 0.909 mmol), ACVA (0.001 g, 0.00363 mmol; [macroCTA]/[ACVA] ratio = 2.5), and 1,3,5-trioxane (0.0136 g, 0.151 mmol) were dissolved in 1,4-dioxane (3.414 mL, 3.516 g) in a Schlenk flask. The reaction mixture was deoxygenated by three freeze–pump–thaw cycles and filled with Argon gas. The flask was placed in preheated oil bath at 65 ^{o}C for 24 hours with continuous stirring. After polymerization, the block copolymer was precipitated into 10-fold hexane and partial air-dried prior to NMR and SEC analyses.

To induce self-assembly, Milli-Q water was injected into the polymer solution at a rate of 1.2 mL $hour^{-1}$ via a syringe pump (NE-4000 dual syringe pump, New Era pump systems) under constant stirring at room temperature. The final concentration of polymer was 1% w/w. Then, the sample was transferred into a dialysis bag (MWCO 3500 Da) and dialyzed against Milli-Q water for 3 days. Water was changed daily.

Block copolymers based on the chain extension of PEGMA (M_n 950)-based macroRAFT agents (theoretical DP = 18) with IPS were prepared via a similar approach to that described

for PEGMA (M_n 950)-b-PMPS, except the block copolymer was dialyzed against THF prior to SEC analysis. A general reaction scheme can be viewed in Figure 4-18. The self-assembly of this block copolymer was induced by addition of Milli-Q water and applying an identical method mentioned in PEGMA (M_n 950)-b-PMPS. The sample was then transferred into a dialysis bag (MWCO 3500 Da) and dialyzed against Milli-Q water for 3 days. Water was changed daily.

2.7.2 Self-Assembly of PLMA-b-PMPS in n-Hexane

A similar approach to that of PEGMA-b-PMPS was applied in preparing $PLMA_{38}$-b-$PMPS_y$ block copolymers, where *y* was the targeted number of MPS units (ranging from 80 to 1000). A general reaction scheme can be viewed in Figure 4-23. These block copolymers were precipitated into an ethanol/water (2:8 volume ratio) mixture prior to characterisations. The self-assembly of this block copolymer was induced by addition of *n*-hexane (a non-solvent for the MPS block) and using similar addition conditions via syringe pump to those described in PEGMA-b-PMPS. Then, the sample was transferred into a dialysis bag (MWCO 3500 Da) and dialyzed against hexane for 3 days. Hexane was changed daily.

2.8 Oil-in-Water Miniemulsion Stabilized by ABC-Type Triblock Copolymers

The synthesis of ABC-type triblock copolymers was similar to the method described in Section 2.6.3, except this process was performed in two steps. An example of the preparation of PEGMA (M_n 950)$_{18}$-b-$PMPS_{20}$-b-$PBzMA_{100}$ at 10% w/w is given. PEGMA (M_n 950)$_{18}$ macroRAFT agent (0.2565 g, 0.0147mmol), MPS (0.07 mL, 0.295 mmol), ACVA (0.0016 g,

0.00571 mmol; [macroCTA]/[ACVA] ratio = 2.5), and 1,3,5-trioxane (0.0044 g, 0.0488 mmol) were dissolved in 1,4-dioxane (2.93 mL, 3.02 g) in a Schlenk flask. The reaction mixture was deoxygenated by three freeze–pump–thaw cycles and filled with Argon gas. The flask was placed in a preheated oil bath at 65 ^{o}C for 24 hours with continuous stirring. After polymerization, an aliquot was taken to determine the conversion of MPS into polymer via ^{1}H NMR. A general reaction scheme can be viewed in Figure 5-2. The block copolymer was precipitated into 10-fold hexane and partially air-dried. The mass of incomplete dry PEGMA (M_n 950)$_{18}$ – PMPS$_{20}$ macroRAFT agent was measured and re-dissolved in dioxane. For the subsequent chain extension with BzMA, PEGMA (M_n 950)$_{18}$ – PMPS$_{20}$ macroRAFT agent (0.2379 g, 0.0111 mmol), BzMA (0.19 mL, 1.11 mmol), ACVA (0.0013 g, 0.00464 mmol; [macroCTA]/[ACVA] ratio = 2.5), and 1,3,5-trioxane (0.0168 g, 0.187 mmol) were dissolved in 1,4-dioxane (3.962 mL, 4.08 g). The reaction was deoxygenated again via free-pump-thaw and placed in an oil bath at 65 ^{o}C for 24 hours. After the reaction completed, the triblock copolymer was precipitated into hexane and the collected copolymer was partially air-dried. The mass of triblock copolymer (not vacuum dried) was recorded and dissolved in toluene at a concentration of 20 % w/w.

A toluene-in-water miniemulsion was formed via the following approach. 1 g of toluene (containing 200 mg of triblock copolymer) was mixed with 0.05 g of hexadecane. The total mass fraction of oil phase was maintained at 20% w/w via addition of MilliQ water to form a biphasic mixture. The mixture was ultrasonicated on ice (Branson Model 450 Digital Sonifier with microtip, 5 mins cycle, 30% amplitude, 200 W) to form a homogeneous milky white solution. The type of the emulsion was confirmed by a drop test.

2.9 Silica Synthesis and Crosslinking

2.9.1 Hydrolysis and Condensation of TEOS to Yield Silica Shells

A typical sol–gel experiment was adapted from the procedure of Tissot et al.[12] Briefly, a volume of ethanolic nanoparticle dispersion (e.g. PMPS-b-PBzMA, see Section 2.6.1) corresponding to 1 g of polymer was diluted with further ethanol to a total amount of solvent 100 g. To this solution, ammonium hydroxide (30% w/w) was added so that the concentration of base was 0.4 M. A separate solution of 15 g of TEOS in 15 g ethanol was injected into the ethanolic dispersion at a rate of 1 mL/hr via syringe pump under constant magnetic stirring at room temperature. A range of parameters were studied such as the total amount of TEOS added, concentration of base and the feed rate. The resulting particle dispersion was centrifuged at 4000 rpm and then redispersed into fresh ethanol. A general schematic diagram can be viewed in Figure 3-14.

2.9.2 Base-Catalysed Cross-linking of MPS-functional Capsules and Miniemulsion Droplets

Different base catalysts were used to induce crosslinking of MPS. For miniemulsions prepared in Section 2.8, 1 mL of the resulting miniemulsion was extracted and 0.112 mL of triethylamine was added to form a catalyst concentration of 0.8 mol L^{-1}. The solution was stirred overnight in an oil bath at 25 ^{o}C. Other catalysts were also utilised such as hydrochloric acid and octylamine. The catalyst concentration was remained the same.

For interfacial crosslinking of the nanoparticle dispersions prepared by the PISA process (Section 2.6.3), 0.208 mL of ammonium hydroxide solution was added to 2 mL of triblock copolymer dispersion to form a catalyst concentration of 0.8 mol L^{-1}. The solution was stirred overnight in an oil bath at 25 ^{o}C. When Nile Red was present, the crosslinked particle dispersion was dialyzed against isopropanol:MilliQ (96:4% v/v) solvent for 3 days. The solvent was changed daily.

2.10 Instrumentation and Analytical Methods

Below are the main characterisation methods used in this thesis.

2.10.1 Nuclear Magnetic Resonance Spectroscopy (NMR)

Proton (^{1}H) spectra were acquired with a 300 MHz Bruker Avance III NMR spectrometer. Deuterated chloroform ($CDCl_3$) or deuterated acetone was used as NMR solvents. ^{1}H NMR was used to determine the fractional conversion of monomer to polymer by comparing the integral of vinylic protons of methacrylate-based monomers (MPS, IPS, PEGMA, LMA, and BzMA, $\delta \sim 5.54$ and 6.10 ppm) before and after polymerization to an internal reference (either 1,3,5-trioxane ($\delta = 5.15$ ppm) or DMF ($\delta = 7.96$ ppm)). 1,3,5-Trioxane was used as reference for solution polymerization; for heterogeneous systems, DMF in acetone-d_6 was used (both the continuous and dispersed phases of the reaction are miscible with both acetone and DMF).

Silicon (^{29}Si) NMR spectra were acquired on the same instrument at a frequency of 79.39 MHz, both with and without TMS as internal reference. Due to solubility issues, $CDCl_3$ or acetone-d_6 containing a small amount of chromium(III) acetylactonate was used as solvent for the macroRAFT agent and diblock copolymer. Chromium(III) acetylactonate is a paramagnetic relaxing agent and used to reduce recycle delay.[13] ^{29}Si NMR spectra were recorded at 298.15 K with 6000 scans and a dwell time of 31.73 μs, with background noise minimized by spectral subtraction method.

2.10.2 Dynamic Light Scattering (DLS)

Hydrodynamic diameters were measured by using a Malvern ZetaSizer Nanoseries integrated with DTS software. The measurement was carried out at 298 K using a 4 mW He–Ne laser with wavelength 633 nm. The scattering angle was 173°. Results were based on the average values of three independent measurements. Highly diluted solutions were used to determine particle sizes (2 drops of the sample in approximately 20 mL of selected solvent).

2.10.3 Scanning Electron Microscopy (SEM)

Particle characteristics (surface structure, size, and shape) were determined by using Hitachi SU-70 Analytical Field Emission SEM. Specimens were prepared by drying a drop of diluted sample solution on aluminium stubs. The accelerating voltage was set to 1.5 kV. Dried sample studs were sputter-coated using a Platinum Coater BalTec SCD050 prior to imaging.

2.10.4 Transmission Electron Microscopy (TEM)

For Chapter 3 and 4, particle features (interior structure, size, and morphology) were determined by using a FEI Tecnai (FEI, OR, USA). The accelerating voltage was 200 kV. Images were recorded digitally using an Eagle 2k CCD camera (FEI) and Digital Micrograph (Gatan).

For Chapter 5, a Hitachi HT 7700 transmission electron microscope was used. The accelerating voltage was set to 80 kV. Images were recorded digitally via using a XR-81 CCD camera (AMT). Sample preparation was identical for both instruments, where all samples were prepared via using a drop-cast method onto carbon-coated 300 mesh copper grids.

2.10.5 Thermogravimetric Analysis (TGA)

Thermal analysis was carried out via using a LABSYS Evo TG-DSC 1600C Thermogravimeter. An aluminium crucible (100 μL) was used to hold the sample in the furnace. Approximately 15 mg of samples were used and heated from 25 °C to 550 °C at a rate of 10 °C min^{-1} in a nitrogen atmosphere.

2.10.6 X-ray Photoelectron Spectroscopy (XPS)

Elemental compositions were analysed through an Escalab250Xi X-ray photoelectron spectrometer (Thermo Scientific). The Al Kα incident radiation (1486.6 eV) was set at 150 W

(13 kV, 12 mA). Survey scans were taken over a binding energy range of 1360–0 eV (1 eV steps) with a dwell time of 100 ms; higher resolution scans were taken with 0.1 eV steps and a 250 ms dwell time. Data was analysed using Avantage software (Thermo Scientific).

2.10.7 Size Exclusion Chromatography (SEC)

In Chapters 3 and 4, polymer molecular weights and distributions were determined via using a Shimadzu system with refractive index detection (RID-10A), four Phenogel columns (105, 104, 103 and 500 Å pore size) and THF as eluent (flow rate 1 mL min^{-1}). All polymer samples were dissolved overnight in the eluent at a concentration ~3 mg mL^{-1}, then filtered through a 450 nm Nylon filter. The columns were housed in a CTO-10AC VP Shimadzu column oven set at 40 °C. Calibration was performed using a series of linear polystyrene standards (Polymer Laboratories) spanning a mass range of 0.6 to 1820 kDa.

In Chapter 5, the polymer sample preparation was maintained the same as above (dissolved overnight in THF at a concentration of ~ 3 mg/mL and filtered through a 450 nm PTFE filter). The polymer molecular weights and distributions were determined via using a Viscotek system with refractive index detection (VE 3580), a PLgel guard column, two PLgel columns (MIXED-C, mixed pore size) and THF as eluent (flow rate 1 mL/min). The columns were warmed in a Phenomenex column oven (TS-430) set at 40 °C. Calibration was performed using a series of linear polystyrene standards (PSS-Polymer) spanning a mass range of 0.27 to 66 kDa.

2.10.8 Ultraviolet–Visible Spectroscopy (UV-Vis)

The samples were prepared by adding 1 ml of dialysed Nile Red solution into 9 ml of fresh dioxane. The samples were allowed to stand for 24 hours before analysis. UV-visible spectra were recorded in a glass cuvette using an UV Mate spectrophotometer (Metertech). The samples were scanned with a wavelength range from 400 to 800 nm.

2.11 References

1. H. Ozaki, A. Hirao and S. Nakahama, *Macromolecules*, 1992, **25**, 1391-1395.
2. M. Rabnawaz, Z. Wang, Y. Wang, I. Wyman, H. Hu and G. Liu, *RSC Advances*, 2015, **5**, 39505-39511.
3. E. Borovin, E. Callone, F. Ribot and S. Diré, *European Journal of Inorganic Chemistry*, 2016, **2016**, 2166-2174.
4. K. Zhang, L. Gao and Y. Chen, *Macromolecules*, 2007, **40**, 5916-5922.
5. T. Boursier, I. Chaduc, J. Rieger, F. D Agosto, M. Lansalot and B. Charleux, *Polymer Chemistry*, 2011, **2**, 355-362.
6. L. Ahmadkhani, M. Abbasian and A. Akbarzadeh, *Designed Monomers and Polymers*, 2017, **20**, 406-418.
7. X. Huang, S. I. Sevimli and V. Bulmus, *European Polymer Journal*, 2013, **49**, 2895-2905.
8. Q. Zheng, G. H. Zheng and C. Y. Pan, *Polymer International*, 2006, **55**, 1114-1123.
9. P. Greenspan and S. D. Fowler, *Journal of Lipid Research*, 1985, **26**, 781-789.
10. P. J. Roth, F. D. Jochum and P. Theato, *Soft Matter*, 2011, **7**, 2484-2492.
11. B. Karagoz, C. Boyer and T. P. Davis, *Macromolecular Rapid Communications*, 2014, **35**, 417-421.
12. I. Tissot, J. P. Reymond, F. Lefebvre and E. Bourgeat-Lami, *Chemistry of Materials*, 2002, **14**, 1325-1331.
13. G. Agrawal, M. Schürings, X. Zhu and A. Pich, *Polymer*, 2012, **53**, 1189-1197.

Chapter 3 : Polymer-Inorganic Hybrid Nanoparticles of Various Morphologies via Polymerization-Induced Self-Assembly and Sol–Gel Chemistry

3.1 Introduction

Polymer-inorganic hybrid materials have been researched intensively over the last few decades. Hybrid materials can combine the beneficial properties of each component and minimize disadvantageous ones, as often single-component materials have limited physical and/or chemical properties for a specific application. Numerous examples of polymer-inorganic and polymer-organic have been demonstrated in different areas such as biomedical applications,[1, 2] fuel cells,[3, 4] membranes,[5, 6] and others. A range of synthetic methods have been utilised to create such materials, mostly using heterophase polymerization approaches such as miniemulsion,[7-9] emulsion[10, 11] and dispersion polymerization,[12-14] in addition to layer-by-layer deposition methods.[15]

Silica (SiO_2) has excellent chemical and physical properties and is one of the most popular components utilized in hybrid material designs.[16-18] External morphology and shape control of pure silica nanoparticles is much less common in comparison to spherical silica nanoparticles with varying internal (i.e. solid, hollow, or mesoporous) structure, which have been widely reported. The morphology and structure of silica nanoparticles are highly influenced by the preparation methods and reaction conditions. Different shapes and structures of pure silica nanoparticles have been studied to enhance the application efficiency, especially in biomedical

applications.[16, 19-22] Polymer@silica (Polymer core / silica shell) nanoparticles have been synthesized through classic emulsion polymerization (using either alkoxysilane functional co-monomer[23, 24] or silica nanoparticles[25]) and dispersion polymerization (where small silica nanoparticles are absorbed onto the polymer nanoparticle surface via acid-base interactions[26]). However, these methods primarily produce spherical nanoparticles.

Hybrid silica nanoparticles with unique and controllable external morphologies were only able to be prepared at low solids content. This limitation is analogous to previous methods used to prepare polymer nanoparticles with rod-like or vesicular morphologies, where the controlled self-assembly of diblock copolymers in selective solvents was only possible at very low concentration.[27, 28] In recent times, polymerization-induced self-assembly (PISA) mediated by RAFT polymerization has become a preferred method to prepare self-assembled block copolymer nanoparticles, as this method offers more flexibility and controls in addition to synthesize nanoparticles with tailored shapes at very high solids content (up to 50 % w/w).[29] PISA is a robust technique and it has been applied in many cases to examine the effect solvent choice,[30-33] charge of the stabilizing block[34, 35] and the nature of the core-forming block[36, 37] as well as the use of novel solvents (e.g. supercritical carbon dioxide) to prepare unique *in-situ* particle architectures.[38]

This chapter reports the preparation of silica shell – polymer core hybrid nanoparticles at high solids content via the combination of PISA and sol-gel chemistry. A diblock copolymer is synthesized by RAFT polymerization, whereby the solvophilic block is a methacrylate bearing an alkoxysilane pendant group, followed by chain extension with the solvophobic block (benzyl methacrylate) in a non-solvent (ethanol). The length of the solvophobic block is varied

in order to use PISA template to direct the morphology to various nanoparticle structures. Due to the presence of alkoxysilane groups at the nanoparticle surface, the growth of a silica shell on the particle surface can be achieved via the hydrolysis and condensation of a silica precursor (TEOS) in a controlled fashion, to produce silica nanoparticles with different morphologies. The surface condensation step is orthogonal to the PISA process and as a result the polymer nanoparticle acts as a template for the construction of silica shells at the surface. To the best of our knowledge, this is the first report on the use of alkoxysilane-containing methacrylates as a stabilizer block in PISA systems, which provides the means to control and generate hybrid nanoparticles with an array of morphologies and with an amenable surface to further functionalization.

3.2 Results and Discussions

3.2.1 Alkoxysilane-containing MacroRAFT Agents

In this work, alkoxysilane-containing monomers such as MPS and IPS were prepared as macroRAFT agents. MPS has been applied in RAFT polymerization previously and reported by Mellon *et al.*[39] (as a macroRAFT agent) and Zhang *et al.*[40] (as a second block during copolymer synthesis). IPS has been utilised in anionic polymerization[41] and via ATRP,[42] however, neither monomer (MPS or IPS) has been used in PISA systems previously. The commercially available MPS monomer was first employed in our study and IPS monomer was prepared in parallel with this work. ^{1}H and ^{29}Si NMR spectra of as-synthesized IPS are shown in Figure 3-1 and Figure 3-2 respectively. One of the ultimate aims of this work was to make alkoxysilane-based macroRAFT agents for subsequent chain extension through the PISA process. The PISA system in this work was briefly outlined in Figure 3-3. A dithiobenzoate (CPADB) and a trithiocarbonate (CDTSPA) based RAFT agents were utilised and they possessed identical leaving groups. These RAFT agents were selected due to efficient RAFT polymerization of tertiary propagating radicals, which require thiocarbonylthio compounds with a tertiary R group and radical stabilizing Z group to improve the rate of addition of radicals to the C=S group of the chain transfer agent.[43] In following sections, dithiobenzoate and trithiocarbonate based RAFT agents were labelled as ‘D’ and ‘T’ respectively. All reactions were performed at 65 ^{o}C to maintain a constant 10 hour half-life of ACVA initiator.[44]

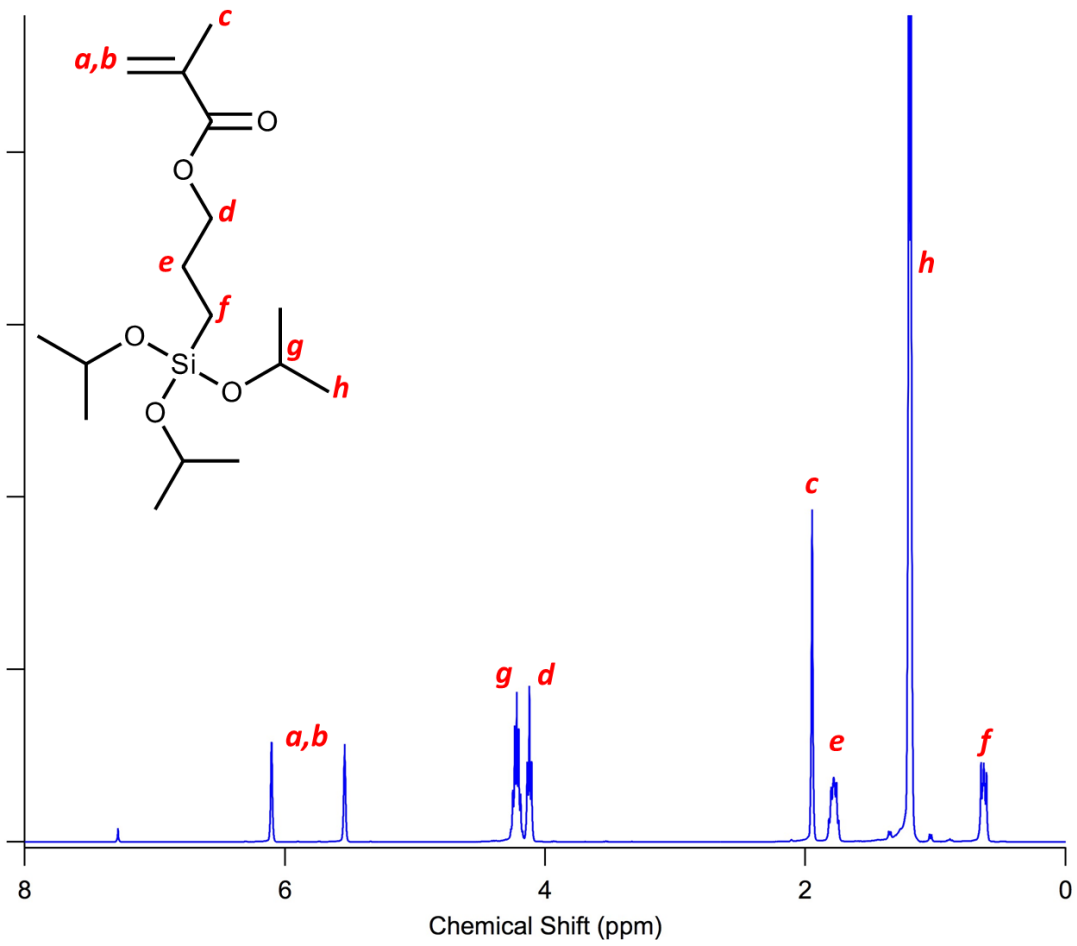

Figure 3-1: Proton NMR spectrum of IPS in $CDCl_3$

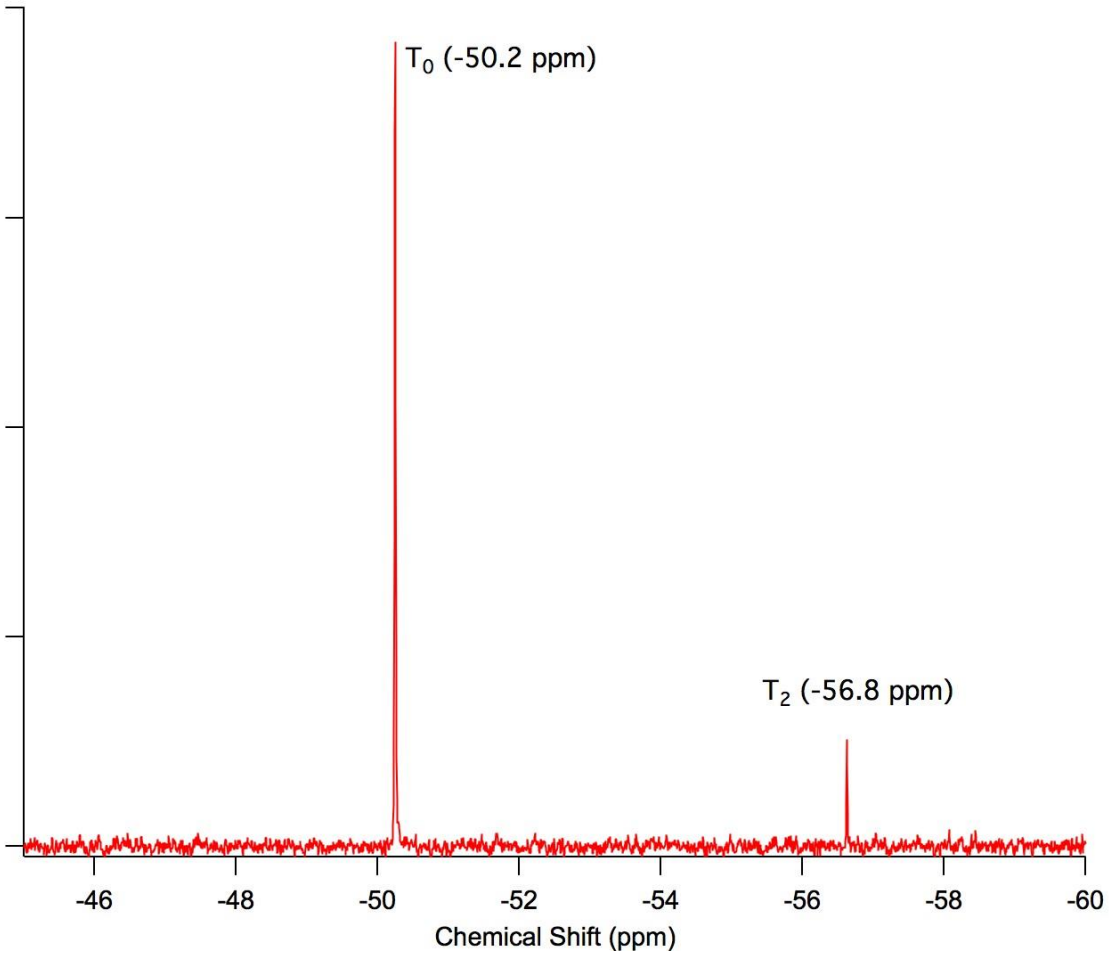

Figure 3-2: ^{29}Si NMR spectrum of IPS in $CDCl_3$. T_0 and T_2 refer to Si atoms with 0 and 2 Si-O-Si linkages respectively.

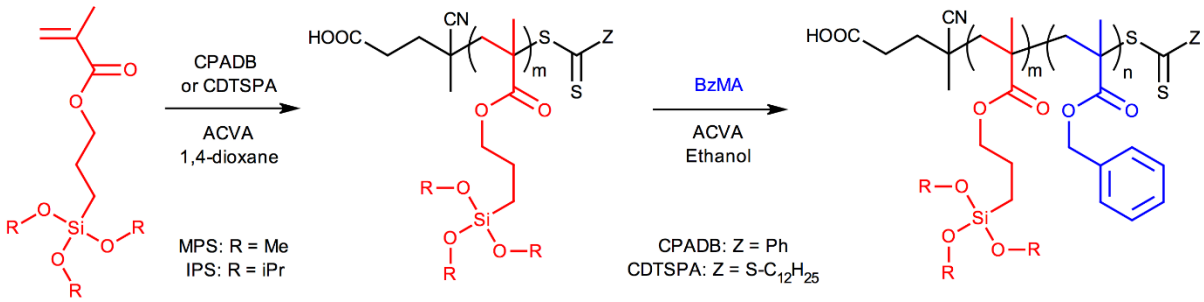

Figure 3-3: Schematic of the PISA process using an alkoxysilane solvophilic block to chain extend benzyl methacrylate in ethanol.

Each macroRAFT agent was prepared to have two targeted degrees of polymerization (DP), namely 40 and 65 monomer repeating units. The characterization data of macroRAFT agents are reported in Table 3-1. The fractional conversion was high (≥ 0.95) in all macroRAFT agent syntheses. Good agreement was established between the theoretical DP (based on the target DP and fractional conversion) and experimental DP determined by ^{1}H NMR spectroscopy of the resultant polymer, assuming every chain carries one RAFT end-group. The ^{1}H NMR of a dithiobenzoate-based MPS macroRAFT agent is shown in Figure 3-4. XPS characterisation was also used to support the agreement where the estimated DP of macroRAFT agents could be calculated via using the Si : S atomic ratio. Assuming no loss or degradation of RAFT end-groups during synthesis or storage, the macroRAFT agents should have two S atoms per endgroup and one Si atom per monomer repeating unit. The XPS data shown in Table 3-2 was based on CPADB macroRAFT agents (D). The estimated DP by XPS was higher than the theoretical DP, especially MPS based macroRAFT agents (Entry 3-1 and 3-2 in Table 3-2).

An important experimental observation was that when poly(MPS) was precipitated and fully dried under vacuum, the dry polymer would not re-dissolve back into any good solvent tested (chloroform, ethanol, DMSO, acetone and THF). Other groups had identified this problem previously, attributed to intra- and inter-molecular crosslinking of the polymer via hydrolysis and condensation of trimethoxysilane group.[39, 40] In this work, all solution-based characterisations (such as NMR and SEC) were prepared by promptly dissolving the precipitated and partially dried sample into the relevant solvent to minimize potential crosslinking. This approach worked well as the solution-state ^{29}Si NMR (Figure 3-5) detected a sole sharp resonance peak at ~ -42.7 ppm (normally defined as T^0 peak),[45] indicative of no crosslinking of the macroRAFT agent and proving that the alkoxysilane based macroRAFT agents were stable in the absence of prolonged drying and storage.

Table 3-1: Characterisation data of macroRAFT agents

Entry	Sample code	Fractional conversion	DP_{th}	DP (^{1}H NMR)	M_n (^{1}H NMR) (kDa)	M_n (SEC) (kDa)	$Đ$ (SEC)
3-1	D-MPS_{40}	0.98	39	41	10.0	16.8	4.03
3-2	D-MPS_{65}	0.97	63	66	15.9	26.3	11.3
3-3	D-IPS_{40}	0.97	39	48	13.3	10.8	1.23
3-4	D-IPS_{65}	0.97	63	72	21.2	21.6	1.49
3-5	T-MPS_{40}	0.95	38	36	9.84	10.4	1.45
3-6	T-MPS_{65}	0.96	62	72	15.8	19.6	2.36
3-7	T-IPS_{40}	0.96	38	48	13.0	9.86	1.20
3-8	T-IPS_{65}	0.97	63	59	21.4	14.8	1.34

Table 3-2: XPS data of CPADB based macroRAFT agents (D)

Entry*	Sample code	Conversion	DP_{th}	DP (^{1}H NMR)	Si, S content (atomic %)	Si : S ratio	DP (XPS)
3-1	D-MPS_{40}	0.98	39	41	7.25, 0.22	33	66
3-2	D-MPS_{65}	0.97	63	66	6.71, 0.15	45	90
3-3	D-IPS_{40}	0.97	39	48	6.85, 0.28	24.5	49
3-4	D-IPS_{65}	0.97	63	72	9.53, 0.25	38	76

** Refer to Table 3-1.*

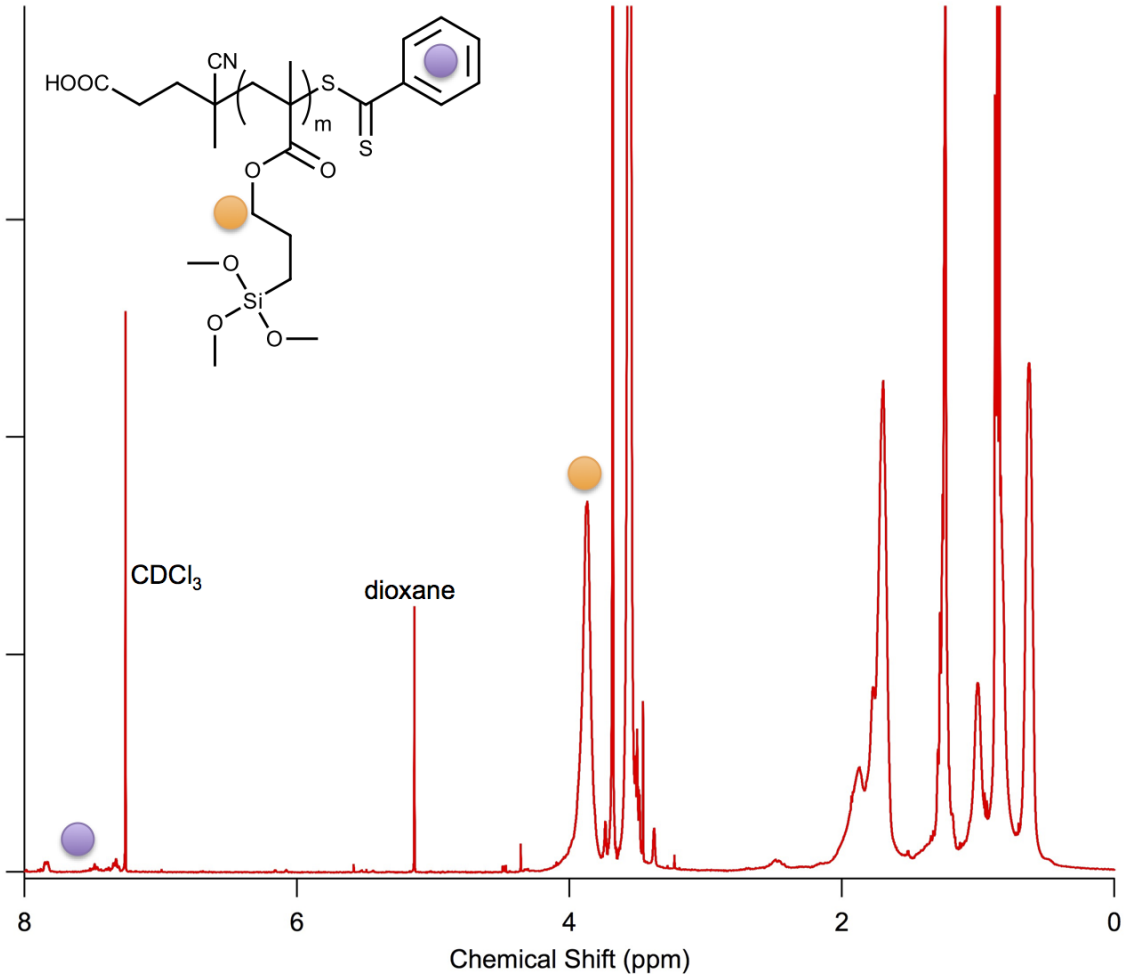

Figure 3-4: ^{1}H NMR spectrum of D-MPS$_{40}$ macroRAFT agent (Entry 3-1 in Table 3-1). Orange circle refers to CH_2 in the MPS backbone and purple circle refers to aromatic ring of RAFT agent.

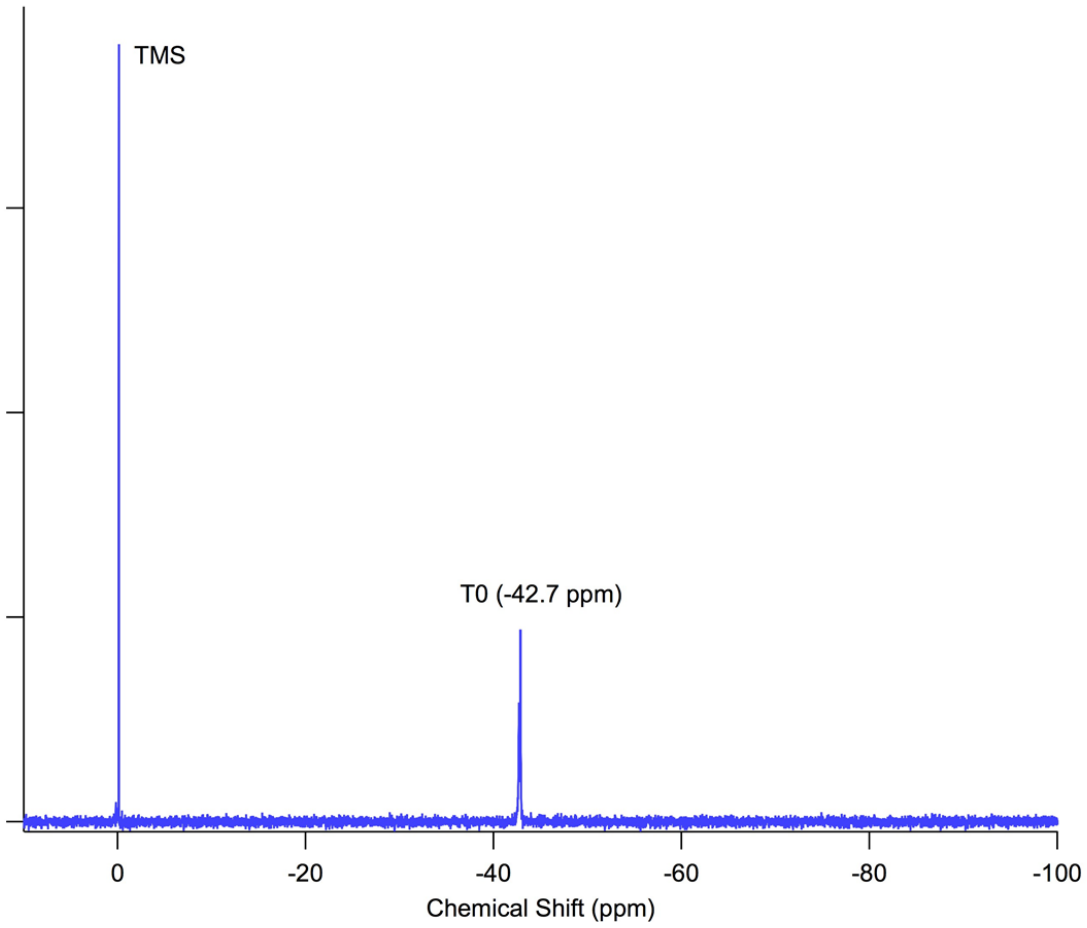

Figure 3-5: Solution-based ^{29}Si NMR spectrum of D-MPS$_{40}$ after precipitation into hexane ($CDCl_3$ + tetramethylsilane (TMS) as internal reference)

The nature of the alkoxysilane group was shown to influence the molecular weight distribution of polymers significantly (see Table 3-1 and Figure 3-6). These results showed a correlation between the nature of the alkoxysilane pendant group and stability towards hydrolysis and condensation. Most MPS-based macroRAFT agents had very high dispersities (specifically Entry 3-1 and 3-2 in Table 3-1), however IPS based macroRAFT agents had dispersities lower than 1.5 and monomodal distributions. This result was attributed to the increased stability of the tri(isopropoxysilyl) group relative to the trimethoxysilyl group with respect to hydrolysis and condensation.[46] While the molecular weight distributions of MPS based macroRAFT

agents might seem extraordinarily broad for a typical RAFT polymerization, it was not due to a poorly controlled polymerization. These high molecular peaks/shoulders were most likely formed during SEC sample preparation; samples were dried as much as possible, dissolved in SEC eluent overnight and then filtered prior to analysis. This hypothesis was supported by the fact that (i) these samples could be effectively chain extended with BzMA under a variety of conditions (see Figure 3-7 and Figure 3-8) and (ii) the absence of T^1, T^2, or T^3 peaks in ^{29}Si NMR spectra of the resulting polymers, suggesting that the samples did not crosslink immediately after preparation. Ozaki *et. al.* reported broad molecular weight distributions after precipitation of trimethoxysilyl or triethoxysilyl-based polymers due to hydrolysis and condensation of alkoxysilane groups.[41] ^{29}Si NMR spectroscopy also confirmed the absence of hydrolysis and condensation after IPS based macroRAFT agents were precipitated into methanol/water mixture (Figure 3-9).

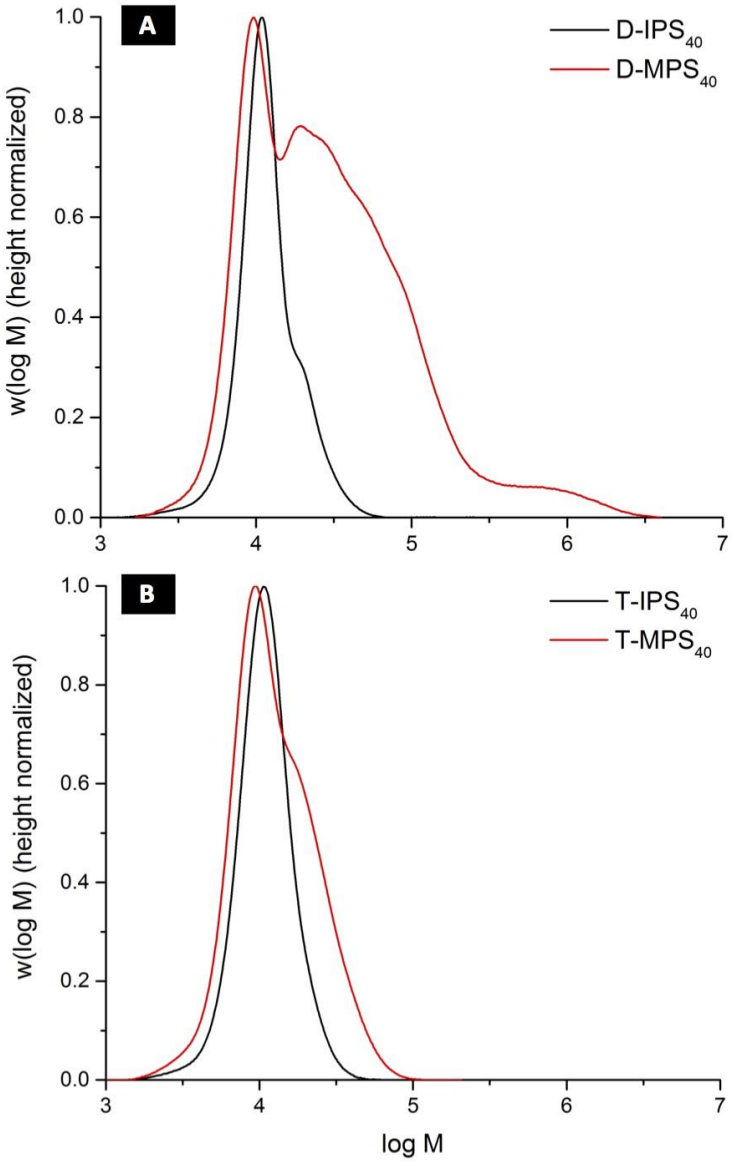

Figure 3-6: Height-normalized SEC molecular weight distributions for (A) dithiobenzoate, and (B) trithiocarbonate mediated RAFT polymerization of MPS (red) and IPS (black)

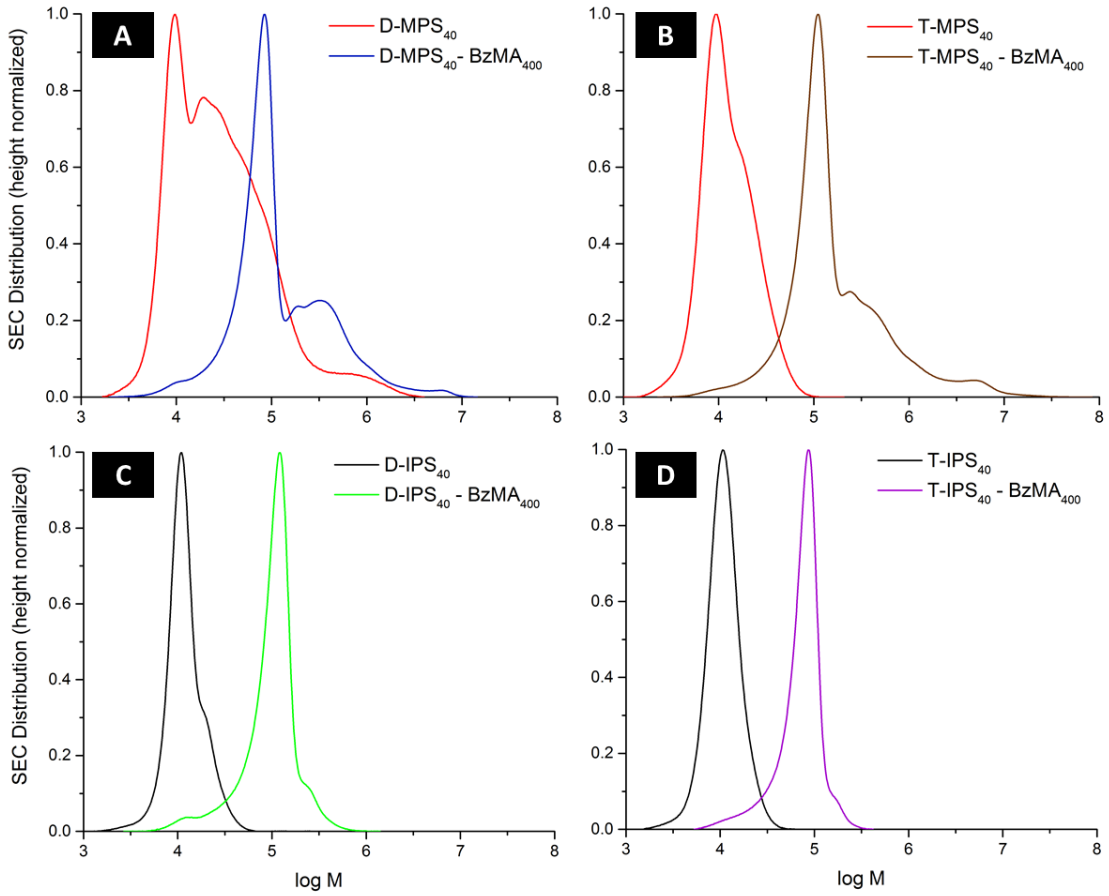

Figure 3-7: Height-normalized SEC molecular weight distributions for chain extension with 400 units of BzMA under different alkoxysilane macroRAFT agents (40 monomer repeating units) and RAFT agent types. (A) Entry 3-27 in Table 3-6; (B) Entry 3-44 in Table 3-6; (C) Entry 3-52 in Table 3-6; and (D) Entry 3-66 in Table 3-6Table 3-8.

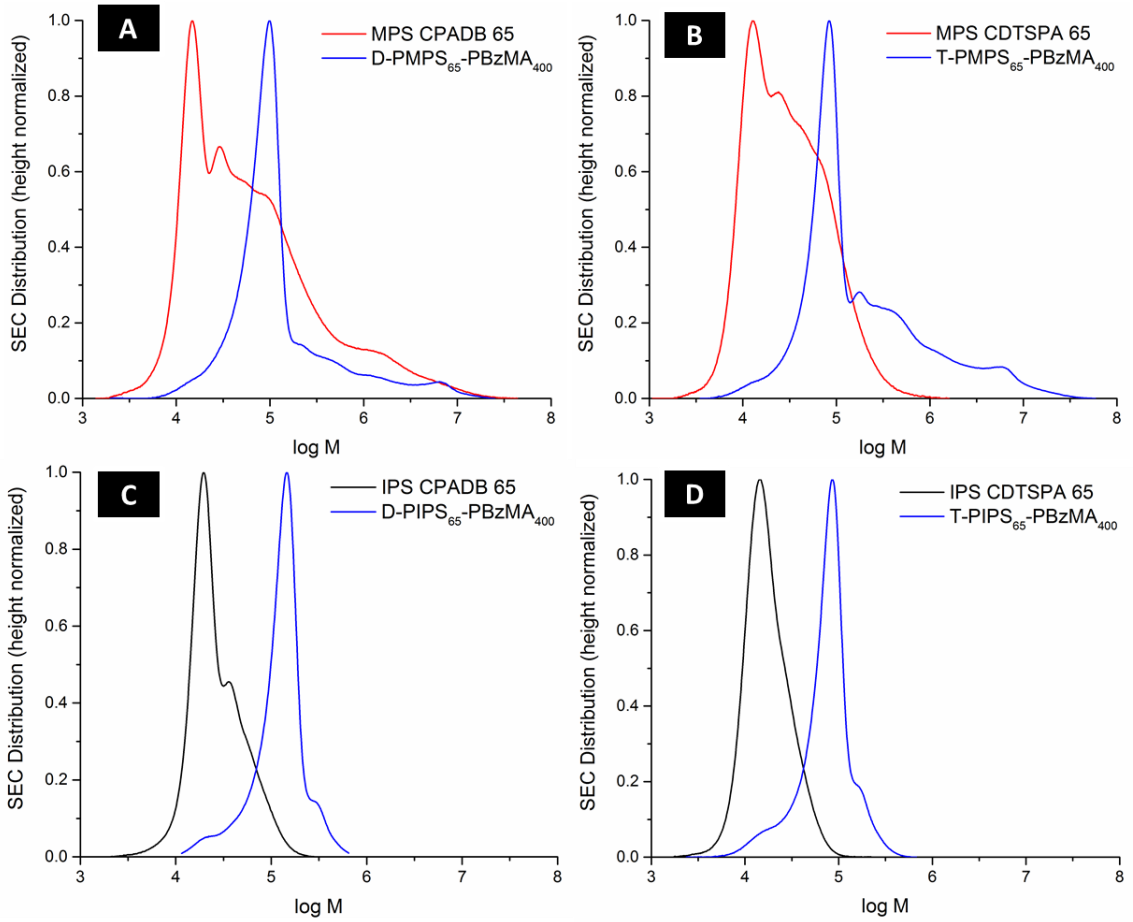

Figure 3-8: Height-normalized SEC molecular weight distributions of MPS- and IPS- based macroRAFT agents with 65 monomer repeating units in the chain extension with 400 units of benzyl methacrylate. (A) Entry 3-40 in Table 3-6; (B) Entry 3-48 in Table 3-6; (C) Entry 3-62 in Table 3-6; and (D) Entry 3-70 in Table 3-6.

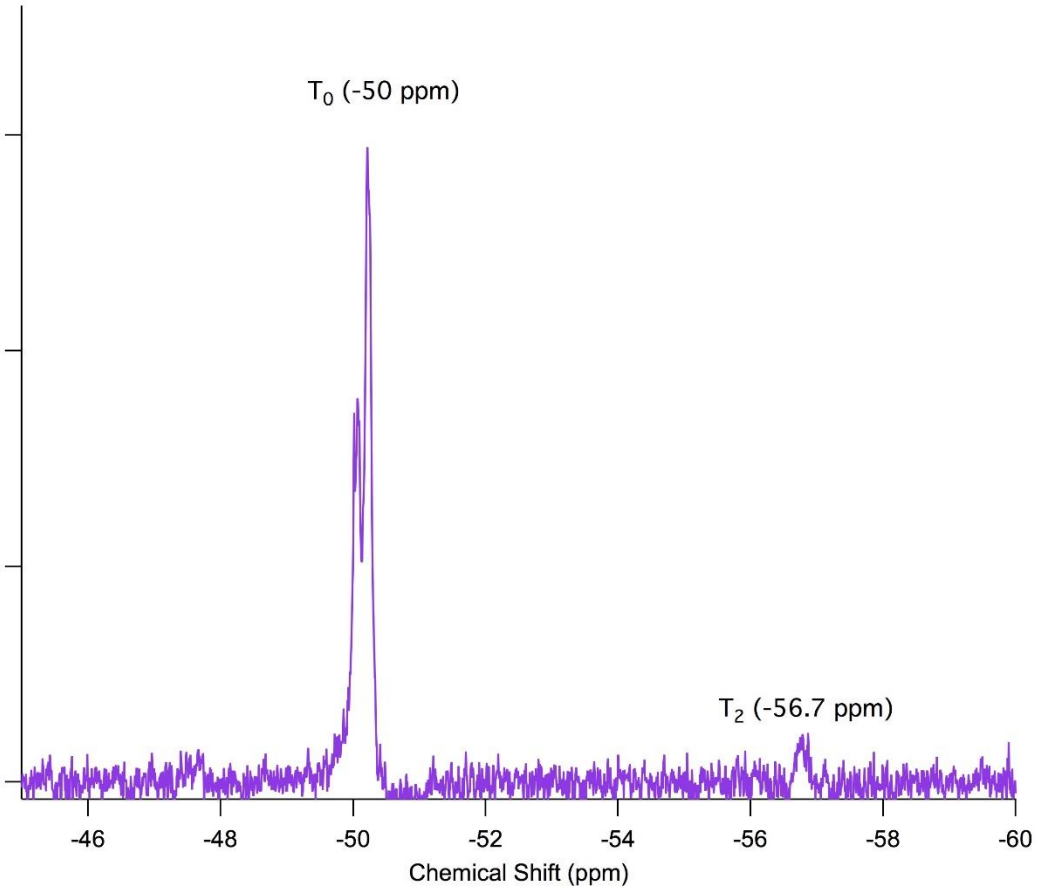

Figure 3-9: Solution-based ^{29}Si NMR spectrum of D-IPS$_{40}$ after precipitation into methanol/water (8:2 v/v)

It is noteworthy that the controlled polymerization of MPS is influenced by the RAFT agent selection. In this work, trithiocarbonate mediated polymerization produced low dispersity polymers (Entry 3-5 and 3-6 in Table 3-1) under similar conditions to those applied for dithiobenzoate-mediated reactions (Entry 3-1 and 3-2 in Table 3-1). The reason for this is unclear as possible inter-molecular crosslinking of chains via condensation is unlikely to be greatly influenced (if at all) by the nature of the chain end. Thermogravimetric analysis showed dried macroRAFT agents had decomposed and a significant residual mass remained at the conclusion of the heating process (~ > 30% of the original mass of the sample, Figure 3-10 and Table 3-3). The residual mass is quite close to the predicted residual mass, based on the assumption that a cross-linked silica residue has formed upon heating (Appendix 1).

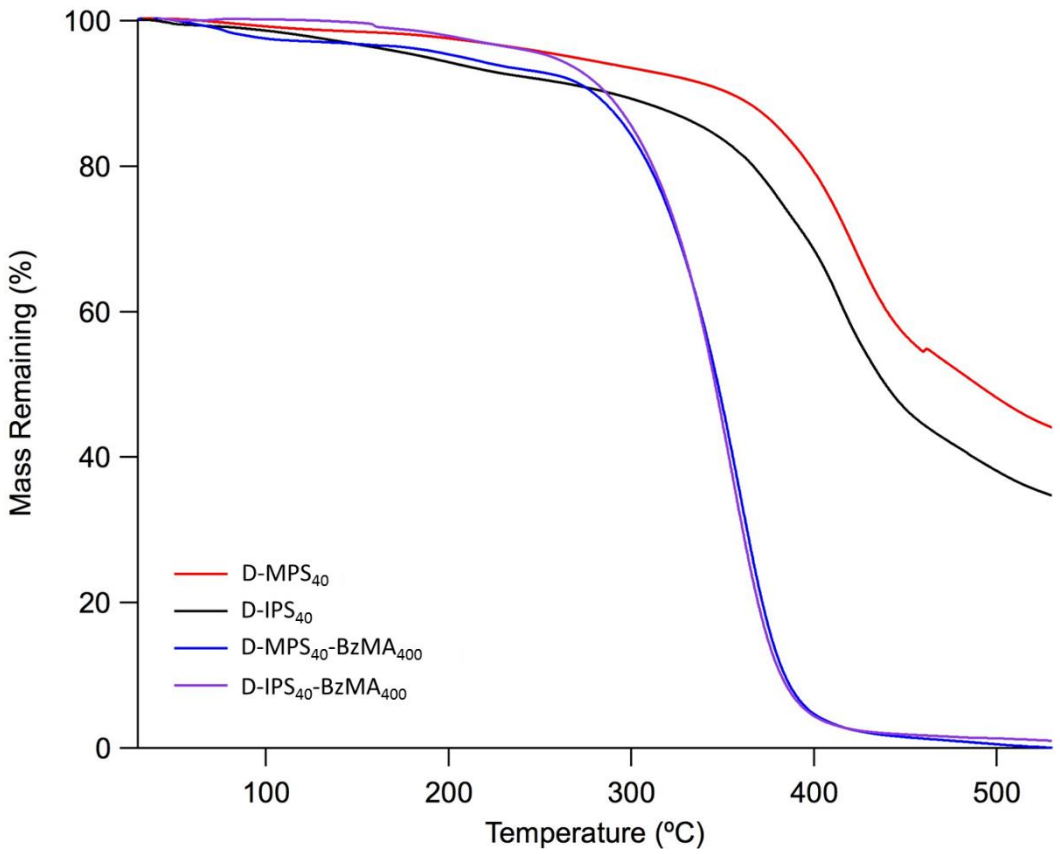

Figure 3-10: Thermogravimetric analysis of MPS (red) and IPS (black) macroRAFT agents in addition to chain extension with 400 units of BzMA (blue and purple curves)

Table 3-3: Residual mass of TGA for different macroRAFT agents

Entry	MacroRAFT agents	Residual mass (%)
3-9	D-MPS$_{40}$	41.8
3-10	D-MPS$_{65}$	40.6
3-11	D-IPS$_{40}$	32.6
3-12	D-IPS$_{65}$	36.5

3.2.2 Nanoparticle Synthesis via the PISA Process

This section discusses the chain extension of alkoxysilane containing macroRAFT agents with benzyl methacrylate (BzMA) in ethanol. As BzMA monomer is soluble in ethanol but its polymer is insoluble, this represents a dispersion polymerization where the PISA process can potentially occur. BzMA is selected as a core-forming block for its high reactivity and a glass transition temperature of poly(BzMA) (55 ^{o}C) is lower than the experimental temperature, which prevents the formation of nanoparticles with kinetically frozen cores.[47, 48] In this work, the target DP of BzMA was adjusted from 100 to 400 units and three different solid contents (based on full conversion) were targeted at 10, 15, and 20 % w/w. *In-situ* self-assembly was demonstrated via the formation of a milky dispersion from an initially clear solution in the absence of any coagulum, demonstrating the ability for the alkoxysilane macroRAFT agent to act as a stabilizer in block copolymer self-assembly. On the other hand, a significant precipitation of polymer was found in the absence of the alkoxysilane solvophilic block (Figure 3-11).

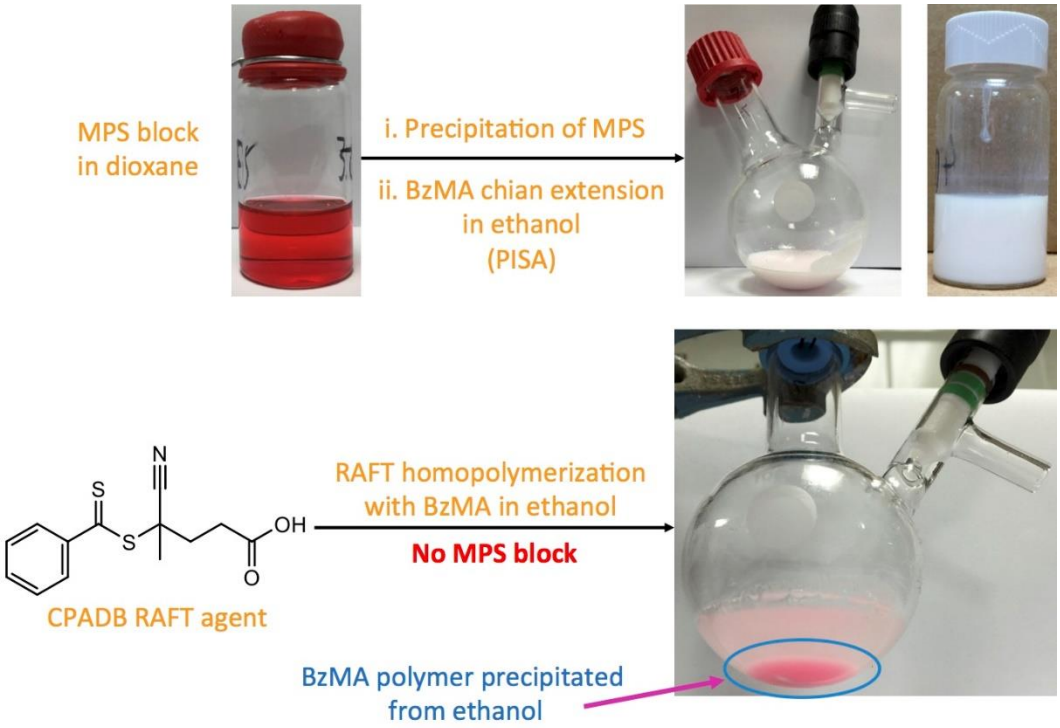

Figure 3-11: RAFT polymerization of BzMA in ethanol. (Top): PISA process in the presence of alkoxysilane solvophilic block; (Bottom): Absence of alkoxysilane solvophilic block, showing polymer precipitation.

The results for PISA systems stabilized by dithiobenzoate and trithiocarbonate based MPS macroRAFT agents are summarised in Table 3-4 and Table 3-5 respectively. The fractional conversion of BzMA was very high in nearly all cases (≥ 0.91) and a range of particle morphologies was observed by SEM and TEM analysis (Figure 3-12). A predictive phase diagram was not the main priority of this work, however some information can be obtained regarding morphological transition. When a shorter alkoxysilane macroRAFT agent was used (D-MPS$_{40}$ and T-MPS$_{40}$), a vesicular morphology was observed at BzMA block lengths greater than 150 repeat units. This vesicle phase was not pure and often a minor fraction of spherical particles could be observed (Figure 3-12B as an example). These macroRAFT agents did not exhibit either pure spherical phase nor a 'worm' phase at low BzMA DP values; only short rod-like structure or fused spherical objects were observed. When using a longer stabilizer block

(MPS_{65}), spherical morphology was observed across a wide range of BzMA DP values. This observation is in agreement with published PISA reports where the solvophilic block length can influence the packing parameter of block copolymer and hence the nanoparticle morphology.[32, 49, 50] A longer stabilizer block can also result in 'kinetically' trapped spherical morphology despite a high DP of core-forming block.[51] Longer stabilizer blocks aid the steric stabilization of nanoparticles, however, they also prevent the efficient 1D fusion of spheres to form higher-order rod-like structures.[51] No evidence showed the solids content had significant impact on the morphology in this alkoxysilane stabilized system. Variation of the Z group had an impact on the morphology of MPS-based block copolymers (e.g. spheres in Entry 3-40 in Table 3-4 (D-MPS_{65}-$BzMA_{400}$) and mixture of vesicles and spheres in Entry 3-48 in Table 3-5 (T-MPS_{65}-$BzMA_{400}$)). IPS-based block copolymer nanoparticles were spherical in nature regardless of the Z group of the RAFT agent.

Table 3-4: Summary of PISA experiments utilizing dithiobenzoate based MPS macroRAFT agents as solvophilic blocks

Entry	MacroRAFT agents	Target BzMA DP	Solids (%)	BzMA conversion	d_z (nm) / PDI (DLS)	Morphology
3-13	D-MPS_{40}	100	10	0.97	72 / 0.05	Rods/fused spheres
3-14			15	0.97	69 / 0.05	Rod/fused spheres
3-15			20	0.99	107 / 0.18	Fused spheres
3-16		125	10	0.96	84 / 0.13	Spheres, mainly fused
3-17			20	0.98	118 / 0.22	Spheres, some fused
3-18		150	20	0.98	225 / 0.08	Vesicles
3-19		200	10	0.91	259 /0.1	Vesicles
3-20			15	0.99	223 / 0.17	Vesicles and spheres
3-21			20	0.96	297 / 0.24	Vesicles
3-22		300	10	0.93	421 / 0.19	Vesicles and spheres
3-23			15	0.99	234 / 0.07	Vesicles, some spheres
3-24			20	0.99	352 / 0.14	Vesicles, some spheres

3-25		400	10	0.98	943 / 0.30	Vesicles, some spheres
3-26			15	0.98	785 / 0.23	Vesicles
3-27			20	0.97	236 / 0.24	Vesicles, some spheres
3-28	D-MPS$_{65}$	100	10	0.95	97 / 0.13	Spheres
3-29			15	0.99	88 / 0.12	Irregular fused spheres
3-30			20	0.95	109 /0.22	Irregular fused spheres
3-31		150	20	0.98	186 /0.24	Spheres, some irregular
3-32		200	10	0.98	119 / 0.14	Spheres
3-33			15	0.96	97 / 0.09	Spheres
3-34			20	0.96	137 / 0.14	Spheres
3-35		300	10	0.91	173 / 0.15	Spheres, some irregular
3-36			15	0.98	239 / 0.27	Spheres
3-37			20	0.93	216 / 0.23	Spheres
3-38		400	10	0.94	180 / 0.14	Spheres
3-39			15	0.97	175 / 0.24	Spheres
3-40			20	0.99	189 / 0.08	Spheres

Table 3-5: Summary of PISA experiments utilizing trithiocarbonate based MPS macroRAFT agents as solvophilic blocks. All experiments were conducted at a solids content of 20 wt%.

Entry	**MacroRAFT agents**	**Target BzMA DP**	**BzMA conversion**	**d_z (nm) / PDI (DLS)**	**Morphology**
3-41	T-MPS$_{40}$	100	0.99	231 / 0.22	Spheres, some vesicles
3-42		200	0.99	930 / 0.04	Vesicles
3-43		300	0.99	648 / 0.07	Vesicles
3-44		400	0.99	995 / 0.18	Vesicles
3-45	T-MPS$_{65}$	100	0.99	219 / 0.82	Rods
3-46		200	0.99	150 / 0.18	Lumpy rods
3-47		300	0.99	570 / 0.55	Rods and spheres
3-48		400	0.91	475 / 0.66	Vesicles and spheres

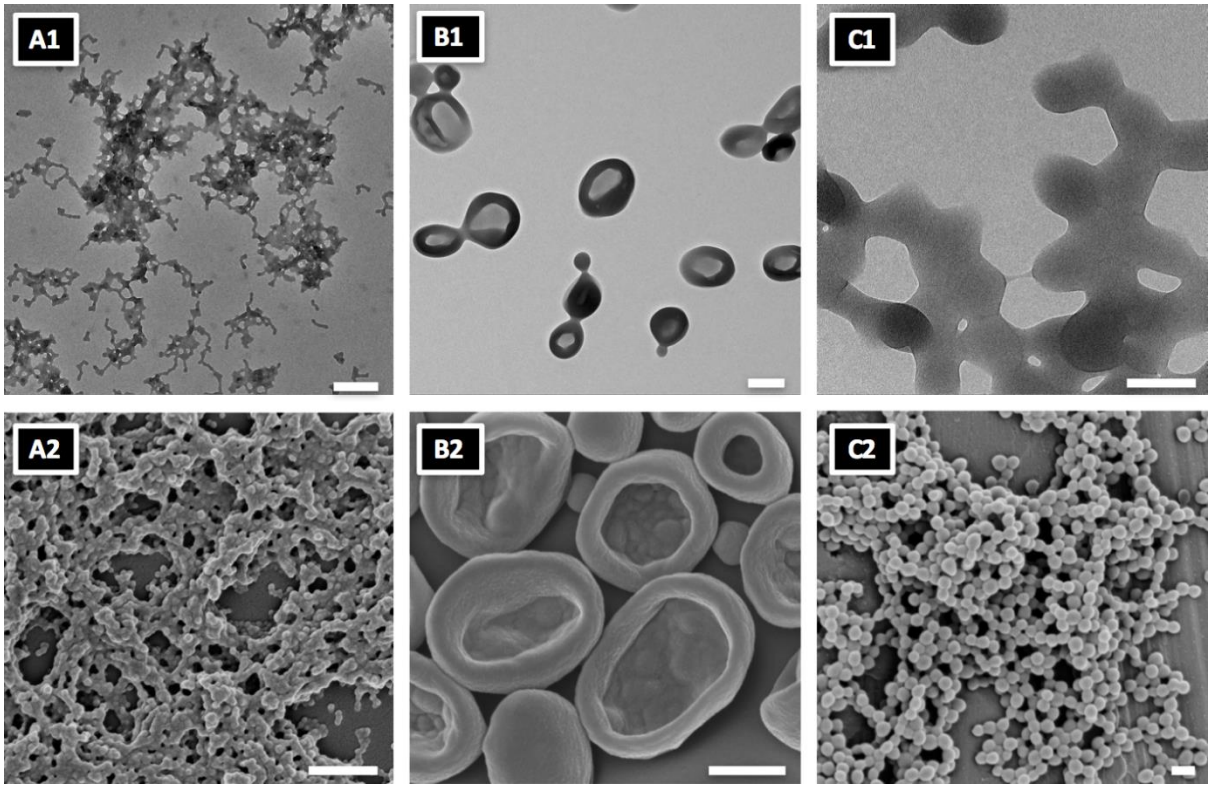

Figure 3-12: TEM (top row) and SEM (bottom row) of various MPS-stabilized nanoparticles: (A) Entry 3-14 in Table 3-4 (D-MPS$_{40}$ – BzMA$_{100}$); (B) Entry 3-26 in Table 3-4 (D-MPS$_{40}$ – BzMA$_{400}$); and (C) Entry 3-40 in Table 3-4 (D-MPS$_{65}$ – BzMA$_{400}$). Scale bars = (A and B) = 500 nm, and (C) = 250 nm.

Using the molecular weight distribution of macroRAFT agents presented in Figure 3-6 as a reference point, we demonstrate that chain extension with BzMA during the PISA process was very effective (Figure 3-7 and Table 3-6). The results shown here all correspond to the extension of 400 BzMA units and so are readily comparable; it is acknowledged that these molecular weight distributions are only semi-quantitative given the likely presence of cross-linked material and molecular weight determination via polystyrene calibration. In all cases, the primary peak in the SEC chromatogram shifts from a relative molecular weight of ~ 10^4 to ~ 10^5 Da. A small residual peak was detected at low molecular weights and this was likely caused by dead chains formed during macroRAFT agent synthesis. High molecular weight peaks found in the poly(MPS-b-BzMA) molecular weight distribution were not the

consequence of termination by combination, but rather to intra- and inter-molecular crosslinking of MPS units. These results support the hypothesis in previous section that MPS based polymer undergoes crosslinking after synthesis. In contrast, the more bulky and stable poly(IPS) macroRAFT agent produced relatively low dispersity and narrow MWD copolymers (~ 1.5) upon the chain extension with BzMA (Figure 3-7 and Table 3-6), with an associated small bimolecular termination peak at high molecular weights. Poly(IPS-b-BzMA) almost fully decomposed during TGA analysis (Figure 3-10) with only a small residual mass remaining (< 1%).

Table 3-6: Number-average molecular weight and dispersity values for various macroRAFT agents after chain extension with 400 BzMA units

Solvophilic block	Entry*	M_n (SEC) (kDa)	$Đ$
MPS	3-27	63.8	3.69
	3-40	68.1	5.12
	3-44	84.2	4.54
	3-48	76.0	8.27
IPS	3-52	68.9	1.62
	3-62	91.8	1.51
	3-66	57.2	1.36
	3-70	54.3	1.55

** Refer to Table 3-4, Table 3-5, Table 3-7, and Table 3-8.*

Highly stable nanoparticle dispersions (Table 3-7 and Table 3-8) were also observed in PISA systems stabilized by IPS-based macroRAFT agents. In all cases high BzMA conversion was achieved, however, the nanoparticle morphology was spherical regardless of the DP of BzMA block, even up to very high values (such as 1800 and 2500 units). As an example, monodisperse spherical nanoparticles stabilized by T-IPS_{40} based macroRAFT agent (PDI by DLS < 0.06) just increased in size from ~129 nm to ~447 nm hydrodynamic diameter upon increasing the BzMA block length. IPS has a much bulkier pendant (tri(isopropoxysilyl)) group compared to MPS, greatly influencing the packing parameter and thus impact on the particle morphology. A bulkier solvophilic block is similar to a large 'head group' surfactant in terms of self-assembly of an amphiphilic species, making the formation of spheres more likely. A longer stabilizing block will also provide more effective steric stabilization and aid in the formation of spherical nanoparticles. Upon increasing DP of the BzMA block, these spherical nanoparticles continue grow in size; both by the increase in molecular weight as well as the mobility of individual copolymer chains between micelles and/or sphere-sphere fusion events.[52] Data in Table 3-7 shows that smaller nanoparticles are observed with using longer stabilizer blocks (DP 65) in contrast to shorter stabilizer blocks (DP 40) when the DP of the BzMA block is held constant . This is due to a longer stabilizer block having a stronger inter-corona chain repulsion, which favours a decreasing in the radius of curvature and form smaller nanoparticles.[53-55] During the self-assembly process, a greater number of shorter stabilizer block copolymers ($PIPS_{40}$-b-PBzMA) are required to associate together for stabilization, as the number of solvophilic IPS units in $PIPS_{40}$ block is lower than $PIPS_{65}$. Therefore, the size of nanoparticles expands as a greater number of shorter block copolymers joining together. The nanoparticles formed at the lowest BzMA DP (100 units, Entry 3-49 and 3-59 in Table 3-7) exhibited different morphologies by different imaging methods: the samples appeared sticky and aggregated by SEM, and fibrous by TEM (Figure 3-13A). This is most likely due to particle

collapse and coalescence during imaging, as opposed to the existence of a worm of fibrous morphology.

Table 3-7: Summary of PISA experiments utilizing dithiobenzoate based IPS macroRAFT agents as solvophilic blocks. All experiments were conducted at a solids content of 20 wt%.

Entry	MacroRAFT agents	Target BzMA DP	BzMA conversion	d_z (nm) / PDI (DLS)	Morphology
3-49	D-IPS$_{40}$	100	0.97	59 / 0.05	Rods/fused spheres
3-50		200	0.99	89 / 0.07	Spheres
3-51		300	0.98	136 / 0.05	Spheres
3-52		400	0.99	123 / 0.03	Spheres
3-53		500	0.99	146 / 0.02	Spheres
3-54		600	0.98	155 / 0.02	Spheres
3-55		800	0.98	169 / 0.02	Spheres
3-56		1100	0.98	292 / 0.05	Spheres
3-57		1400	0.99	232 / 0.02	Spheres
3-58		1800	0.98	283 / 0.03	Spheres
3-59	D-IPS$_{65}$	100	0.98	92 / 0.25	Rods/fused spheres
3-60		200	0.98	76 / 0.05	Spheres
3-61		300	0.99	87 / 0.04	Spheres
3-62		400	0.98	97 / 0.04	Spheres
3-63		500	0.99	132 / 0.03	Spheres
3-64		600	0.99	127 / 0.04	Spheres
3-65		1200	0.97	158 / 0.03	Spheres

Table 3-8: Summary of PISA experiments utilizing trithiocarbonate based IPS macroRAFT agents as solvophilic blocks. All experiments were conducted at a solids content of 20 wt%.

Entry	MacroRAFT agents	Target BzMA DP	BzMA conversion	d_z (nm) / PDI (DLS)	Morphology
3-66	T-IPS$_{40}$	400	0.98	129 / 0.06	Spheres
3-67		800	0.93	180 / 0.03	Spheres
3-68		1200	0.85	262 / 0.02	Spheres
3-69		2500	0.99	447 / 0.05	Spheres
3-70	T-IPS$_{65}$	400	0.99	132 / 0.15	Spheres
3-71		1000	0.96	144 / 0.07	Spheres

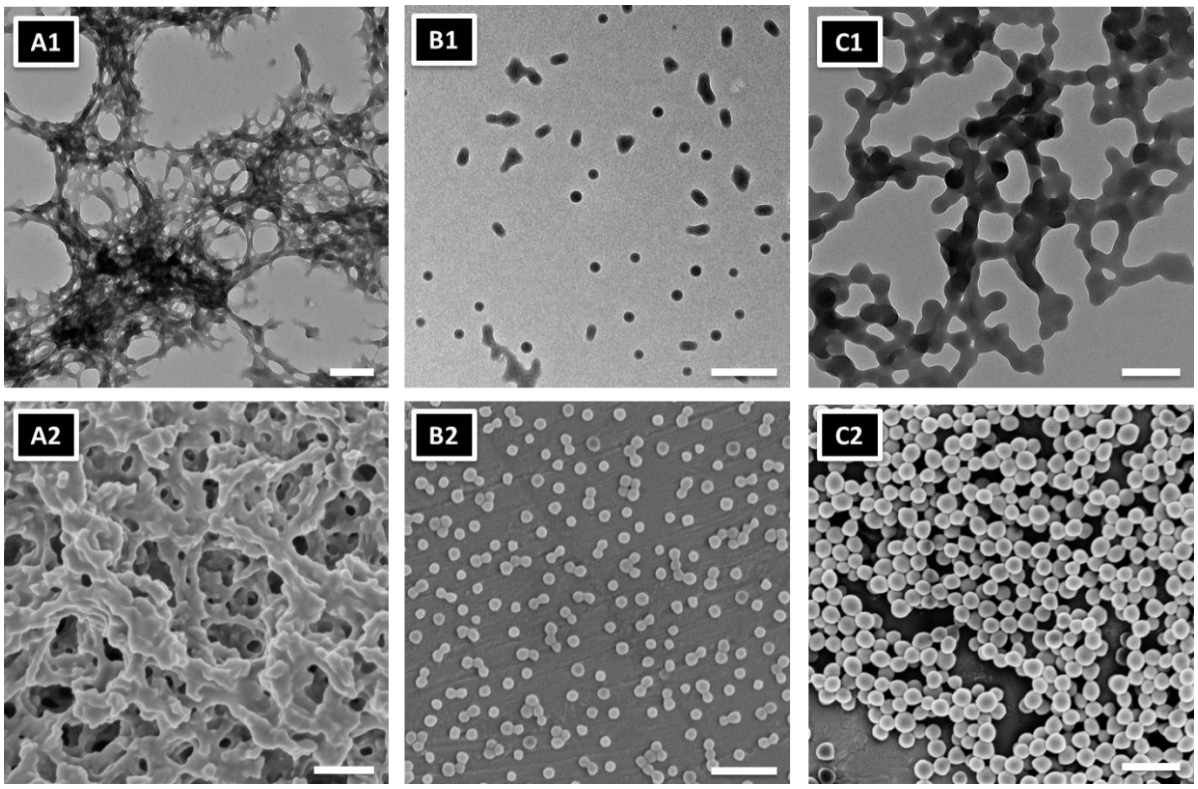

Figure 3-13: TEM (top row) and SEM (bottom row) of various IPS-stabilized nanoparticles: (A) Entry 3-59 in Table 3-7 (D-IPS$_{65}$ – BzMA$_{100}$); (B) Entry 3-52 in Table 3-7 (D-IPS$_{40}$ – BzMA$_{400}$); and (C) Entry 3-56 in Table 3-7 (D-IPS$_{40}$ -BzMA$_{1100}$). All scale bar = 500 nm.

3.2.3 Growth of Silica Shells

As each repeating unit in the stabilizer block consists of a reactive alkoxysilane group, the nanoparticles prepared in the above section were subsequently used as a template to create hybrid polymer-silica nanoparticles. This was accomplished via base-catalysed hydrolysis and condensation of TEOS at the particle surface, achieved by slow feed of TEOS into the reaction mixture to minimize the nucleation of new SiNPs. The procedure is briefly described in Figure 3-14. Base catalysis (ammonia) was used in this experiment to produce stable nanoparticles with highly crosslinked, branched and fully dense silica networks; in contrast, acid catalysis may form weakly crosslinked structures and produce aggregation.[11]

MPS-functional vesicles (Entry 3-26 in Table 3-4) and IPS-functional nanospheres (Entry 3-52 in Table 3-7) were selected for the formation of a silica coating. For MPS stabilized vesicles, a uniform thick silica shell is observed at the particle surface by TEM and noticeable changes to surface morphology are seen by SEM (Figure 3-14A). SEM analysis also supports the successful growth of silica shells by showing strong contrast to the previously (non-crosslinked) collapsed vesicles (Figure 3-12B); the crosslinked silica shell is more rigid and retains its structural integrity under the conditions of the electron microscope. In comparison to MPS-stabilized systems, multi-lobed (also referred to as 'raspberry-like') structures were discovered at the surface of IPS-functional nanospheres after growth of the silica shell at the particle surface (Figure 3-14B).

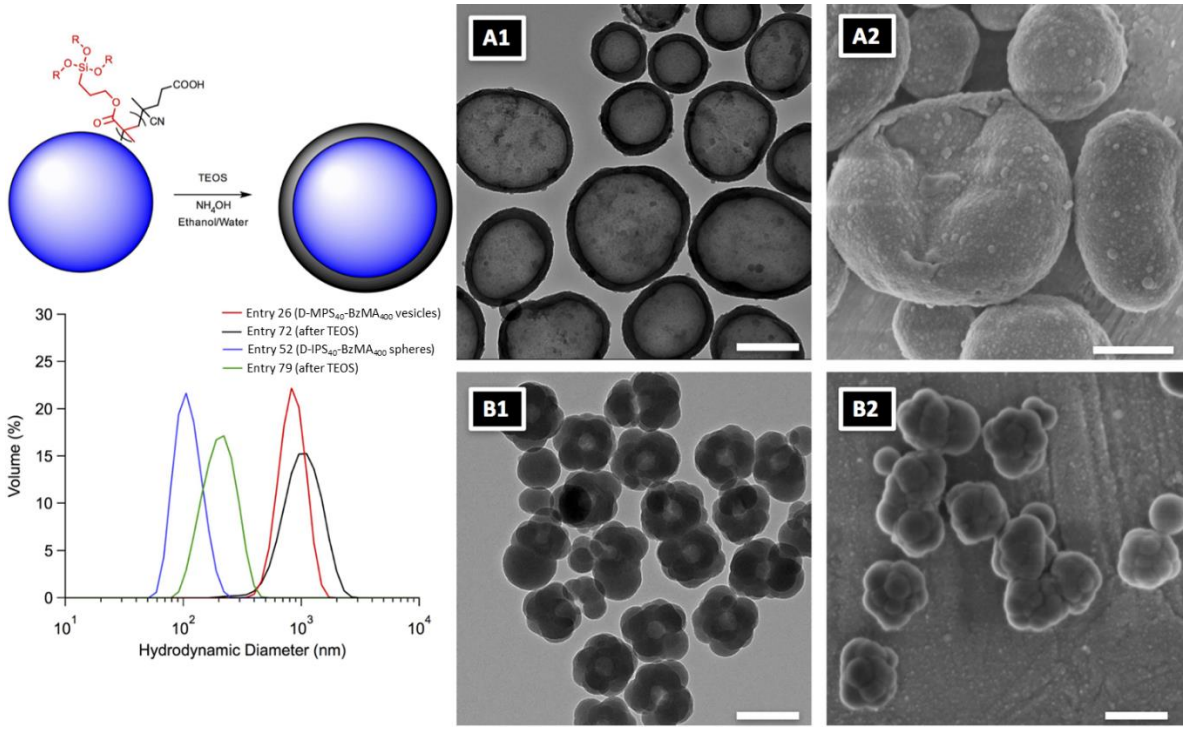

Figure 3-14: (Top left) Schematic diagram of growth of silica shell on particle surface with alkoxysilane groups (via TEOS hydrolysis and condensation); (Bottom left) DLS volume distributions before and after silica shell growth for sphere and vesicles particles; (Right panel) TEM and SEM images of particles following silica shell growth. A1/A2: Entry 3-72 in Table 3-9 (scale bars = 500 nm). B1/B2: Entry 3-79 in Table 3-9 (scale bars = 200 nm).

The different morphologies of these particles (smooth shells versus raspberry-like structures) are attributed to the different hydrolysis rates of the isopropoxysilyl and methoxysilyl groups. Davies *et al.* reported on the half-life of various alkylsilyl compounds with respect to acid and base-catalysed hydrolysis;[46] the half-life of trimethylsilyl and triethylsilyl groups was < 1 minute while the triisopropylsilyl group had a half-life of > 24 hours. The longer half-life and greater stability of the isopropylsilyl group is analogous to the isopropoxysilyl groups at the surface of the IPS functional particles prepared here. TEOS is thus more likely to hydrolyse and self-condense as opposed to crosslink with surface IPS groups. As a result, clustered

domains of silica form at the IPS surface as opposed to the growth of a smooth and even shell. Raspberry-like structures were retained even at greatly reduced TEOS feed rates.

With knowledge of the initial particle size and amount of TEOS added into the system, it is possible to predict the final particle size after the growth of silica shell through the sol-gel process.[23] This prediction is valid if all added TEOS hydrolyses and condenses at the particle surface without secondary nucleation. This predictive model can be found in Appendix 2. The *z*-average hydrodynamic diameter (measured by DLS) and predicted particle size are shown in Table 3-9. For IPS based precursors (spherical nanoparticles), the agreement between predicted size and hydrodynamic diameter by DLS was quite good, except when the ammonia concentration was significantly increased (Entry 3-84 and 3-85 in Table 3-9). An approximate 40-60 nm increase in hydrodynamic diameter was observed after silica shell growth, in conjunction with low polydispersity of the particle size distribution.

Table 3-9: Particle size (experimental and predicted) of MPS- and IPS- stabilized nanoparticles after growth of a silica shell

Entry	Variation*	d_z (nm) / PDI (DLS)	d_{pred} (nm)
MPS vesicle (Entry 3-26)		785 / 0.23	-
3-72	None	826 / 0.29	1198
3-73	0.1 x mass TEOS	713 / 0.33	848
3-74	0.2 x mass TEOS	899 / 0.22	902
3-75	0.4 x mass TEOS	799 / 0.56	995
3-76	2 x mass TEOS	1870 / 0.36	1435
3-77	0.6 M NH_4OH	1506 / 0.82	1198
MPS sphere (D-MPS$_{65}$ – BzMA$_{400}$)^		129 / 0.04	-
3-78	None	210 / 0.10	197
IPS sphere (Entry 3-52)		123 / 0.03	-
3-79	None	168 / 0.05	171
3-80	0.5 x mass TEOS	162 / 0.10	147
3-81	1.25 x mass TEOS	166 / 0.11	174
3-82	2 x feed rate	190 / 0.13	171
3-83	0.5 x feed rate	189 / 0.05	171
3-84	0.6 M NH_4OH	259 / 0.05	171
3-85	0.8 M NH_4OH	1779 / 0.29	171

** Relative to procedure described in Experimental Section. ^ BzMA conversion was 0.98 and the solids content was 20 wt%.*

The predicted size was quite different from the actual particle size of MPS-based vesicles. In most cases (Entry 3-72 to 3-75 in Table 3-9), the predicted size was bigger than the observed size, which implied that some TEOS did not condense at the particle surface. The overestimation of size is potentially due to simultaneous growth of the silica shell from the inner and outer surface of the vesicle structure. As a result, some TEOS is consumed in the growth of the inner surface of the vesicle, which would not contribute to increasing particle diameter. Electron microscopy and DLS of particles prior to centrifugation, washing and redispersion in fresh solvent demonstrated the nucleation of new particles (~ 50 nm diameter, occupying around 5-10% of the total volume distribution), which would further reduce the amount of available TEOS to condense at the particle surface and therefore contribute to the overestimation in the predicted size.

All silica shell growth experiments were carried out at the same mass concentration of polymer precursor dispersed in ethanol. This would result in a lower number of seed particles per unit volume for larger MPS vesicles in comparison to smaller IPS spheres at the same mass concentration. A reduction in number of seed particles decreases the total available seed surface area for TEOS to condense, hence increasing the likelihood of secondary nucleation (this is similar to the mechanism of secondary nucleation in seeded emulsion polymerization systems and its dependence on particle number[56]). To support this, small MPS stabilized spheres (Entry 3-78 in Table 3-9) with a higher seed particle number density were tested in the growth of silica shells. The analysis indicated good agreement between predicted particle size and that observed experimentally.

3.3 Conclusions

This work demonstrates the preparation of hybrid polymer-silica nanoparticles of differing morphologies through the use of reactive alkoxysilane monomers. This work clearly shows the nature of alkoxysilane group (present within the solvophilic block) has a significant impact on the resulting morphology of nanoparticles produced by the PISA process, and the morphology of the silica shell that grows from the surface of such particles. When alkoxysilane monomers are used as a solvophilic block for subsequent chain extension, the bulkier IPS monomer containing a triisopropoxysilyl group yields spherical nanoparticles only, while the less bulky MPS monomer can access to higher order morphologies such as vesicles. The different reactivities of these alkoxysilane monomers with respect to hydrolysis and condensation also causes a significant effect on the controlled growth of silica shell at particle surface, resulting smooth (MPS) or lobed silica shells (IPS).

The stability of these two alkoxysilane monomers represents a synthetic and characterization challenge. Both monomers are difficult to work with (especially MPS), and purification and storage of the resulting polymers can be troublesome as alkoxysilane monomers are moisture and temperature sensitive, resulting in undesired crosslinking. Redissolution in common solvents and subsequent analysis by SEC is thus complicated and hindered by additional peaks at higher molecular weights which are highly caused by crosslinking and the formation of aggregated structures. Despite these challenges, effective chain extension of alkoxysilane based macroRAFT agents has been demonstrated and the self-assembly of resulting diblock copolymers via the PISA mechanism in a block-selective solvent with good colloidal stability has been shown. Overall, the approach outlined in this chapter demonstrates a pathway towards

the preparation of hybrid nanoparticles, where the inorganic component (silica) is prepared orthogonally to the morphology-directing component (the PISA step). The potential exists for the process to be performed in a one-pot synthesis upon appropriate choice of second block monomer and solvent. This work is also quite attractive and important to polymer field as hybrid polymer-silica nanoparticles vesicles can be easily produced by this method, providing access to a morphology that is not typically achievable via other colloidal nanocomposite synthetic approaches.

3.4 References

1. P. R. Supronowicz, P. M. Ajayan, K. R. Ullmann, B. P. Arulanandam, D. W. Metzger and R. Bizios, *Journal of Biomedical Materials Research*, 2002, **59**, 499-506.
2. A. Bianco, B. M. Bozzo, C. D. Gaudio, I. Cacciotti, I. Armentano, M. Dottori, F. D'Angelo, S. Martino, A. Orlacchio and J. M. Kenny, *Journal of Bioactive and Compatible Polymers*, 2011, **26**, 225-241.
3. B. P. Tripathi and V. K. Shahi, *Progress in Polymer Science*, 2011, **36**, 945-979.
4. K. Feng, B. B. Tang and P. Y. Wu, *ACS Applied Materials & Interfaces*, 2013, **5**, 1481-1488.
5. S. P. Nunes, K. V. Peinemann, K. Ohlrogge, A. Alpers, M. Keller and A. T. N. Pires, *Journal of Membrane Science*, 1999, **157**, 219-226.
6. C. N. Berger, M. Dirschka and A. Vijayaraghavan, *Nanoscale*, 2016, **8**, 17928-17939.
7. K. Landfester, *Angewandte Chemie International Edition*, 2009, **48**, 4488-4507.
8. K. Y. van Berkel and C. J. Hawker, *Journal of Polymer Science Part A: Polymer Chemistry*, 2010, **48**, 1594-1606.
9. D. Qi, Z. Cao and U. Ziener, *Advances in Colloid and Interface Science*, 2014, **211**, 47-62.
10. N. S. Othman and E. Bourgeat-Lami, *Langmuir*, 2009, **25**, 10121-10133.
11. E. Bourgeat-Lami, I. Tissot and F. Lefebvre, *Macromolecules*, 2002, **35**, 6185-6191.
12. M. Kim, Y. K. Kim, J. Kim, S. Cho, G. Lee and J. Jang, *RSC Advances*, 2016, **6**, 27460-27465.
13. H. Zhu, Q. Zhang and S. Zhu, *Dalton Transactions*, 2015, **44**, 16752-16757.
14. P. B. Zetterlund, S. C. Thickett, S. Perrier, E. Bourgeat-Lami and M. Lansalot, *Chemical Reviews*, 2015, **115**, 9745-9800.
15. Y. Wang, A. S. Angelatos and F. Caruso, *Chemistry of Materials*, 2008, **20**, 848-858.
16. I. I. Slowing, B. G. Trewyn, S. Giri and V. S. Y. Lin, *Advanced Functional Materials*, 2007, **17**, 1225-1236.
17. F. Flaig, J. Rinck, M. Stephan, T. Bocksrocker, M. Bruns, C. Kubel, A. Powell, G. Ozin and U. Lemmer, *Nano Letters*, 2013, **13**, 475-480.
18. R. Mitran, D. Berger, C. Munteanu and C. Matei, *Journal of Physical Chemistry C*, 2015, **119**, 15177-15184.
19. B. G. Trewyn, J. A. Nieweg, Y. Zhao and V. S. Y. Lin, *Chemical Engineering Journal*, 2008, **137**, 23-29.
20. Q. G. Xiao, X. Tao, H. K. Zou and J. F. Chen, *Chemical Engineering Journal*, 2008, **137**, 38-44.
21. S. Santra, H. Yang, D. Dutta, J. T. Stanley, P. H. Holloway, W. Tan, B. M. Moudgil and R. A. Mericle, *Chemical Communications*, 2004, **0**, 2810-2811.
22. J. X. Wang, L. X. Wen, Z. H. Wang and J. F. Chen, *Materials Chemistry and Physics*, 2006, **96**, 90-97.
23. I. Tissot, C. Novat, F. Lefebvre and E. Bourgeat-Lami, *Macromolecules*, 2001, **34**, 5737-5739.
24. I. Tissot, J. P. Reymond, F. Lefebvre and E. Bourgeat-Lami, *Chemistry of Materials*, 2002, **14**, 1325-1331.
25. M. J. Percy, J. I. Amalvy, D. P. Randall, S. P. Armes, S. J. Greaves and J. F. Watts, *Langmuir*, 2004, **20**, 2184-2190.

26. M. J. Percy, V. Michailidou, S. P. Armes, C. Perruchot, J. F. Watts and S. J. Greaves, *Langmuir*, 2003, **19**, 2072-2079.
27. Z. Gao, S. K. Varshney, S. Wong and A. Eisenberg, *Macromolecules*, 1994, **27**, 7923-7927.
28. L. Zhang and A. Eisenberg, *Science*, 1995, **268**, 1728-1731.
29. S. L. Canning, G. N. Smith and S. P. Armes, *Macromolecules*, 2016, **49**, 1985-2001.
30. S. Sugihara, A. Blanazs, S. P. Armes, A. J. Ryan and A. L. Lewis, *Journal of the American Chemical Society*, 2011, **133**, 15707-15713.
31. N. J. Warren, O. O. Mykhaylyk, D. Mahmood, A. J. Ryan and S. P. Armes, *Journal of the American Chemical Society*, 2014, **136**, 1023-1033.
32. L. A. Fielding, M. J. Derry, V. Ladmiral, J. Rosselgong, A. M. Rodrigues, L. P. D. Ratcliffe, S. Sugihara and S. P. Armes, *Chemical Science*, 2013, **4**, 2081-2087.
33. X. Zhang, J. Rieger and B. Charleux, *Polymer Chemistry*, 2012, **3**, 1502-1509.
34. M. Semsarilar, V. Ladmiral, A. Blanazs and S. P. Armes, *Langmuir*, 2012, **28**, 914-922.
35. M. Semsarilar, V. Ladmiral, A. Blanazs and S. P. Armes, *Langmuir*, 2013, **29**, 7416-7424.
36. P. Yang, L. P. D. Ratcliffe and S. P. Armes, *Macromolecules*, 2013, **46**, 8545-8556.
37. X. Zhang, S. Boisse, C. Bui, P. A. Albouy, A. Brulet, M. H. Li, J. Rieger and B. Charleux, *Soft Matter*, 2012, **8**, 1130-1141.
38. S. Dong, W. Zhao, F. P. Lucien, S. Perrier and P. B. Zetterlund, *Polymer Chemistry*, 2015, **6**, 2249-2254.
39. V. Mellon, D. Rinaldi, E. Bourgeat-Lami and F. D'Agosto, *Macromolecules*, 2005, **38**, 1591-1598.
40. Y. Zhang, S. Luo and S. Liu, *Macromolecules*, 2005, **38**, 9813-9820.
41. H. Ozaki, A. Hirao and S. Nakahama, *Macromolecules*, 1992, **25**, 1391-1395.
42. M. Rabnawaz, Z. Wang, Y. Wang, I. Wyman, H. Hu and G. Liu, *RSC Advances*, 2015, **5**, 39505-39511.
43. E. Rizzardo, J. Chiefari, R. T. A. Mayadunne, G. Moad and S. H. Thang, in *Controlled/Living Radical Polymerization*, ed. K. Matyjaszewski, American Chemical Society, 2000, vol. 768, ch. 20, pp. 278-296.
44. S. P. Vernekar, N. D. Ghatge and P. P. Wadgaoknar, *Journal of Polymer Science Part A: Polymer Chemistry*, 1988, **26**, 953-958.
45. D. J. Kang and B. S. Bae, *Journal of Non-Crystalline Solids*, 2008, **354**, 4975-4980.
46. J. S. Davies, C. L. Higginbotham, E. J. Tremeer, C. Brown and R. C. Treadgold, *Journal of the Chemical Society, Perkin Transactions 1*, 1992, **0**, 3043-3048.
47. İ. Kaya and Ç. Y. Pala, *Fluid Phase Equilibria*, 2014, **374**, 63-69.
48. Y. Ma and T. P. Lodge, *Macromolecules*, 2016, **49**, 3639-3646.
49. D. Zehm, L. P. D. Ratcliffe and S. P. Armes, *Macromolecules*, 2013, **46**, 128-139.
50. Y. Pei, O. R. Sugita, L. Thurairajah and A. B. Lowe, *RSC Advances*, 2015, **5**, 17636-17646.
51. M. J. Derry, L. A. Fielding, N. J. Warren, C. J. Mable, A. J. Smith, O. O. Mykhaylyk and S. P. Armes, *Chemical Science*, 2016, **7**, 5078-5090.
52. E. R. Jones, O. O. Mykhaylyk, M. Semsarilar, M. Boerakker, P. Wyman and S. P. Armes, *Macromolecules*, 2016, **49**, 172-181.
53. L. Wang, J. Zhou, X. Dong, T. Chen, Q. Yang, C. Chen and X. Chen, *Nanotechnology*, 2006, **17**, 2745-2751.
54. A. Choucair, C. Lavigueur and A. Eisenberg, *Langmuir*, 2004, **20**, 3894-3900.
55. D. A. Canelas, D. E. Betts and J. M. DeSimone, *Macromolecules*, 1996, **29**, 2818-2821.
56. R. G. Gilbert, *Emulsion polymerization: a mechanistic approach*, Academic Press, 1995.

Chapter 4 : Self-Assembly of Block Copolymers with an Alkoxysilane-Based Core Forming Block: A Study of Synthetic Approaches and Copolymer Composition

4.1 Introduction

As detailed in Chapter 1, polymeric based colloidal nanocomposites have become a popular research topic recently, especially integrated with either an organic or inorganic phase at the nanoscale. Numerous materials can be used to prepare such nanocomposites such as natural and synthetic clays,[1-3] (semi-) metal oxide nanoparticles,[4-12] graphene-derived nanosheets,[13-17] carbon nanotubes,[18, 19] and quantum dots.[20-22] In general, such hybrid materials are prepared by dispersing organic/inorganic materials into the monomer phase (for miniemulsion polymerization)[23, 24] or the continuous phase (for emulsion and dispersion polymerization)[25-28] and then radical polymerization leads to the formation of an *in-situ* composite.

Polymer-silica hybrid nanocomposite has received significant research attention in recent decades.[29-31] Modified silica nanoparticles have been used to prepare the reverse silica@polymer (silica core / polymer shell) structure via "grafting from" or "grafting to". As "grafting to" has some limitations (e.g. low grafting density),[32] a combination of "grafting from" and reversible deactivation radical polymerization has been developed in recent times, known as surface-initiated reversible deactivation radical polymerization (SI-RDRP).[25] SI-RDRP has been demonstrated as a powerful tool in emulsion polymerization (such as RAFT-assisted encapsulating emulsion polymerization[10-12, 18, 22, 33]) to further advance the design of colloidal

nanocomposite where the organic/inorganic phase can be enclosed by a living polymer shell. This method is established on physisorption of a specifically designed amphiphilic RAFT copolymer onto the surface of the organic/inorganic nanomaterial, with a subsequent starved-feed emulsion polymerization.

Alkoxysilane functional monomers such as 3-(trimethoxysilyl)propyl methacrylate (MPS) are highly prone to hydrolysis and condensation when dispersed in water and this process has been formerly used to prepare colloidal nanocomposites.[34-37] A straightforward route was showed by van der Wel and co-workers in producing colloidal organosilica with variable particle size.[34] This approach involved stirring MPS in water at room temperature in the presence of ammonium hydroxide catalyst. Using a base catalyst in preparing hybrid colloids is quite common and has been reported elsewhere, e.g. MPS based emulsification to prepare hybrid colloids at room temperature.[35-37] This step precedes the free-radical polymerization of the unreacted vinyl groups present in the MPS colloid, "solidifying" the particle and creating a polymer-silica hybrid.

Polymerization-induced self-assembly (PISA) has been widely used in preparing polymer-silica colloidal nanocomposites.[38-43] Surface-initiated PISA was recently applied to assemble silica nanoparticles (~15 nm diameter, dispersed in ethanol) into "strings" and vesicles by Benicewicz and coworkers,[38, 39] while the transformation was governed by the balance of solvophilic and solvophobic polymers grafted onto the silica surface. Bourgeat-Lami and coworkers also performed nitroxide-mediated PISA in the presence of aqueous silica nanoparticles so that the poly((PEGMA)-*co*-styrene) macroalkoxyamine could be absorbed onto the surface of silica nanoparticles.[40] This led the block copolymers to self-assemble into

various morphologies at the silica surface under the influence of pH. A potential application of polymeric vesicles prepared by PISA is demonstrated in loading silica nanoparticles into the vesicle core, and the release mechanism is triggered by order-order and order-disorder transitions.[41, 42]

In Chapter 3, the synthesis of polymer/silica nanocomposites with various morphologies via the combination of PISA and sol-gel chemistry was demonstrated. MPS was selected as the solvophilic block in this instance, allowed to undergo chain extension with benzyl methacrylate in ethanol, yielding spherical and vesicular morphologies. The presence of alkoxysilane groups at the particle surface allowed for the controlled condensation of a silica precursor (tetraethylorthosilicate, TEOS) to occur and form a silica shell at the particle interface. In this Chapter, the design of colloidal nanocomposites with an alkoxysilane-functional core is investigated, initially via the PISA process. The first investigated system was the use of a hydrophilic PEG-based macroRAFT agent to mediate aqueous RAFT emulsion polymerization of MPS under different approaches (*ab initio*, seeded, and different initiating systems). Due to various shortcomings and limitations of this method from a mechanistic perspective, solvent-driven self-assembly of pre-prepared block copolymers[44, 45] is utilized in an attempt to prepare targeted nanostructures. The effect of changing the steric bulk of the alkoxysilane core (through the use of the monomer 3-(triisopropoxysilyl) propyl methacrylate, IPS) with respect to the particle morphology is also studied. Lastly, self-assembly of MPS-based block copolymers is demonstrated in an organic solvent (*n*-hexane) through the use of an appropriate lipophilic macroRAFT agent, demonstrating the versatility of MPS in different solvents to form nanoparticles.

4.2 Results and Discussions

4.2.1 Attempts at Aqueous PISA Formulations Using MPS as Solvophobic Monomer

Approaches toward the preparation of MPS-based polymer nanoparticles via the PISA method in aqueous solution are described in this section. As MPS monomer and the corresponding poly(MPS) homopolymer are insoluble in water, this represents a typical emulsion polymerization.[46] The total solids content was set to 10 % w/w in all cases. A trithiocarbonate based solvophilic block (poly(ethylene glycol) methyl ether methacrylate, PEGMA, monomer M_n = 950 Da) was chain extended with MPS in pH 7 buffer to reduce the possibility of MPS hydrolysis, which is accelerated under acidic or basic conditions.[47-49] The overall procedure is illustrated in Figure 4-1. Three PEGMA macroRAFT agents with different degree of polymerization were prepared, all of which possessed a narrow molecular weight distribution ($Đ$ ~ 1.1; refer to Figure 4-2 and Table 4-1).

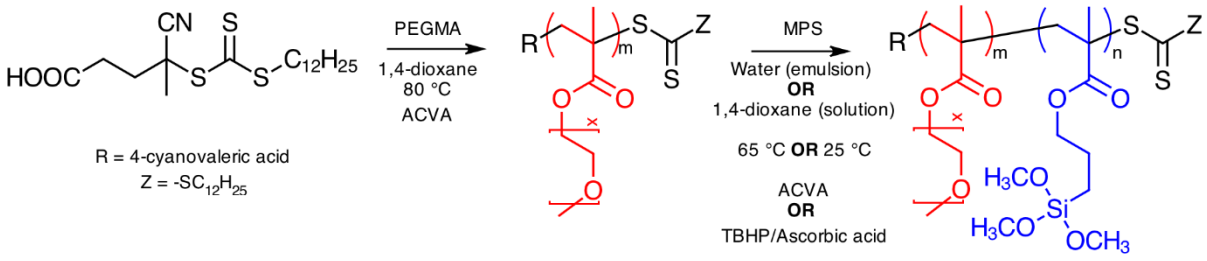

Figure 4-1: Overview of PEGMA-b-PMPS block copolymer synthesis via either RAFT mediated solution polymerization or emulsion polymerization

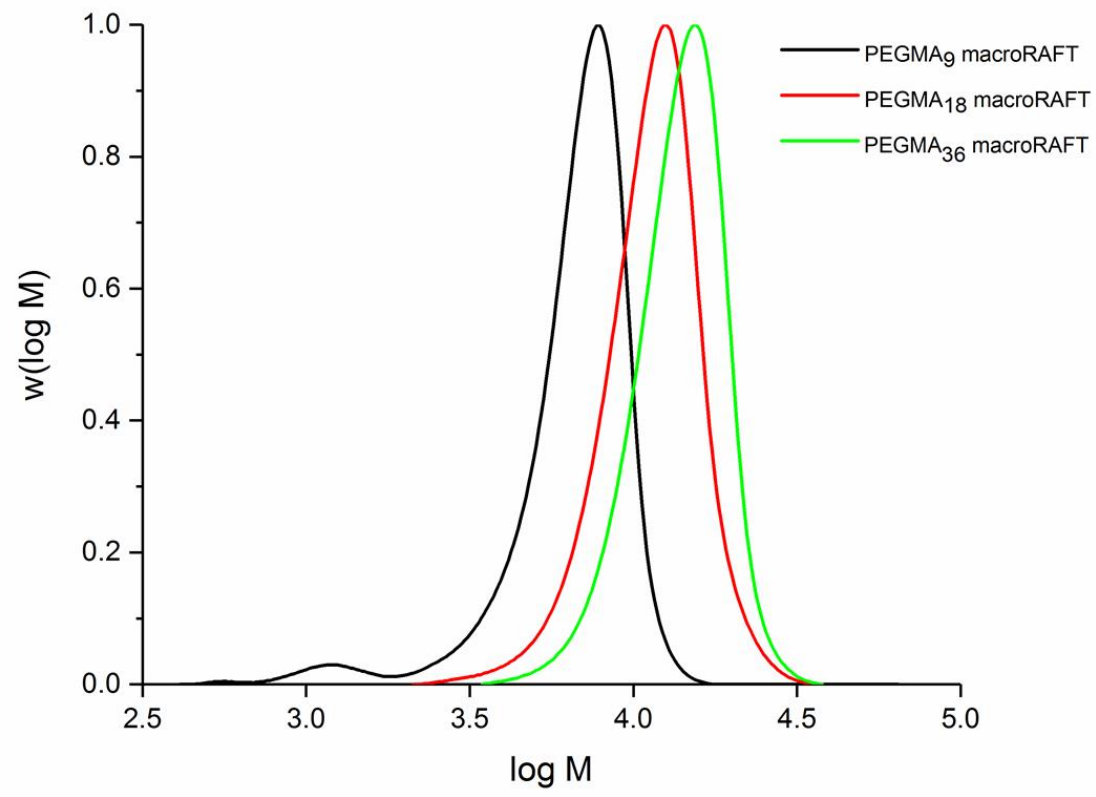

Figure 4-2: SEC distributions of the three different PEGMA macroRAFT agents used in this Chapter

Table 4-1: SEC data of the three different PEGMA macroRAFT agents shown in Figure 4-2

Target PEGMA DP	**PEGMA conversion**	**DP_{th}**	**M_n (kDa)**	**$Đ$**
10	0.89	9	5.7	1.23
20	0.89	18	11.9	1.13
40	0.87	36	14.4	1.10

The results of the RAFT-mediated emulsion polymerizations (using ACVA as initiator) are reported in Table 4-2. Extensive coagulum was observed in nearly all RAFT-mediated emulsion polymerizations, making it difficult to determine the MPS conversion (values ranged from 27% to 92%, according to the latex that was formed). Electron microscopy (Figure 4-3) and DLS analysis revealed the formation of spherical polymer nanoparticles, however, there

was no clear trend in particle size across these experiments. The extensive coagulum was caused by the MPS block, as opposed to the possibility of poor colloidal stability provided by the PEGMA stabilizer block. This was demonstrated through the use of the $PEGMA_{18}$ macroRAFT agent to polymerize another methacrylate-based hydrophobic monomer (benzyl methacrylate) in water to high conversion, resulting in the formation of stable nanoparticles with no coagulum (Sample 4-S in Table 4-4).

Table 4-2: Summary of ab initio RAFT-mediated emulsion polymerization of MPS at 65 °C for 24 hours. All the experiments were conducted at 10% w/w except where noted.

Sample code	**PEGMA MacroRAFT agents**	**Target MPS DP**	**MPS conversion[a]**	**d_z (nm) (PDI)**
4-A	$PEGMA_9$	80	0.92	160 (0.41)
4-B		100	0.57	98 (0.38)
4-C		200	0.92	111 (0.29)
4-D	$PEGMA_{18}$	80	0.55	80 (0.13)
4-E		100	0.70	89 (0.14)
4-F		200	0.27	148 (0.26)
4-G	$PEGMA_{36}$	200	n/a[c]	150 (0.25)
4-H		400[b]	n/a[c]	190 (0.38)
4-I		600[b]	n/a[c]	357 (0.25)

[a] In all samples, extensive coagulum was observed. Conversion was based on stable latex only and values listed above were underestimate. [b] Target solids content was 20% w/w. [c] No meaningful conversion was measured due to high level of coagulum.

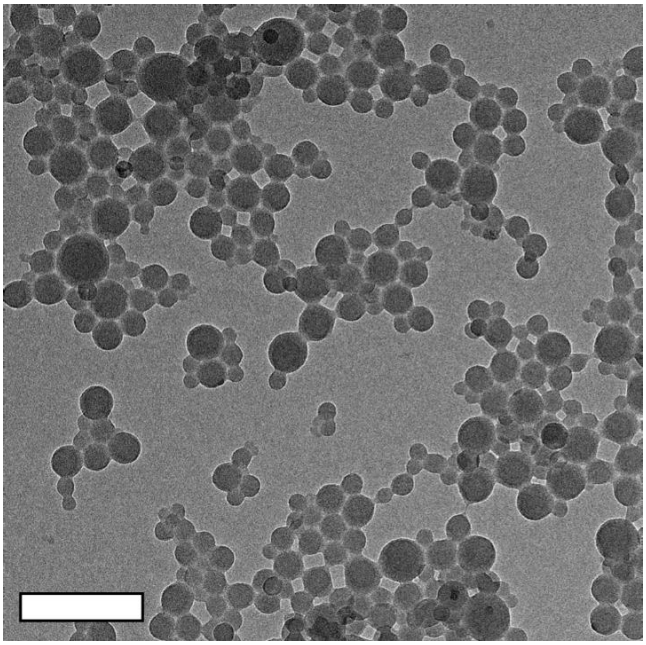

Figure 4-3: TEM image of Sample 4-F (in Table 4-2) prepared by RAFT-mediated emulsion polymerization. Scale bar= 200 nm.

Due to presence of extensive coagulum, SEC analysis was inconsistent and troublesome in evaluating successful chain extension. The coagulum was often insoluble in THF, providing data that only partially represented the molecular weight distribution (MWD) of the polymer formed. This can be seen in Figure 4-4(A). No detectable chain extension and a significant low molecular weight "tail" in the distribution was observed. When the PEGMA macroRAFT agents were replaced with a poly(ethylene glycol) methyl ether (PEG-2000)-CDTSPA RAFT agent, similar results were obtained. The synthesis of (PEG-2000)-CDTSPA RAFT via esterification is shown in Figure 4-5. Upon attempted RAFT emulsion polymerization of MPS, comparable coagulum again occurred, with formation of low molecular weight polymer (Table 4-3, Figure 4-6, and Figure 4-7).

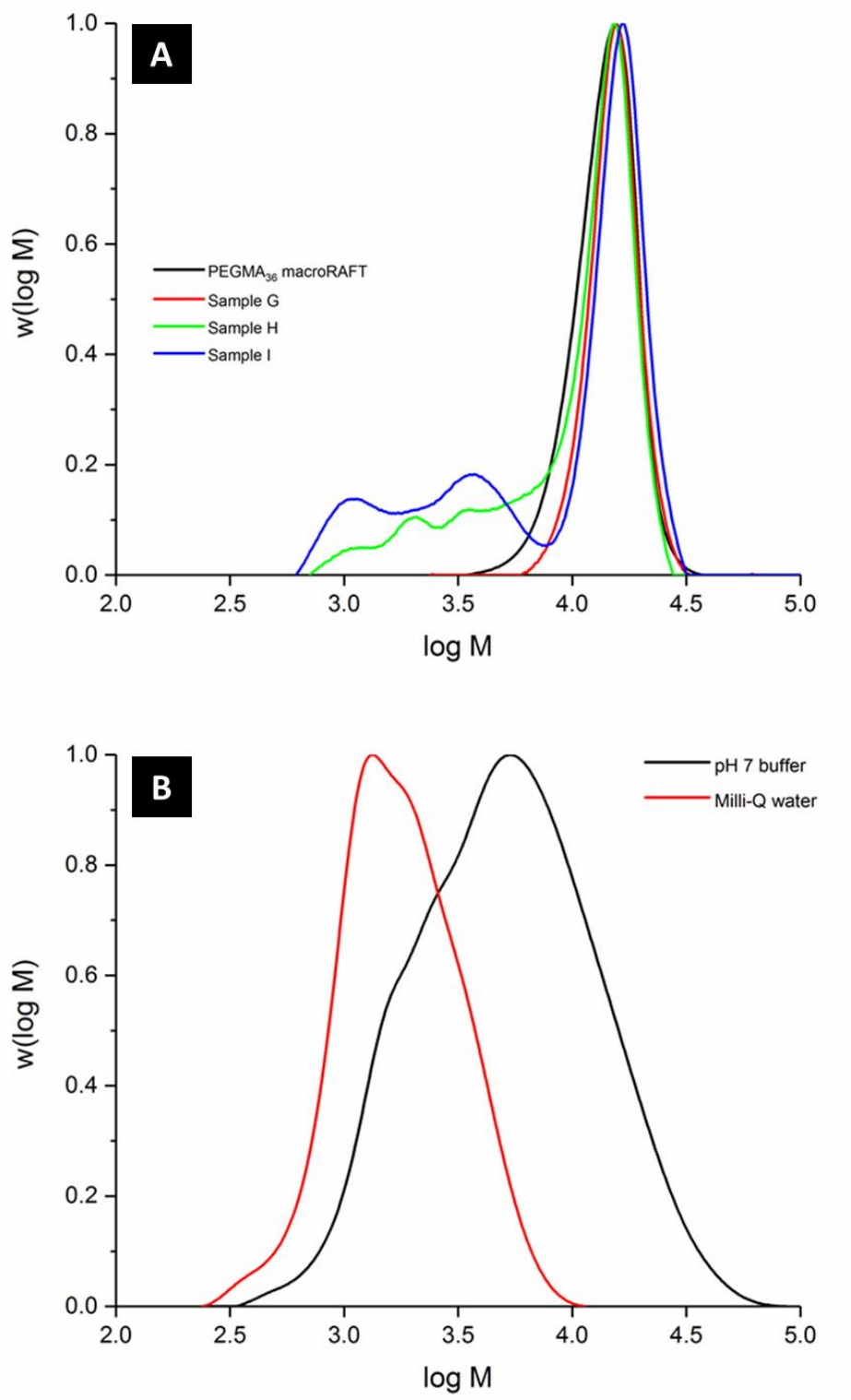

Figure 4-4: Height-normalized SEC molecular weight distributions of: (A) $PEGMA_{36}$ macroRAFT agent and subsequent emulsion polymerization of MPS; (B) Precipitate formed during the emulsification of MPS in pH 7 buffer (black line) and Milli-Q water (red line) at 65 ^{o}C.

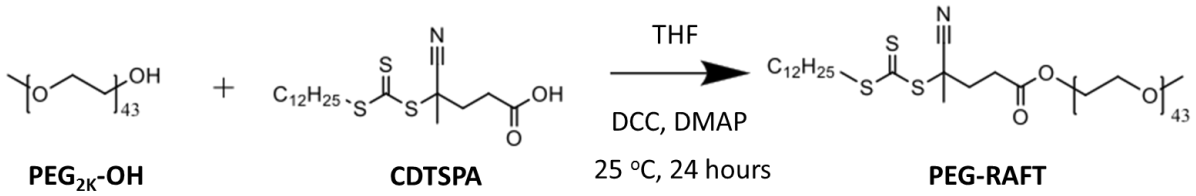

Figure 4-5: Synthesis of (PEG-2000)-CDTSPA RAFT via esterification reaction with hydroxy-functional PEG.

Table 4-3: Summary of ab initio RAFT-mediated emulsion polymerization of MPS using (PEG-2000)-CDTSPA RAFT at 65 °C for 24 hours.

Sample code	Solids content (% w/w)	Target MPS DP	MPS conversion[a]	d_z (nm) (PDI)
4-J	20	100	0.66	139 (0.16)
4-K		200	0.53	180 (0.25)
4-L		300	0.62	200 (0.02)
4-M		400	0.64	218 (0.23)
4-N	10	80	0.66	92 (0.17)
4-O		100	0.68	106 (0.20)
4-P		200	0.60	180 (0.02)
4-Q		300	0.63	241 (0.03)
4-R		400	0.54	255 (0.03)

[a] *In all samples, extensive coagulum was observed. Conversion was based on stable latex only and values listed were underestimated.*

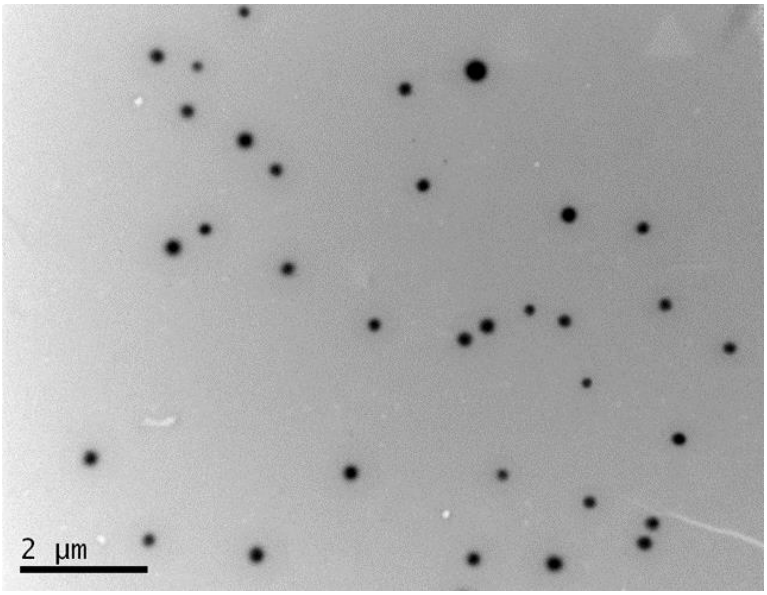

Figure 4-6: TEM image of Sample 4-M in Table 4-3.

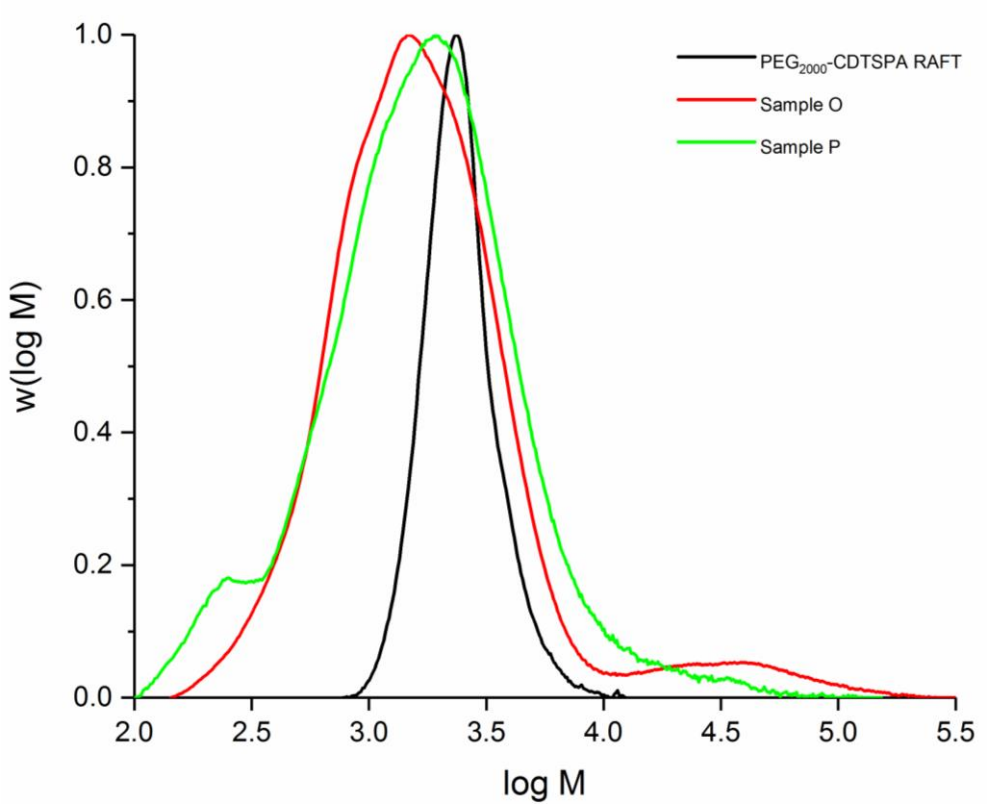

Figure 4-7: Height-normalized SEC distributions of PEGylated RAFT agent and attempted RAFT-mediated emulsion polymerization of MPS.

To further explore the above results, the stability of the MPS monomer alone was investigated under our experimental conditions. In the absence of the stabilizer block (macroRAFT agent) and initiator, MPS was stirred vigorously in either Milli-Q water or pH 7 buffer at 65 ^{o}C for 24 hours. The MPS weight fraction was maintained at 10% w/w to simulate the conditions used in the PISA formulations. In both cases, an oligomeric precipitate formed (buffer: M_n = 3.6 kDa, $Đ$ = 2.2; Milli-Q water: M_n = 1.5 kDa, $Đ$ = 1.4; refer to Figure 4-4(B)). The mass of the precipitate was approximately 79% of the initial mass of the MPS present. This observation (oligomers obtained in this molecular weight range) was similar to previously published work,[50] where MPS was also hydrolysed without catalyst; however in that work MPS-based oligomers took more than 7 days to form at room temperature. The molecular weight distributions reported previously spanned a similar molecular weight range to the polymer produced in above emulsion polymerization experiments (Figure 4-4(A)).

The oligomeric precipitate described above was analysed by NMR spectroscopy. For ^{1}H NMR analysis, resonances attributed to the vinylic protons of MPS (~ 5.58 and 6.03 ppm) were still present after 24 hours reaction (Figure 4-8), however, the integral of the singlet at 3.52 ppm (three methoxy groups) had reduced by ~ 83% relative to the initial value. ^{29}Si NMR analysis of the precipitate (Figure 4-9) also revealed four distinct peaks at -42.3 ppm, -50.6 ppm, -58.9 ppm, and -68.5 ppm which corresponded to T^0, T^1, T^2, and T^3 groups respectively. The superscript number (T^0 to T^3) refer to Si atoms with 0, 1, 2, and 3 Si-O-Si linkages respectively.[51] Both NMR analyses strongly supported precipitate formation was via the hydrolysis and condensation of the trimethoxysilyl moiety under catalyst-free conditions used here. A similar experiment performed at 25 ^{o}C was precipitate-free and no condensation of the MPS monomer was observed by ^{29}Si NMR (Figure 4-9), emphasizing the importance of reaction temperature.

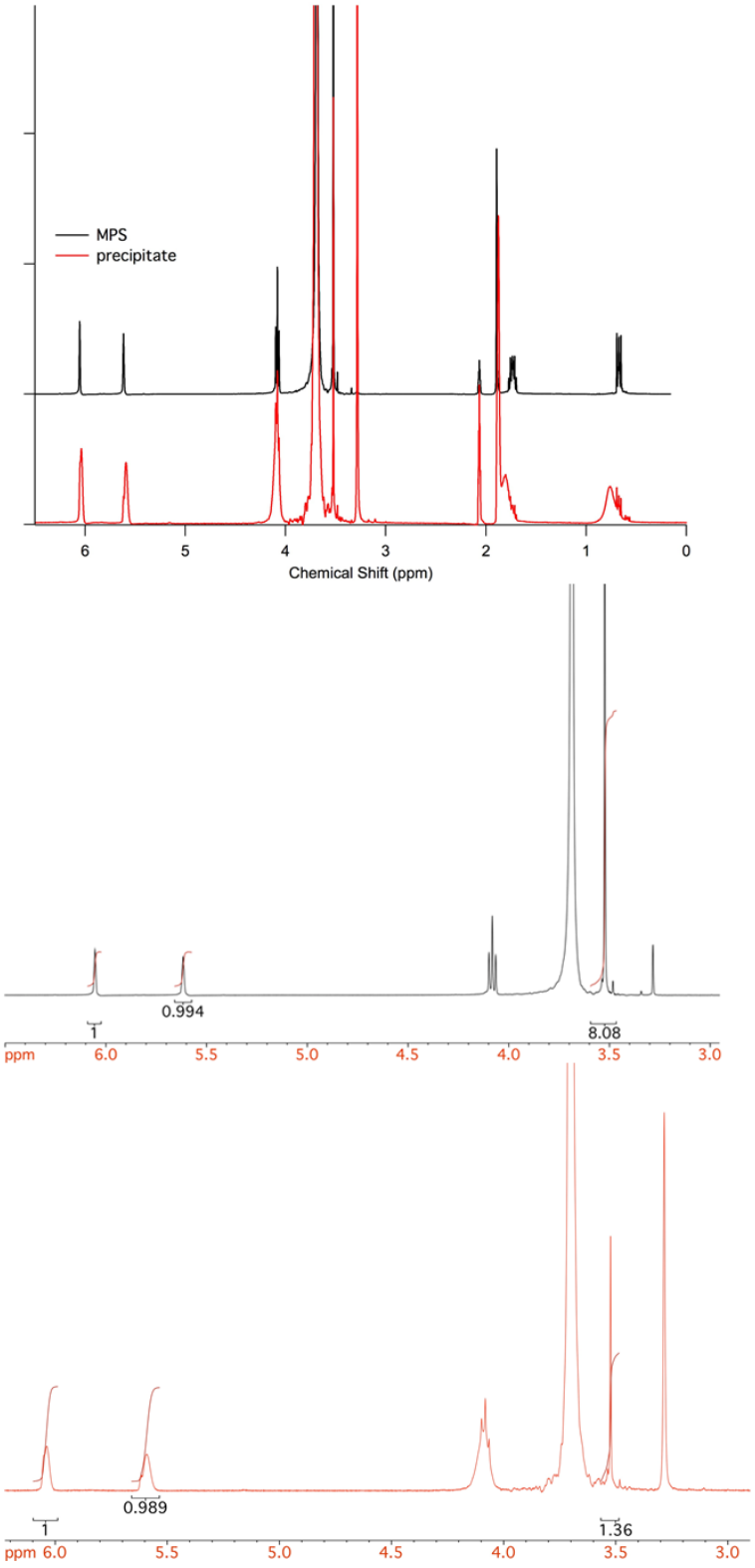

Figure 4-8: (Top): ^{1}H NMR spectra of MPS/water emulsion (black line) and precipitate (red line) after stirring at 65 ^{o}C for 24 hours. (Middle): Enlarged region of MPS/water spectrum showing vinyl resonance at 5.58 and 6.03 ppm and trimethoxy resonance at 3.52 ppm. (Bottom): The precipitate showed that the vinyl resonances were still present and the integral of the trimethoxy resonance had decreased significantly.

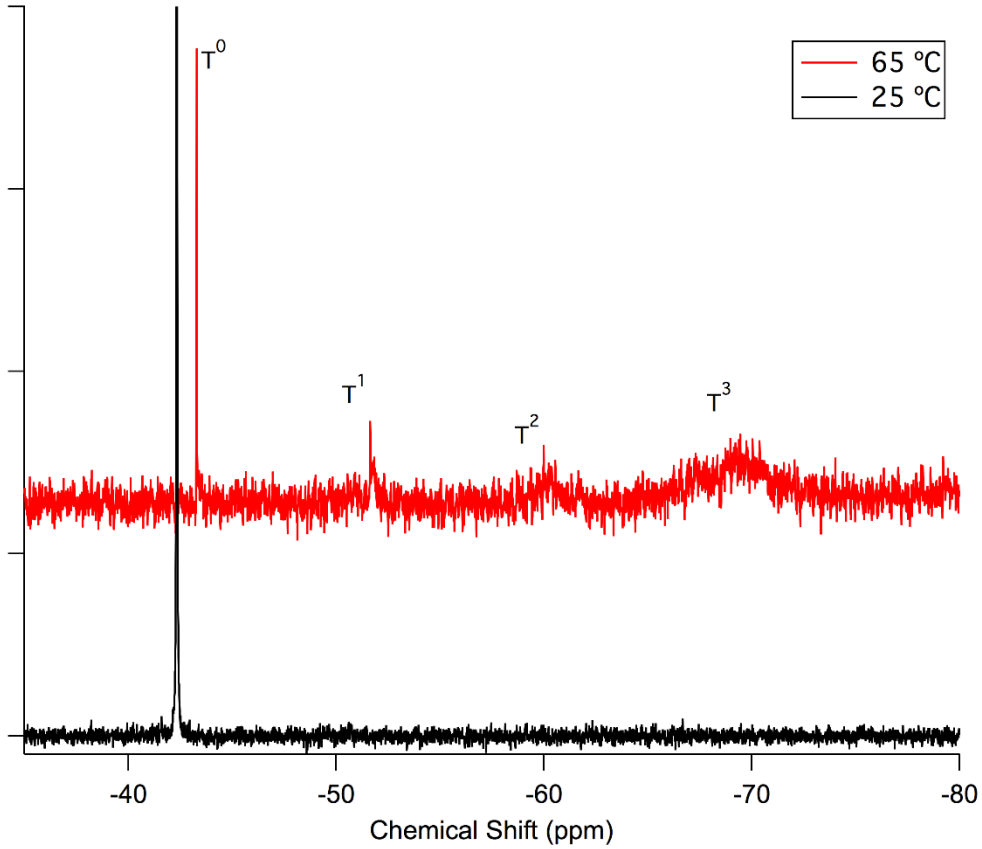

Figure 4-9: ^{29}Si NMR of the precipitate formed during emulsification of MPS in water at 65 °C for 24 hours (red curve) and at 25 °C (black curve, no precipitate).

Based on these observations, we conclude that under these conditions the *ab initio* RAFT emulsion polymerization of MPS was not possible due to the inherent instability of the monomer in water. The hydrolysis and subsequent condensation of MPS led to the formation of polymeric species through siloxane linkages, which greatly compromised the ability for monomer addition and chain extension via the RAFT process. This also explains the broad and low molecular weight distributions seen in these attempted PISA systems (Figure 4-4).

Comparing these results to previously published work, it is worth noting that MPS has been used in radical emulsion polymerization systems to produce hybrid latex particles via copolymerization with styrene.[52, 53] In those publications, the pH was maintained at 7 (similar in this work) to minimize MPS hydrolysis and condensation, and no MPS side reactions were reported. However, MPS was added in a second step after particle nucleation,[53] avoiding the formation of MPS droplets in the aqueous continuous phase. In an *ab initio* system under RAFT control such as those used here, the particle nucleation does not commence until the solvophobic block is sufficiently long to induce self-assembly. This prolongs the length of time where the MPS monomer would exist as droplets in the aqueous continuous phase and therefore increasing the chance of hydrolysis and condensation.

The results reported here are supported by published data regarding alkoxysilane hydrolysis. Savard *et al.* showed that the hydrolysis of MPS was pseudo first order in nature, with the rate coefficient for hydrolysis to trisilanol calculated as $k = \sim 1.5 \times 10^{-2}$ hour^{-1} at pH 7 (25 ^{o}C).[47] With reported activation energy data for trialkoxysilane hydrolysis ($E_a = \sim 27$ to 43 kJ mol^{-1} depending on the mechanism of hydrolysis),[48] the degree of MPS hydrolysis after 24 hours at 65 ^{o}C was estimated between 73% and 95%. However, these calculations were based on dilute solution kinetic data, and our experiment was a heterogeneous system of MPS droplets in water. Nonetheless, MPS hydrolysis in our experiment is likely to be significant where the hydrolysis can occur at the MPS droplet/water interface. Savard *et al.* also stated that "the rate of condensation became as rapid as the rate of hydrolysis" under neutral and alkaline pH conditions, supporting our experimental observation of a significant precipitate of oligomers from MPS.

In an attempt to resolve the issue of MPS stability in water at elevated temperature in *ab initio* systems, two different sets of experiments were proposed and conducted: (i) seeded PISA, where self-assembly occurred using another monomer prior to polymerization of MPS; and (ii) low temperature PISA of MPS in water via redox initiation (Table 4-4). In the case of seeded PISA using a $PEGMA_{18}$ macroRAFT agent, benzyl methacrylate (target addition of 100 monomer units) was used as the core forming block, followed by MPS of varying target DP (from 80 to 200). The MPS conversion was high ($\geq$ 84%) and the systems were coagulum-free. Upon increasing the target DP of the MPS block, bimodal particle size distributions were observed by DLS and TEM analysis (Figure 4-10(A, B)). This result suggested that the poly(BzMA) seed was not growing uniformly with further addition of MPS, again attributed to the hydrolytic instability of MPS at elevated temperature. For redox experiments, ascorbic acid and tert-butylhydroperoxide (TBHP) were used as a redox pair to initiate the *ab initio* RAFT emulsion polymerization of MPS at 25 ^{o}C, using the $PEGMA_{18}$ macroRAFT agent. Small and relatively monodisperse nanoparticles were produced and determined by DLS and TEM analysis (Table 4-4 and Figure 4-11). In the redox system, the fractional conversion of MPS was relatively high and the experiments were coagulum free.

Table 4-4: Summary of seeded and redox-initiated RAFT-mediated emulsion polymerization of MPS, using a $PEGMA_{18}$ macroRAFT agent. All the experiments were conducted at 10% w/w.

Sample code	Target MPS DP	MPS conversion	d_z (nm) (PDI)
Seeded			
4-S	Seed (100 units of BzMA)	n/a[a]	50 (0.17)
4-T	80	0.87	100 (0.28)
4-U	100	0.94	145 (0.24)
4-V	200	0.84	244 (0.25)
Redox			
4-W	80	0.68	43 (0.13)
4-X	100	0.74	49 (0.14)
4-Y	200	0.77	52 (0.09)

[a] *Fractional conversion of BzMA was 0.87.*

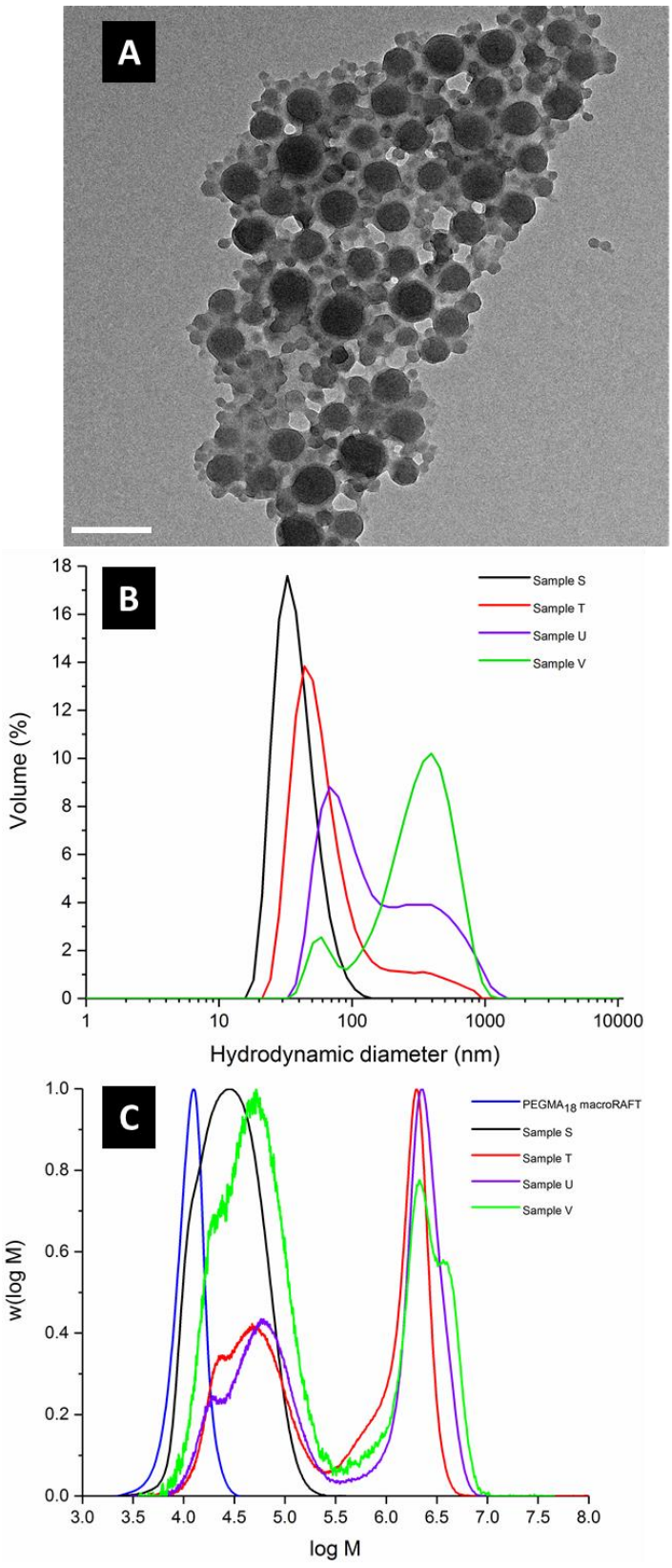

Figure 4-10: Seeded RAFT-mediated emulsion polymerization of MPS. (A) TEM image of Sample 4-V in Table 4-4; (B) DLS volume distributions of seeded experiments; (C) Height-normalized SEC distributions of seeded polymerizations. Scale bar = 200 nm in panel (A).

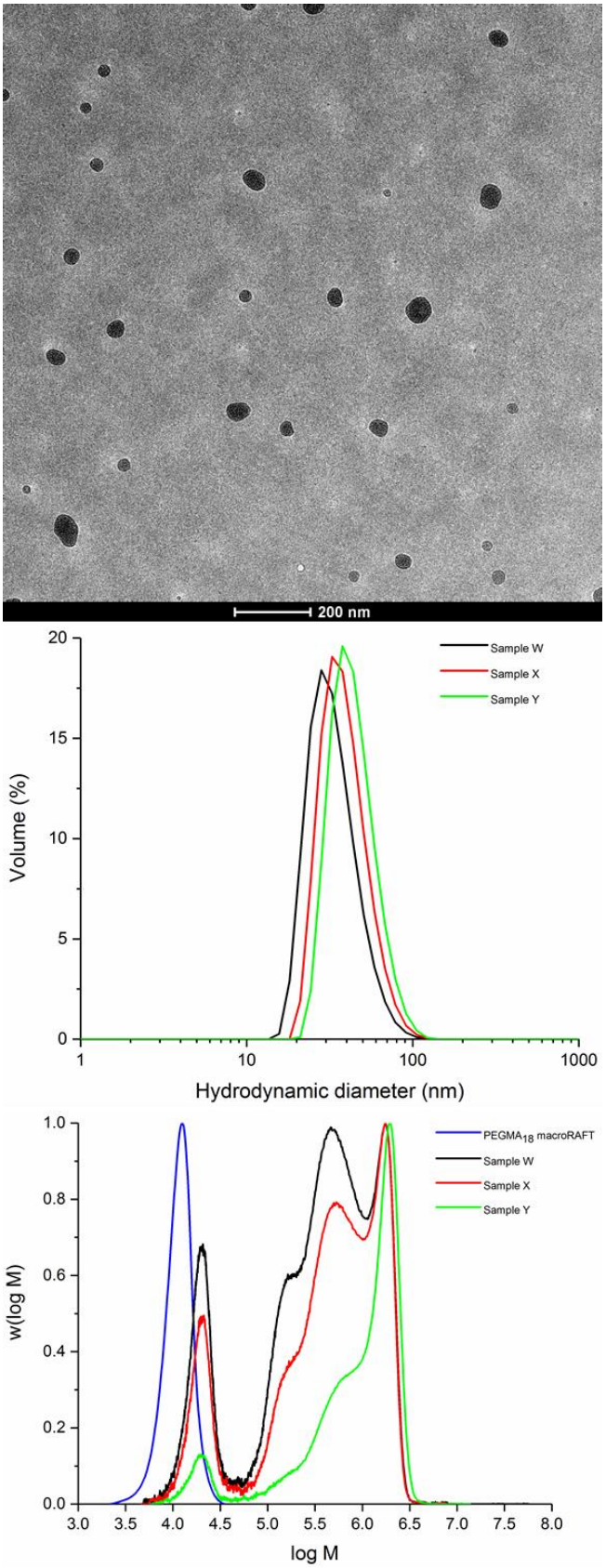

Figure 4-11: Redox-initiated RAFT emulsion polymerization of MPS. (Top): TEM image of Sample 4-Y in Table 4-4; (Middle): DLS volume distributions of samples; (Bottom): Height-normalized SEC distributions of samples.

Unexpected features were observed in the molecular weight distributions of seeded and redox emulsion polymerization systems. A narrow peak at extremely high molecular weight (> 10^6 g mol^{-1}) was observed in all seeded samples (Figure 4-10(C)), in addition to polymer in the "expected" molecular range (10^4 – 10^5 Da). There was some evidence of chain extension of the PEGMA macroRAFT agents. The SEC chromatograms for redox-initiated systems are shown in Figure 4-11 and the peak at extremely high molecular weights is outside the calibration range of the SEC. These unexpected features warrant further discussion, given how different they are to those seen in Figure 4-4. The narrow and extremely high molecular weight peak is attributed to crosslinked polymer nanoparticles that passing through the SEC columns as a single entity, as opposed to individual chains. This is analogous to recent published results in template polymerization in self-assembled polymeric micelles, where the resultant nanoparticles could not be dissociated into individual chains for molecular weight analysis.[54] To achieve such a molecular distribution, the PEGMA macroRAFT agent needs to be successfully chain extended with MPS, with subsequent partial hydrolysis of the polyMPS block promoting *in-situ* crosslinking following self-assembly.

4.2.2 Solution Self-Assembly of PEGMA-b-MPS Copolymers upon Addition of Selective Non-Solvent

As an alternative to RAFT aqueous emulsion polymerization, the solution self-assembly of pre-formed diblock copolymers was performed. For this method, poly(PEGMA-b-MPS) copolymers were prepared by RAFT polymerization in 1,4-dioxane, a good solvent to both blocks. A $PEGMA_{18}$ macroRAFT agent was selected as a stabilizer block and the target MPS DP was varied from 80 to 1000 (Table 4-5 and Figure 4-12). The SEC chromatograms showed a shift towards increased molecular weight with increased target DP of the MPS block as expected. However, a small residual population of PEGMA macroRAFT agent was found in most samples that did not undergo successful chain extension. This was possibly due to steric hindrance of the bulky PEGMA macroRAFT agent that may cause lower re-initiation efficiency. M_p values (representative of the PEGMA-b-PMPS copolymer population) show a linear increase with DP_{th}, indicative of the living nature of the polymerization (Figure 4-13). The polymerization was also confirmed to be first order in nature with respect to the consumption of MPS (Figure 4-14).

Table 4-5: Summary of $PEGMA_{18}$-b-$PMPS_y$ block copolymers via RAFT solution polymerization and their self-assembly upon addition of selective solvent (water). All the experiments were conducted at 10% w/w.

Sample code	Target MPS DP	MPS conversion[a]	DP_{th}	M_n (kDa)	M_p (kDa)	$Đ$[b]	d_z (nm) (PDI)	d_z (nm) (PDI) (post-dialysis)
4-Z	80	0.87	70	11.4	13.7	1.33	37 (0.17)[c]	41 (0.39)
4-AA	100	0.85	85	12.3	17.2	1.68	51 (0.20)[c]	46 (0.23)
4-AB	200	0.78	156	20.7	33.3	1.75	88 (0.20)	53 (0.21)
4-AC	400	0.67	268	28.2	58.6	2.14	105 (0.06)	89 (0.08)
4-AD	600	0.63	378	31.3	73.1	2.38	113 (0.05)	104 (0.03)
4-AE	800	0.53	424	35.0	83.7	2.49	151 (0.03)	147 (0.03)
4-AF	1000	0.42	420	64.8	89.6	2.98	185 (0.06)	185 (0.07)

[a] Determined by NMR spectroscopy, [b] Dispersity of entire distribution (including macroRAFT agent), [c] Self-assembly took place by rapid addition of water via pipette in one shot, in lieu of slow addition via syringe pump.

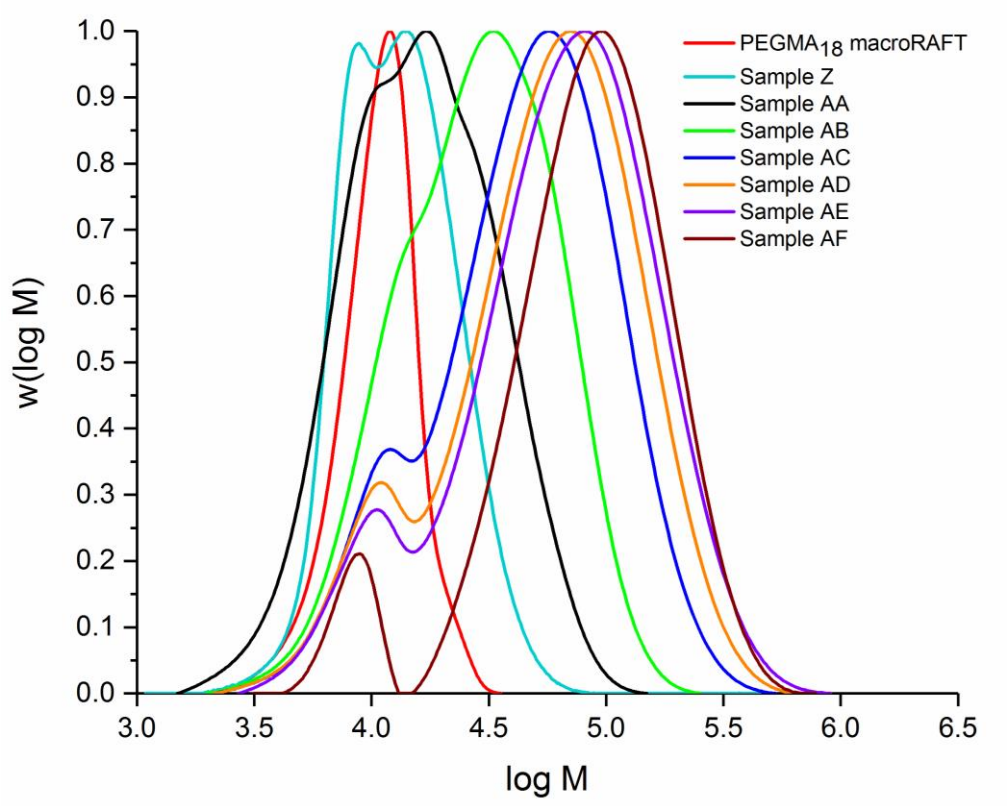

Figure 4-12: Height-normalized SEC molecular weight distributions for PEGMA-b-PMPS block copolymers prepared by RAFT solution polymerization.

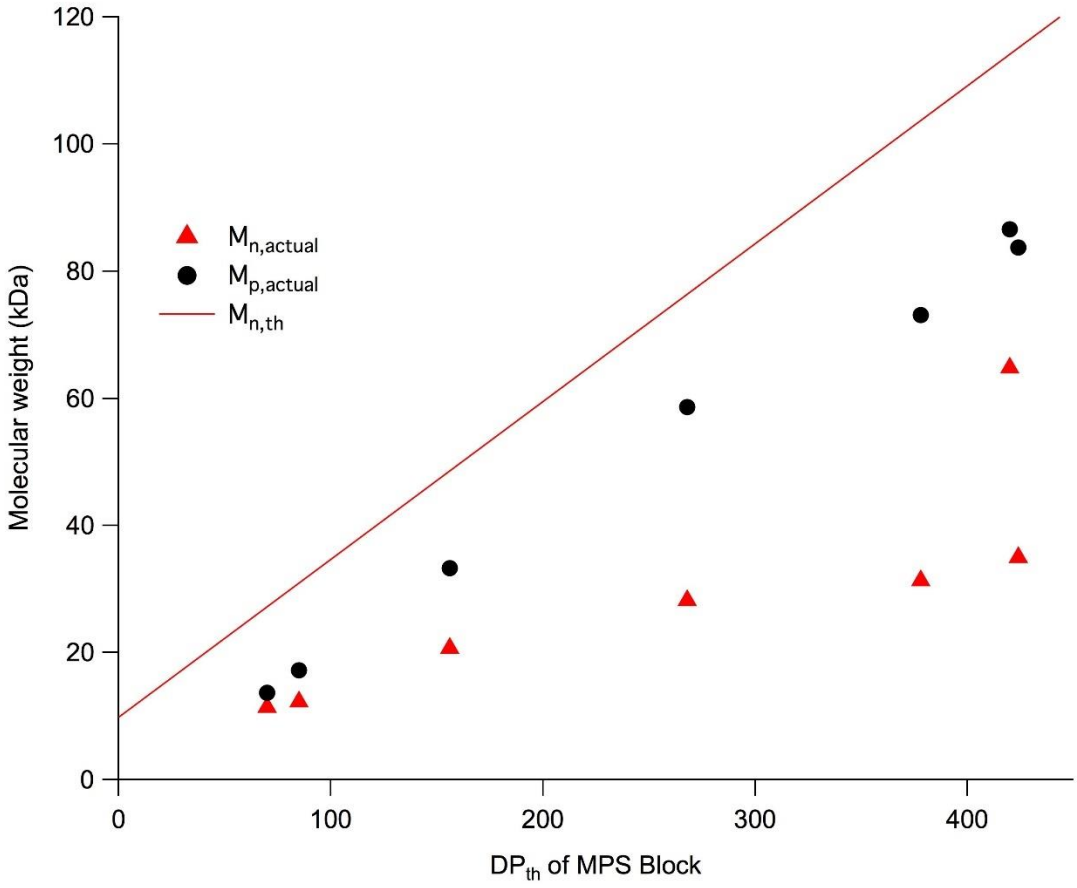

Figure 4-13: Variation of M_n (red triangles) and M_p (black circles) of the PEGMA-b-PMPS block copolymers (from SEC measurements, relative to PMMA standards) reported in Table 4-5. The red line is the theoretical M_n value based on the theoretical DP of the MPS block.

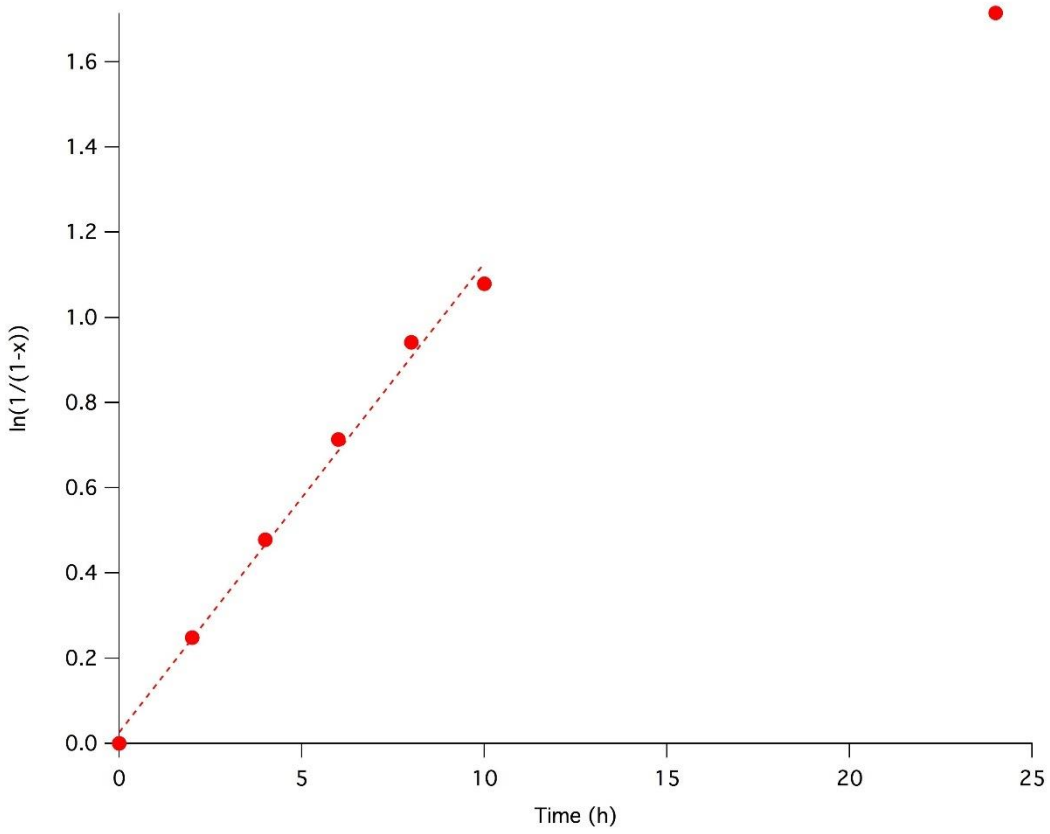

Figure 4-14: Plot of ln(1/(1-x)) vs time (x = fractional conversion of MPS) for the synthesis of $PEGMA_{18}$-b-$PMPS_{200}$ (Sample 4-AB in Table 4-5). A linear fit (R^2 = 0.994) is provided for the first 10 hours of polymerization, indicative of the first-order nature of the consumption of MPS.

Self-assembly of these block copolymers was induced by the slow addition of water which is a poor solvent for the PMPS block. The resultant block copolymers did not undergo purification prior to addition of water. Upon continual addition of water, the solution gradually became turbid and ultimately a milky-white colour. Samples were then dialyzed against water to remove residual 1,4-dioxane. DLS and TEM analyses revealed the resulting nanoparticles were small, and the diameter of relatively monodisperse spheres ranged from ~40 to ~190 nm (Table 4-5, Figure 4-15, and Figure 4-16(A)). For samples with shorter MPS blocks (Samples 4-Z and 4-AA in Table 4-5), a broad size distribution was observed upon slow addition of water, and the samples were not colloidally stable. However, rapid addition of water in a single shot

produced stable nanoparticles for these samples with a moderate polydispersity in size distribution. The hydrodynamic diameter scaled with a 0.65 power law dependence of the DP of the MPS core-forming block (Figure 4-16(B)), a value that is typical of block copolymer self-assembly in the strong segregation limit.[55]

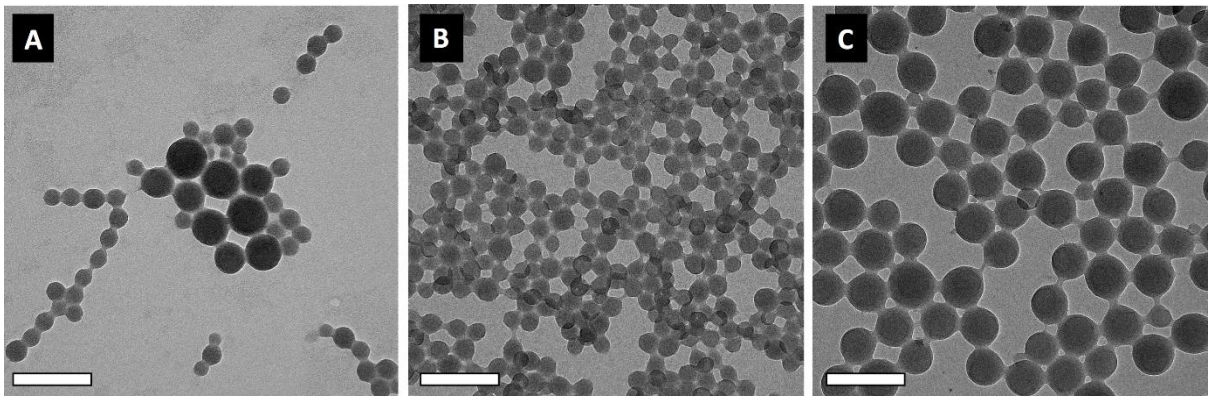

*Figure 4-15: TEM images of nanoparticles prepared by addition of water to a solution of PEGMA-b-PMPS in 1,4 dioxane. (**A**) Sample 4-Z in Table 4-5, (**B**) Sample 4-AC in Table 4-5, and (**C**) Sample 4-AE in Table 4-5. Scale bar = 200 nm in all cases.*

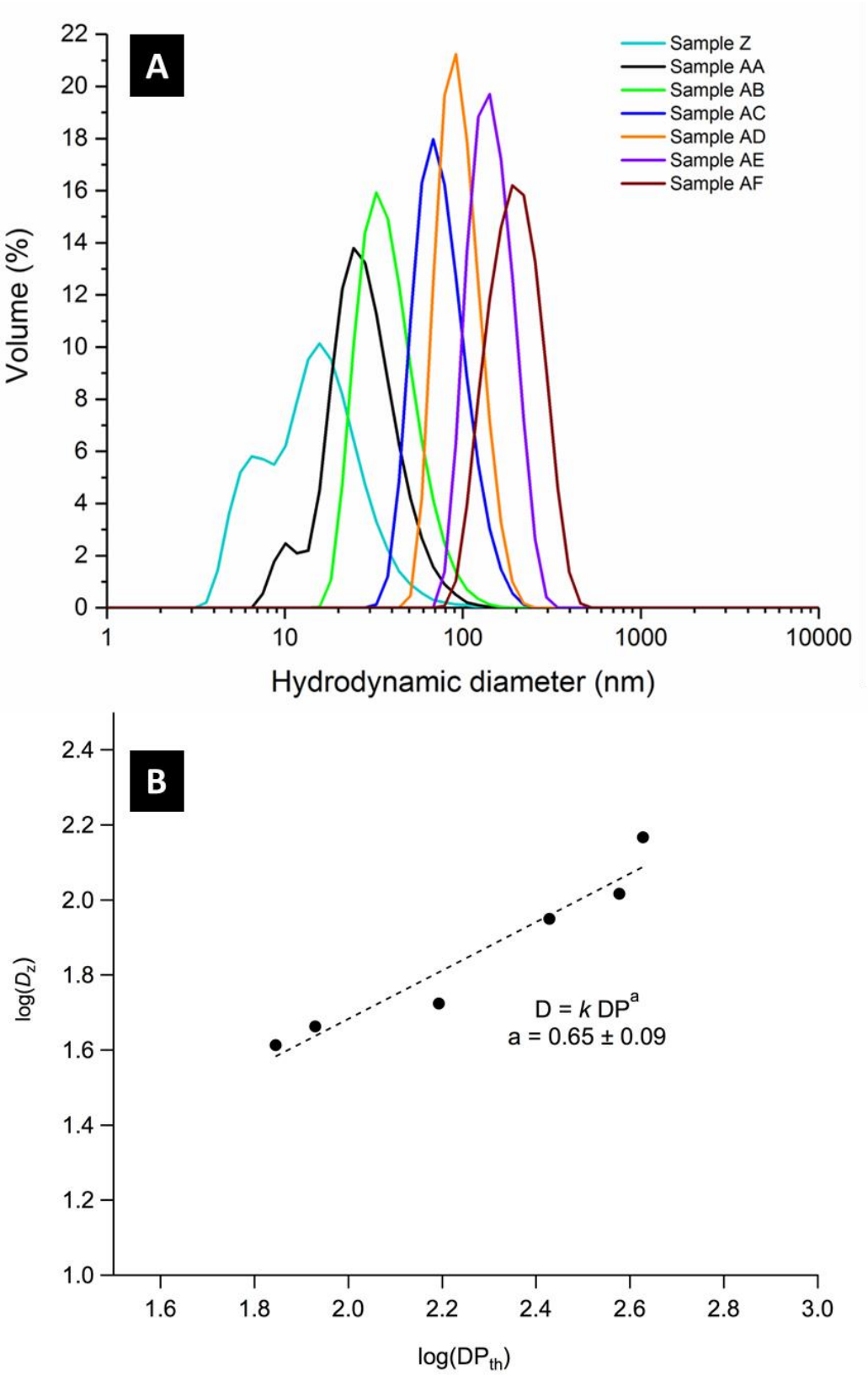

Figure 4-16: (A) DLS volume distributions and (B) variation of hydrodynamic diameter with theoretical MPS DP for self-assembled nanoparticles described in Table 4-5.

Despite the strong asymmetry in the polymer composition upon increasing MPS block length (e.g. Sample 4-AE in Table 4-5 is nominally $PEGMA_{18}$-b-$PMPS_{424}$, with a volume fraction of the MPS block $f_{MPS} \sim 0.96$), all resultant nanoparticles were still spherical. This was unexpected as the thermodynamic of self-assembly suggests that lower curvature shapes should be produced such as rods, vesicles, and lamellae during the self-assembly of highly asymmetric block copolymers.[44, 45, 56, 57] The observed spherical structures could be rationalized either on the basis of the bulky nature of PEGMA-based solvophilic "head group," or that rearrangement beyond spherical micelles was impossible due to kinetic trapping or chemical reaction.[56] It was further shown that the polymer nanoparticles did not dissociate when added to excess miscible good solvent for both blocks after self-assembly. Sample 4-AC (in Table 4-5) was added into 1,4-dioxane and a negligible change in particle size was observed (d_z (initial, in water) = 89 nm; d_z (final, in dioxane) = 84 nm, see Figure 4-17). We presume this is attributed to *in-situ* core crosslinking of the nanoparticles via the trimethoxysilyl groups present along the polymer backbone; this crosslinking traps the morphology and enables the formation of only spherical nanoparticles. This interpretation also matches with the SEC distributions seen in Figure 4-10(C) where an extraordinarily high molecular weight peak is observed; this peak can be attributed to crosslinking of self-assembled polymer chains.

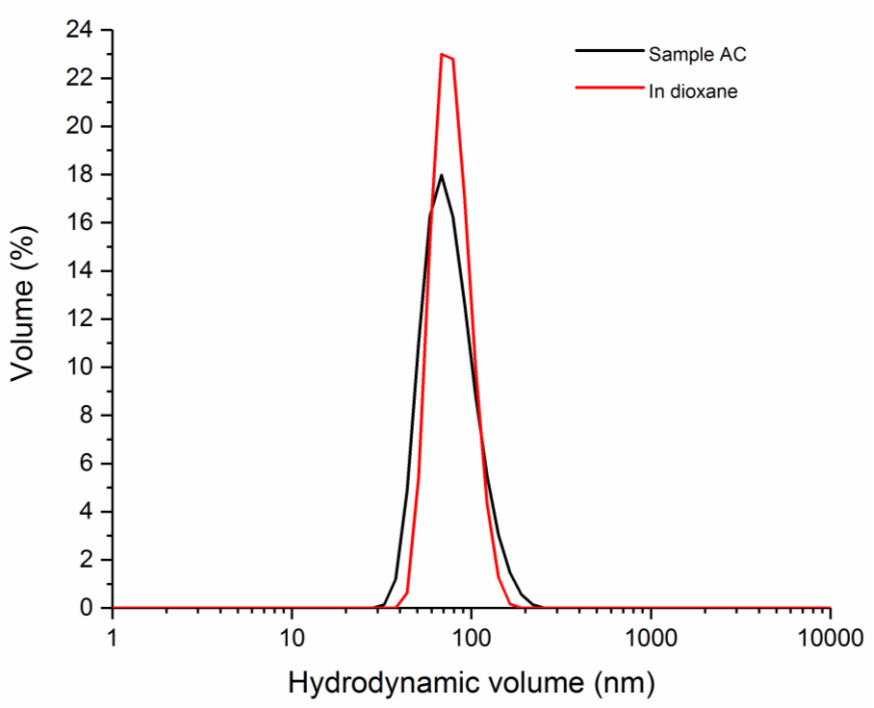

Figure 4-17: DLS volume distributions of Sample 4-AC in Table 4-5 (self-assembled PEGMA-b-PMPS block copolymer in water, black curve); upon adding aqueous dispersion of Sample 4-AC (in Table 4-5) to a miscible good solvent, 1,4 dioxane (red curve).

4.2.3 Self-Assembly of PEGMA-b-IPS Block Copolymers in Water: Effect of Changing the Alkoxysilane Group

In the preceding section, the bulky PEGMA headgroup has the effect of lowering the effective packing parameter of PEGMA-b-PMPS diblock copolymers, favouring the formation of spherical structures. In an attempt to access higher order morphologies, a bulkier monomer (3-(triisopropoxysilyl) propyl methacrylate, IPS) was used to replace MPS as the solvophobic block for self-assembly in water. A similar approach to prepare PEGMA-b-PMPS block copolymers was applied here: a $PEGMA_{18}$ macroRAFT agent was utilised, followed by chain extension with IPS in 1,4-dioxane. At the end of the reaction, the resultant polymer solution

was added with water via syringe pump to induce self-assembly. Once water was completely injected, dialysis was applied to remove residual 1,4-dioxane. The overall synthetic process is shown in Figure 4-18.

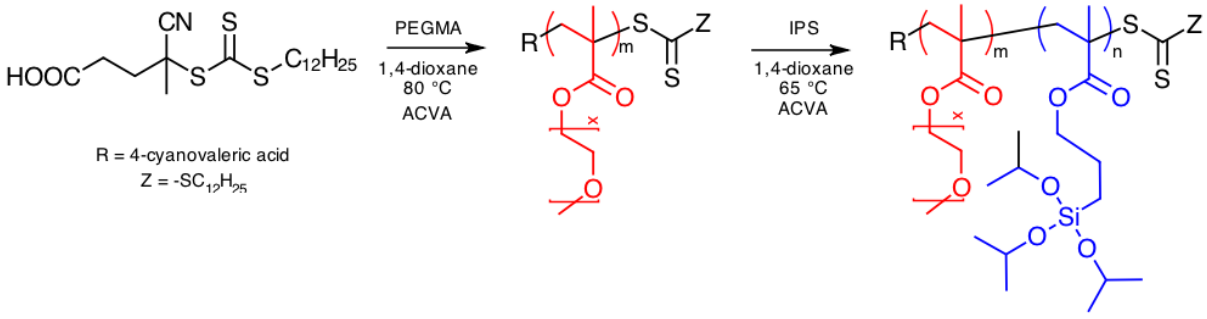

Figure 4-18: Overview of PEGMA-b-PIPS block copolymer synthesis via RAFT mediated solution polymerization

The results of block copolymer synthesis are shown in Table 4-6 and Figure 4-19. A range of target DPs of the IPS block were considered, from 80 to 600 units. All fractional conversions were moderately high and the SEC distributions shifted towards higher molecular weights with increased target DP of the IPS block as expected. A low molecular weight shoulder peak, corresponding to macroRAFT agent that had not undergone chain extension was also observed. We presume this peak is caused by the slow macroRAFT agent consumption during polymerization, causing some block copolymer chains form earlier than others and produce a broader molecular weight distribution. For the isolation of PEGMA-b-PIPS block copolymer, the polymer solution was dialyzed against THF due to PEGMA homopolymer is soluble in methanol/water mixture and this is a typical solvent combination to precipitate PIPS. Similar to PEGMA-b-PMPS block copolymers, it was difficult to achieve PEGMA-b-PIPS copolymers

with a theoretical DP of the core-forming block greater than 450 monomer units (Table 4-5 and Table 4-6).

Table 4-6: Summary of $PEGMA_{18}$-b-$PIPS_x$ diblock copolymers via RAFT solution polymerization and their self-assembly upon addition of selective solvent (water)

Sample code	**Target IPS DP**	**IPS conversion[a]**	**DP_{th}**	**M_n (kDa)**	**$Đ^b$**	**d_z (nm) (PDI)**	**d_z (nm) (PDI) (post-dialysis)**
4-AG	80	0.88	70	27.3	1.71	48.5 (0.12)[c]	49.8 (0.15)
4-AH	100	0.72	72	18.4	2.28	100 (0.21)[c]	97 (0.23)
4-AI	200	0.70	140	33.1	2.38	156 (0.07)	156 (0.07)
4-AJ	400	0.74	296	41.8	2.54	154 (0.04)	154 (0.02)
4-AK	600	0.66	396	48.7	2.70	208 (0.014)	209 (0.03)

[a] Determined by NMR spectroscopy, [b] Dispersity of entire distribution (including macroRAFT agent), [c] Self-assembly took place by rapid addition of water via pipette in one shot, in lieu of slow addition via syringe pump.

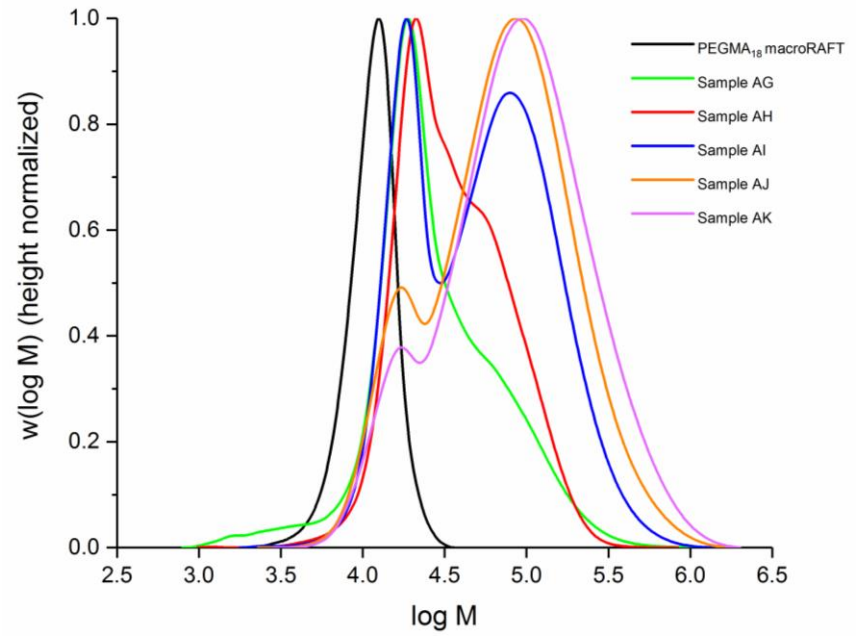

Figure 4-19: Height-normalized SEC molecular weight distributions for PEGMA-b-PIPS block copolymers prepared by RAFT solution polymerization.

Upon the continual addition of water, the solution of PEGMA-b-PIPS gradually became turbid and milky white. DLS and TEM analyses of the post-dialysis dispersion revealed the formation of small spherical nanoparticles ranging from ~ 50 nm to ~ 210 nm diameter (Table 4-6, Figure 4-20 and Figure 4-21). No higher-order morphologies were again observed. Because of the nature of the IPS repeating unit, the particle size and copolymer molecular weight were much higher than the PEGMA-b-PMPS at a comparable core block length. A similar observation with short MPS blocks was also observed in IPS-based systems, where a broad size distribution formed upon slow addition of water, and the samples were not colloidally stable. This was again addressed by a one-shot addition of water into these systems to induce self-assembly.

Over an equivalent range of core-forming block lengths as those studied in PEGMA-b-PMPS systems, only spherical nanoparticles were observed in PEGMA-b-PIPS systems. This is attributed to the greater volume of the IPS-based core-forming block being still insufficient to overcome the large effective headgroup area of the PEGMA-based stabilizer block to potentially form worms or vesicles. The DLS distribution (Figure 4-22) shows insignificant change after adding sample 4-AG (in Table 4-6) into dioxane. This may be due to slow crosslinking of PIPS block during/or after self-assembly in water, which cannot be suppressed completely. As a result, dioxane swollen the partial crosslinking PIPS network and increased DLS particle size slightly (d_z (initial, in water) = 49.8 nm and d_z (final, in dioxane) = 52.5 nm).

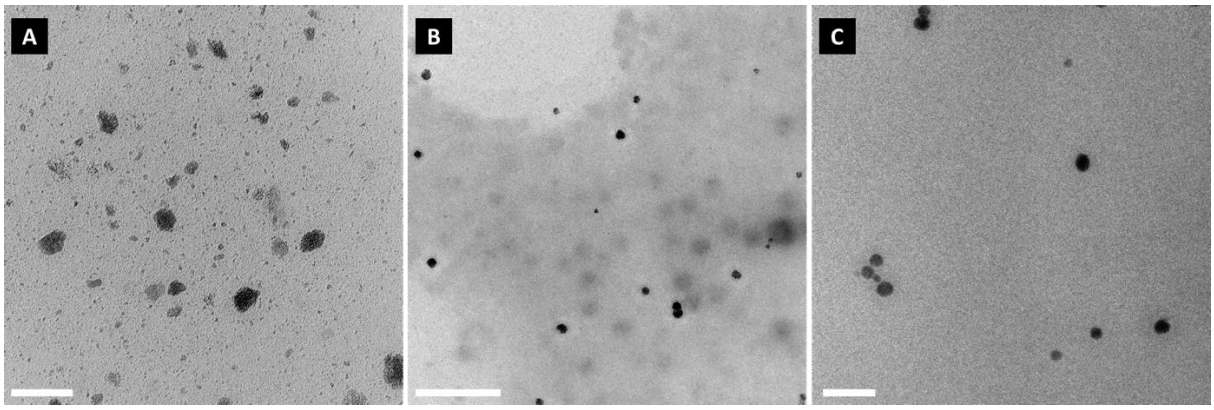

Figure 4-20: TEM images of nanoparticles prepared by addition of water to a solution of PEGMA-b-PIPS in 1,4 dioxane. (A) Sample 4-AG in Table 4-6, (B) Sample 4-AH in Table 4-6, and (C) Sample 4-AJ in Table 4-6. Scale bar = (A) 100 nm, (B) 500 nm, and (C) 200 nm.

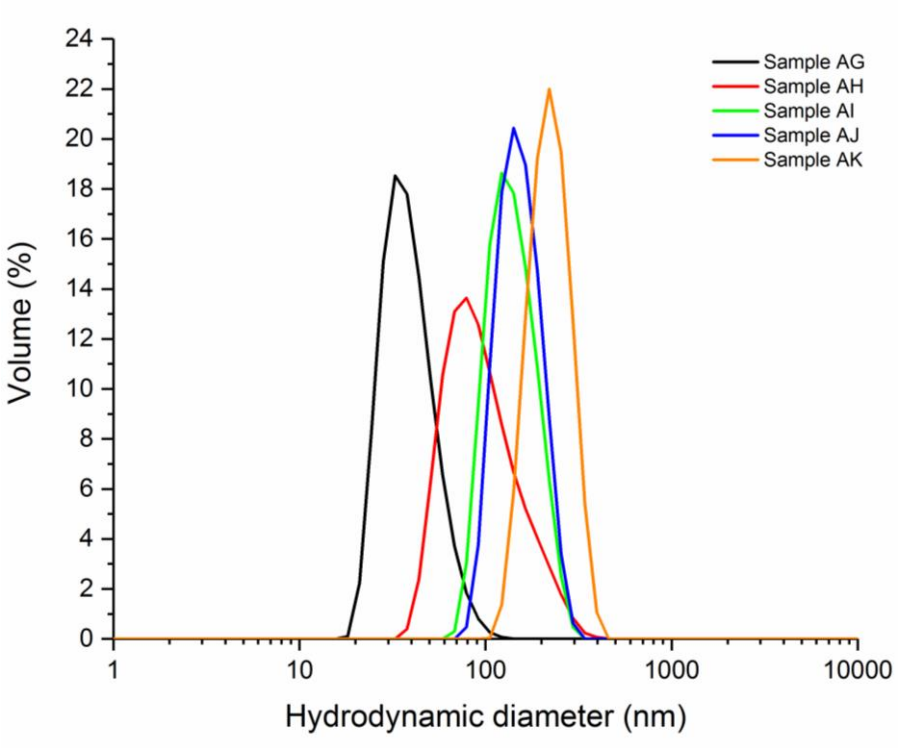

Figure 4-21: DLS volume distributions of PEGMA-b-PIPS after dialysis against water.

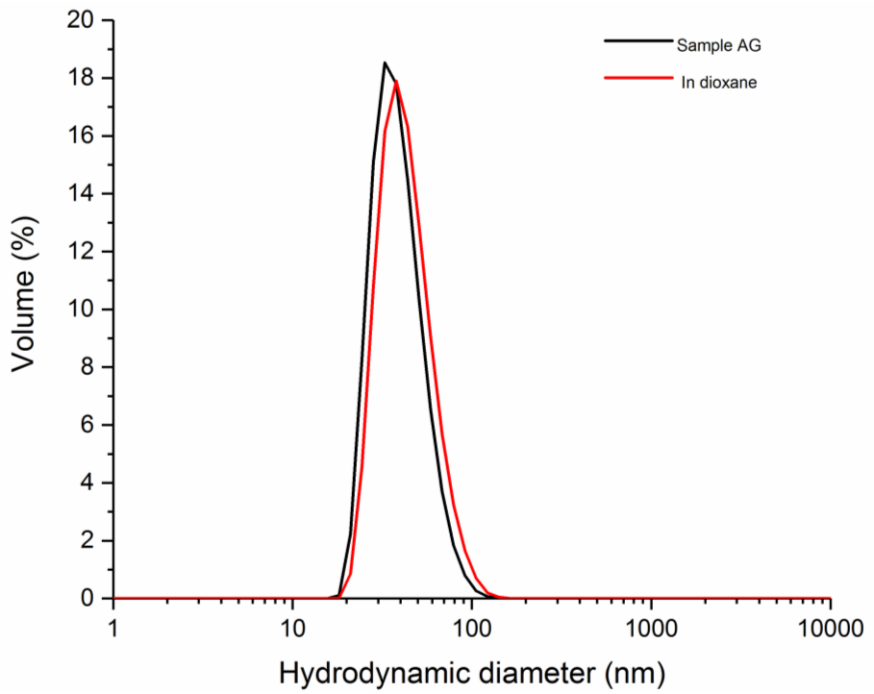

Figure 4-22: DLS volume distribution of Sample 4-AG in Table 4-6 (self-assembled PEGMA-b-PIPS in water, black curve); upon addition of Sample 4-AG (in Table 4-6) into dioxane (red curve)

4.2.4 Self-Assembly of MPS-based Block Copolymers in a Non-Polar Organic Solvent

In this section, the solution self-assembly of diblock copolymers containing an MPS core-forming block in a non-polar organic solvent (*n*-hexane) is demonstrated. Lauryl methacrylate (LMA) was used as a hydrophobic stabilizer, followed by chain extension with MPS in a good solvent for both blocks (1,4-dioxane) via RAFT polymerization. Self-assembly of a 10 % w/w solution of the PLMA-b-PMPS block copolymer in 1,4-dioxane was induced by addition of *n*-hexane, eliciting a turbid white dispersion. A $PLMA_{38}$ macroRAFT agent was used and the target MPS DP was adjusted from 80 to 400 repeating units (Table 4-7). A shorter $PLMA_{18}$ macroRAFT agent was used initially, however in this instance colloidally stable nanoparticles could not be formed via self-assembly, prompting the use of a longer LMA stabilizing block. The reaction scheme is shown in Figure 4-23.

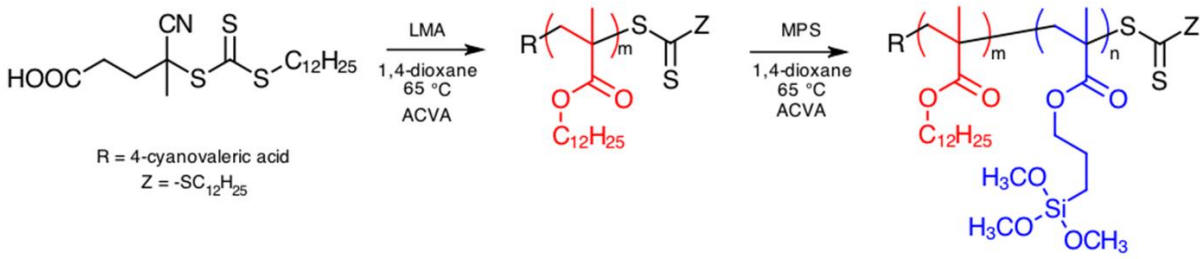

Figure 4-23: The preparation of PLMA-b-PMPS block copolymer via RAFT polymerization in dioxane

Table 4-7: Summary of $PLMA_{38}$-b-$PMPS_y$ diblock copolymers via RAFT solution polymerization and their self-assembly upon addition of selective solvent (n-hexane)

Sample code	**Target MPS DP**	**MPS conversion[a]**	**DP_{th}**	**M_n (kDa)**	**$Đ^b$**	**d_z (nm) (PDI)**	**d_z (nm) (PDI) (post-dialysis)**
4-AL	80	0.88	70	9.73	1.45	43 (0.2)	39 (0.1)
4-AM	100	0.87	87	13.2	1.56	50 (0.11)	50 (0.22)
4-AN	200	0.77	154	28.2	1.55	98 (0.13)	91 (0.11)
4-AO	400	0.63	252	39.2	2.64	371 (0.28)	360 (0.34)

[a] Determined by NMR spectroscopy, [b] Dispersity of entire distribution (including macroRAFT agent)

The SEC chromatograms of the resulting polymers show a shift towards higher molecular weights upon increasing target MPS DP (Figure 4-24), proving effective chain extensions of the PLMA macroRAFT agent in solution. A low molecular weight shoulder was observed in all distributions, likely corresponding to the initial macroRAFT agent. The dispersity was higher than a 'typical' RAFT polymerization and the conversion of MPS monomer into polymer decreased with increasing target MPS DP.

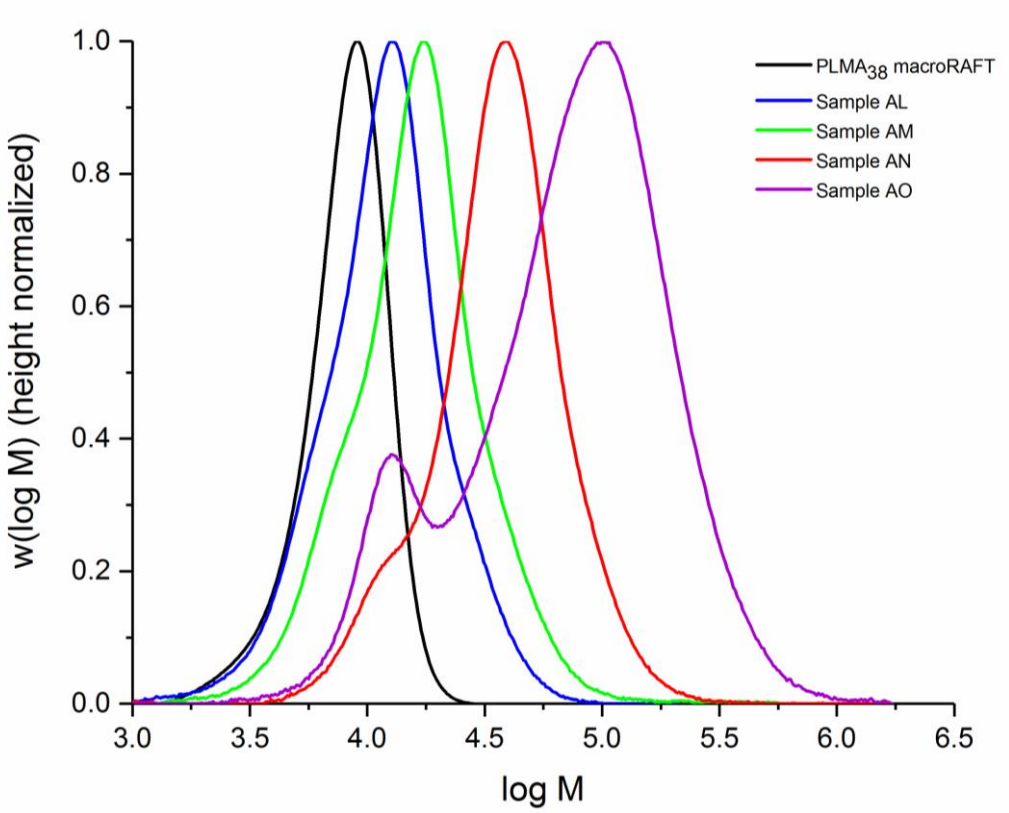

Figure 4-24: Height-normalized SEC molecular weight distributions for PLMA-b-PMPS block copolymers prepared by RAFT solution polymerization.

TEM analysis revealed a transition across different nanoparticle morphologies for self-assembled PLMA-b-PMPS block copolymers (Figure 4-25). When the MPS block was relatively short, TEM revealed small and monodisperse spherical nanoparticles (Samples 4-AL to 4-AN). At the longest MPS length studied, the resulting morphology was a mixed phase consisting of spheres, rods and vesicles (Sample 4-AO (in Table 4-7), Figure 4-25(C) and Figure 4-26). This demonstrated that higher order morphologies such as vesicles were possible with a MPS core-forming block. DLS measurements supported the observation of small and monodisperse objects with an effective particle size range of ~ 40 to ~90 nm (Samples 4-AL to 4-AN), with a large increase in average particle size of the mixed phase (as DLS measurements assume a spherical morphology, the change in effective particle size is indicative

of the nature of diffusion in solution of different particle morphologies). Compared to the PEGMA-b-PMPS system discussed in Section 4.2.2, the non-spherical morphologies observed here can be attributed to a less bulky solvophilic block. The DLS distribution (Figure 4-27) shows the particles did not dissociate into a good solvent (dioxane) (d_z (initial, in hexane) = 39 nm; d_z (final, in dioxane) = 35 nm). It is proposed that the MPS crosslinking process can occur and continue at a minimum rate if any one of the trimethoxysilyl groups is hydrolysed. In the supplied MPS monomer, 1 % of trimethoxysilyl groups have been hydrolysed based on the supplier data (Sigma Aldrich), which may be promoted in the presence of trace water in both solvents. According to the specification test results, the hexane used in this experiment had a maximum acidity of 0.0002 meq g^{-1}, which could have the catalyst effect in crosslinking the alkoxysilyl groups.

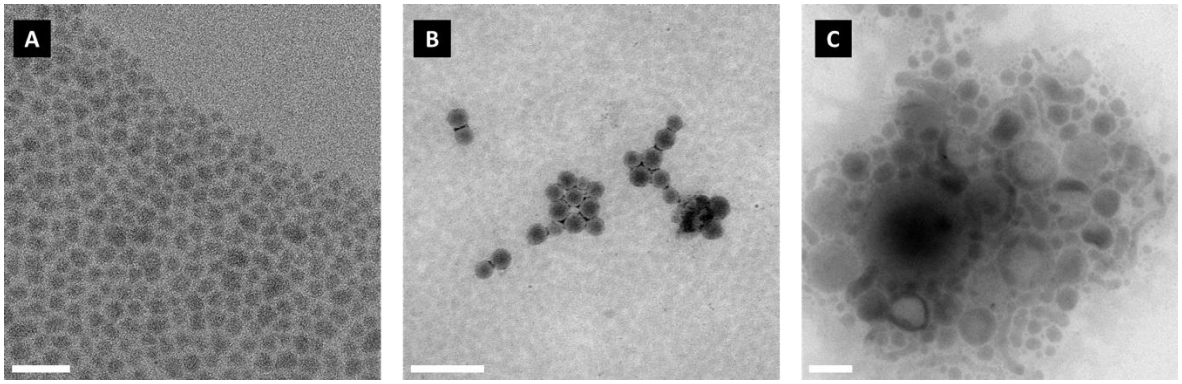

Figure 4-25: TEM images of nanoparticles prepared by addition of hexane to a solution of PLMA-b-PMPS in 1,4 dioxane. (A) Sample 4-AM in Table 4-7, (B) Sample 4-AN in Table 4-7, and (C) Sample 4-AO in Table 4-7. Scale bar = (A) 100 nm, (B) 200 nm, and (C) 500 nm.

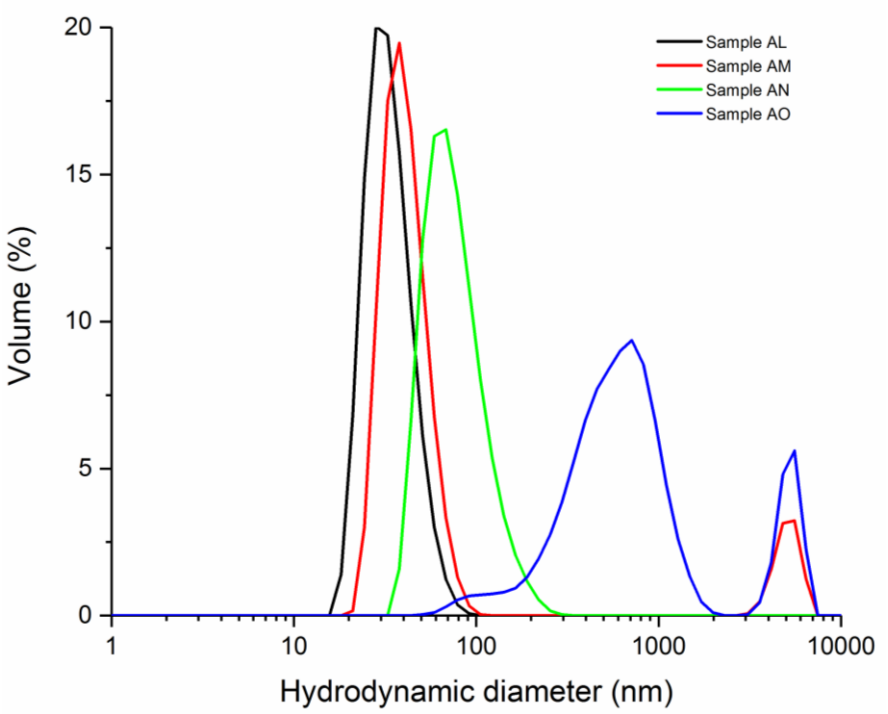

Figure 4-26: DLS volume distributions of PLMA-b-PMPS after dialysis against hexane.

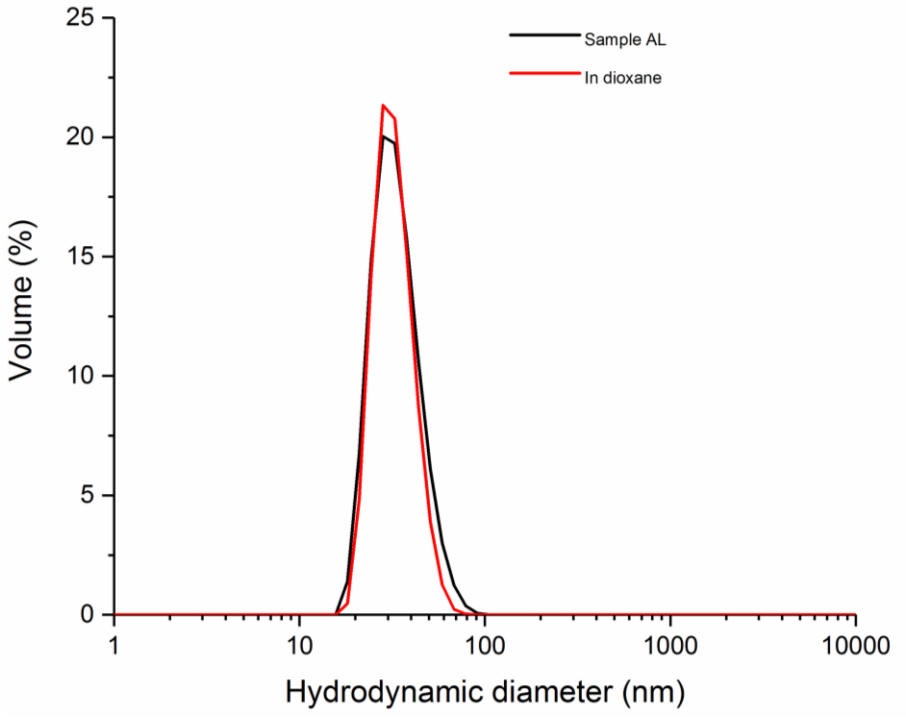

Figure 4-27: DLS volume distributions of Sample 4-AL in Table 4-7 (self-assembled of PLMA-b-PMPS in hexane, black curve); upon addition of Sample 4-AL (in Table 4-7) into dioxane (red curve)

4.2.5 Comparison Between Emulsion Polymerization and Solution Self-Assembly Polymerization Used in This Study

Different approaches (emulsion polymerization and solution self-assembly polymerization) have been investigated in this study and they have distinct impacts to hybrid nanoparticles. Low temperature emulsion polymerization and solution polymerization are suitable for MPS monomers. These systems produce coagulum free product and breakthrough the MPS stability issue in high temperature emulsion polymerization. Both systems also use neutral solvent to reduce the MPS crosslinking risk. However, emulsion polymerization has an obstacle in SEC analysis where an extremely high molecular weight peak (outside calibration range) is observed, impacting the accuracy of molecular weight and dispersity. This problem is not found in solution polymerization. The selection of redox catalyst is also limited compares to a wide range initiator can be applied in solution polymerization. Temperature control is also crucial in emulsion polymerization as any increasing temperature may boost MPS hydrolysis and condensation rates. Overall, solution polymerization is a better choice than emulsion polymerization for this tricky MPS monomer. Solution polymerization has proved the chain extension/molecular weight distribution is good and higher order morphology is obtained despite the process involves multiple steps. When the experiment requires low temperature and a solvent which cannot dissolve MPS monomer, redox emulsion polymerization is a primary choice.

4.3 Conclusions

In this Chapter, the RAFT polymerization of alkoxysilane-functional monomers (MPS and IPS) to produce silica core-polymer shell nanoparticles via different self-assembly approaches was studied. The PISA process was not possible in a classic and elevated temperature (65 ^{o}C) RAFT emulsion polymerization due to instability of the MPS monomer in the reaction medium (water). The alkoxysilane groups of MPS were shown to hydrolyse and condense in the absence of an acid or base catalyst via SEC and ^{1}H/^{29}Si NMR characterisations. Intermolecular condensation also produced MPS based oligomers which reduced colloidal stability and resulted in poor chain extension with a PEGMA-based macroRAFT agent. Lower reaction temperature (redox initiation) and seeded systems were also chosen in attempts to suppress MPS crosslinking, however, these systems provided mixed results. In both cases, coagulum was minimal due a reduction in monomer hydrolysis and condensation, but their chain extension was not effectively quantified via SEC.

Because of the above-mentioned issues, the traditional method of diblock copolymer self-assembly in solution at low total solids content was performed via adding a poor solvent. While the technical advantages of the PISA method were lost, control and quantification of the polymer synthesis could be easier to achieve in the absence of water as reaction solvent. Even with highly asymmetric diblock copolymers, only spherical nanoparticles were obtained using both MPS and IPS as the core-forming block. The formation of non-equilibrium morphologies was attributed to the bulky PEGMA headgroup and *in-situ* crosslinking of the MPS block, trapping the spherical structures formed upon addition of water, which could not return to their dissolved unimer state in a good solvent. The use of an oil-soluble stabilizer block (lauryl

methacrylate) to prepare diblock copolymers with a MPS core block demonstrated the ability to prepare mixed morphology nanoparticles upon addition of *n*-hexane.

4.4 References

1. S. I. Ali, J. P. A. Heuts, B. S. Hawkett and A. M. van Herk, *Langmuir*, 2009, **25**, 10523-10533.
2. M. A. M. Mballa, S. Ali, J. P. Heuts and A. M. v. Herk, *Polymer International*, 2012, **61**, 861-865.
3. S. A. F. Bon and P. J. Colver, *Langmuir*, 2007, **23**, 8316-8322.
4. S. Chakraborty, K. Jähnichen, H. Komber, A. A. Basfar and B. Voit, *Macromolecules*, 2014, **47**, 4186-4198.
5. C. Kaewsaneha, P. Tangboriboonrat, D. Polpanich, M. Eissa and A. Elaissari, *Journal of Polymer Science Part A: Polymer Chemistry*, 2013, **51**, 4779-4785.
6. S. F. Medeiros, A. M. Santos, H. Fessi and A. Elaissari, *Journal of Colloid Science and Biotechnology*, 2012, **1**, 99-112.
7. J. F. Dechezelles, V. Malik, J. J. Crassous and P. Schurtenberger, *Soft Matter*, 2013, **9**, 2798-2802.
8. J. Moraes, K. Ohno, T. Maschmeyer and S. Perrier, *Chemical Communications*, 2013, **49**, 9077-9088.
9. F. Zhang, S. Yu, G. Hou, N. Xu, Z. Wu and L. Yue, *Colloid and Polymer Science*, 2015, **293**, 1893-1902.
10. D. Nguyen, B. T. T. Pham, V. Huynh, B. J. Kim, N. T. H. Pham, S. A. Bickley, S. K. Jones, A. Serelis, T. Davey, C. Such and B. S. Hawkett, *Polymer*, 2016, **106**, 238-248.
11. D. Nguyen, C. Such and B. Hawkett, *Journal of Polymer Science Part A: Polymer Chemistry*, 2012, **50**, 346-352.
12. D. Nguyen, H. S. Zondanos, J. M. Farrugia, A. K. Serelis, C. H. Such and B. S. Hawkett, *Langmuir*, 2008, **24**, 2140-2150.
13. E. Bourgeat-Lami, J. Faucheu and A. Noel, *Polymer Chemistry*, 2015, **6**, 5323-5357.
14. S. H. Che Man, S. C. Thickett, M. R. Whittaker and P. B. Zetterlund, *Journal of Polymer Science Part A: Polymer Chemistry*, 2013, **51**, 47-58.
15. H. M. Etmimi and R. D. Sanderson, *Macromolecules*, 2011, **44**, 8504-8515.
16. H. Kim, A. A. Abdala and C. W. Macosko, *Macromolecules*, 2010, **43**, 6515-6530.
17. T. Kuilla, S. Bhadra, D. Yao, N. H. Kim, S. Bose and J. H. Lee, *Progress in Polymer Science*, 2010, **35**, 1350-1375.
18. D. Nguyen, C. H. Such and B. S. Hawkett, *Journal of Polymer Science Part A: Polymer Chemistry*, 2013, **51**, 250-257.
19. W. Zhong, J. N. Zeuna and J. P. Claverie, *Journal of Polymer Science Part A: Polymer Chemistry*, 2012, **50**, 4403-4407.
20. T. de Roo, S. Huber and S. Mecking, *ACS Macro Letters*, 2016, **5**, 786-789.
21. A. Fokina, K. Klinker, L. Braun, B. G. Jeong, W. K. Bae, M. Barz and R. Zentel, *Macromolecules*, 2016, **49**, 3663-3671.
22. P. Das and J. P. Claverie, *Journal of Polymer Science Part A: Polymer Chemistry*, 2012, **50**, 2802-2808.
23. K. Landfester, *Angewandte Chemie International Edition*, 2009, **48**, 4488-4507.
24. D. Qi, Z. Cao and U. Ziener, *Advances in Colloid and Interface Science*, 2014, **211**, 47-62.
25. P. B. Zetterlund, S. C. Thickett, S. Perrier, E. Bourgeat-Lami and M. Lansalot, *Chemical Reviews*, 2015, **115**, 9745-9800.

26. W. Mitsuru and T. Toshiyuki, *Journal of Polymer Science Part A: Polymer Chemistry*, 2006, **44**, 4736-4742.
27. J. Zhou, H. Yao and J. Ma, *Polymer Chemistry*, 2018, **9**, 2532-2561.
28. J. B. Jun, J. K. Hong, J. G. Park and K. D. Suh, *Macromolecular Chemistry and Physics*, 2003, **204**, 2281-2289.
29. Z. Zhang, P. Zhang, Y. Wang and W. Zhang, *Polymer Chemistry*, 2016, **7**, 3950-3976.
30. E. Bourgeat-Lami, A. J. P. G. França, T. C. Chaparro, R. D. Silva, P. Y. Dugas, G. M. Alves and A. M. Santos, *Macromolecules*, 2016, **49**, 4431-4440.
31. J. A. Balmer, A. Schmid and S. P. Armes, *Journal of Materials Chemistry*, 2008, **18**, 5722-5730.
32. B. Radhakrishnan, R. Ranjan and W. J. Brittain, *Soft Matter*, 2006, **2**, 386-396.
33. A. C. Perreira, S. Pearson, D. Kostadinova, F. Leroux, F. D Agosto, M. Lansalot, E. Bourgeat-Lami and V. Prevot, *Polymer Chemistry*, 2017, **8**, 1233-1243.
34. C. van der Wel, R. K. Bhan, R. W. Verweij, H. C. Frijters, Z. Gong, A. D. Hollingsworth, S. Sacanna and D. J. Kraft, *Langmuir*, 2017, **33**, 8174-8180.
35. M. Youssef, T. Hueckel, G. R. Yi and S. Sacanna, *Nature Communications*, 2016, **7**, 12216.
36. S. Sacanna, W. T. M. Irvine, P. M. Chaikin and D. J. Pine, *Nature*, 2010, **464**, 575.
37. S. Sacanna, L. Rossi and A. P. Philipse, *Langmuir*, 2007, **23**, 9974-9982.
38. Y. Zheng, Y. Huang, Z. M. Abbas and B. C. Benicewicz, *Polymer Chemistry*, 2016, **7**, 5347-5350.
39. Y. Zheng, Y. Huang, Z. M. Abbas and B. C. Benicewicz, *Polymer Chemistry*, 2017, **8**, 370-374.
40. X. G. Qiao, O. Lambert, J. C. Taveau, P. Y. Dugas, B. Charleux, M. Lansalot and E. Bourgeat-Lami, *Macromolecules*, 2017, **50**, 3796-3806.
41. R. Deng, M. J. Derry, C. J. Mable, Y. Ning and S. P. Armes, *Journal of the American Chemical Society*, 2017, **139**, 7616-7623.
42. C. J. Mable, M. J. Derry, K. L. Thompson, L. A. Fielding, O. O. Mykhaylyk and S. P. Armes, *Macromolecules*, 2017, **50**, 4465-4473.
43. G. H. Teo, R. P. Kuchel, P. B. Zetterlund and S. C. Thickett, *Polymer Chemistry*, 2016, **7**, 6575-6585.
44. Z. Gao, S. K. Varshney, S. Wong and A. Eisenberg, *Macromolecules*, 1994, **27**, 7923-7927.
45. L. Zhang and A. Eisenberg, *Science*, 1995, **268**, 1728-1731.
46. R. G. Gilbert, *Emulsion polymerization: a mechanistic approach*, Academic Press, 1995.
47. S. Savard, L. P. Blanchard, J. Léonard and R. E. Prud'homme, *Polymer Composites*, 1984, **5**, 242-249.
48. H. Jiang, Z. Zheng, Z. Li and X. Wang, *Industrial & Engineering Chemistry Research*, 2006, **45**, 8617-8622.
49. M. C. Brochier Salon, P. A. Bayle, M. Abdelmouleh, S. Boufi and M. N. Belgacem, *Colloids and Surfaces A: Physicochemical and Engineering Aspects*, 2008, **312**, 83-91.
50. K. Piana and U. Schubert, *Chemistry of Materials*, 1994, **6**, 1504-1508.
51. Y. Abe, Y. Honda and T. Gunji, *Applied Organometallic Chemistry*, 1998, **12**, 749-753.
52. I. Tissot, C. Novat, F. Lefebvre and E. Bourgeat-Lami, *Macromolecules*, 2001, **34**, 5737-5739.
53. I. Tissot, J. P. Reymond, F. Lefebvre and E. Bourgeat-Lami, *Chemistry of Materials*, 2002, **14**, 1325-1331.
54. A. Tardy, K. A. Bhullar, D. Q. Lim, S. C. Thickett and P. B. Zetterlund, *Journal of Polymer Science Part A: Polymer Chemistry*, 2017, **55**, 1590-1600.

55. S. Förster, M. Zisenis, E. Wenz and M. Antonietti, *The Journal of Chemical Physics*, 1996, **104**, 9956-9970.
56. Y. Mai and A. Eisenberg, *Chemical Society Reviews*, 2012, **41**, 5969-5985.
57. L. A. Fielding, M. J. Derry, V. Ladmiral, J. Rosselgong, A. M. Rodrigues, L. P. D. Ratcliffe, S. Sugihara and S. P. Armes, *Chemical Science*, 2013, **4**, 2081-2087.

Chapter 5 : Preparation of Particles and Capsules with a Crosslinked Interface via Alkoxysilane-Functional Triblock Copolymers

5.1 Introduction

Self-assembled block copolymer nanoparticles are becoming increasingly popular in recent times, due to the rise of several synthetic techniques that enable block copolymers to be readily synthesized. For the design of hybrid polymer-organic or polymer-inorganic materials, the controlled polymerization of monomers with a specific functional group, followed by self-assembly, is a popular route. Monomers containing (for example) inorganic functional groups are commercially available, and Reversible Deactivation Radical Polymerization (RDRP) techniques can be used to integrate inorganic structures into polymeric materials; examples prepared include fluorinated,[1, 2] silicon[3, 4] and phosphorus-based polymeric materials.[5, 6] Besides benefits from inorganic functional groups, inorganic containing amphiphilic copolymers also can be used as polymeric surfactants.[7-10] Silicon (Si) is one of the most popular elements to integrate into hybrid polymeric materials, as many types (functionalized with other inorganic groups, monomers, porous *etc.*) and forms (solid and liquid) of silicon containing materials are easily accessible.

In the preparation of block copolymer nanoparticles, one of the traditional methods involves the slow addition of a block-selective solvent to induce self-assembly.[11-13] While block copolymers have low critical micelle concentration or critical aggregation concentration values

compared to low molecular weight surfactants, block copolymer nanoparticles can dissociate into individual chains when a major change to the system occurs (e.g. very low concentration, high temperature, good solvent *etc.*) This problem is particularly relevant to cargo-loaded nanoparticles for delivery of a therapeutic payload.[14-16] As a result, numerous strategies have been developed to covalently crosslink block copolymer nanoparticles to prevent dissociation; these methods can be cross-linking the core, corona, and at the interfacial junction between the solvophilic and solvophobic domains.[17] Shell crosslinking is normally carried out by using crosslinking agents (organosilicon (for example: (3-aminopropyl)trimethoxysilane and 1,2-bis(trimethoxysilyl)ethane), divinylbenzene, diethylene glycol dimethacrylate, glutaraldehyde *etc.*),[18-27] Michael addition reaction,[28, 29] UV-irradiation,[30-34] "click" chemistry,[35-37] and others. All these methods require very low diblock copolymer concentration to proceed crosslinking and avoid intermicellar couplings.[17]

Shell-crosslinked nanoparticles also can be subjected to additional surface functionalization and further extend the applications of these nanoparticles. Surface functionalization can be completed via three routes: using a functionalized initiator species,[38, 39] randomly integrating functional groups into the shell after formation of particles[40-42] or one of many "click" reactions.[17] However, all of the above methods mainly form a crosslinked shell that can potentially degrade at high temperature. If the shell is crosslinked with an organosilicon crosslinking reagent, a robust crosslinked inorganic (silica) shell is formed through sol-gel chemistry.[43-45] The crosslinked silica also enables surface functionalization via reaction with commercial available alkoxysilanes that contain various functional groups (e.g. amino, glycidyl, thiol).[46-48]

Hybrid polymer-silica nanoparticles are traditionally prepared via "grafting from" and "grafting to" methods and these methods produce silica core / polymer shell nanoparticles.[49] By tuning the position of the crosslinking precursor (such as an alkoxysilane) in the block copolymer as well as reaction conditions, hybrid polymer nanoparticles with a silica core or silica shell can be easily obtained via an acid or base catalysed hydrolysis and condensation process.[50-56] Highly crosslinked silicon networks have been widely used to reduce the leaching of incorporated dyes[57] and increase air/gas permeation rates inside the polymer matrix.[58, 59] In addition to shell crosslinking, periphery/end terminal shell crosslinking (where terminally functionalized polymeric surfactants at the extremity of the shell are crosslinked) has been used to improve the structural integrity of the resultant nanoparticles.[60-63] Periphery shell crosslinking is quite useful as this method can create a significant free volume within the particle (as well as a thin outer shell) that increase cargo loading efficiency and diffusion. For example, triethoxysilyl-terminated triblock copolymers were used as surfactants in stabilizing oil-in-water miniemulsions.[64] Stable and hybrid nanoparticles with large internal cavity were obtained after the terminal silyl functional groups were crosslinked at the outermost shell.

The advent of Polymerization-Induced Self-Assembly (PISA) mediated by RAFT technique has enabled the preparation of *in-situ* self-assembled organic-inorganic polymer nanoparticles with various morphologies at high solids content.[65-68] Similar to the stabilization of block copolymer nanoparticles prepared by solvent-induced methods, cross-linking methods to stabilize a particular particle morphology have been adopted. By incorporating functional groups into the copolymer that are amenable to crosslinking, morphology control and post-polymerization crosslinking can be completed in two steps through the use of the PISA method.[69-71] This method (PISA and crosslinking) makes nanoparticles resistant to external stimuli and fix the nanoparticle morphologies (sphere, rod and vesicle). Chambon and co-

workers reported the linear poly(glycerol monomethacrylate-block-2-hydroxypropyl methacrylate) (PGMA-b-PHPMA) vesicles had disintegrated when cationic surfactant or DMF was added into the system.[72] However, they enhanced the vesicular structure by copolymerizing with ethylene glycol dimethacrylate (EGDMA) to form a triblock copolymer (PGMA-b-PHPMA-b-PEGDMA). PEGDMA crosslinking was successfully achieved as the DLS particle size increased in the presence of surfactant and no nanoparticle dissolution was observed. Interfacial crosslinking of self-assembled nanoparticles has been demonstrated via the use of a triblock copolymer where the middle block is crosslinked.[73-77] Interfacial crosslinking can retain the mobility and nature of hydrophilic and hydrophobic blocks which is much better than whole corona shell and core crosslinking. In addition, interfacial crosslinking can be carried out at high copolymer concentration as the intermicellar coupling is avoided by steric stabilization polymer chains at the outermost shell.[78]

The results reported in the previous chapters document the use of alkoxysilane functional polymers both as a solvophilic and solvophobic block in copolymer self-assembly. In this chapter, RAFT polymerization is used to prepare triblock copolymers that contain PMPS as a "middle" block, where the aim is to ultimately create block copolymer nanoparticles with a crosslinked interface, as opposed to a crosslinked core or corona. The triblock copolymers have an ABC-type composition, with a hydrophilic poly(ethylene glycol) methyl ether methacrylate (PEGMA) block, a short PMPS block, and a hydrophobic poly(benzyl methacrylate) (PBzMA) block. The composition of these triblock copolymers is studied in two settings; i) pre-formed copolymers as polymeric surfactants to stabilize O/W miniemulsion droplets, and ii) *in-situ* copolymer formation via RAFT-mediated PISA. Following self-assembly, the PMPS block is subsequently crosslinked via base-catalysed hydrolysis and condensation. Interfacial crosslinking was shown to be successful in both methods, however the colloidal stability of

crosslinked emulsions was relatively poor. The PISA approach was much more successful with respect to *in-situ* colloidal stability, however only spherical nanoparticles were formed with no observed morphology transitions. The encapsulation of a dye (Nile Red) into the particle core was also achieved during the self-assembly process, and the retention of Nile Red in the particle core was improved when the alkoxysilyl moieties at the particle interface were crosslinked.

5.2 Results and Discussions

5.2.1 Oil-in-Water Droplets Stabilized by Alkoxysilane Containing Triblock Copolymers

The use of alkoxysilane-functional triblock copolymers as a polymeric surfactant in O/W miniemulsions is discussed in this section. The triblock copolymers consist of a PEGMA hydrophilic block (P), MPS interfacial block (M) and hydrophobic BzMA block (B) (denoted as $P_xM_yB_z$ where *x*, *y* and *z* are the respective DPs of the three blocks). By designing the alkoxysilane-functional block as the middle block, MPS moieties can be distributed near to the droplet interface. Three PEGMA (M_n 300) ($P300_x$) and three PEGMA (M_n 950) ($P950_x$) macroRAFT agents of different degree of polymerization (M_n 300: 19, 39, and 58; M_n 950: 9, 18, and 36) were prepared. The PEGMA macroRAFT agent was first chain extended with MPS and then BzMA in dioxane in a two-step approach. The SEC data of these macroRAFT agents are tabulated in Table 5-1. All macroRAFT agents possessed narrow molecular weight distributions ($Đ$ ~ 1.2; see Figure 5-1). The preparation of these triblock copolymers is illustrated in Figure 5-2.

Table 5-1: Fractional conversion and SEC data of PEGMA macroRAFT agents

Entry	Target PEGMA macroRAFT agents	Fractional conversion	DP_{th}	M_n (SEC) (kDa)	$Đ$ (SEC)
5-1	PEGMA $(M_n\ 300)_{20}$	0.97	19	5.94	1.22
5-2	PEGMA $(M_n\ 300)_{40}$	0.98	39	12.2	1.19
5-3	PEGMA $(M_n\ 300)_{60}$	0.97	58	14.3	1.20
5-4	PEGMA $(M_n\ 950)_{10}$	0.90	9	9.60	1.11
5-5	PEGMA $(M_n\ 950)_{20}$	0.90	18	14.2	1.09
5-6	PEGMA $(M_n\ 950)_{40}$	0.89	36	22.6	1.19

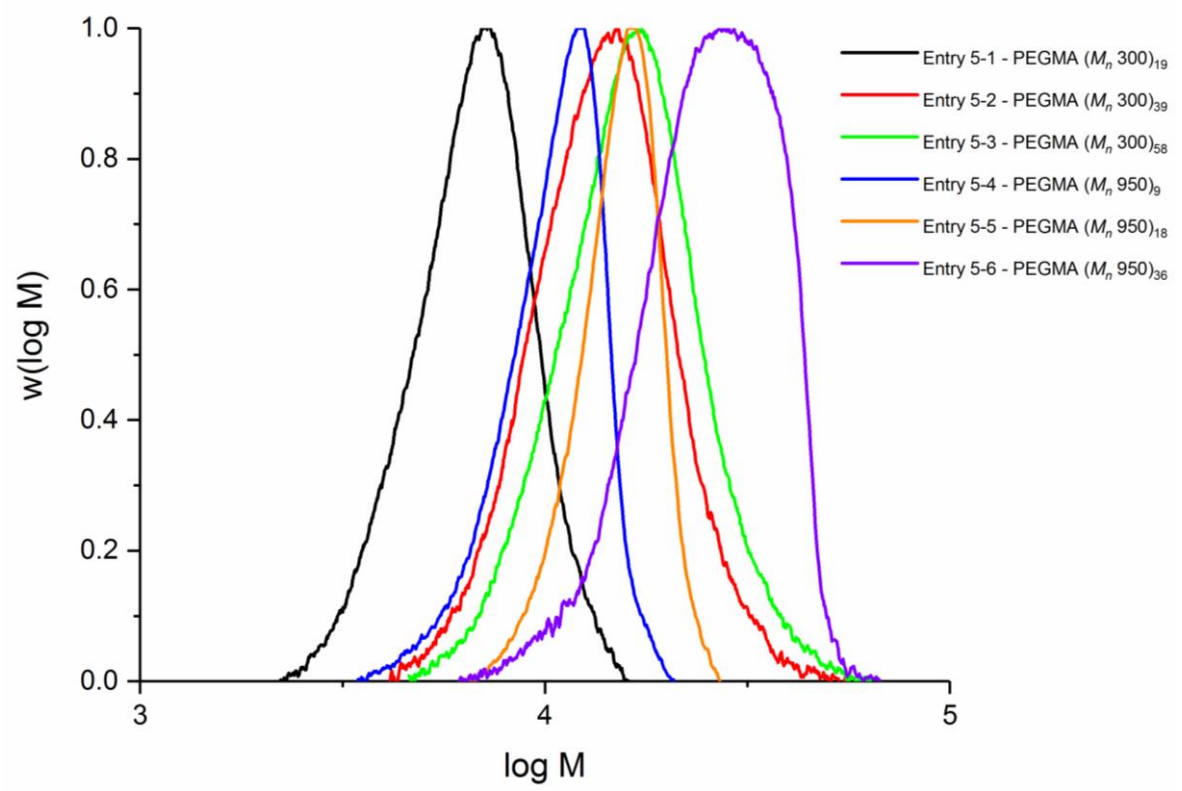

Figure 5-1: Height normalized SEC distributions of PEGMA macroRAFT agents

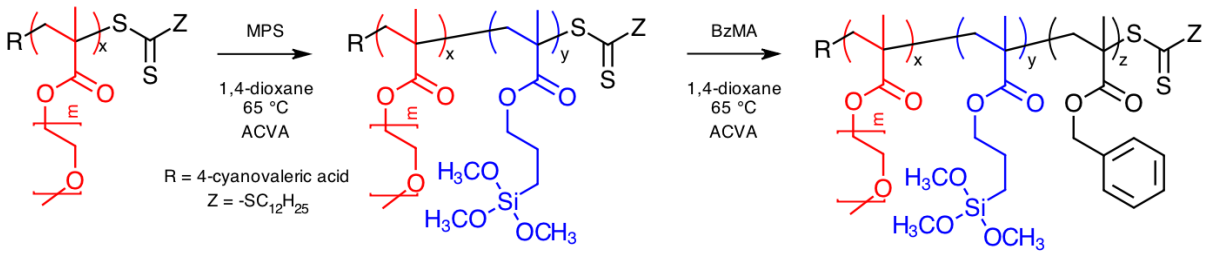

Figure 5-2: RAFT-mediated solution polymerization of PEGMA triblock copolymer in dioxane

Monomer conversion data for the chain extension polymerization of MPS and BzMA is summarized in Table 5-2. In all cases, the conversions of MPS and BzMA were moderately high (≥ 74% and ≥ 76% respectively). Due to extensive crosslinking of polymers during SEC preparation and analysis and irreproducible molecular weight distributions (as reported in Chapters 3 and 4), attributed to the highly reactive nature of the MPS block, SEC was not performed to analyse these triblock copolymers. The overall molecular weight of the triblock copolymer was varied according to the target degree of polymerization of each block. As the application of these triblock copolymers was to act as a polymeric surfactant, Griffin's equation was used to target an approximate hydrophilic–lipophilic balance (HLB) value for the polymeric structure.[79-81] Griffin's equation is suitable for non-ionic surfactants such as PEGMA, defined below:

$$HLB = 20 \times \left(\frac{M_h}{M}\right)$$

where M_h is the total molecular mass of hydrophilic groups (repeating ethylene glycol units in PEGMA block; PEGMA (M_n 950): ~ 19 units, and PEGMA (M_n 300): ~ 5 units) and M is the molecular mass of entire triblock copolymer ($P_xM_yB_z$) including the RAFT agent. The calculated HLB values are also tabulated in Table 5-2, suggesting an appropriate composition for an O/W stabilizer. The miniemulsion type was confirmed via a drop test. A drop of

miniemulsion (without catalyst) was transferred into toluene and water respectively; the observation showed the drop could completely disperse in water while the white drop sank in toluene and unable to disperse (Figure 5-3). This proved that the minimemulsion was an O/W system despite the polymeric surfactant being initially dissolved in the oil phase.

Table 5-2: PEGMA triblock copolymers with different target DP and conversions of MPS and BzMA and their HLB values

Entry	**PEGMA MacroRAFT agents from Table 5-1**	**Target composition**	**Conversion**		**Theoretical**	
			MPS	**BzMA**	**Composition**	**HLB value**
5-7	5-1	$P300_{19}M_{10}B_{30}$	0.88	0.89	$P300_{19}M_{9}B_{27}$	6.5
5-8	5-2	$P300_{39}M_{20}B_{60}$	0.83	0.82	$P300_{39}M_{17}B_{49}$	6.9
5-9	5-3	$P300_{58}M_{30}B_{90}$	0.79	0.82	$P300_{58}M_{24}B_{74}$	6.9
5-10	5-4	$P950_{9}M_{10}B_{50}$	0.83	0.90	$P950_{9}M_{8}B_{45}$	8.0
5-11	5-5	$P950_{18}M_{20}B_{100}$	0.76*	0.82*	$P950_{18}M_{15}B_{82}$	8.4
5-12	5-5	$P950_{18}B_{100}$	-	0.85	$P950_{18}B_{85}$	9.3
5-13	5-6	$P950_{36}M_{40}B_{200}$	0.74^	0.76^	$P950_{36}M_{30}B_{152}$	8.7

** Average conversion based on six experiments. ^ Average conversion based on two experiments.*

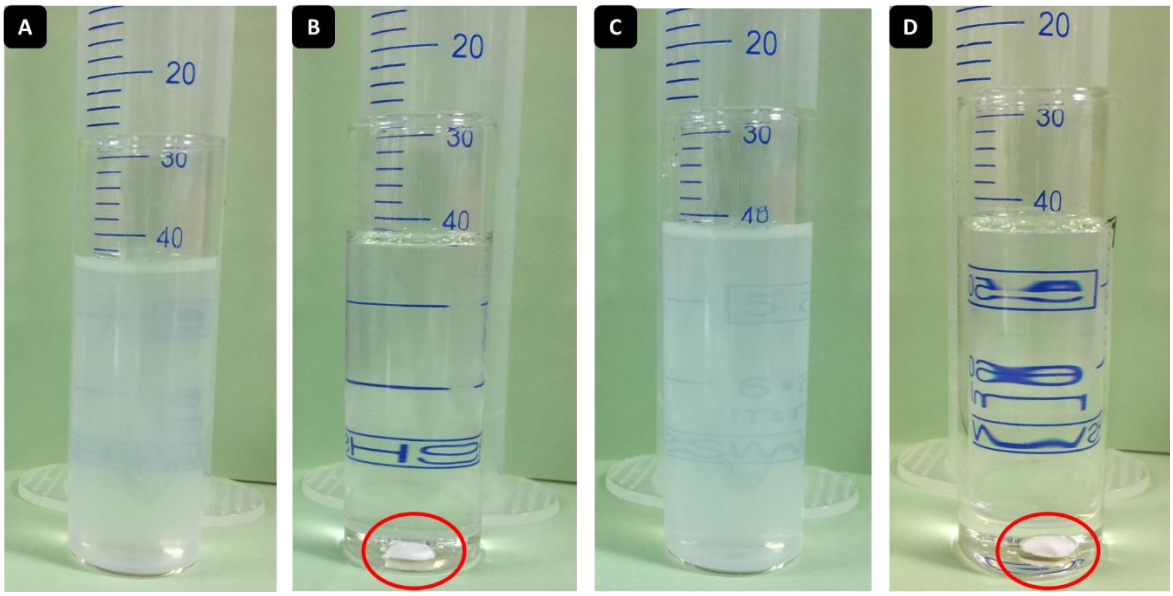

Figure 5-3: Drop test of miniemulsion: (A) Entry 5-7 in Table 5-2 ($P300_{19}M_9B_{27}$) in water, (B) Entry 5-7 in Table 5-2 ($P300_{19}M_9B_{27}$) in toluene, (C) Entry 5-10 in Table 5-2 ($P950_9M_8B_{45}$) in water, and (D) Entry 5-10 in Table 5-2 ($P950_9M_8B_{45}$) in toluene. Both miniemulsions were prepared at 20 % w/w polymer loading (with respect to oil phase) and 20 % w/w oil phase. Red circle shows the white drop sank in toluene.

The results of the toluene-in-water miniemulsions stabilized by $P_xM_yB_z$ triblock copolymers under different conditions are reported in Table 5-3 to Table 5-6. The weight fraction of the oil phase was kept at 20 % w/w and the reaction temperature was maintained at 25 ^oC unless otherwise noted, and the MPS block was subsequently crosslinked after formation of the miniemulsion. The reaction conditions studied included type of catalyst to induce crosslinking, catalyst concentration, PEGMA macroRAFT agent, chain length of triblock copolymers, polymer loading, and temperature. Each of these variables are discussed in the following paragraphs. Miniemulsions were studied by comparing the DLS volume distributions before (in both water and 1,4-dioxane) and after crosslinking (in 1,4-dioxane). Dioxane is a good solvent for the triblock copolymer and when dioxane is added, the non-crosslinked droplets should dissociate into individual chains, resulting in a very small particle diameter. In contrast, after crosslinking the droplets should not dissociate; dioxane will swell the crosslinked particles

slightly and the resultant DLS volume distribution should be comparable close to the distribution in water, as the particle structure has been "fixed" (if completely crosslinked). The DLS volume distributions in water (before crosslinking) represent the particle sizes after ultrasonication in the absence of catalyst. The volume mean diameter, d_z, and PDI values were also considered. The stability of after crosslinked miniemulsion was much concerned in this work and it varied across different conditions. According to observations, the uncrosslinked miniemulsion had slightly better stability (stability in crosslinked miniemulsion plus additional up to 2 days) than crosslinked miniemulsion.

Table 5-3: Effect of catalyst selections on the particles size and stability of $P950_{18}M_{15}B_{82}$

Entry	Condition		Volume mean diameter before crosslinking		d_z before crosslinking		Volume mean diameter after crosslinking		d_z after crosslinking		After crosslinking stability
	Type of catalyst	[Catalyst] (mol L^{-1})	Dioxane (nm)	Water (nm)	Dioxane (nm) (PDI)	Water (nm) (PDI)	Dioxane (nm)	Water (nm)	Dioxane (nm) (PDI)	Water (nm) (PDI)	
$P950_{18}M_{15}B_{82}$											
5-14	HCl	0.4	12.3	351	500 (0.706)	248 (0.188)	3706	384	364 (0.901)	621 (0.479)	Overnight
5-15	NH_4OH	0.4	12.3	351	500 (0.706)	248 (0.188)	1166	399	845 (0.715)	1542 (0.871)	Overnight
5-16	TEA	0.4	7.98	1740	597 (0.66)	231 (0.234)	364	1086	433 (0.63)	259 (0.19)	< 2 days

5-17	TEA	0.8	7.98	1740	597 (0.66)	231 (0.234)	195	244	320 (0.477)	297 (0.365)	2 days
5-18	Octylamine	0.8	19.2	355	3680 (1.0)	403 (0.328)	47.8	509	1198 (1.0)	1472 (0.871)	A few hours

In the above experiments, the polymer loading was 10 % w/w and the reaction temperature was 25 ^{o}C. HCl = hydrochloric acid, NH_4OH = ammonium hydroxide, TEA = triethylamine.

Table 5-4: Effect of polymer loading on particle size and stability of $P950_{18}M_{15}B_{82}$

Entry	Condition	Volume mean diameter before crosslinking		d_z before crosslinking		Volume mean diameter after crosslinking		d_z after crosslinking		After crosslinking stability
	Polymer loading in toluene (wt %)	Dioxane (nm)	Water (nm)	Dioxane (nm) (PDI)	Water (nm) (PDI)	Dioxane (nm)	Water (nm)	Dioxane (nm) (PDI)	Water (nm) (PDI)	
$P950_{18}M_{15}B_{82}$										
5-19	15	9.43	336	125 (0.266)	323 (0.265)	162	299	177 (0.412)	348 (0.435)	~ 2 days
5-20	20	10.6	545	104 (0.654)	474 (0.236)	1226	442	649 (0.616)	527 (0.487)	3 days

In the above experiments, TEA catalyst was used with a concentration of 0.8 mol L^{-1}. The reaction temperature was 25 ^{o}C.

Table 5-5: Different lengths of PEG and triblock copolymer were investigated and their impacts on the particle size and stability

Entry	Condition	Volume mean diameter before crosslinking		d_z before crosslinking		Volume mean diameter after crosslinking		d_z after crosslinking		After crosslinking stability
	Chain lengths of PEG and triblock copolymer	Dioxane (nm)	Water (nm)	Dioxane (nm) (PDI)	Water (nm) (PDI)	Dioxane (nm)	Water (nm)	Dioxane (nm) (PDI)	Water (nm) (PDI)	
5-21	$P300_{19}M_9B_{27}$	41.1	697	119 (0.355)	1206 (0.428)	910	805	1083 (0.665)	1158 (0.368)	< 3 days
5-22	$P300_{39}M_{17}B_{49}$	7.14	824	188 (0.313)	581 (0.688)	2285	1253	262 (0.602)	504 (0.592)	3 days
5-23	$P300_{58}M_{24}B_{74}$	785	778	84.5 (0.443)	1109 (0.565)	791	593	471 (0.676)	1215 (0.74)	3 days
5-24	$P950_9M_8B_{45}$	5.52	1033	2831 (1.0)	255 (0.263)	75.4	286	114 (0.374)	267 (0.279)	< 3 days

5-25	$P950_{36}M_{30}B_{152}$	82.9	529	53.6 (0.995)	519 (0.31)	753	457	538 (0.679)	485 (0.377)	3 days

In the above experiments, TEA catalyst was used with a concentration of 0.8 mol L^{-1}. The polymer loading was fixed at 20 % w/w and reaction temperature was 25 ^{o}C.

Table 5-6: Effect of high reaction temperature on the particle size and stability of $P950_xM_yB_z$ triblock copolymers

Entry	Condition	Volume mean diameter before crosslinking		d_z before crosslinking		Volume mean diameter after crosslinking		d_z after crosslinking		After crosslinking stability
	Temperature (ºC)	Dioxane (nm)	Water (nm)	Dioxane (nm) (PDI)	Water (nm) (PDI)	Dioxane (nm)	Water (nm)	Dioxane (nm) (PDI)	Water (nm) (PDI)	
$P950_{18}M_{15}B_{82}$										
5-26	65	10.8	459	209 (0.334)	428 (0.275)	2322	314	467 (0.469)	554 (0.569)	Overnight
$P950_{36}M_{30}B_{152}$										
5-27	65	37.7	534	56.5 (0.589)	502 (0.317)	495	507	576 (0.594)	572 (0.533)	Overnight

In the above experiments, TEA catalyst was used with a concentration of 0.8 mol L^{-1}. The polymer loading was 20 % w/w.

Acid vs Base Catalysis. Using the $P950_{18}M_{15}B_{82}$ triblock copolymer, the influence of acid or base catalysis was studied on the interfacial crosslinking of o/w droplets. The loading of polymer in the toluene phase was 10 % w/w. The concentration of HCl and NH_4OH in the aqueous phase was 0.4 mol L^{-1} (Entry 5-14 and 5-15 in Table 5-3). The volume distributions of the non-crosslinked droplets decreased significantly in 1,4-dioxane, showing distinct dissociation into individual chains (Figure 5-4). After cross-linking with both catalysts, there is no evidence of dissociation into unimers upon addition to 1,4-dioxane. Catalysis with NH_4OH revealed a volume distribution closer to the parent distribution in water, with much larger effective particle size when acid catalysis was used. An acidic environment has a much faster hydrolysis rate than condensation, causing the PMPS block to have majority silanol groups (Si-OH) and minor crosslinked network (Si-O-Si).[82-84] It is postulated that this may result in interparticle crosslinking and the formation of larger aggregates via the presence of silanol groups. However, both solutions phase separated overnight after crosslinking.

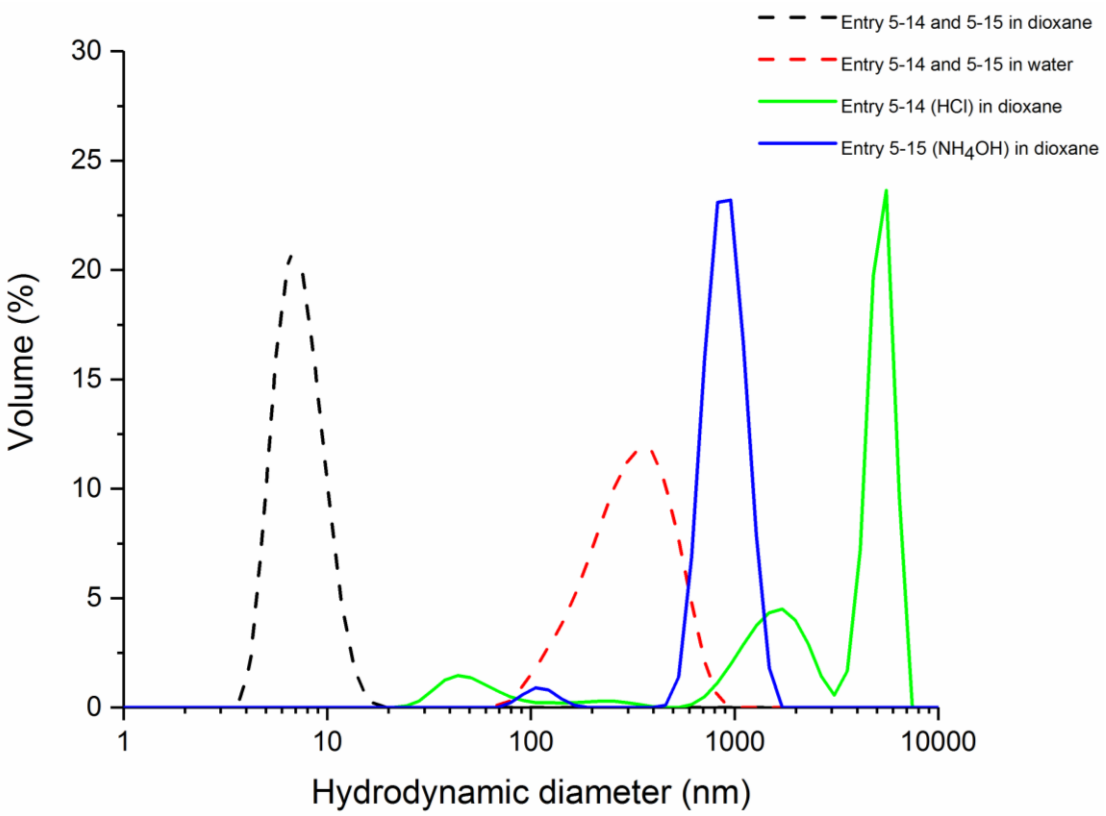

Figure 5-4: DLS volume distributions of Entry 5-14 and 5-15 (in Table 5-3) in dioxane and water, using HCl and NH_4OH catalysts. Dash line represents before crosslinking (no catalyst) and solid line represents after crosslinking (with catalyst).

Base Catalysis: Effect of Water Solubility. The effectiveness of two other catalysts of differing water solubility (triethylamine (TEA) and octylamine) was studied, as a comparison to the NH_4OH discussed above. The water solubility of octylamine and TEA at 25 ^oC is 0.2 and 69 g L^{-1} respectively.[85] A moderately water-soluble base (TEA) was tested to crosslink the MPS groups at the droplet interface. Two different concentrations of TEA were used (Entry 5-16 and 5-17 in Table 5-3; 0.4 and 0.8 mol L^{-1} respectively) and the same precursor polymer was used. A peak at large particle size (~ 5 µm; Figure 5-5) was observed in water for the uncrosslinked miniemulsion (Entry 5-16 and 5-17 in Table 5-3) and this peak was possibly due to an insufficient level of polymeric surfactant. After TEA-induced catalysis, a bimodal

distribution and large particle size were obtained in the DLS distribution when using high concentration (0.8 mol L^{-1}). A significant increase in the size distribution was noticed when the crosslinked miniemulsion dispersed in 1,4-dioxane (compared to without crosslinking) (Figure 5-5). This result suggested moderate levels of interfacial crosslinking of MPS units and higher catalyst concentration had a closer preservation of the initial droplet size in water. After crosslinking, the dispersion was stable for up to 2 days, representing an improvement on ammonium hydroxide catalyst. A highly water insoluble catalyst (octylamine, Entry 5-18 in Table 5-3) was subsequently investigated and the catalyst concentration was fixed at 0.8 mol L^{-1}, since higher catalyst concentration had a better performance. Figure 5-5 shows the octylamine did not effectively crosslink the PMPS block at the droplet interface; upon addition to 1,4-dioxane, the volume distribution was only slightly larger than dissociated unimers (see orange and purple curves). The crosslinked miniemulsion catalysed by octylamine also phase separated within a few hours. Therefore, TEA catalyst was selected and applied in the remaining miniemulsion experiments.

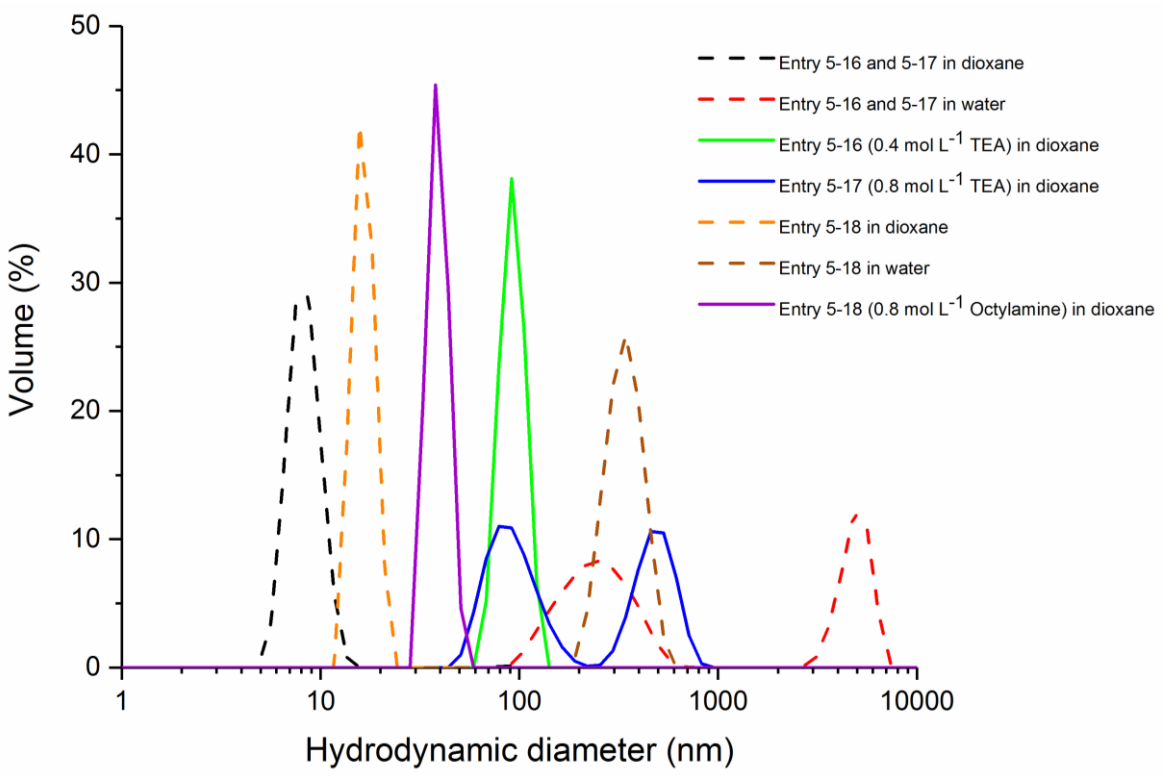

Figure 5-5: DLS volume distributions of Entry 5-16, 5-17 and 5-18 (in Table 5-3) in dioxane and water, using TEA and octylamine catalysts. Dash line represents before crosslinking (no catalyst) and solid line represents after crosslinking (with catalyst).

Polymer Loading. The influence of increasing the polymer loading was further examined, using 0.8 mol L^{-1} catalyst concentration. Two different polymer loadings (15 and 20 % w/w; Entry 5-19 and 5-20 (in Table 5-4) respectively) were tested. The crosslinked miniemulsion was stable for up to 3 days at a polymer loading of 20 % w/w. Figure 5-6 shows a large particle size and unimodal distribution were observed at a polymer loading of 20 % w/w (see purple curve) when dispersed in dioxane, significantly larger than the parent distribution in water. The DLS distribution for 15 % w/w polymer loading was comparable to the result at 10 % w/w (Entry 5-17 in Table 5-3; Figure 5-5). The increased polymer concentration will result in a more densely packed droplet interface which can improve the droplet stability and also likely enhance the level of MPS crosslinking. In Figure 5-6, it can be seen that the particle size (Entry

5-20 in Table 5-4) after crosslinking (in dioxane) is slightly bigger than its uncrosslinked miniemulsion in water, most likely due to swelling of the polymer domains in a good solvent.

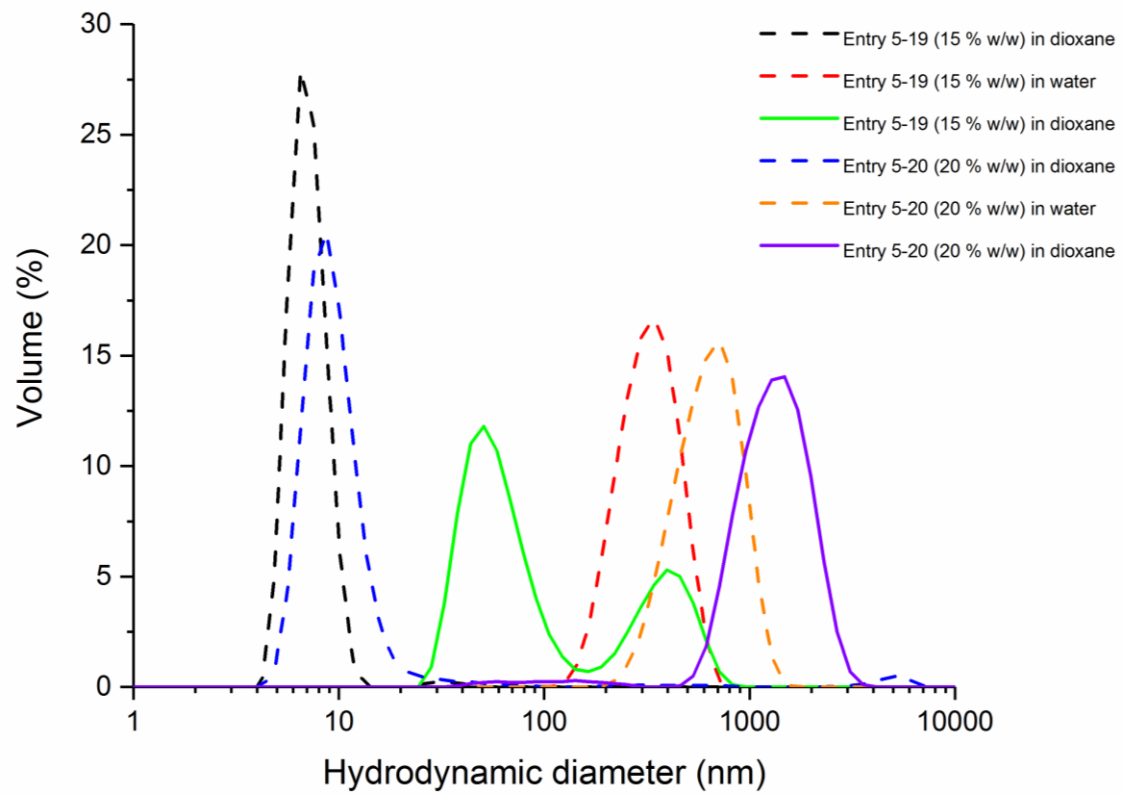

Figure 5-6: DLS volume distributions of different polymer loading experiments (Entry 5-19 and 5-20 in Table 5-4) in dioxane and water. Dash line represents before crosslinking (no catalyst) and solid line represents after crosslinking (with catalyst).

Influence of PEG and Triblock Copolymer Chain Lengths. Different lengths of PEG and triblock copolymer were then studied for miniemulsions prepared under the above-optimised conditions (0.8 mol L^{-1} TEA, 20 % w/w polymer loading). Figure 5-7 and Figure 5-8 show the DLS volume distributions of miniemulsions stabilized by polymers with a PEGMA (M_n 300) and PEGMA (M_n 950) block respectively. In the case of P300 triblocks (Figure 5-7), there was clear evidence of successful interfacial crosslinking – the unimer peak at low particle size

disappeared (comparing before and after crosslinking distributions in dioxane); in nearly all cases the primary peak in dioxane was comparable to the precursor size distribution in water. When the chain length of triblock copolymer was increased (while keeping the block ratios identical), there was moderate improvement in the dispersion stability after crosslinking (phase separation after three days), which was still undesirable for long term storage. There was no obvious trend in particle size and PDI when the chain length of triblock copolymer increased. TEM images (Figure 5-9 and Figure 5-10) showed hollow "capsule-like" structures were produced. TEM images were taken by diluting crosslinked solution with MilliQ. The capsules appear collapsed under electron microscopy due to their hollow nature and relatively thin crosslinked interface. Both electron microscopy images also illustrated the hollow capsules maintained the same structure before and after crosslinking and TEA catalyst did not degrade the polymeric surfactants. The size of crosslinked capsules was comparable to the DLS volume distributions.

In comparison, when P950 was used as the hydrophilic block, there was a much greater level of variation in successfully crosslinking the droplet interface (see Figure 5-8). For the triblock copolymer of shortest chain length (Entry 5-24 in Table 5-5), insufficient crosslinking was observed to stabilize the droplets (light green curve). The efficacy of crosslinking improved with increasing polymer chain length, as the parent size distribution was preserved to a greater extent (when comparing distributions in water and dioxane, see orange and purple curves). This is likely attributed to reduced mobility of the higher molecular weight triblock copolymer when adsorbed at the droplet interface, in addition to a greater number of MPS units available for crosslinking. TEM revealed hollow structure nanoparticles were also obtained when longer P950 macroRAFT agent was used (Figure 5-11; Entry 5-25 in Table 5-5). This observation was similar to nanoparticles produced with using P300 macroRAFT agent in miniemulsions.

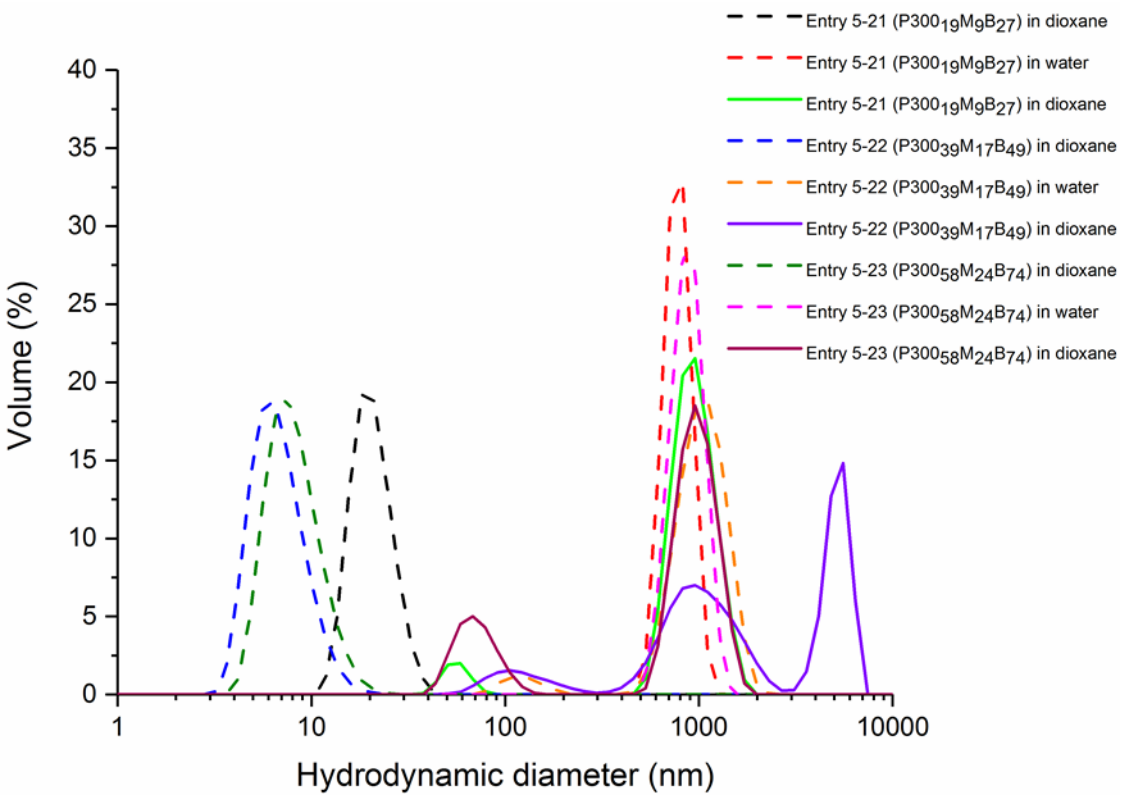

Figure 5-7: DLS volume distributions of P300$_x$M$_y$B$_z$ (Entry 5-21, Entry 5-22 and Entry 5-23 in Table 5-5) in dioxane and water. Dash line represents before crosslinking (no catalyst) and solid line represents after crosslinking (with catalyst).

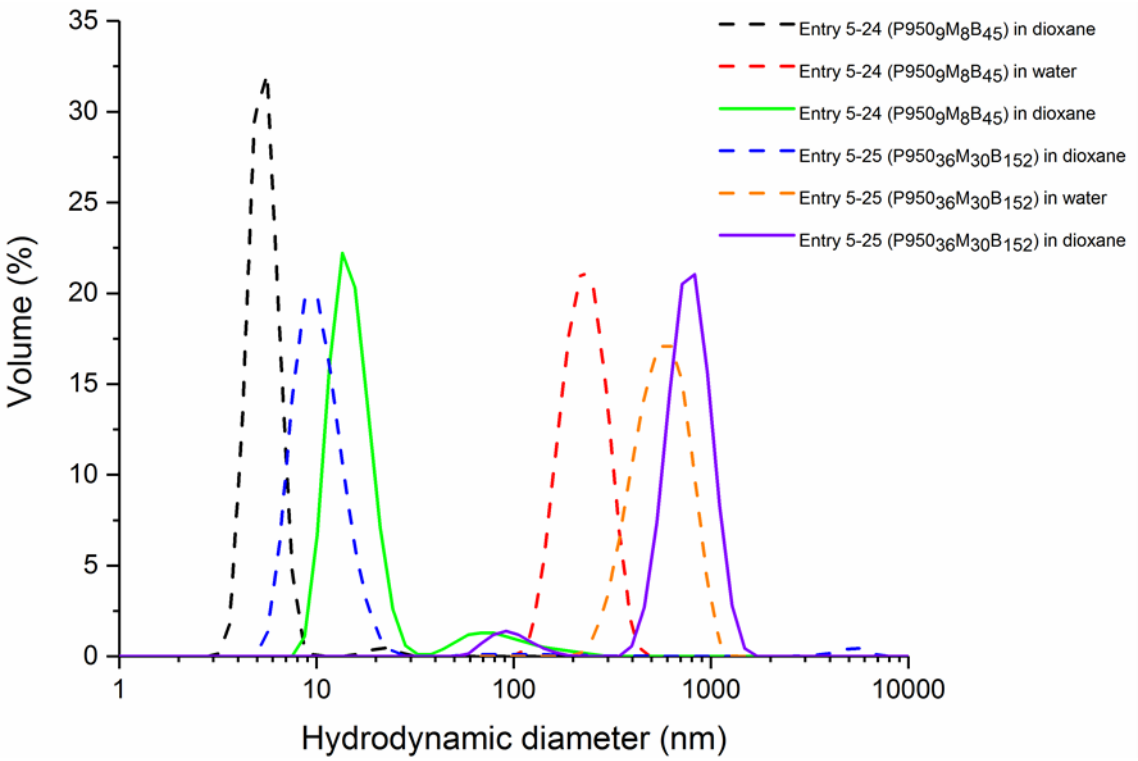

Figure 5-8: DLS volume distributions of P950$_x$M$_y$B$_z$ (Entry 5-24 and Entry 5-25 in Table 5-5) in dioxane and water. Dash line represents before crosslinking (no catalyst) and solid line represents after crosslinking (with catalyst).

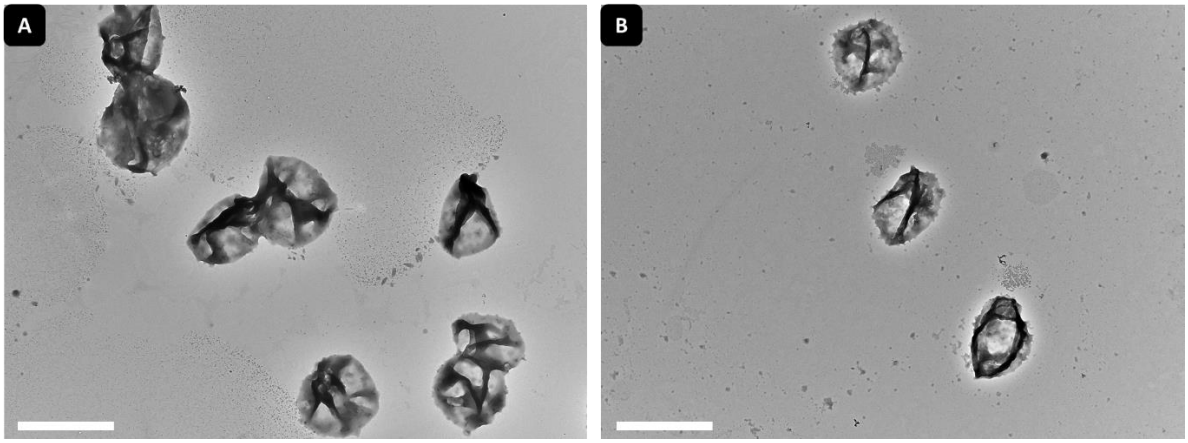

Figure 5-9: TEM images of Entry 5-21 (in Table 5-5, P300$_{19}$M$_9$B$_{27}$) in MilliQ: (A) before crosslinking, and (B) after crosslinking. Scale bar: (A) and (B) = 2 µm

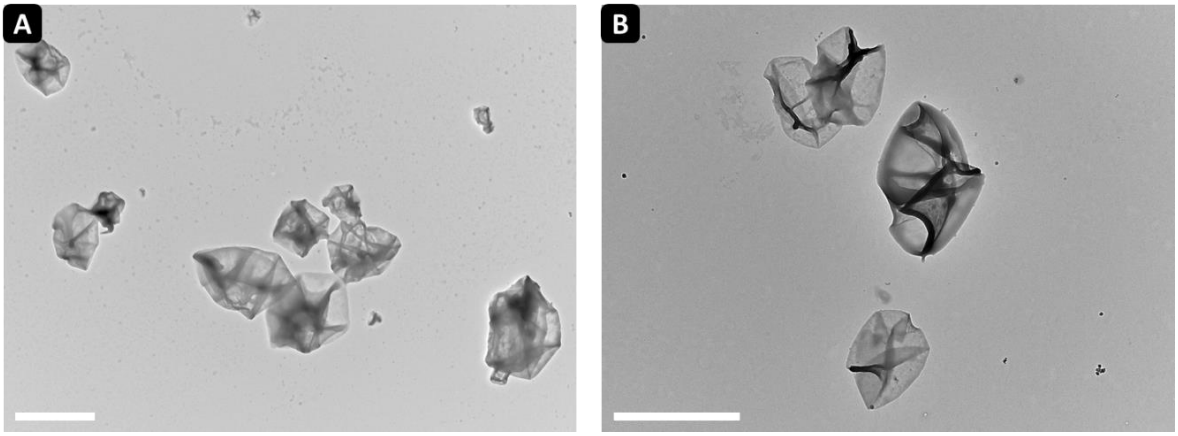

Figure 5-10: TEM images of Entry 5-23 (in Table 5-5, $P300_{58}M_{24}B_{74}$) in MilliQ: (A) before crosslinking, and (B) after crosslinking. Scale bar: (A) and (B) = 2 µm

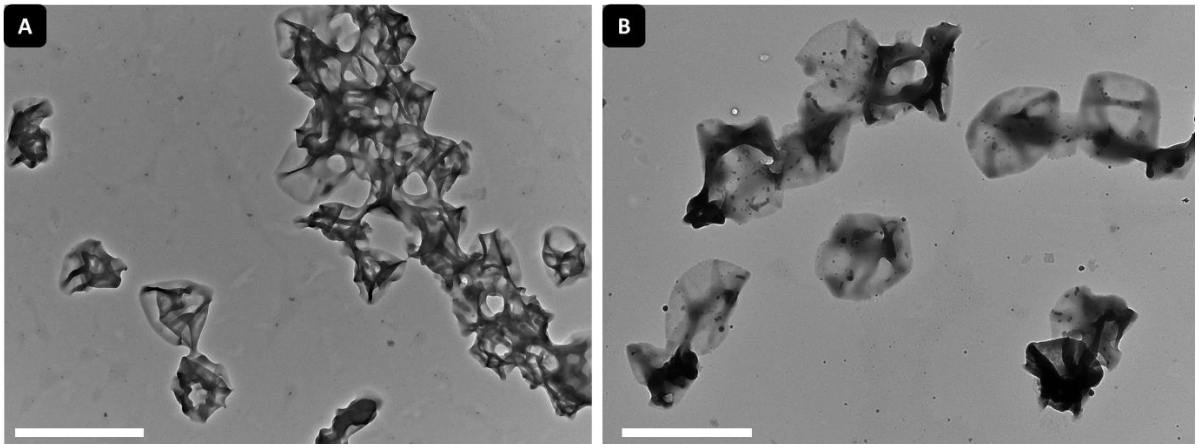

Figure 5-11: TEM images of Entry 5-25 (in Table 5-5, $P950_{36}M_{30}B_{152}$) in MilliQ: (A) before crosslinking, and (B) after crosslinking. Scale bar: (A) and (B) = 2 µm

Influence of Temperature. Rates of hydrolysis and condensation of alkoxysilyl are temperature sensitive. At elevated temperatures, the rate of hydrolysis of MPS units will increase with the presence of catalyst and consequently condensation reaction.[86-89] A more rapid condensation could potentially "lock" the droplets promptly via forming a silica shell. Two different P950-based triblock copolymers (Entry 5-26 and 5-27 in Table 5-6) were studied

under higher temperature and the particle size distributions are shown in Figure 5-12. There was excellent correspondence between the parent droplet distribution before (water) and after (dioxane) crosslinking, with no evidence of residual unimers. However, the stability was poor and the dispersions phase separated overnight.

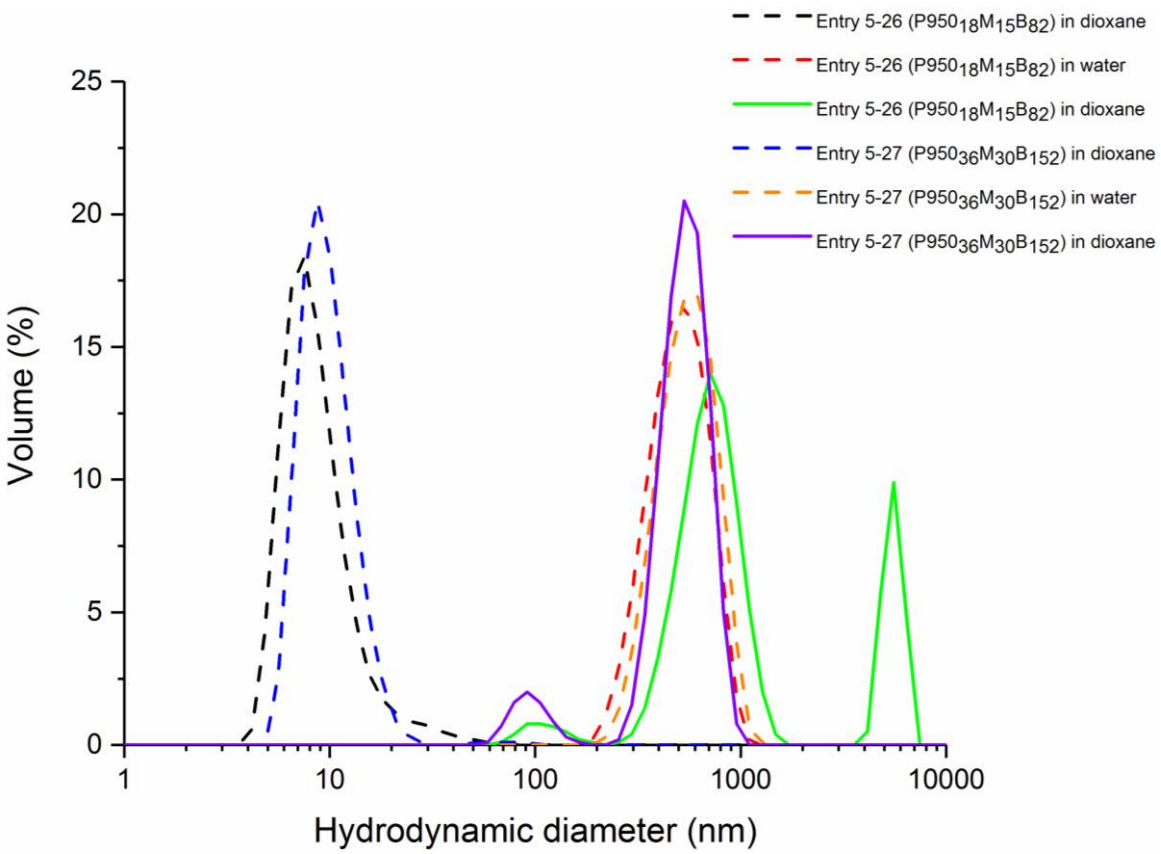

Figure 5-12: DLS volume distributions of higher reaction temperature experiments (Entry 5-26 and 5-27 in Table 5-6) in dioxane and water. Dash line represents before crosslinking (no catalyst) and solid line represents after crosslinking (with catalyst).

Absence of MPS Block. Lastly, the effect of the presence of the PMPS block was studied. A diblock copolymer without an PMPS block ($P950_{18}B_{85}$; Entry 5-28 in Table 5-7) was prepared and applied as polymeric surfactant in O/W minimeulsion (no TEA catalyst). DLS measurement in dioxane showed complete dissociation of the stabilized droplets upon transfer from miniemulsion to dioxane, as expected (Figure 5-13). However, this dispersion showed the greatest stability (at least 5 days) before phase separation, suggesting that the PMPS block has a negative effect on colloidal stability. The reason for this is not clear, however the crosslinking of MPS obviously impacts on the mobility of the polymer chains at the interface. Furthermore, residual uncrosslinked groups (methoxysilyl and silanol) present near the particle surface may result in aggregation and destabilization over time. In term of particle structure, Figure 5-14 indicated a mixed morphology of hollow and sphere was obtained. This observation was slightly different to triblock copolymer containing PMPS block where all the resultant nanoparticles were hollow structure.

Table 5-7: Particle size and stability of PEGMA diblock copolymer without PMPS block

Entry	**Condition**	**Volume mean diameter**		***d_z***		**Stability**
	Diblock copolymer composition (No PMPS block)	**Dioxane (nm)**	**Water (nm)**	**Dioxane (nm) (PDI)**	**Water (nm) (PDI)**	
5-28	$P950_{18}B_{85}$	29.3	1219	138 (0.357)	348 (0.261)	5 days

In the above experiment, the polymer loading was fixed at 20 % w/w and reaction temperature was 25 ^{o}C.

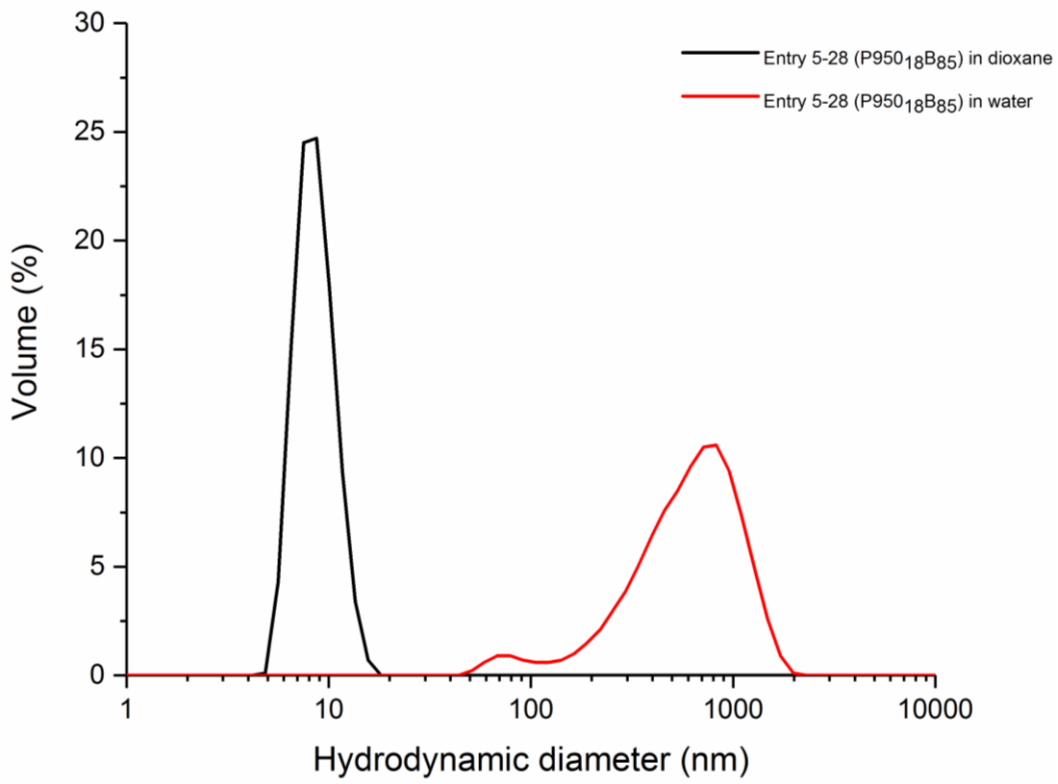

Figure 5-13: DLS volume distribution of P950$_{18}$B$_{85}$ diblock copolymer (Entry 5-28 in Table 5-7) in dioxane and water

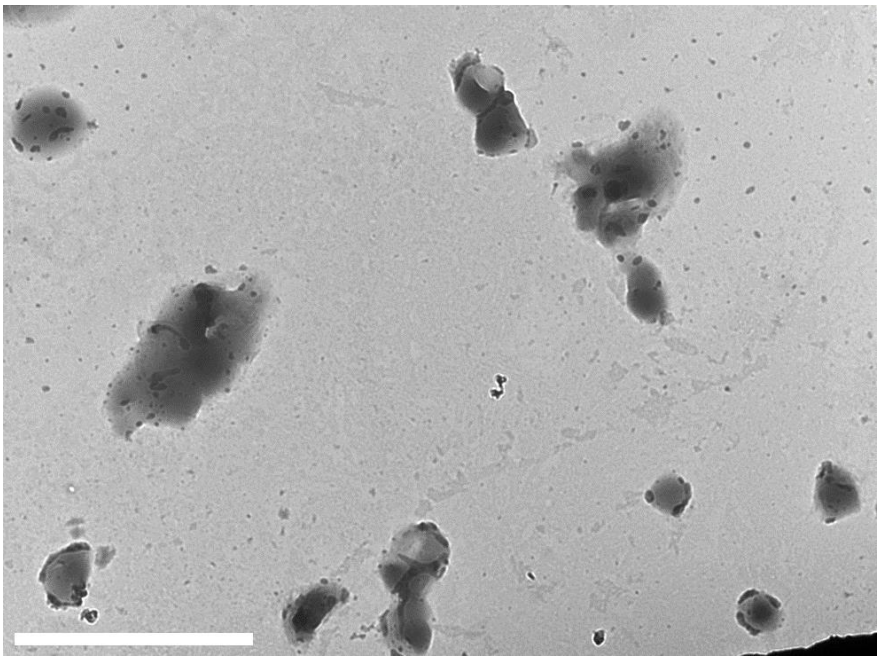

Figure 5-14: TEM image of Entry 5-28 (in Table 5-7, P950$_{18}$B$_{85}$) in MilliQ (no crosslinking). Scale bar = 2 µm.

5.2.2 Self-Assembly of Alkoxysilane-Containing Triblock Copolymers via Polymerization-Induced Self-Assembly

As the O/W miniemulsions stabilized by triblock copolymers reported in the previous section had limited colloidal stability, an alternative method of triblock copolymer self-assembly was investigated. In this section, Polymerization-Induced Self-Assembly (PISA) mediated by RAFT polymerization was used to synthesize triblock copolymers of similar composition to those prepared in Section 5.2.1. One PEGMA (M_n 300) and two PEGMA (M_n 950) macroRAFT agents of different degree of polymerization (M_n 300: 19 units; M_n 950: 9 and 18 units) were prepared for this study. The SEC data of these macroRAFT agents were tabulated in Table 5-1 (Entry 5-1, 5-4, and 5-5) and they possessed narrow molecular weight distributions (see Figure 5-1; black, blue, and orange curves). The pre-synthesized PEGMA macroRAFT agent was first chain extended with MPS in isopropanol and then BzMA in isopropanol:water (96:4 % v/v) under a one-pot approach. Water was added to create an isopropanol:water (96:4 % v/v) mixture for chain extension with BzMA in order to prevent UCST-type behaviour of PEGMA in isopropanol during storage.[90] It was observed that when pure isopropanol was used as the reaction solvent for PISA syntheses, the resultant triblock copolymer (PEGMA-PMPS-PBzMA) precipitated from solution when the temperature dropped from the reaction temperature to room temperature. The system was completely stable at room temperature when water was present. The synthesis of this triblock copolymer via one-pot approach is illustrated in Figure 5-15.

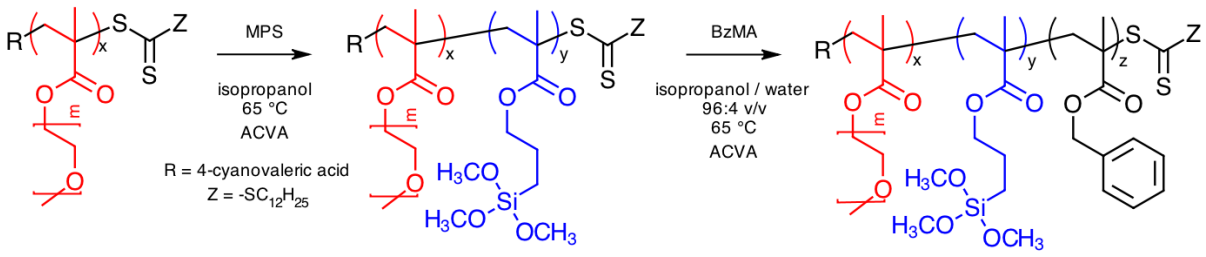

Figure 5-15: PISA mediated by RAFT polymerization of PEGMA-PMPS-PBzMA triblock copolymer in isopropanol:water (96:4 % v/v)

The target degree of polymerization of MPS was kept at 20 while the length of the BzMA block was varied from 100 up to 1000 units. The reaction was completed as a one-pot process and no purification was performed prior to chain extension with BzMA. As the conversion of MPS into polymer was moderate, some remaining MPS units were then incorporated into the growing polymer chains during BzMA chain extension, producing the triblock copolymer with the expected structure of PEGMA-*block*-PMPS-*block*-(PMPS-*gradient*-PBzMA) (P_x-*b*-M_{20-y}-*b*-(M_y-*grad*-B_z), where *x* and *z* are the respective DPs of PEGMA and BzMA, *y* is the remaining units of MPS monomer incorporated into the BzMA block). The results of the chain extension of MPS and BzMA are summarised in Table 5-8 to Table 5-10. The fractional conversion of BzMA was quite high (≥ 85 %) in most cases, however, the fractional conversion of MPS was lower when higher molecular weight PEGMA macroRAFT agents were used. This was attributed to longer/heavier PEGMA macroRAFT agent having a reduced reinitiation efficiency[91] and steric hindrance from the bulky pendant group.[92, 93]

Table 5-8: Conversion and stability of $P300_{19}$ triblock copolymers

Entry	Target composition	Conversion		Theoretical composition	Stability (No gelation)
		MPS	BzMA		
5-29	$P300_{19}M_{20}B_{100}$	0.86	0.99	$P300_{19}$-*b*-M_{17}-*b*-(M_3-*grad*-B_{99})	≥ 7 days
5-30	$P300_{19}M_{20}B_{200}$	0.79	0.98	$P300_{19}$-*b*-M_{16}-*b*-(M_4-*grad*-B_{196})	~ 5 days
5-31*	$P300_{19}M_{20}B_{200}$	0.83	0.95	$P300_{19}$-*b*-M_{17}-*b*-(M_3-*grad*-B_{190})	~ 5 days
5-32	$P300_{19}M_{20}B_{400}$	0.83	0.99	$P300_{19}$-*b*-M_{17}-*b*-(M_3-*grad*-B_{396})	2 days
5-33	$P300_{19}M_{20}B_{600}$	0.79	0.97	$P300_{19}$-*b*-M_{16}-*b*-(M_4-*grad*-B_{582})	~ 1 day
5-34	$P300_{19}M_{20}B_{800}$	0.77	0.96	$P300_{19}$-*b*-M_{15}-*b*-(M_5-*grad*-B_{768})	A few hours
5-35^	$P300_{19}M_{20}B_{800}$	0.72	0.97	$P300_{19}$-*b*-M_{14}-*b*-(M_6-*grad*-B_{776})	A few hours

** Nile Red was applied in the experiment. ^ Aliquot was extracted immediately once the reaction stopped and the solution was still hot.*

Table 5-9: Conversion and stability of $P950_9$ triblock copolymers

Entry	Target composition	Conversion		Theoretical composition	Stability (No gelation)
		MPS	BzMA		
5-36	$P950_9M_{20}B_{100}$	0.78	0.97	$P950_9$-*b*-M_{16}-*b*-(M_4-*grad*-B_{97})	≥ 7 days
5-37	$P950_9M_{20}B_{200}$	0.60	0.98	$P950_9$-*b*-M_{12}-*b*-(M_8-*grad*-B_{196})	
5-38	$P950_9M_{20}B_{400}$	0.77	0.97	$P950_9$-*b*-M_{15}-*b*-(M_5-*grad*-B_{388})	
5-39*	$P950_9M_{20}B_{400}$	0.76	0.95	$P950_9$-*b*-M_{15}-*b*-(M_5-*grad*-B_{380})	
5-40	$P950_9M_{20}B_{600}$	0.74	0.97	$P950_9$-*b*-M_{15}-*b*-(M_5-*grad*-B_{582})	~ 5 days
5-41	$P950_9M_{20}B_{800}$	0.64	0.95	$P950_9$-*b*-M_{13}-*b*-(M_7-*grad*-B_{760})	
5-42	$P950_9M_{20}B_{1000}$	0.68	0.98	$P950_9$-*b*-M_{14}-*b*-(M_6-*grad*-B_{980})	

** Nile Red was applied in the experiment.*

Table 5-10: Conversion and stability of $P950_{18}$ triblock copolymers

Entry	Target composition	Conversion		Theoretical composition	Stability (No gelation)
		MPS	BzMA		
5-43	$P950_{18}M_{20}B_{100}$	0.63	0.91	$P950_{18}$-*b*-M_{13}-*b*-(M_7-*grad*-B_{91})	≥ 7 days
5-44	$P950_{18}M_{20}B_{200}$	0.57	0.85	$P950_{18}$-*b*-M_{11}-*b*-(M_9-*grad*-B_{170})	
5-45	$P950_{18}M_{20}B_{400}$	0.62	0.95	$P950_{18}$-*b*-M_{12}-*b*-(M_8-*grad*-B_{380})	
5-46*	$P950_{18}M_{20}B_{400}$	0.62	0.94	$P950_{18}$-*b*-M_{12}-*b*-(M_8-*grad*-B_{376})	
5-47	$P950_{18}M_{20}B_{600}$	0.60	0.96	$P950_{18}$-*b*-M_{12}-*b*-(M_8-*grad*-B_{576})	
5-48	$P950_{18}M_{20}B_{800}$	0.63	0.95	$P950_{18}$-*b*-M_{13}-*b*-(M_7-*grad*-B_{760})	~ 6 days
5-49	$P950_{18}M_{20}B_{1000}$	0.66	0.94	$P950_{18}$-*b*-M_{13}-*b*-(M_7-*grad*-B_{940})	

** Nile Red was applied in the experiment.*

Influence of Hydrophobic Chain Length. A range of target BzMA DPs were investigated in three different PEGMA macroRAFT agent systems. For all compositions, no variation in particle morphology was observed; all resultant nanoparticles were spherical in shape, even at very high target BzMA DPs. Typical TEM images of spherical nanoparticles formed by the PISA process for these systems are shown in Figure 5-16. The use of different PEGMA macroRAFT agents ($P300_{19}$ and $P950_9$) also resulted in the exclusive formation of spherical nanoparticles, despite this being a dispersion polymerization system. This phenomenon was attributed to the bulky/long stabilizer block or the higher order morphology was not possible due to kinetic trapping,[94-99] however as will be discussed later, the presence of the MPS block also contributes to this exclusive spherical morphology.

The stability of the resulting dispersions (prior to MPS crosslinking) also varied across the systems (Table 5-8 to Table 5-10). When lower molecular weight PEGMA macroRAFT agents were used and a high BzMA DP was targeted, the uncrosslinked dispersion would gel after a few hours (Entry 5-34 in Table 5-8), in contrast to 6 days (Entry 5-48 in Table 5-10) stability with high molecular weight PEGMA macroRAFT agent at an identical target DP of BzMA. This gel issue was possibly due to strong interactions of long fused sphere network (see Figure 5-17). DLS particle size before crosslinking (Entry 5-33 in Table 5-11) showed very large particle size in isopropanol:water and water. The DLS particle size was comparable to that observed by TEM (Figure 5-17). Wang and co-workers reported fractal-type connected bead structure was caused by random spheres fusion and diffusion limited aggregation and growth processes.[100] The gelation was reversible into the liquid state upon heating, however, significant coagulum was observed. The reversible transition from gel to liquid was attributed to solvent plasticization of the core-forming block at high temperature.[101-103] Because of the rapid gelation of Entry 5-34 (in Table 5-8), an identical experiment was performed however the particle size was measured directly while the reaction dispersion was still hot (Entry 5-35 in Table 5-11). The particle size of Entry 5-35 (in Table 5-11) before crosslinking was typical for a dispersion of this composition and demonstrated good reproducibility of particle size without the effects of aggregation and gelation. TEM images of particles prepared in these experiments are shown in Figure 5-18.

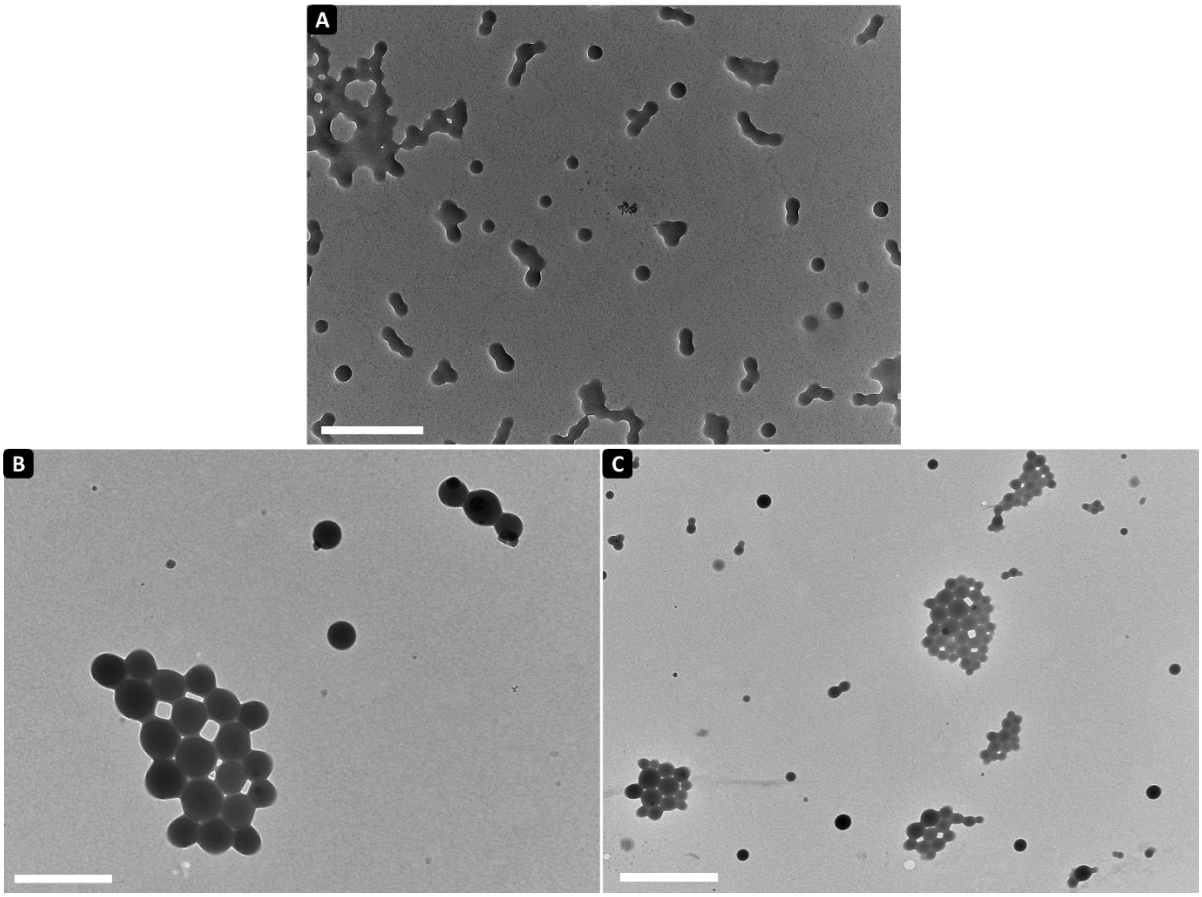

Figure 5-16: TEM images of self-assembled nanoparticles in isopropanol:water (96:4 % v/v) and before crosslinking: (A) Entry 5-30 in Table 5-11, (B) Entry 5-42 in Table 5-12, and (C) Entry 5-49 in Table 5-13. Scale bar = (A) 500 nm, (B) 1 µm, and (C) 2 µm.

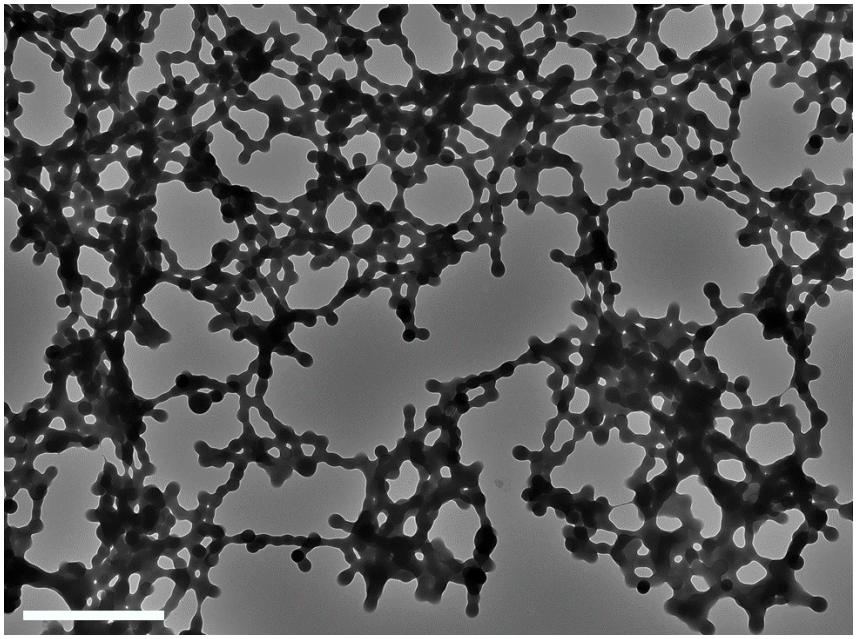

Figure 5-17: TEM image of Entry 5-33 (in Table 5-11, $P300_{19}M_{20}B_{600}$) in isopropanol:water (96:4 % v/v) (before crosslinking). Scale bar = 2 µm.

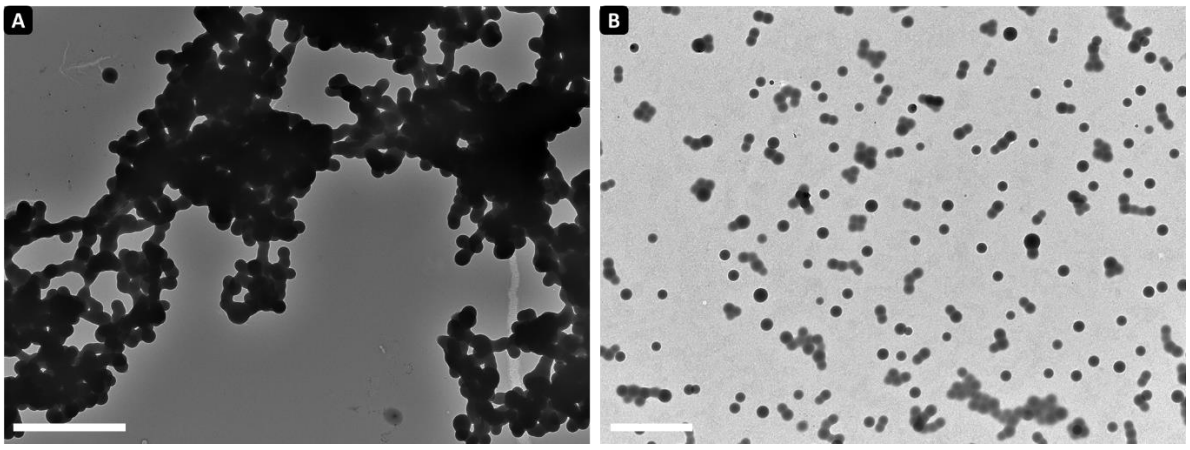

Figure 5-18: TEM images of $P300_{19}M_{20}B_{800}$ in isopropanol:water (96:4 % v/v): (A) Entry 5-34 in Table 5-11 (before crosslinking) and (B) Entry 5-35 in Table 5-11 (before crosslinking). Scale bar: (A) and (B) = 2 µm.

Crosslinking via Using NH_4OH Catalyst. After the self-assembled nanoparticles were produced, the interfacial PMPS block was initially crosslinked with TEA at a concentration 0.8 mol L^{-1}. Although TEA was the best catalyst for interfacial crosslinking in Section 5.2.1, the PISA system became unstable and polymer precipitated out once TEA catalyst was added. The system instability in this PISA approach was possibly due to different solvents used. As a result, ammonium hydroxide was used at the same concentration, resulting in stable nanoparticle dispersions. The results of DLS measurements (before and after crosslinking) in isopropanol:water (96:4 % v/v), dioxane, and water are listed in Table 5-11 to Table 5-13. Each experiment was assessed by comparing DLS measurements between dioxane and isopropanol:water (96:4 % v/v), to study if the self-assembled nanoparticle would disassemble in a good solvent (dioxane) or not. The average particle size in isopropanol:water (96:4 % v/v) and water were comparable, with an increase in particle size upon increasing the length of the BzMA block. Prior to cross-linking, the effective particle size in dioxane was relatively small (~ 11 to 37 nm hydrodynamic diameter); after cross-linking, the particle size in dioxane was much larger (see Figure 5-19, Figure 5-21 and Figure 5-23). The *z*-average diameter in dioxane was typically slightly larger than the particle size in both isopropanol:water and water, due to the swelling of the polymer phase with a good solvent; the particles however were unable to dissociate due to the interfacial cross-linking of the MPS block. There was no evidence of unimers in the particle size distribution after crosslinking and addition to dioxane, suggesting a high level of interfacial cross-linking. Most of the DLS volume distributions (after crosslinking) overlapped with their parent distributions in isopropanol:water (Figure 5-20, Figure 5-22 and Figure 5-24), showing particle size distribution was not influenced by the crosslinking process.

An additional benefit of interfacial cross-linking was that the colloidal stability of the resulting dispersion was improved. All crosslinked dispersions did not gel after 7 days of storage. Figure 5-25 shows the comparison between nanoparticle dispersions that were either cross-linked or not crosslinked; the lack of gelation (after crosslinking) is emphasised via vial inversion. TEM also disclosed the crosslinking could prevent sphere-sphere fusion and avoid long network entanglement (Figure 5-26) and the particle size was comparable to DLS measurement (Table 5-11). Large DLS particle sizes were noted in Entries 5-33 and 5-34 (Table 5-11). The unusual particle size of Entry 5-33 (in Table 5-11) before crosslinking was perhaps an effect of slow gelation over time as it had a maximum stability up to a day. Unintended PMPS crosslinking was ruled out in this case and a clear particle size shift (when added to dioxane) could be observed in Figure 5-19. As long as the solution had not fully gelled, crosslinking of Entry 5-33 (in Table 5-11) was still possible, producing a moderate DLS particle size. The large DLS particle size in Entry 5-34 (in Table 5-11) was expected since this sample gelled quickly, making true determination of particle size difficult.

Table 5-11: Particle size diameter of $P300_{19}$ triblock copolymer before and after crosslinking

Entry number from Table 5-8	**Theoretical composition**	**d_z before crosslinking**			**d_z after crosslinking**		
		Isopropanol:Water 96:4 % v/v (nm) (PDI)	**Dioxane (nm) (PDI)**	**Water (nm) (PDI)**	**Isopropanol:Water 96:4 % v/v (nm) (PDI)**	**Dioxane (nm) (PDI)**	**Water (nm) (PDI)**
5-29	$P300_{19}$-*b*-M_{17}-*b*-(M_3-*grad*-B_{99})	95.3 (0.142)	12.6 (0.237)	89 (0.164)	105 (0.164)	108 (0.113)	100 (0.181)
5-30	$P300_{19}$-*b*-M_{16}-*b*-(M_4-*grad*-B_{196})	93.9 (0.081)	13.3 (0.199)	87.7 (0.145)	94.8 (0.081)	124 (0.01)	87.6 (0.086)
5-32	$P300_{19}$-*b*-M_{17}-*b*-(M_3-*grad*-B_{396})	208 (0.291)	19 (0.196)	198 (0.321)	165 (0.11)	268 (0.068)	153 (0.107)
5-33	$P300_{19}$-*b*-M_{16}-*b*-(M_4-*grad*-B_{582})	1295 (0.443)	23.1 (0.205)	1186 (0.831)	354 (0.293)	689 (0.23)	326 (0.376)
5-34	$P300_{19}$-*b*-M_{15}-*b*-(M_5-*grad*-B_{768})	2821 (0.982)	25.2 (0.194)	3556 (0.565)	2966 (0.754)	1552 (0.338)	3344 (0.799)

5-35^	$P300_{19}$-*b*-M_{14}-*b*-(M_6-*grad*-B_{776})	246 (0.022)	26.2 (0.198)	244 (0.018)	245 (0.032)	457 (0.05)	232 (0.034)

^ *Aliquot was extracted immediately once the reaction stopped and the solution was still hot.*

Table 5-12: Particle size diameter of P950$_9$ triblock copolymer before and after crosslinking

Entry number from Table 5-9	**Theoretical composition**	**d_z before crosslinking**			**d_z after crosslinking**		
		Isopropanol:Water 96:4 % v/v (nm) (PDI)	**Dioxane (nm) (PDI)**	**Water (nm) (PDI)**	**Isopropanol:Water 96:4 % v/v (nm) (PDI)**	**Dioxane (nm) (PDI)**	**Water (nm) (PDI)**
5-36	P950$_9$-*b*-M$_{16}$-*b*-(M$_4$-*grad*-B$_{97}$)	80.9 (0.127)	11.6 (0.227)	74.4 (0.133)	79.6 (0.093)	92.1 (0.09)	77.6 (0.146)
5-37	P950$_9$-*b*-M$_{12}$-*b*-(M$_8$-*grad*-B$_{196}$)	88.5 (0.136)	14.5 (0.286)	81 (0.135)	88.3 (0.106)	103 (0.06)	82.8 (0.142)
5-38	P950$_9$-*b*-M$_{15}$-*b*-(M$_5$-*grad*-B$_{388}$)	125 (0.097)	18.5 (0.163)	125 (0.118)	122 (0.069)	208 (0.008)	116 (0.098)
5-40	P950$_9$-*b*-M$_{15}$-*b*-(M$_5$-*grad*-B$_{582}$)	142 (0.067)	21 (0.137)	138 (0.106)	135 (0.058)	210 (0.014)	129 (0.062)
5-41	P950$_9$-*b*-M$_{13}$-*b*-(M$_7$-*grad*-B$_{760}$)	188 (0.033)	23.7 (0.181)	186 (0.084)	180 (0.037)	331 (0.106)	171 (0.066)

5-42	$P950_9$-*b*-M_{14}-*b*-(M_6-*grad*-B_{980})	416 (0.074)	37.4 (0.23)	412 (0.016)	420 (0.093)	666 (0.261)	399 (0.007)

Table 5-13: Particles size diameter of $P950_{18}$ triblock copolymer before and after crosslinking

Entry number from Table 5-10	**Theoretical composition**	**d_z before crosslinking**			**d_z after crosslinking**		
		Isopropanol:Water 96:4 % v/v (nm) (PDI)	**Dioxane (nm) (PDI)**	**Water (nm) (PDI)**	**Isopropanol:Water 96:4 % v/v (nm) (PDI)**	**Dioxane (nm) (PDI)**	**Water (nm) (PDI)**
5-43	$P950_{18}$-*b*-M_{13}-*b*-(M_7-*grad*-B_{91})	129 (0.266)	11.3 (0.237)	124 (0.304)	126 (0.237)	120 (0.236)	125 (0.268)
5-44	$P950_{18}$-*b*-M_{11}-*b*-(M_9-*grad*-B_{170})	150 (0.109)	12.7 (0.147)	144 (0.133)	150 (0.12)	171 (0.114)	144 (0.127)
5-45	$P950_{18}$-*b*-M_{12}-*b*-(M_8-*grad*-B_{380})	104 (0.162)	14.6 (0.223)	101 (0.212)	104 (0.148)	141 (0.073)	99.7 (0.169)
5-47	$P950_{18}$-*b*-M_{12}-*b*-(M_8-*grad*-B_{576})	121 (0.202)	21.5 (0.188)	120 (0.229)	122 (0.169)	181 (0.04)	120 (0.226)
5-48	$P950_{18}$-*b*-M_{13}-*b*-(M_7-*grad*-B_{760})	146 (0.094)	24.4 (0.17)	145 (0.113)	144 (0.119)	225 (0.06)	141 (0.117)

5-49	$P950_{18}$-*b*-M_{13}-*b*-(M_7-*grad*-B_{940})	213 (0.055)	31.6 (0.197)	207 (0.072)	212 (0.042)	348 (0.121)	202 (0.031)

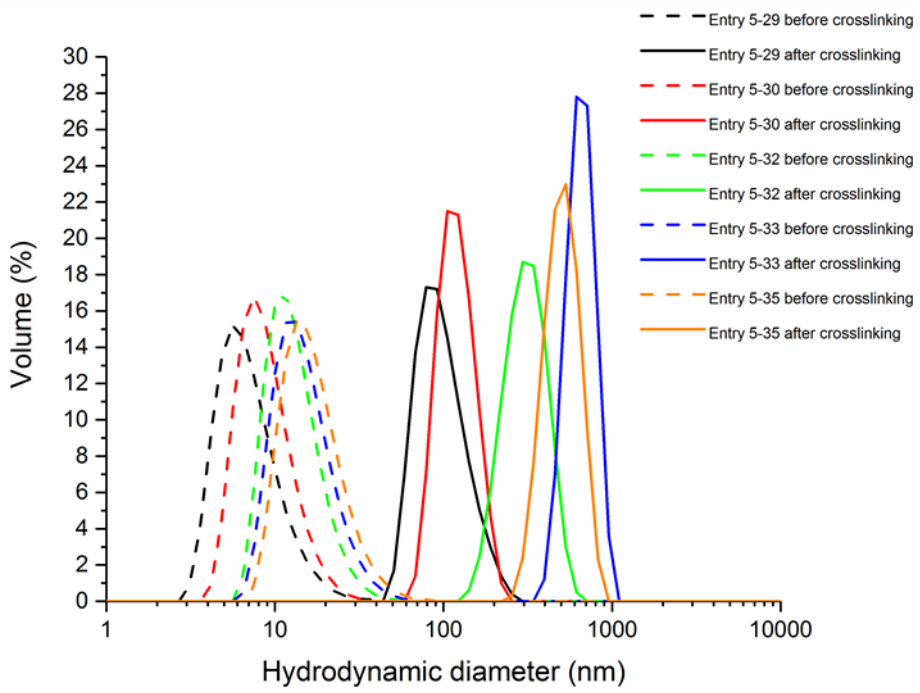

Figure 5-19: DLS volume distributions of $P300_{19}$-b-$PMPS_{20\text{-}y}$-b-($PMPS_y$-grad-$PBzMA_z$) in dioxane. Dash line represents before crosslinking (no catalyst) and solid line represents after crosslinking (with catalyst).

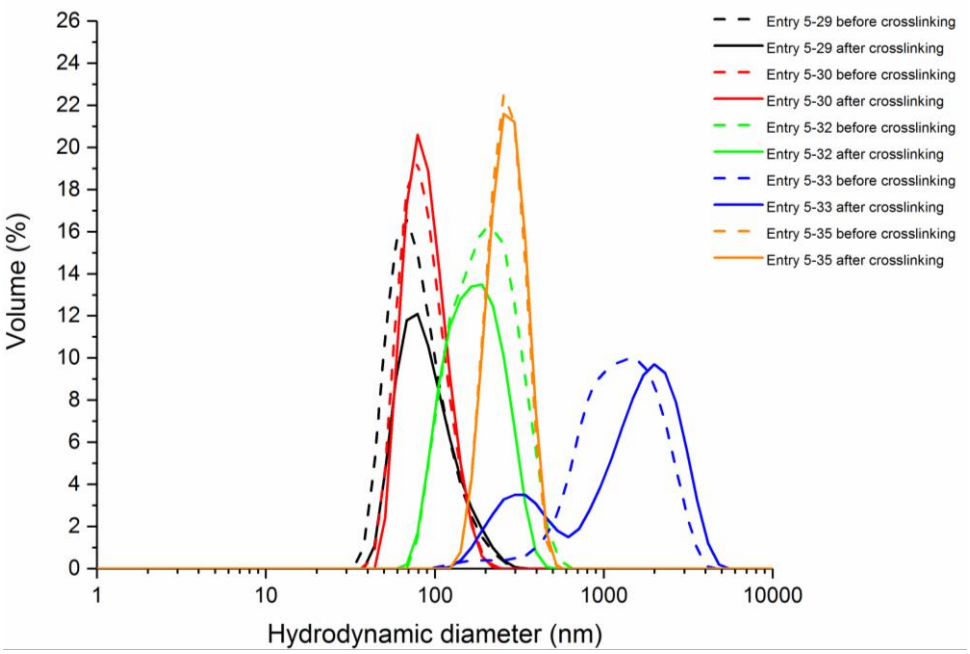

Figure 5-20: DLS volume distributions of $P300_{19}$-b-$PMPS_{20\text{-}y}$-b-($PMPS_y$-grad-$PBzMA_z$) in isopropanol:water (96:4 % v/v). Dash line represents before crosslinking (no catalyst) and solid line represents after crosslinking (with catalyst).

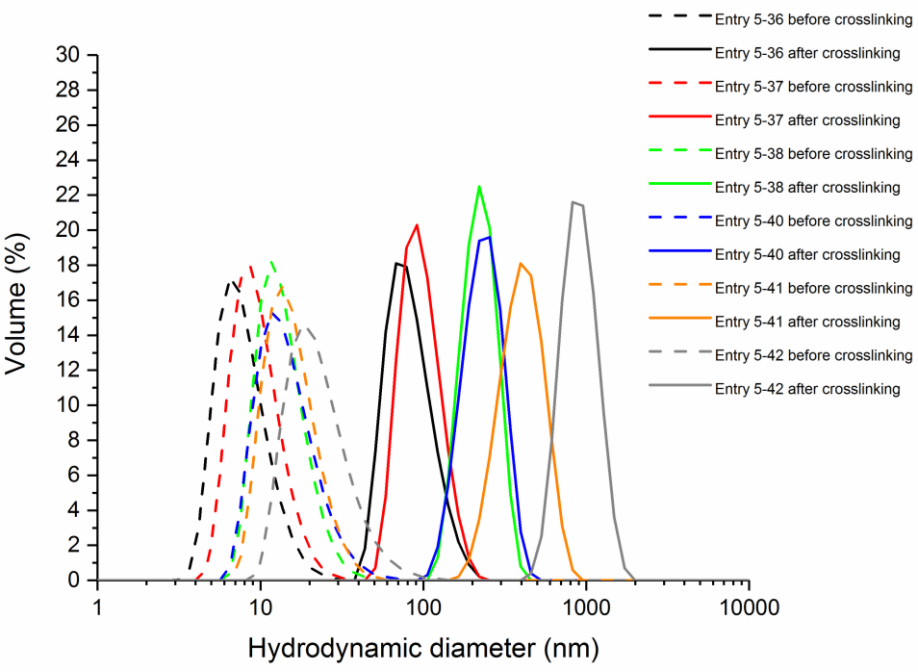

Figure 5-21: DLS volume distributions of P950$_9$-b-PMPS$_{20-y}$-b-(PMPS$_y$-grad-PBzMA$_z$) in dioxane. Dash line represents before crosslinking (no catalyst) and solid line represents after crosslinking (with catalyst).

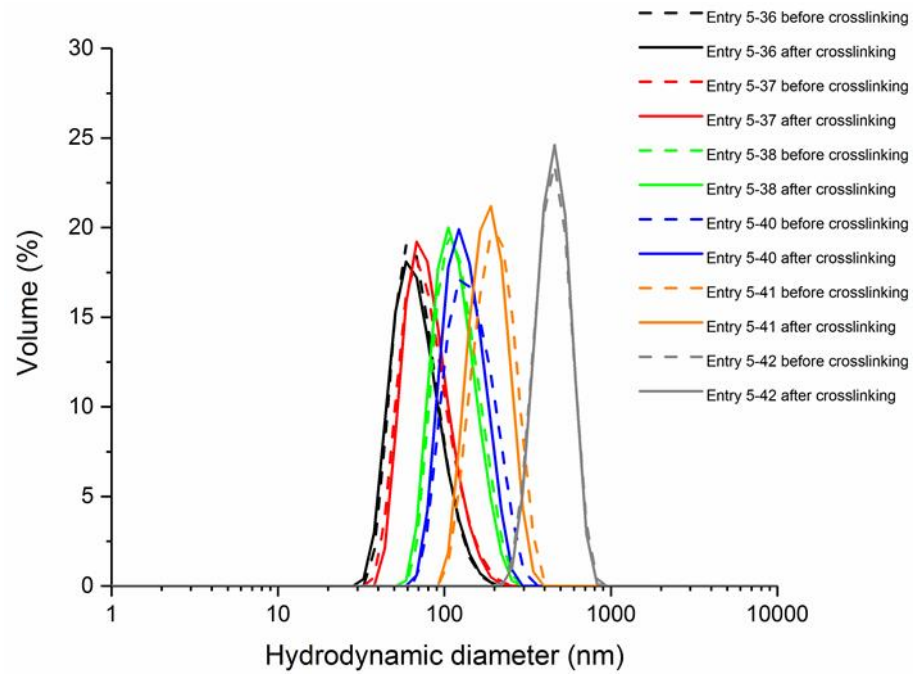

Figure 5-22: DLS volume distributions of P950$_9$-b-PMPS$_{20-y}$-b-(PMPS$_y$-grad-PBzMA$_z$) in isopropanol:water (96:4 % v/v). Dash line represents before crosslinking (no catalyst) and solid line represents after crosslinking (with catalyst).

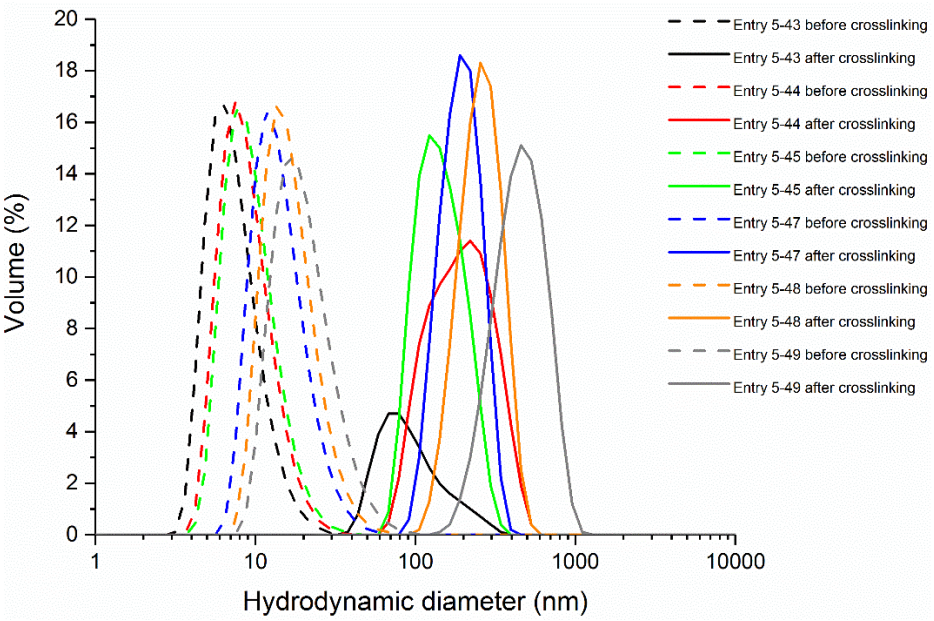

Figure 5-23: DLS volume distributions of $P950_{18}$-b-$PMPS_{20\text{-}y}$-b-($PMPS_y$-grad-$PBzMA_z$) in dioxane. Dash line represents before crosslinking (no catalyst) and solid line represents after crosslinking (with catalyst).

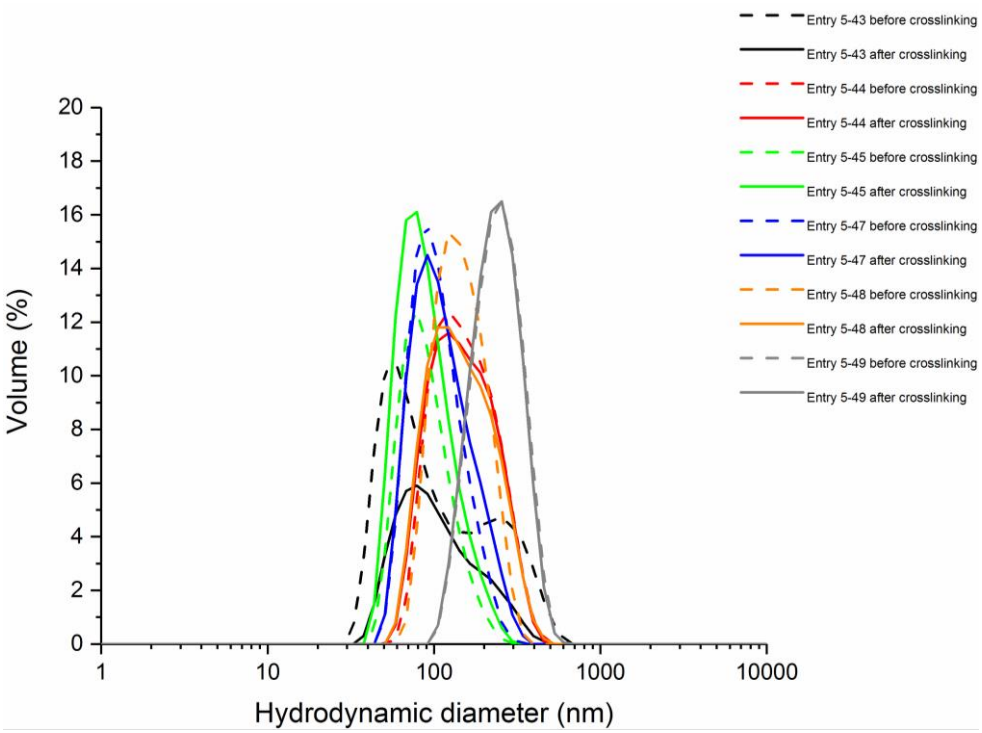

Figure 5-24: DLS volume distributions of $P950_{18}$-b-$PMPS_{20\text{-}y}$-b-($PMPS_y$-grad-$PBzMA_z$) in isopropanol:water (96:4 % v/v). Dash line represents before crosslinking (no catalyst) and solid line represents after crosslinking (with catalyst).

Figure 5-25: Images of non-crosslinking and after crosslinking of Entry 5-35 (in Table 5-11, $P300_{19}$-b-M_{14}-b-(M_6-grad-B_{776})): (A) gel formation after a few hours (no crosslinking), and (B) white liquid (after crosslinking with catalyst).

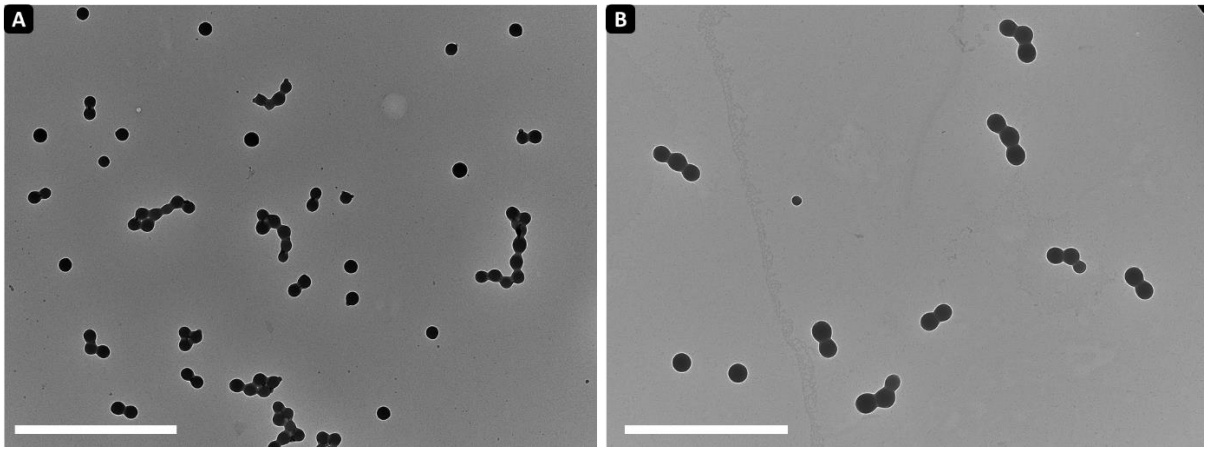

Figure 5-26: TEM images of nanoparticles in isopropanol:water (96:4 % v/v): (A) Entry 5-33 in Table 5-11 (after crosslinking) and (B) Entry 5-35 in Table 5-11 (after crosslinking). Scale bar: (A) and (B) = 2 µm.

Absence of PMPS block. In this section, the impact of the PMPS block on the particle morphology was studied. A low molecular weight PEGMA macroRAFT agent ($P300_{19}$) was directly chain extended with different lengths of BzMA block to form diblock copolymer nanoparticles in isopropanol/water (96:4 % v/v). The fractional conversion of BzMA was high and the DLS particle size increased with increasing the chain length of PBzMA (Table 5-14). However, the dispersion stability decreased when the chain length of PBzMA increased, ranging from more than 7 days ($P300_{19}B_{196}$) to ~ 1 day ($P300_{19}B_{760}$). Figure 5-27 shows three different $P300_{19}B_z$ dispersions, with the precipitate noted in images B and C. An almost clear liquid phase was observed in Entry 5-52 (in Table 5-14, $P300_{19}B_{760}$) while pale white liquid was observed in Entry 5-51 (in Table 5-14, $P300_{19}B_{332}$). The precipitation was attributed to an insufficient stabilization from $P300_{19}$ when targeting high BzMA DP. Interestingly, in the absence of an MPS block, vesicle-type morphologies were observed by electron microscopy (Figure 5-28). This result showed a contrasting observation to Entry 5-30 in Table 5-11 (Figure 5-16) where PMPS block was included and only spheres were observed. This result strongly suggests that the MPS block is preventing the formation of higher order morphologies beyond spherical nanoparticles; as the MPS block is soluble in the reaction medium, the solvophilic block in these systems actually consists of the PEGMA block as well as the MPS block. IPS was not studied in this case, as IPS is soluble in the reaction medium and has a bulky structure which can further increase the effective headgroup area. In the absence of catalyst, the particles are not interfacially cross-linked, and so the differing chemical nature of the solvophilic block is preventing a morphology transition, even at very long BzMA block lengths.

Table 5-14: Conversion and DLS data of $P300_{19}B_z$

Entry	**Target BzMA DP**	**BzMA conversion**	**Theoretical composition**	d_z		
				Isopropanol: Water (96:4 % v/v) (nm) (PDI)	**Dioxane (nm) (PDI)**	**Water (nm) (PDI)**
5-50	200	0.98	$P300_{19}B_{196}$	403 (0.197)	11 (0.128)	383 (0.22)
5-51	400	0.83	$P300_{19}B_{332}$	1234 (0.123)	14.9 (0.092)	1269 (0.793)
5-52	800	0.95	$P300_{19}B_{760}$	2630 (0.764)	20.7 (0.161)	2296 (0.919)

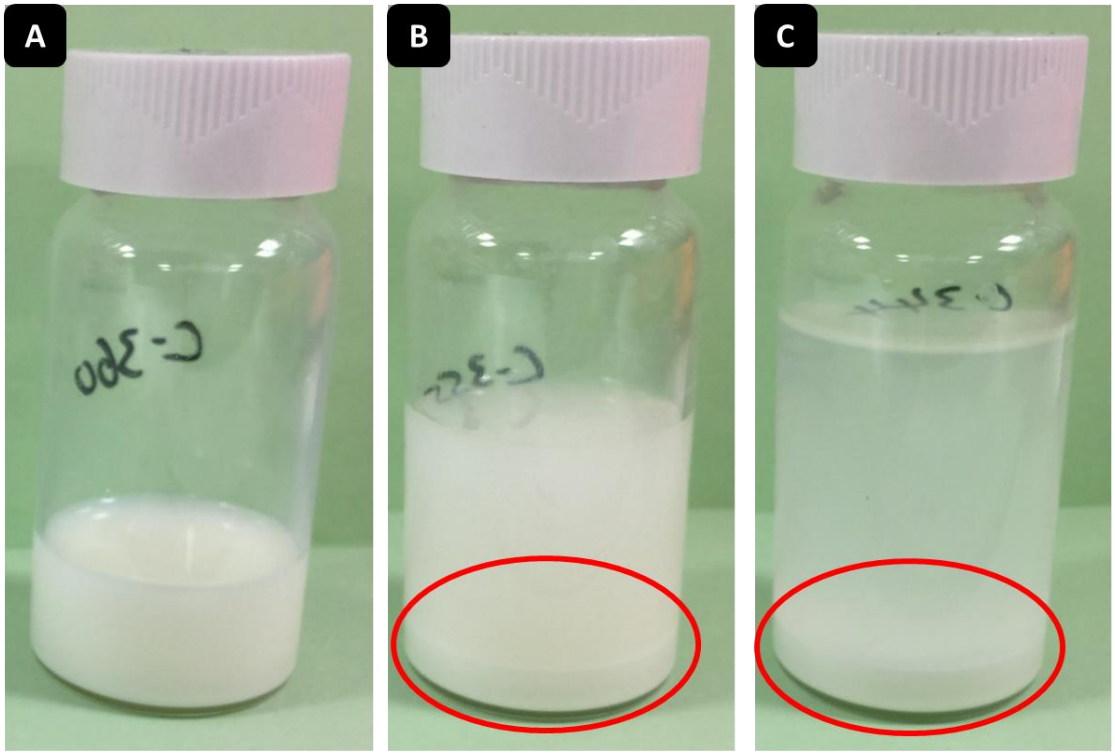

Figure 5-27: $P300_{19}B_z$ solutions (in isopropanol:water (96 % v/v)) and their stability: (A) Entry 5-50 in Table 5-14, (B) Entry 5-51 in Table 5-14, and (C) Entry 5-52 in Table 5-14. Red circle shows the precipitated polymer.

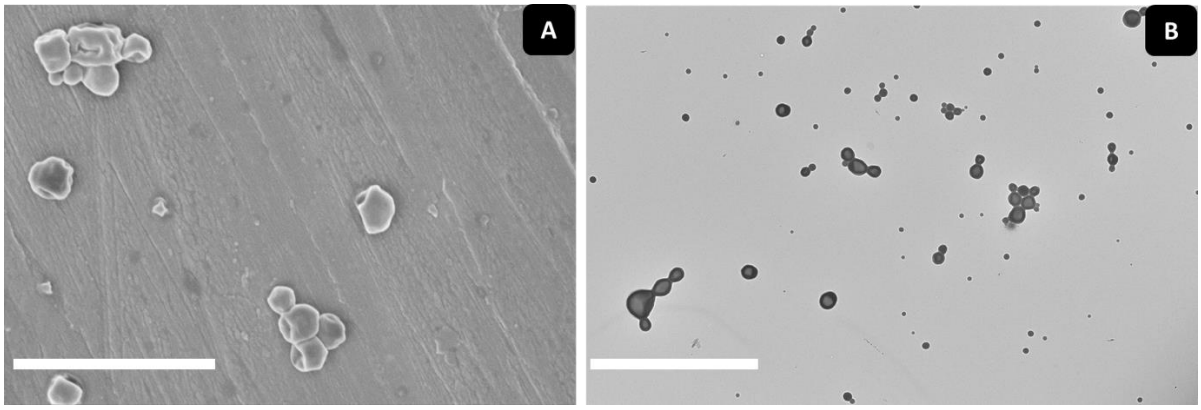

Figure 5-28: Electron microscopy images of Entry 5-50 (in Table 5-14) in isopropanol:water (96 % v/v): (A) SEM image (no crosslinking) and (B) TEM image (no crosslinking). Scale bar: (A) 2 µm and (B) 5 µm.

Encapsulation of Nile Red into Nanoparticle Core. Nile Red is a hydrophobic dye with a water solubility of < 1 μg mL^{-1}.[104] In this work, the maximum absorption wavelength of Nile Red in dioxane was 519 nm and the molar absorption coefficient was determined to be 18825 ± 126 M^{-1} cm^{-1}. Nile Red was introduced together with the addition of BzMA into the reaction vessel in order to simultaneously encapsulate Nile Red into the particle core during the self-assembly process.[105] The Nile Red encapsulated nanoparticles were subsequently crosslinked with using NH_4OH, followed by 3 days dialysis against isopropanol:water (96 % v/v) to remove Nile Red that was not encapsulated (the possibility of Nile Red leaching from the particle core also exists). Figure 5-29 shows a notable colour difference of the nanoparticle dispersion before (a dark reddish pink) and after dialysis (pale pink), indicating large amount of non-encapsulated Nile Red was eliminated during dialysis, which is discussed in the next paragraph. The presence of Nile Red also did not affect the stability of the dispersion.

The concentration of encapsulated Nile Red was determined by using UV-vis spectroscopy in dioxane. Dioxane is a good solvent to both Nile Red and the triblock copolymer; as a result, non-crosslinked particles will dissociate into unimers in dioxane (releasing any encapsulated Nile Red) while crosslinked nanoparticles (after dialysis) will not dissociate, with any Nile Red released from the particle is due to diffusion through the cross-linked interface. The DLS particle size results of experiments in the presence of Nile Red is presented in Table 5-15. A major particle size change in dioxane (before and after crosslinking) was observed in Figure 5-30 and this phenomenon had been described in the previous section. Figure 5-31 shows the crosslinked distributions sufficiently close to their non-crosslinked parent distributions in isopropanol:water (96:4 % v/v) (after dialysis). Table 5-16 shows the data of Nile Red experiments and the retention efficiency attributed to interfacial crosslinking. The concentration of non-encapsulated Nile Red was varied with the type of PEGMA macroRAFT

agent used; this is primarily due to the mass ratio between Nile Red and PEGMA macroRAFT agent used in each experiment was held constant. The retention efficiency of crosslinked nanoparticles was relatively low, which may be attributed to leakage of Nile Red across the cross-linked interface when swollen with dioxane. However, this result demonstrated crosslinking could retain some cargo within the core even a good solvent was used. For example, 1.41 μmol L^{-1} of Nile Red was encapsulated in non-crosslinked particles (Entry 5-31 in Table 5-16) after dialysis and all dye was released when dioxane was added. After the particles were crosslinked and dialysed, 1.11 μmol L^{-1} of Nile Red was released in dioxane through diffusion, meaning that 0.3 μmol L^{-1} of Nile Red remained in the particle core. The retention efficiency of Entry 5-39 (in Table 5-16) was quite high (56.3 %) compared to other systems tested; and this was possibly due to the structure of the polymer. Entry 5-39 (in Table 5-9) possessed a PBzMA chain twice that of Entry 5-31 (in Table 5-8), which would increase the aromatic ring interaction by twofold and therefore retained more Nile Red.[106] TEM images (Figure 5-32) showed that the morphology was still spherical (and some fused spheres) after loaded with Nile Red, crosslinking and dialysis.

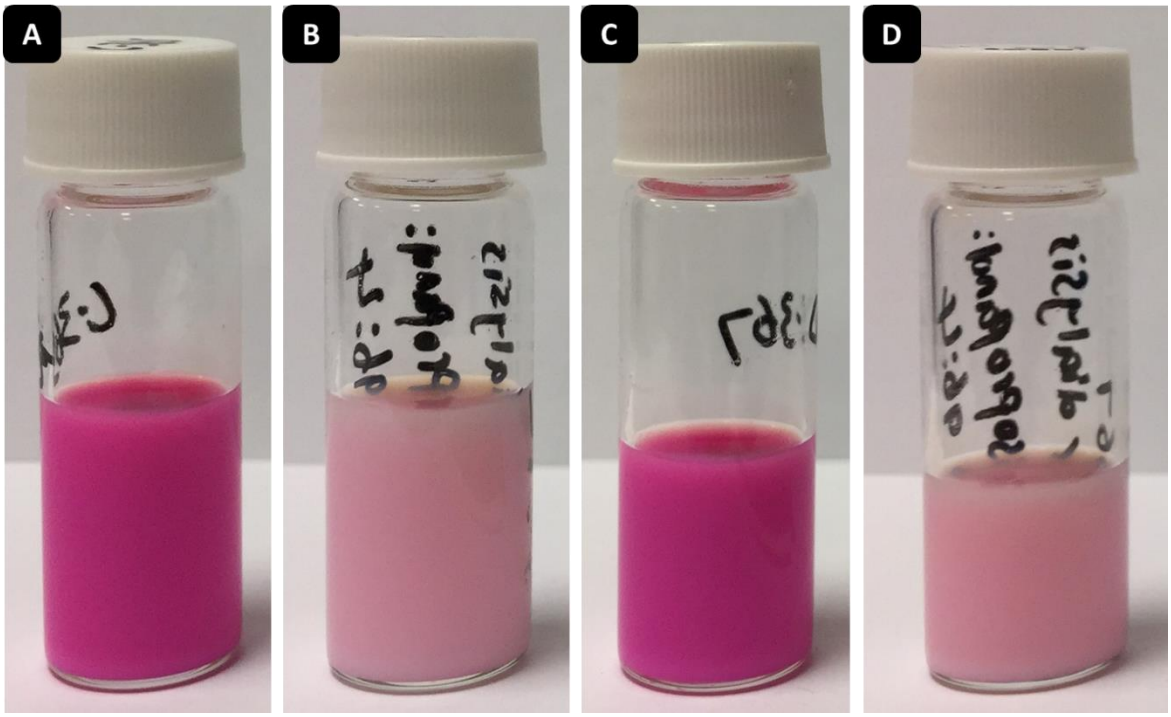

Figure 5-29: Nile Red encapsulation experiment (Entry 5-31 in Table 5-8; $P300_{19}$-b-M_{17}-b-(M_3-grad-B_{190})): (A) solution before crosslinking and dialysis, (B) solution before crosslinking and after dialysis, (C) solution after crosslinking and before dialysis, and (D) solution after crosslinking and dialysis.

Table 5-15: Particle size of Nile Red experiments

Entry from Table 5-8, Table 5-9 and Table 5-10	**Theoretical composition**	**Description**	**d_z before crosslinking**			**d_z after crosslinking**		
			Isopropanol:Water 96:4 % v/v (nm) (PDI)	**Dioxane (nm) (PDI)**	**Water (nm) (PDI)**	**Isopropanol:Water 96:4 % v/v (nm) (PDI)**	**Dioxane (nm) (PDI)**	**Water (nm) (PDI)**
5-31	$P300_{19}$-*b*-M_{17}-*b*-(M_3-*grad*-B_{190})	Before dialysis	109 (0.047)	15.3 (0.252)	104 (0.086)	110 (0.057)	150 (0.032)	102 (0.049)
		After dialysis	113 (0.056)	22.8 (0.255)	107 (0.066)	228 (0.186)	182 (0.038)	229 (0.279)
5-39	$P950_9$-*b*-M_{15}-*b*-(M_5-*grad*-B_{380})	Before dialysis	111 (0.081)	16.7 (0.123)	106 (0.107)	126 (0.073)	205 (0.015)	119 (0.096)
		After dialysis	128 (0.089)	23.6 (0.221)	123 (0.1)	153 (0.086)	212 (0.014)	147 (0.133)
5-46	$P950_{18}$-*b*-M_{12}-*b*-(M_8-*grad*-B_{376})	Before dialysis	116 (0.172)	17 (0.181)	115 (0.222)	114 (0.177)	154 (0.075)	112 (0.212)

		After dialysis	110 (0.093)	19.4 (0.204)	106 (0.157)	109 (0.158)	142 (0.061)	105 (0.187)

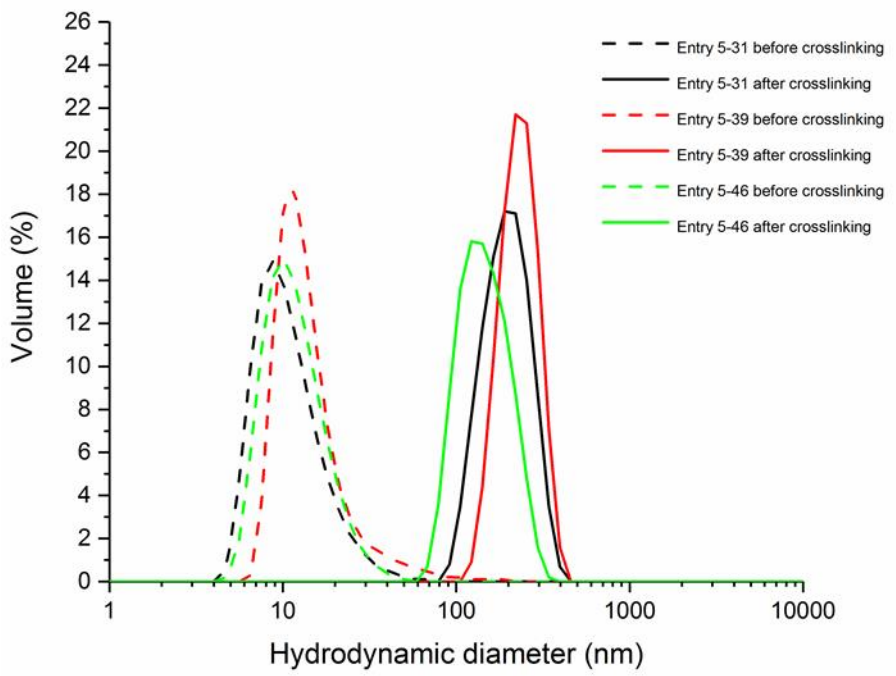

Figure 5-30: DLS volume distributions of Nile Red experiments (after dialysis) in dioxane. Dash line represents before crosslinking (no catalyst) and solid line represents after crosslinking (with catalyst).

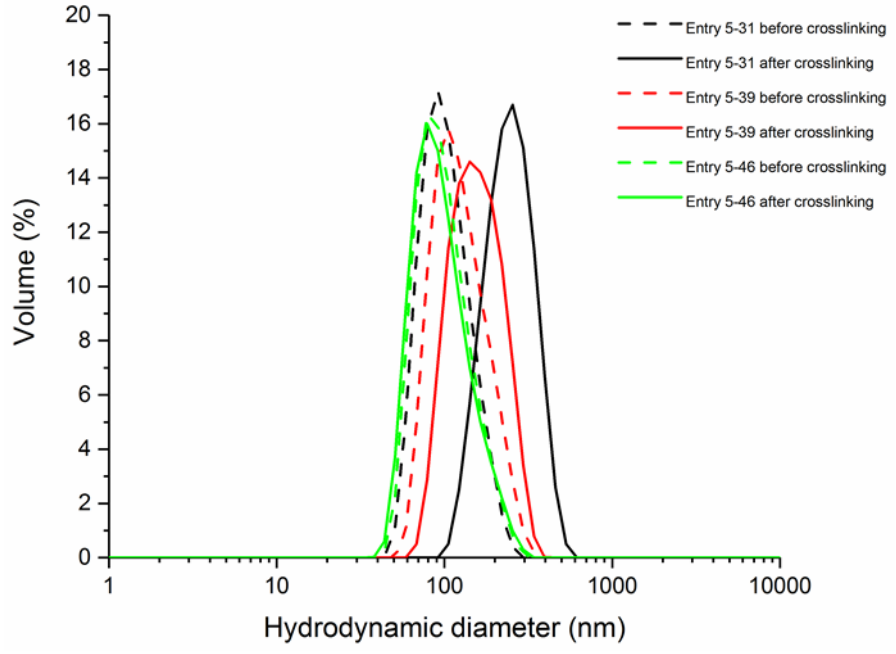

Figure 5-31: DLS volume distributions of Nile Red experiments (after dialysis) in isopropanol:water (96:4 % v/v). Dash line represents before crosslinking (no catalyst) and solid line represents after crosslinking (with catalyst).

Table 5-16: Data of Nile Red experiments and the retention efficiency

Entry from Table 5-8, Table 5-9, and Table 5-10	**Theoretical composition**	**Concentration of non-encapsulated Nile Red (μmol L^{-1})**	**Concentration of encapsulated Nile Red released in dioxane (after dialysis) (μmol L^{-1})**		**Remaining concentration of encapsulated Nile Red in the particle core after dioxane added (after dialysis) (μmol L^{-1})**		**Retention efficiency (%)[#]**
			Before Crosslinking	**After Crosslinking**	**Before Crosslinking**	**After Crosslinking**	
5-31	$P300_{19}$-*b*-M_{17}-*b*-(M_3-*grad*-B_{190})	40.9	1.41	1.11	0	0.3	21.3
5-39	$P950_{9}$-*b*-M_{15}-*b*-(M_5-*grad*-B_{380})	15.6	2.61	1.14	0	1.47	56.3
5-46	$P950_{18}$-*b*-M_{12}-*b*-(M_8-*grad*-B_{376})	47.6	5.28	4.11	0	1.17	22.2

[#] *The retention efficiency of Nile Red in the core was calculated by using 1- ([encapsulated Nile Red released in dioxane (after crosslinking)] / [encapsulated Nile Red released in dioxane (before crosslinking)]).*

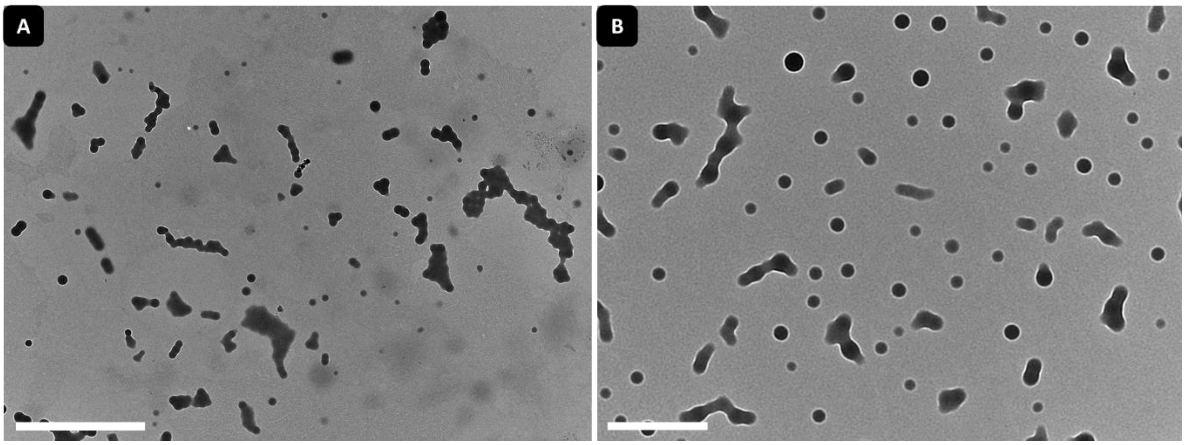

Figure 5-32: TEM images of Entry 5-46 (in Table 5-15; $P950_{18}$-b-M_{12}-b-(M_8-grad-B_{376})) in isopropanol:water (96:4 % v/v): (A) before dialysis (after crosslinking) and (B) after dialysis (after crosslinking). Scale bar: (A) 2 µm and (B) 500 nm.

5.3 Conclusions

In this work, the use of triblock copolymers with a reactive middle block have been explored to create interfacially crosslinked polymer nanoparticles and capsules. Two different methods were pursued, involving either a pre-synthesized triblock copolymer to stabilize a miniemulsion system, or *in-situ* self-assembly of a targeted copolymer. Both methods had comparative successes and limitations to their approach.

Pre-synthesized triblock copolymers used as polymeric surfactants in stabilizing toluene/water miniemulsion showed the ability to effectively crosslink the interface by base catalysed hydrolysis and condensation, yielding hollow capsules. The capsules did not dissociate upon addition to dioxane, as opposed to the starting copolymer. Despite a series of optimisation with respect to polymer loading, polymer composition, temperature and catalyst type, the main deficiency of this approach was the stability of crosslinked dispersion. These dispersions were not suitable for long term storage, as the miniemulsion phase separated within days. The stability of the dispersion may be improved by partially crosslinking the MPS (to retain some of the solvophilic character of MPS), increasing the HLB value of polymeric surfactant, or using a highly oil soluble hydrophobic block (e.g by replacing BzMA with lauryl methacrylate).

PISA mediated by RAFT polymerization provided an alternative approach towards the synthesis of triblock copolymers with similar composition to the approach above. *In-situ* self-assembled nanoparticles were generated when the chain length of PBzMA block increased. Many factors were considered and studied to access higher order morphology, however, the morphology was still restricted to spherical nanoparticles, with vesicles only formed in the

absence of the middle PMPS block. The stability of the un-crosslinked PISA dispersion was varied with the type of PEGMA macroRAFT agent used and target BzMA DP. Gelation of the nanoparticle dispersion was observed upon storage, however this could be avoided and stability could be improved by crosslinking the interfacial PMPS block with the addition of a base catalyst. Crosslinked nanoparticles were shown to enhance the retention efficiency of Nile Red in the particle core in comparison to non-crosslinked particles. This shows the possibility of using nanoparticles with an interfacial alkoxysilyl block can be a potential candidate for the controlled release of hydrophobic materials.

5.4 References

1. S. Perrier, S. G. Jackson, D. M. Haddleton, B. Améduri and B. Boutevin, *Macromolecules*, 2003, **36**, 9042-9049.
2. B. P. Koiry, A. Chakrabarty and N. K. Singha, *RSC Advances*, 2015, **5**, 15461-15468.
3. K. Huan, L. Bes, D. M. Haddleton and E. Khoshdel, *Journal of Polymer Science Part A: Polymer Chemistry*, 2001, **39**, 1833-1842.
4. K. I. Fukukawa, L. Zhu, P. Gopalan, M. Ueda and S. Yang, *Macromolecules*, 2005, **38**, 263-270.
5. K. J. Sykes, S. Harrisson and D. J. Keddie, *Macromolecular Chemistry and Physics*, 2016, **217**, 2310-2320.
6. J. Huang and K. Matyjaszewski, *Macromolecules*, 2005, **38**, 3577-3583.
7. H. Guo, P. Liu, H. Li, C. Cheng and Y. Gao, *Langmuir*, 2018, **34**, 5750-5758.
8. P. S. Mohanty, H. Dietsch, L. Rubatat, A. Stradner, K. Matsumoto, H. Matsuoka and P. Schurtenberger, *Langmuir*, 2009, **25**, 1940-1948.
9. Y. Liu and X. Wang, *Polymer Chemistry*, 2011, **2**, 2741-2757.
10. P. Raffa, A. A. Broekhuis and F. Picchioni, *Journal of Petroleum Science and Engineering*, 2016, **145**, 723-733.
11. H. Yu, J. Zhu and W. Jiang, *Journal of Polymer Science Part B: Polymer Physics*, 2008, **46**, 1536-1545.
12. L. Zhang and A. Eisenberg, *Journal of the American Chemical Society*, 1996, **118**, 3168-3181.
13. Y. Yu and A. Eisenberg, *Journal of the American Chemical Society*, 1997, **119**, 8383-8384.
14. B. Louage, Q. Zhang, N. Vanparijs, L. Voorhaar, S. Vande Casteele, Y. Shi, W. E. Hennink, J. Van Bocxlaer, R. Hoogenboom and B. G. De Geest, *Biomacromolecules*, 2015, **16**, 336-350.
15. Z. L. Tyrrell, Y. Shen and M. Radosz, *Progress in Polymer Science*, 2010, **35**, 1128-1143.
16. H. Wei, X. Zhang, C. Cheng, S. X. Cheng and R. X. Zhuo, *Biomaterials*, 2007, **28**, 99-107.
17. R. K. O'Reilly, C. J. Hawker and K. L. Wooley, *Chemical Society Reviews*, 2006, **35**, 1068-1083.
18. Y. Li, W. Du, G. Sun and K. L. Wooley, *Macromolecules*, 2008, **41**, 6605-6607.
19. L. Yukun, C. T. Leela, F. V. L. Fong, Z. Jiong and C. Chong, *Journal of Polymer Science Part A: Polymer Chemistry*, 2014, **52**, 3250-3259.
20. A. M. Mukkaram and H. D. H. Stöver, *Journal of Polymer Science Part A: Polymer Chemistry*, 2006, **44**, 156-171.
21. G. Jiang, *Journal of Applied Polymer Science*, 2009, **114**, 3472-3478.
22. A. N. Koo, H. J. Lee, S. E. Kim, J. H. Chang, C. Park, C. Kim, J. H. Park and S. C. Lee, *Chemical Communications*, 2008, **0**, 6570-6572.
23. L. N. Pilon, S. P. Armes, P. Findlay and S. P. Rannard, *European Polymer Journal*, 2006, **42**, 1487-1498.
24. E. S. Read and S. P. Armes, *Chemical Communications*, 2007, **0**, 3021-3035.
25. S. I. Ali, J. P. A. Heuts and A. M. van Herk, *Soft Matter*, 2011, **7**, 5382-5390.
26. J. Liu, Q. Yang, L. Zhang, H. Yang, J. Gao and C. Li, *Chemistry of Materials*, 2008, **20**, 4268–4275.

27. D. Niu, Y. Li, X. Qiao, L. Li, W. Zhao, H. Chen, Q. Zhao, Z. Ma and J. Shi, *Chemical Communications*, 2008, **0**, 4463-4465.
28. L. He, E. S. Read, S. P. Armes and D. J. Adams, *Macromolecules*, 2007, **40**, 4429-4438.
29. B. D. Mather, K. Viswanathan, K. M. Miller and T. E. Long, *Progress in Polymer Science*, 2006, **31**, 487-531.
30. S. Sugihara, S. Ito, S. Irie and I. Ikeda, *Macromolecules*, 2010, **43**, 1753-1760.
31. J. Ding and G. Liu, *Macromolecules*, 1998, **31**, 6554-6558.
32. J. S. Kim and J. H. Youk, *Macromolecular Research*, 2009, **17**, 926-930.
33. X. Jiang, S. Luo, S. P. Armes, W. Shi and S. Liu, *Macromolecules*, 2006, **39**, 5987-5994.
34. Y. Liu, V. Piñón and M. Weck, *Polymer Chemistry*, 2011, **2**, 1964-1975.
35. M. J. Joralemon, R. K. O'Reilly, C. J. Hawker and K. L. Wooley, *Journal of the American Chemical Society*, 2005, **127**, 16892-16899.
36. R. K. O'Reilly, M. J. Joralemon, K. L. Wooley and C. J. Hawker, *Chemistry of Materials*, 2005, **17**, 5976-5988.
37. X. Jiang, G. Zhang, R. Narain and S. Liu, *Langmuir*, 2009, **25**, 2046-2054.
38. M. J. Joralemon, K. S. Murthy, E. E. Remsen, M. L. Becker and K. L. Wooley, *Biomacromolecules*, 2004, **5**, 903-913.
39. K. Qi, Q. Ma, E. E. Remsen, C. G. Clark and K. L. Wooley, *Journal of the American Chemical Society*, 2004, **126**, 6599-6607.
40. D. Pan, J. L. Turner and K. L. Wooley, *Chemical Communications*, 2003, **0**, 2400-2401.
41. J. L. Turner, D. Pan, R. Plummer, Z. Chen, A. K. Whittaker and K. L. Wooley, *Advanced Functional Materials*, 2005, **15**, 1248-1254.
42. J. L. Turner, M. L. Becker, X. Li, J.-S. A. Taylor and K. L. Wooley, *Soft Matter*, 2005, **1**, 69-78.
43. K. Wei, X. Peng and F. Zou, *International Journal of Pharmaceutics*, 2014, **464**, 225-233.
44. A. Khanal, Y. Inoue, M. Yada and K. Nakashima, *Journal of the American Chemical Society*, 2007, **129**, 1534-1535.
45. D. Niu, Y. Li and J. Shi, *Chemical Society Reviews*, 2017, **46**, 569-585.
46. P. K. Jal, S. Patel and B. K. Mishra, *Talanta*, 2004, **62**, 1005-1028.
47. Y. P. He, S. Q. Wang, C. R. Li, Y. M. Miao, Z. Y. Wu and B. S. Zou, *Journal of Physics D: Applied Physics*, 2005, **38**, 1342-1350.
48. T. K. H. Ta, M. T. Trinh, N. V. Long, T. T. M. Nguyen, T. L. T. Nguyen, T. L. Thuoc, B. T. Phan, D. Mott, S. Maenosono, H. T. Van and V. H. Le, *Colloids and Surfaces A: Physicochemical and Engineering Aspects*, 2016, **504**, 376-383.
49. J. Moraes, K. Ohno, T. Maschmeyer and S. Perrier, *Chemical Communications*, 2013, **49**, 9077-9088.
50. H. Chen, X. Wu, H. Duan, Y. A. Wang, L. Wang, M. Zhang and H. Mao, *ACS Applied Materials & Interfaces*, 2009, **1**, 2134-2140.
51. W. Li, C. H. Kuo, I. Kanyo, S. Thanneeru and J. He, *Macromolecules*, 2014, **47**, 5932-5941.
52. J. Du and Y. Chen, *Macromolecules*, 2004, **37**, 6322-6328.
53. J. Du and Y. Chen, *Macromolecular Rapid Communications*, 2005, **26**, 491-494.
54. C. G. Gamys, E. Beyou, E. Bourgeat-Lami, L. David and J. Oberdisse, *Soft Matter*, 2012, **8**, 6564-6572.
55. R. Wang, W. Z. Wang, S. Lu and T. Liu, *Macromolecules*, 2009, **42**, 4993-5000.
56. S. Czarnecki and A. Bertin, *Chemistry – A European Journal*, 2018, **24**, 3354-3373.
57. M. M. E. Severin-Vantilt and E. W. J. L. Oomen, *Journal of Non-Crystalline Solids*, 1993, **159**, 38-48.

58. M. Kanezashi, in *Encyclopedia of Membrane Science and Technology*, eds. E. M. Hoek, V. V. Tarabara and M. Kanezashi, John Wiley & Sons, Inc., 2013, DOI: 10.1002/9781118522318.emst043.
59. T. Suzuki and Y. Otsuki, *Polymer Journal*, 2018, **50**, 177-186.
60. C. Nardin, T. Hirt, J. Leukel and W. Meier, *Langmuir*, 2000, **16**, 1035-1041.
61. T. F. Yang, C. N. Chen, M. C. Chen, C. H. Lai, H. F. Liang and H. W. Sung, *Biomaterials*, 2007, **28**, 725-734.
62. K. Youngjong and T. T. Andrew, *Angewandte Chemie International Edition*, 2005, **44**, 409-412.
63. G. Liang, J. Xu and X. Wang, *Journal of the American Chemical Society*, 2009, **131**, 5378-5379.
64. R. McHale, N. Ghasdian, N. S. Hondow, P. M. Richardson, A. M. Voice, R. Brydson and X. Wang, *Macromolecules*, 2010, **43**, 6343-6347.
65. V. Ladmiral, M. Semsarilar, I. Canton and S. P. Armes, *Journal of the American Chemical Society*, 2013, **135**, 13574-13581.
66. L. Shen, H. Guo, J. Zheng, X. Wang, Y. Yang and Z. An, *ACS Macro Letters*, 2018, **7**, 287-292.
67. M. Huo, Y. Zhang, M. Zeng, L. Liu, Y. Wei and J. Yuan, *Macromolecules*, 2017, **50**, 8192-8201.
68. L. Esser, N. P. Truong, B. Karagoz, B. A. Moffat, C. Boyer, J. F. Quinn, M. R. Whittaker and T. P. Davis, *Polymer Chemistry*, 2016, **7**, 7325-7337.
69. J. Huang, H. Zhu, H. Liang and J. Lu, *Polymer Chemistry*, 2016, **7**, 4761-4770.
70. S. L. Canning, G. N. Smith and S. P. Armes, *Macromolecules*, 2016, **49**, 1985-2001.
71. S. J. Byard, M. Williams, B. E. McKenzie, A. Blanazs and S. P. Armes, *Macromolecules*, 2017, **50**, 1482-1493.
72. P. Chambon, A. Blanazs, G. Battaglia and S. P. Armes, *Macromolecules*, 2012, **45**, 5081-5090.
73. Q. Qu, G. Liu, X. Lv, B. Zhang and Z. An, *ACS Macro Letters*, 2016, **5**, 316-320.
74. P. Chambon, A. Blanazs, G. Battaglia and S. P. Armes, *Langmuir*, 2012, **28**, 1196-1205.
75. C. A. Figg, A. Simula, K. A. Gebre, B. S. Tucker, D. M. Haddleton and B. S. Sumerlin, *Chemical Science*, 2015, **6**, 1230-1236.
76. S. Fujii, Y. Cai, J. V. M. Weaver and S. P. Armes, *Journal of the American Chemical Society*, 2005, **127**, 7304-7305.
77. X. Xu, A. E. Smith, S. E. Kirkland and C. L. McCormick, *Macromolecules*, 2008, **41**, 8429-8435.
78. V. Bütün, X. S. Wang, M. V. de Paz Báñez, K. L. Robinson, N. C. Billingham, S. P. Armes and Z. Tuzar, *Macromolecules*, 2000, **33**, 1-3.
79. R. C. Pasquali, M. P. Taurozzi and C. Bregni, *International Journal of Pharmaceutics*, 2008, **356**, 44-51.
80. W. C. Griffin, *Journal of The Society of Cosmetic Chemists*, 1954, **5**, 249-256.
81. W. C. Griffin, *Journal of The Society of Cosmetic Chemists*, 1949, **1**, 311-326.
82. U. Schubert, in *The Sol‐Gel Handbook*, ed. D. L. a. M. Zayat, Wiley-VCH Verlag GmbH & Co., 2015, DOI: 10.1002/9783527670819.ch01, pp. 1-27.
83. G. Wheeler, in *Alkoxysilanes and the Consolidation of Stone*, ed. P. Pardo, Getty Publications, 2005, ch. 2, pp. 13-26.
84. Z. ALOthman, *Materials*, 2012, **5**, 2874-2902.
85. S. H. Yalkowsky, Y. He and P. Jain, *Handbook of Aqueous Solubility Data (Second Edition)*, CRC Press, 2003.
86. H. Jiang, Z. Zheng, Z. Li and X. Wang, *Industrial & Engineering Chemistry Research*, 2006, **45**, 8617-8622.

87. B. D. Benito, F.Velasco, F.J.Martínez and N.Encinas, *Colloids and Surfaces A: Physicochemical and Engineering Aspects*, 2010, **369**, 53-56.
88. M. Mazúr, V. Mlynárik, M. Valko and P. Pelikán, *Applied Magnetic Resonance*, 2000, **18**, 187-197.
89. A. Muzafarov, in *Chemistry Beyond Chlorine*, eds. P. Tundo, L. N. He, E. Lokteva and C. Mota, Springer International Publishing, 2016, DOI: 10.1007/978-3-319-30073-3_11, pp. 317-330.
90. P. J. Roth, F. D. Jochum and P. Theato, *Soft Matter*, 2011, **7**, 2484-2492.
91. W. Zhao, G. Gody, S. Dong, P. B. Zetterlund and S. Perrier, *Polymer Chemistry*, 2014, **5**, 6990-7003.
92. H. Peng, W. Xu and A. Pich, *Polymer Chemistry*, 2016, **7**, 5011-5022.
93. D. Pavlovic, S. Lafond, A. Margaillan and C. Bressy, *Polymer Chemistry*, 2016, **7**, 2652-2664.
94. E. R. Jones, M. Semsarilar, A. Blanazs and S. P. Armes, *Macromolecules*, 2012, **45**, 5091-5098.
95. L. A. Fielding, M. J. Derry, V. Ladmiral, J. Rosselgong, A. M. Rodrigues, L. P. D. Ratcliffe, S. Sugihara and S. P. Armes, *Chemical Science*, 2013, **4**, 2081-2087.
96. D. Zehm, L. P. D. Ratcliffe and S. P. Armes, *Macromolecules*, 2013, **46**, 128-139.
97. M. J. Derry, L. A. Fielding, N. J. Warren, C. J. Mable, A. J. Smith, O. O. Mykhaylyk and S. P. Armes, *Chemical Science*, 2016, **7**, 5078-5090.
98. A. Hanisch, P. Yang, A. N. Kulak, L. A. Fielding, F. C. Meldrum and S. P. Armes, *Macromolecules*, 2016, **49**, 192-204.
99. A. Blanazs, A. J. Ryan and S. P. Armes, *Macromolecules*, 2012, **45**, 5099-5107.
100. G. Wang, M. Schmitt, Z. Wang, B. Lee, X. Pan, L. Fu, J. Yan, S. Li, G. Xie, M. R. Bockstaller and K. Matyjaszewski, *Macromolecules*, 2016, **49**, 8605-8615.
101. L. A. Fielding, J. A. Lane, M. J. Derry, O. O. Mykhaylyk and S. P. Armes, *Journal of the American Chemical Society*, 2014, **136**, 5790-5798.
102. Y. Pei, N. C. Dharsana, J. A. van Hensbergen, R. P. Burford, P. J. Roth and A. B. Lowe, *Soft Matter*, 2014, **10**, 5787-5796.
103. Y. Pei, K. Jarrett, M. Saunders, P. J. Roth, C. E. Buckley and A. B. Lowe, *Polymer Chemistry*, 2016, **7**, 2740-2750.
104. P. Greenspan and S. D. Fowler, *The Journal of Lipid Research*, 1985, **26**, 781-789.
105. B. Karagoz, C. Boyer and T. P. Davis, *Macromolecular Rapid Communications*, 2014, **35**, 417-421.
106. S. Kumar, A. Mohr, A. Kumar, S. K. Sharma and R. Haag, *The International journal of artificial organs*, 2011, **34**, 84-92.

Chapter 6 : Conclusions and Future Work

6.1 Conclusions

This thesis has focussed on the design, preparation and characterization of colloidal nanocomposites, specifically polymer/silica nanoparticles. Silica nanoparticles produced by traditional methods (e.g. emulsion, Stöber *etc.*) are typically spherical in structure, with some control over porosity. This work has used Reversible-Deactivation Radical Polymerization (RDRP) to explore a route to access nanoparticles of differing morphology via Polymerization-Induced Self-Assembly (PISA). PISA mediated by RAFT polymerization provides a level of control of polymer synthesis in addition to particle size and shape. This thesis aimed to use the PISA process to produce polymer-silica nanoparticles with different shapes through the use of the self-assembled polymer nanoparticle as a scaffold for further chemistry.

The design of polymer@silica (polymer core/silica shell) nanoparticles via a combination of PISA and sol-gel chemistry was successfully demonstrated. This was achieved through the use of an alkoxysilane-functional methacrylate as the solvophilic block and subsequent chain-extension and self-assembly of poly(benzyl methacrylate) in ethanol. This was the first reported example of using monomers such as MPS (3-(trimethoxysilyl)propyl methacrylate) and IPS (3-(triisopropoxysilyl)propyl methacrylate) as the stabilizer block in a PISA formulation. A range of morphologies were observed, however the bulkier IPS stabilizer only generated spherical nanoparticles; polymeric vesicles were achieved in the MPS-BzMA system. The alkoxysilane at the particle surface was used to grow a shell of silica in a controlled fashion via a base-catalysed sol-gel process with tetraethylorthosilicate (TEOS). The growth of the silica

shell was verified via electron microscopy and the shell thickness could be adjusted by controlling the TEOS volume.

Attempts to prepare block copolymer nanoparticles with the alkoxysilane block in the particle core proved a greater synthetic challenge. PISA mediated by RAFT emulsion polymerization was attempted to produce PEGMA-b-PMPS particles in aqueous buffer, however the hydrolysis and condensation of the MPS monomer under the reaction conditions used resulted in ineffective chain extension and extensive coagulum. Self-assembly was achieved via preparing diblock copolymers (PEGMA-PMPS, PEGMA-PIPS and PLMA-PMPS) by RAFT solution polymerization and then inducing self-assembly through the addition of a poor solvent (water or hexane). Only sphere nanoparticles were obtained when using PEGMA stabilizer block (both PEGMA-PMPS and PEGMA-PIPS). PLMA-PMPS vesicles were observed in hexane, suggesting that the bulky PEGMA stabilizer block hindered the access to low curvature morphologies in aqueous solution. *In-situ* crosslinking of the PMPS block during and/or after self-assembly was also observed, as all the self-assembled nanoparticles reported (PEGMA-PMPS, PEGMA-PIPS and PLMA-PMPS) were unable to dissociate into unimers upon addition to an excess good solvent that solvated both blocks.

Lastly, MPS-based block copolymers were used to explore the concept of interfacial crosslinking of nanoparticles. Triblock copolymers with alkoxysilane functionality in the middle block (e.g. PEGMA-PMPS-PBzMA) were designed and studied via two approaches. Triblock copolymers were first prepared by RAFT solution polymerization and then used as polymeric surfactants to stabilize toluene-in-water miniemulsions, following by interfacial crosslinking through addition of base catalyst. Various reaction conditions were optimized

however colloidal stability was only of the order of a few days. Despite the relatively low stability, hollow capsules could be observed by cross-linking the interface; the crosslinked structure was also confirmed by DLS measurements in a good solvent (dioxane). As an alternative, PISA mediated by RAFT dispersion polymerization was used to prepare self-assembled nanoparticles of the same triblock composition. Self-assembly to form nanoparticles was observed, and the product stability varied from a few hours to more than a week, depending on the type of PEGMA macroRAFT agent and PBzMA chain length. Only spherical structures were observed, with the exception of removing the MPS block entirely, upon which vesicles formed, suggesting a critical role of the MPS block in trapping the spherical morphology formed. Successful interfacial crosslinking was again observed, and enhanced retention of a model hydrophobic compound (Nile Red) in the crosslinked particle core was reported.

In summary, the versatility and applicability of alkoxysilane-functional monomers such as MPS has been demonstrated through its dual application in chain growth polymerization and as a precursor in sol-gel chemistry to create inorganic materials. This thesis has reported the synthesis of hybrid organic-inorganic nanoparticles via RAFT polymerization and self-assembly through a variety of different approaches. Hybrid nanoparticles with a range of morphologies have been demonstrated, offering a new approach to the preparation of composite materials with different structures. The concepts developed in this thesis can readily be applied to other polymer-organic or polymer-inorganic hybrid nanoparticles in the future.

6.2 Future Work

This work serves as a platform for the continued study of the preparation of colloidal nanocomposites via RDRP methods. Some suggestions and recommendations for future work are given below:

- Surface modification: the surface chemistry of hybrid polymer@silica nanoparticles can be modified to vary their potential application and function. A range of functionalized alkoxysilanes are commercially available, such as fluorinated silanes (e.g. 1H,1H,2H,2H-perfluorodecyltriethoxysilane) and amine based (e.g. (3-aminopropyl) trimethoxysilane). The surface of silica particles can be readily functionalized by modification with these silanes. A fluorinated surface would make the particles much more hydrophobic; an amine-rich surface provides a simple route for further covalent modification at the particle surface.

- Light-mediated polymerization: Numerous challenges were encountered in the preparation of MPS-based block copolymers in aqueous solution, due to the instability of the monomer in the reaction medium at elevated temperatures. Room-temperature redox initiation was applied in this work however challenges with respect to characterization still remained. Given the growth in light-mediated polymerization techniques involving RAFT polymerization, it would be interesting to pursue photopolymerization (.e.g PET-RAFT[1, 2]) as a method to prepare MPS-based block copolymers (and self-assembly). Specifically, the absence of a thermal initiation step may aid in the synthesis of block copolymers without unwanted side-reactions of the MPS monomer.

- Interfacial cross-linking and monolith formation: As shown in Chapter 5, the formation of ABC-type triblock copolymers with MPS as the middle block was effective with respect to interfacial crosslinking of emulsions and polymeric nanoparticles. As block copolymers are routinely used to stabilize and prepare polymerizable high internal phase emulsions (polyHIPEs), the copolymers reported here would be interesting in polyHIPE preparation as the droplet interface can be readily stabilized via crosslinking, reinforcing the pore structure and contributing to the mechanical strength of the monolith.

6.3 References

1. K. Tu, T. Xu, L. Zhang, Z. Cheng and X. Zhu, *RSC Advances*, 2017, **7**, 24040-24045.
2. J. Yeow, J. Xu and C. Boyer, *ACS Macro Letters*, 2015, **4**, 984-990.

Appendices

Appendix 1:

The predicted residual mass of alkoxysilane macroRAFT agents is estimated as follows, based on the below assumptions:

- Effects due to polymer end-groups (dithiobenzoate and trithiocarbonate) are neglected;
- The remaining residual (silica) obtained at the conclusion of TGA measurement is purely produced by the alkoxysilane groups within the polymer backbone upon elevated heating.
- All carbon, hydrogen (and some oxygen) within the polymeric structure are lost via thermal decomposition.
- Silicon (Si) in the silica produced is derived from Si in the polymeric structure.
- The chamber is completely sealed and under an inert atmosphere.

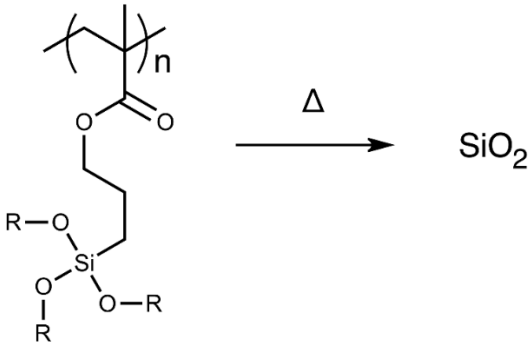

For MPS (248 g/mol) and IPS (332 g/mol) respectively, the mass fraction of Si in the structure is:

MPS: % Si = 28/248 = 11.3% (by mass)

IPS: % Si = 28/332 = 8.4% (by mass)

Assuming all available Si is converted into SiO_2 (60 g/mol), the predicted residual mass is:

Residual mass (MPS): 60/248 = 24.3%

Residual mass (IPS): 60/332 = 18.1%

However, this predicted mass represents a lower bound on the actual value, which is ~ 15% greater. It is postulated that a significant carbon content remains, potentially incorporated into the cross-linked residue.

Appendix 2:

Size prediction of hybrid polymer-silica particles after TEOS growth:

$$d_{pred} = d_{seed} \sqrt[3]{\frac{1.8x + 1.18}{1.8x}}$$

$$x = \frac{\text{seed (g)}}{\text{silica (g)}}; \text{silica}(g) = \frac{m_{TEOS} \times 61}{208}$$

The density of the silica shell is assumed to be ~ 1.8 g/cm^3 and the density of the seed particle is assumed to be equivalent to the density of poly(benzyl methacrylate), which is 1.18 g/cm^3.

Reference: I. Tissot, C. Novat, F. Lefebvre and E. Bourgeat-Lami, Macromolecules, 2001, 34, 5737-5739.